Interlocked Host Structures for Anion Recognition and Lanthanide Complexation

Xiaoxiong Li

Wadham College, University of Oxford



A thesis submitted for the degree of Doctor of Philosophy

Inorganic Chemistry Laboratory

University of Oxford

Michaelmas Term 2018

Interlocked Host Structures for Anion Recognition and Lanthanide Complexation

Xiaoxiong Li, Wadham College, University of Oxford

Abstract of thesis submitted for the degree of Doctor of Philosophy, Michaelmas Term 2018

This thesis describes the utilisation of interlocked host structures for anion recognition and lanthanide complexation. Halogen bonding is used as an intermolecular interaction when designing the interlocked anion hosts.

Chapter 1 introduces the field of supramolecular host-guest chemistry, in particular anion recognition, followed by mechanically interlocked host molecules for guest recognition.

Chapter 2 describes halogen bonding interlocked structures for anion recognition using bifunctional bis-iodotriazole motifs. The synthesis and anion binding properties of a cationic Re(I) complexed halogen bonding rotaxane is reported, and furthermore acid-regulated switching of metal cation and anion guest binding in halogen bonding [2]rotaxanes is demonstrated.

Chapter 3 investigates the preparation of halogen bonding cryptand hosts which contain multiple iodotriazole groups for anion recognition. A naphthalene-containing cryptand host capable of the selective recognition of spherical halide guest species is demonstrated, and attempts to construct halogen bonding cryptand-based interlocked anion hosts are reported.

Chapter 4 details the preparation of novel interlocked rotaxane hosts for lanthanide complexation. The stability and photo-physical properties of the resulting lanthanide complexes are investigated.

Chapter 5 summarises the conclusions of this thesis.

Chapter 6 describes the experimental procedures used in this work, and details the characterisation of novel compounds presented in Chapters 2–4.

Acknowledgements

First, I am immensely grateful to Professor Paul Beer for the opportunity to work in this fascinating group for three years. His supervision and encouragement not only help me progress in chemistry but also have a tremendous influence on my academic career. I feel so fortunate and proud to have such a friendly, trusting and supportive supervisor in my DPhil journey.

Also, acknowledgement should go to Dr. Asha Brown and Dr. Jason Y. C. Lim. They are always there for me when I feel depressed. Asha is so kind to teach me all kinds of knowledge and techniques with endless patience. Jason is my best friend, respectable mentor and admiring model. His diligence and intelligence always encourage me to be confident when I confront problems not to mention his companion everyday makes me feel no longer lonely.

In addition, I am grateful to all my colleagues in Beer group. Especially, I want to express my gratitude to Dr. Jessica Pancholi, Dr. Tim Barendt, Dr. Stuart Cornes, Hena Bagha and Dr. Valentine Bunchuay, Jane Liew, Luiza Bondila, Robert Hein, Harry Klein, Andrew Docker, Grace Turner, Sam Sutton, Tom Mole, Arseni Borissov, TJ and Richard Tse for their help and friendship. It is impossible for me to have this tremendous progress and happy time without them. I am also grateful to my collaborators, Xuejian Zhang and Professor Steve Faulkner, who contribute to the work in Chapter 4, and Dr. Antonio Martinez for the help on crystallography.

Besides, I am lucky enough to get the financial support from China Scholarship Council (CSC) and the Great Britain-China Educational Trust (GBCET).

Last but definitely not least, my heartfelt appreciation is to my loving wife Tiantian Wang (Alice) and my son Hongxuan Li (Maxwell). Their unwavering and unconditional support is always my impetus to go ahead. I love them beyond anything. Many thanks have been given to my parents and grandparents for their

concern and love. Their dedication and encouragement has been valuable beyond words.

This thesis is dedicated to my family.

Xiaoxiong Li

December 2018

长风破浪会有时 直挂云帆济沧海

“Someday, with my sail piercing the clouds, I will mount the wind, break the waves, and traverse the vast, rolling sea.”

Previously published work

Some of the work described in this thesis has already been published:

Peer-reviewed journal articles

"Cationic all-halogen bonding rotaxanes for halide anion recognition"
X. Li, J. Y. C. Lim and P. D. Beer, *Faraday Discuss.* **2017**, 203, 245–255.

"Acid‐regulated Switching of Metal Cation and Anion Guest Binding in Halogen Bonding Rotaxanes"
X. Li, J. Y. C. Lim and P. D. Beer, *Chem. – Eur. J.* **2018**, 24, 17788-17795

Poster presentations

"Acid-regulated Switching of Metal Cationic and Anionic Guest Binding in Neutral Halogen Bonding [2]Rotaxanes"
Xiaoxiong Li and Paul Beer. 13th International Symposium on Macrocyclic and Supramolecular Chemistry, July 2018, Québec City, Canada.

Glossary of abbreviations

δ	chemical shift
λ	wavelength
μ	micro
+ve	positive
Å	Angstrom
AcO^-	acetate anion
aq	aqueous
ATP	adenosine triphosphate
a.u.	arbitrary units
bipy	2,2'-bipyridine, 2,2'-bipyridyl
Boc	*tert*-butoxycarbonyl
br.	broad
Bu	butyl
BzO^-	benzoate anion
ºC	degrees Celsius
cat.	catalytic
conc.	concentrated
COSY	homonuclear correlation spectroscopy
CuAAC	copper(I)-catalyzed azide–alkyne cycloaddition
d	deuterated
d	doublet
DBU	1,8-Diazabicyclo[5.4.0]undec-7-ene
DMF	*N,N'*-dimethylformamide
DMSO	dimethylsulfoxide
DNA	deoxyribonucleic acid
DO3A	1,4,7,10-tetraazacyclododecane-1,4,7-triacetic acid
DOTA	1,4,7,10-tetraazacyclododecane-1,4,7,10-tetraacetic acid
E	potential
$E_{1/2}$	half-wave potential
e.g.	*exempli gratia*
eqv.	equivalent
ES	electrospray
Et	ethyl
eT	energy transfer
ET	electron transfer
Fc	ferrocene
Fc^+	ferrocenium
g	gram
Grubbs' II	Grubbs' second generation catalyst
H	enthalpy
HB	hydrogen bond

hr	hour
HRMS	high resolution mass spectrometry
Hz	Hertz
IUPAC	International Union of Pure and Applied Chemistry
J	coupling constant
^{2}J	two bond coupling constant
^{3}J	three bond coupling constant
K	Kelvin
K_a	association constant
L	litre
Ln	lanthanide
m	milli, multiplet
M	moles per litre
Me	methyl
min	minute(s)
MLCT	metal-to-ligand charge transfer
mol	mole
MS	mass spectrometry
Ms	mesyl
m/z	mass/charge ratio
NMR	nuclear magnetic resonance
p	*para*
PBP	phosphate binding protein
PET	photo-induced electron transfer
Ph	phenyl
pH	$-\log_{10}[H^+]$
pK_a	$-\log_{10}K_a$
ppm	parts per million
q	quartet
R	alkyl or aryl substituent
RCM	ring closing metathesis
ROESY	rotating-frame nuclear Overhauser effect correlation spectroscopy
rt	room temperature
s	singlet
S	entropy
sat.	saturated
SBP	sulfate binding protein
t	triplet
t, tert	*tertiary*
TBA^+	tetrabutylammonium cation
TBTA	tris[(1-benzyl-1,2,3-triazol-4-yl)methyl]amine
TFA	trifluoroactetic acid
TfO^-	triflate anion

THF	tetrahydrofuran
TLC	thin layer chromatography
Ts	4-toluenesulfonyl
UV	ultraviolet
vdW	van der Waals
X	halogen atom
XB	halogen bond

Table of contents

Chapter 1 Introduction 1
1.1 Supramolecular Chemistry 1
1.1.1 Fundamental Aspects of Supramolecular Host-Guest Chemistry 3
1.2 Fundamental Aspects and Applications of Anion Recognition 11
1.2.1 The Importance and Challenges of Anion Recognition 11
1.2.2 Biotic Anion Receptors 12
1.2.3 Artificial Anion Receptors 13
1.2.4 Applications of Anion Recognition 24
1.3 Mechanically Interlocked Host Molecules for Guest Recognition 35
1.3.1 Strategies for Synthesis of Interlocked Molecules 35
1.3.2 Interlocked Host Molecules for Guest Recognition and Sensing 45
1.4 Project Aims 49
1.5 References 50

Chapter 2 Halogen Bonding Interlocked Structures for Anion Recognition using Bifunctional Bis-iodotriazole Motifs 55
2.1 Introduction 55
2.1.1 Bifunctional Properties of 1,2,3-Triazole Derivatives 55
2.1.2 Active Metal Template Synthesis using Triazole Motifs 58
2.1.3 Chapter Aims 59
2.2 Cationic All-XB Re(I)-Containing Rotaxanes for Anion Recognition 60
2.2.1 Design of Target Rotaxanes 60
2.2.2 Synthesis of Target Rotaxanes 60
2.2.3 Anion Binding Studies 72
2.3 Re(I)-bis-iodotriazole-amine based XB Anion Receptor 77
2.3.1 Design of Target Receptors 77
2.3.2 Synthesis and Anion Recognition Properties of Acyclic Systems 77
2.3.3 Attempted Synthesis of Interlocked Systems 83
2.4 Acid-regulated Switching of Metal Cation and Anion Guest Binding in XB Rotaxanes 92
2.4.1 Design and Synthesis of Target Rotaxanes 92
2.4.2 Guest Binding Properties of Neutral Rotaxanes 97
2.4.3 Acid-triggered Regulations in Rotaxane's Guest Binding Behaviour 105
2.5 Towards XB Catenanes Capable of Acid-regulated Switching of Metal Cation and Anion Guest Binding 115
2.5.1 Design of Target Catenanes 115
2.5.2 Active Metal Templation 115
2.5.3 Passive Metal Templation 116
2.6 Conclusion and Future Work 120
2.7 References 122

Chapter 3 Halogen Bonding Cryptands and Cryptand-based Interlocked Structures for Anion Recognition 124
3.1 Introduction 124
3.1.1 Cryptands for Anion Recognition 124
3.1.2 Cryptand-based Interlocked Structures 126
3.1.3 Chapter aims 128
3.2 Halogen Bonding Cryptands for Anion Recognition 130
3.2.1 Tripodal Capping Synthesis and Anion Binding Properties of XB Cryptands 130
3.2.2 Macrocyclic Bridging Synthesis and Anion Binding Properties of XB Cryptands 132
3.3 Towards Halogen Bonding Cryptand-based Interlocked Structures for Anion Recognition 142
3.3.1 Attempted Synthesis via Active Metal Templation 142
3.3.2 Attempted Synthesis via HB Templation 144
3.4 Conclusions and Future Work 146
3.5 References 147

Chapter 4 Novel Rotaxane Ligands for Lanthanide Complexation 148
4.1 Introduction 148
4.1.1 Fundamental Properties of Lanthanides 148
4.1.2 Lanthanide-containing Interlocked Structures 149
4.1.3 Chapter Aims 151
4.2 Synthesis and Characterisation of Rotaxane Ligands 153
4.2.1 Synthesis of Macrocycle Components 153
4.2.2 Synthesis of Axle Components 154
4.2.3 Synthesis and Characterisation of Rotaxanes 155
4.3 Lanthanide Binding Studies 162
4.3.1 Preliminary Qualitative Complexation Studies 162
4.3.2 Association Constant Determination 166
4.4 Conclusions and Future Work 169
4.6 References 171

Chapter 5 Conclusions 172

Chapter 6 Experimental 176
6.1 General Considerations 176
6.1.1 Instrumentation 176
6.1.2 ^{1}H NMR Titration protocols 176
6.1.3 Optical Titration protocols 177
6.2 Synthetic Procedures 178
6.2.1 Solvents and Reagents 178
6.2.2 Synthesis of Novel Compounds from Chapter 2 179
6.2.3 Synthesis of Novel Compounds from Chapter 3 203

6.2.4 Synthesis of Novel Compounds from Chapter 4 217
6.3 References 230

Appendices 231
A: Crystallographic Data 231
B: Computational Studies 236
C: Terbium Titration Spectra 237
References 238

Chapter 1: Introduction

1.1 Supramolecular Chemistry

Supramolecular chemistry refers to the domain of chemistry 'beyond the molecule'. As described by Nobel Prize Laureate Jean-Marie Lehn in his Nobel Lecture:

'Supramolecular chemistry is the chemistry of the intermolecular bond, covering the structures and functions of the entities formed by association of two or more chemical species.'[1]

The history of supramolecular chemistry can be dated back to the 19th century. In 1873, Johannes Diderik van der Waals first proposed the existence of intermolecular forces followed by Hermann Emil Fischer's 'lock and key' hypothesis for enzyme specificity which set the early stage for molecular recognition and host-guest chemistry.[2,3] In 1920, Latimer and Rodebush first used the word 'bond' for the weak interactions between water molecules and since then hydrogen bonding gradually gained mainstream scientific acceptance.[4,5] Hydrogen bonding was used to explain the interactions between two separate strands of nucleotides forming the double helical structure of DNA proposed by James Watson and Francis Crick. The synthesis of artificial crown ether hosts by Charles Pedersen marked a breakthrough for host-guest chemistry in 1967 due to their ability to bind alkali metal cations.[6,7] The pioneers Jean-Marie Lehn and Donald Cram also contributed to the seminal developments in this field and as a consequence shared the 1987 Nobel Prize in Chemistry '*for their development and use of molecules with structure-specific interactions of high selectivity*'. The increasing importance and applications of supramolecular chemistry led to further ground-breaking advances such as self-assembly,[8] molecular recognition,[9] mechanically interlocked structures[10] and molecular machinery,[11] the result of which was recognised by the 2016 Nobel Prize in chemistry being awarded to Jean-Pierre Sauvage, Fraser Stoddart and Ben Feringa '*for the design and synthesis of molecular machines*'.

Supramolecular chemistry encompasses the major areas of host-guest chemistry and self-assembly. Host-guest chemistry describes intermolecular association of two distinct species composed of a larger host or receptor and a smaller guest substrate. The classical examples include crown ethers,[6] cryptands[12] and spherands,[13] which act as hosts for alkali metal cation guests (Figure 1.1).

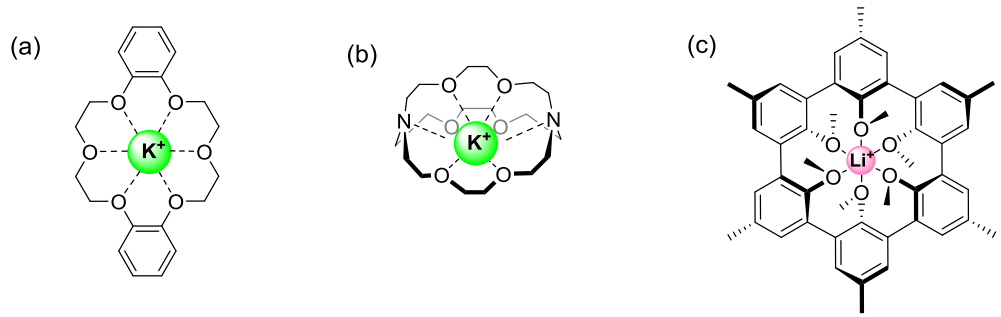


Figure 1.1. Alkali metal cation receptors: (a) dibenzo-18-crown-6;[6] (b) [2,2,2]cryptand;[12] (c) spherand.[13]

In contrast, self-assembly refers to the formation of high-ordered, organised systems arranged and constructed spontaneously from multiple components. Impressive examples include Stoddart's Borromean rings[14] and Fujita's tetravalent Goldberg polyhedral cage[15] (Figure 1.2).

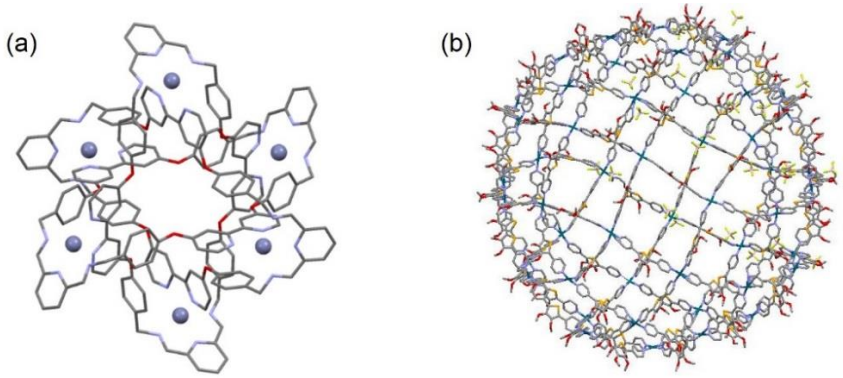


Figure 1.2. Crystal structures of (a) Stoddart's Borromean rings[14] and (b) Fujita's tetravalent Goldberg polyhedral cage.[15]

The theme of this thesis is the construction of elaborate host systems for the recognition of charged guest species, in particular anions. Hence, this introduction chapter

will focus initially on the fundamental aspects of supramolecular host-guest chemistry followed by a review of aspects of anion recognition as well as mechanically interlocked host molecules for guest recognition.

1.1.1 Fundamental Aspects of Supramolecular Host-Guest Chemistry

1.1.1.1 Host-Guest Complementarity

The field of host-guest chemistry is inspired by natural enzymes which can selectively catalyse chemical reactions with specific substrates in their active sites. The first step for catalysis requires the binding of substrates arising from size and geometric complementarity between the enzyme's binding site and substrate. The 'lock and key' model was first proposed by Fischer to explain enzyme specificity.[3] In this analogy, the lock is the enzyme and the key is the substrate, where binding only occurs when a key (substrate) of the correct size and geometry fits into the keyhole (active site) of the lock (enzyme). Subsequently, a modified 'induced fit' model was postulated by Koshland in the 1950s,[16] which assumed that the substrate can influence the final conformation of the enzyme resulting in an enhancement of binding affinity. From these fundamental principles, researchers can elucidate and assess the importance of host-guest complementarity to achieve selective binding. Importantly, optimising and maximising the attractive non-covalent interactions between host and guest is crucial.

1.1.1.2 Non-Covalent Interactions Employed in Host-Guest Chemistry

An appreciation of non-covalent interactions is essential for understanding binding processes in supramolecular host-guest chemistry. Other than electrostatic interactions, non-covalent interactions are generally weaker than covalent bonds. However, this property facilitates reversibility of binding, which is not easily achieved using covalent bonds. The widely-exploited non-covalent interactions employed in host-guest chemistry are discussed below.

Electrostatic Interactions

Electrostatic interactions include ion-ion, ion-dipole and dipole-dipole interactions (Figure 1.3), which obey Coulomb's law. The energy of attractive ion-ion interactions between oppositely charged species can be comparable in strength to a covalent bond but are non-directional. This strong attraction can be utilised for anion binding, especially in competitive solvent media, such as water, in order to enhance binding affinity. Ion-dipole and dipole-dipole interactions, such as hydrogen bonding, are weaker in strength but are more directional, which can be exploited to enhance complementarity and selectivity in host-guest chemistry.[17]

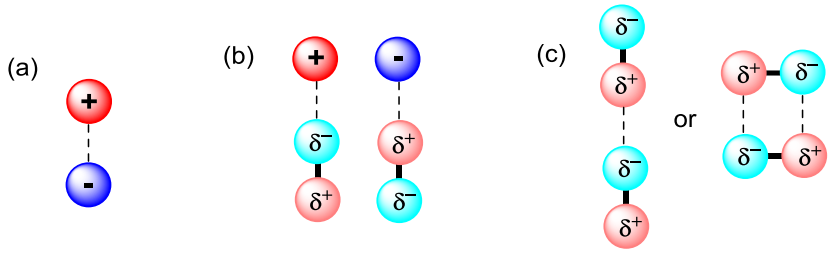


Figure 1.3. Electrostatic interactions: (a) ion-ion; (b) ion-dipole; (c) dipole-dipole interactions.

Hydrogen Bonding (HB)

Hydrogen bonding (HB) is a special case of dipole interaction which occurs between a polarised hydrogen atom covalently bonded to an electronegative atom (e.g. nitrogen, oxygen and fluorine) and a Lewis base.[18] HB interactions are ubiquitous in nature such as the double-helix structure of DNA which is achieved by complementary nucleotide base pair hydrogen bonds (Figure 1.4). The energies of HB interactions vary in the range of 1-170 kJ/mol,[19,20] depending on the nature of the donor and acceptor atoms. Their inherent directionality has been extensively exploited in the design of anion selective HB donor host systems (*vide infra*).[21]

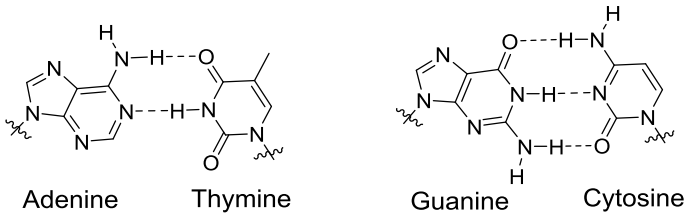


Figure 1.4. DNA base pairs linkage by HB interactions.

Halogen Bonding (XB) and other σ-Hole Interactions

Halogen bonding (XB) is defined by IUPAC as "a net attractive interaction between an electrophilic region on a halogen atom X belonging to a molecule or a molecular fragment RX (where R can be another atom, including X, or a group of atoms) and a nucleophilic region of a molecule, or molecular fragment, YZ."[22] When a halogen atom is covalently linked to an electron withdrawing group (R-X), the halogen atom is polarised, forming a specific region of partial positive charge at the halogen atom's pole terminus of the R-X covalent bond, which is called the 'σ-hole' (Figure 1.5).[23] Governed by the σ-hole, the XB interaction is highly anisotropic, with the R-X···B bond angle close to 180°.[24] The nature of XB is under heated debate with the relative extent of electrostatic, polarisation, charge transfer, covalent and dispersion contributions being considered to be dependent upon the nature of XB donor and Lewis base acceptor.[25,26] The binding energies of XB interactions (10-200 kJ/mol) are of a similar range spanned by HB, with the strength increasing with greater polarizability of the halogen atom (F < Cl < Br < I) and the greater electron-withdrawing nature of the R group.[27,28] XB interactions have long been widely exploited in crystal engineering and materials design, while only in the last decade or so has XB been applied in solution phase anion recognition and catalysis.[29]

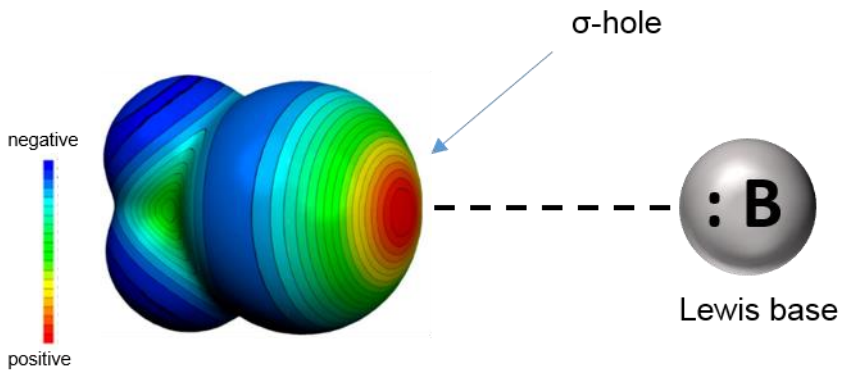


Figure 1.5. The molecular electrostatic potential, in Hartrees, at the 0.001 electrons Bohr^{-3} iso-density surface of CF_3I and XB with a Lewis base. Reproduced from reference 23.

Similar to XB interactions, when other main group atoms (Group 14-16) are covalently bonded to electron-withdrawing groups, the electron-density can be anisotropically polarised resulting in the formation of different numbers of σ-holes, which can interact with Lewis bases.[30] For example, in the presence of different electron-withdrawing substituents, chalcogen atoms can form either one or two σ-holes depending on their bonding characteristics (e.g. one σ-hole on Se atom in $SeCF_2$ and two σ-holes on Se atom in $Se(CF_3)_2$).[31] These σ-hole interactions are known as chalcogen bonding (Group 16), pnictogen bonding (Group 15) and tetrel bonding (Group 14) respectively. Importantly, σ-hole interactions are receiving an ever increasing attention in supramolecular host-guest chemistry, especially in anion receptor design.[30,32]

Cation-π, Anion-π, and π–π Interactions

Cation-π interactions occur between a cation and the planar face of an electron-rich aromatic ring. For example, as shown in Figure 1.6(a), K^+ has a stronger affinity with benzene (19 kcal/mol) in the gas phase than with water molecules (18 kcal/mol).[33] The strength of cation-π interactions follows the same trends as electrostatic interactions, which means that small, more positively charged cations and aromatic systems with more negative quadrupoles can lead to stronger affinity.[34] Cation-π interactions have been widely used in host-guest recognition,[35] catalysis[36] and transmembrane transport.[37]

Anion-π interactions refer to a weak association between an anion and an electron-deficient aromatic ring. Despite the name, the π electrons of the aromatic ring do not play any role in the interaction; detailed computational studies[34,38,39] showed that anion–π interactions arise mainly from electrostatic forces and anion-induced polarisation effects. Thus, small anions such as F^- and Cl^- can have strong interactions with electron-deficient aromatic rings due to strong polarizing effects at shorter distances. Anion-π interactions have been observed in gas,[40] solution[41,42] and solid phases[41–43] (Figure 1.6(b)), and increasingly in anion recognition[44] (Figure 1.6(c)) and membrane transportation.[45–47]

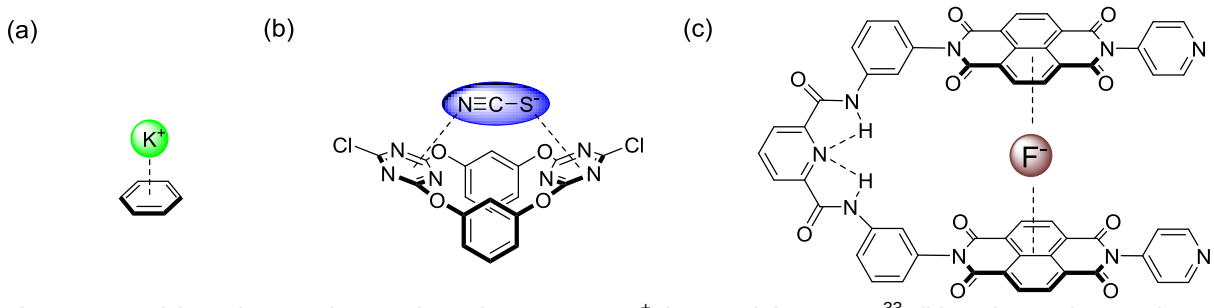


Figure 1.6. (a) cation-π interactions between a K^+ ion and benzene;[33] (b) anion-π interactions between a tetraoxocalix[2]arene[2]triazine macrocycle with thiocyanide anion;[41] (c) naphthalene diimide-containing colorimetric receptor selective for fluoride recognition using anion-π interactions.[44]

Besides interactions between charged species with aromatic rings, π-π interactions can occur between two aromatic systems. Actually, the term 'π-π interactions' is misleading because the π electrons do not play significant roles in the association,[48,49] and can sometimes even hinder the attractive interactions.[50] The Hunter and Sanders model emphasises the importance of electrostatic interactions between aromatic rings, in which the π electrons create a quadrupole moment with partial negative charge above aromatic faces as well as a partial positive charge around the periphery. Thus, the two aromatic rings prefer to adopt a parallel displaced or edge-to-face geometrical arrangement instead of forming sandwich complexes due to the repulsion (Figure 1.7).[51] Besides electrostatics, recent studies have shown that π-π interactions also involve solvation effects and dispersion forces.[48]

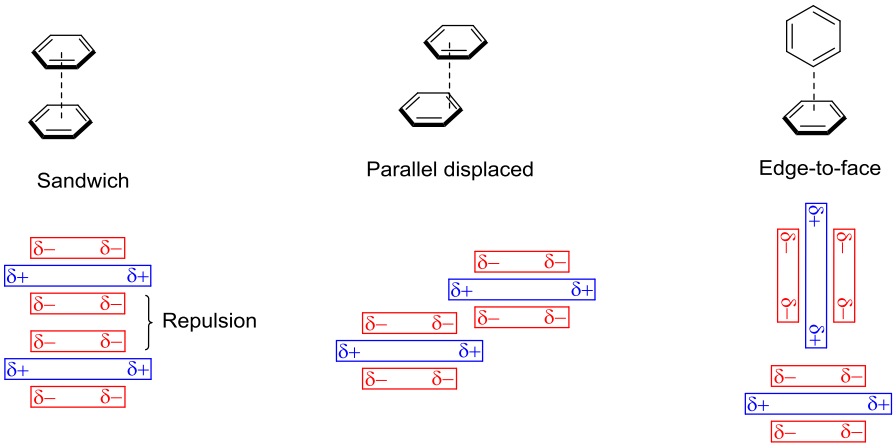


Figure 1.7. The electrostatic interaction models of π-π interactions.

Solvophobic Interactions

Solvophobic interactions refer to the association of non-polar solutes in polar solvents to minimise the energy of the system. When the polar solvent is water, it is termed the 'hydrophobic effect'. The 'classical' hydrophobic effect is driven by an increase in entropy, where the association of non-polar solutes release water molecules from their hydration shells.[52] In contrast, the 'non-classical' hydrophobic effect is characterised by an exothermic contribution where the liberated water molecules from a hydrophobic binding site form cohesive HB interactions with the bulk water.[53,54]

Coordinate Bonds

Coordinate bonds between Lewis acids (including main group atoms such as boron and transition metal cations) and Lewis bases contain significant degrees of orbital overlap depending on the nature of the interacting atoms and therefore may sometimes not be considered strictly non-covalent. Nonetheless, some coordinate bonds are labile for host-guest chemistry applications and are utilised in metal cation recognition (Figure 1.8 (a))[55] and in the design of anion host molecules (Figure 1.8(b)).[56]

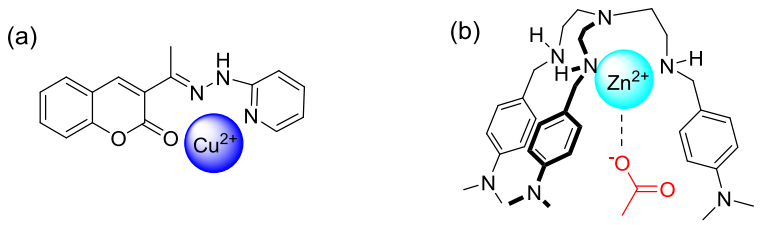


Figure 1.8. (a) A Cu^{2+} host molecule using coordinate bonds[55] and (b) an anion receptor using coordinate bond.[56]

1.1.1.3 Host Design Principles

The chelate effect and macrocyclic effect are concepts originating from metal coordination chemistry that have since been applied in supramolecular host-guest design. The chelate effect refers to the greater stability of complexes that contain chelate rings compared to mono-dentate systems, mainly due to the favourable entropy change of solvation resulting from releasing solvent molecules upon complexation.[57] The stronger guest binding by a macrocyclic host molecule compared to an acyclic analogue is called the 'macrocyclic effect', which arises from a combination of favourable entropy (fewer degrees of freedom being lost upon complexation) and enthalpy (less solvation of the donor atoms in the confined macrocycle cavities).[58] Both effects can be included in the concept of preorganisation, first introduced by Cram in the 1980s, which refers to hosts adopting favourable conformations prior to guest binding. As an example, a rigid tetra-triazole macrocyclic receptor exhibits the highest Cl^- binding affinity in comparison with flexible cyclic and acyclic analogues in CH_2Cl_2 (Figure 1.9).[59] Thus, to maximise the strength of association for a particular guest, a structurally-rigid cyclic host design that contains a complementarily sized cavity is commonly targeted.[60]

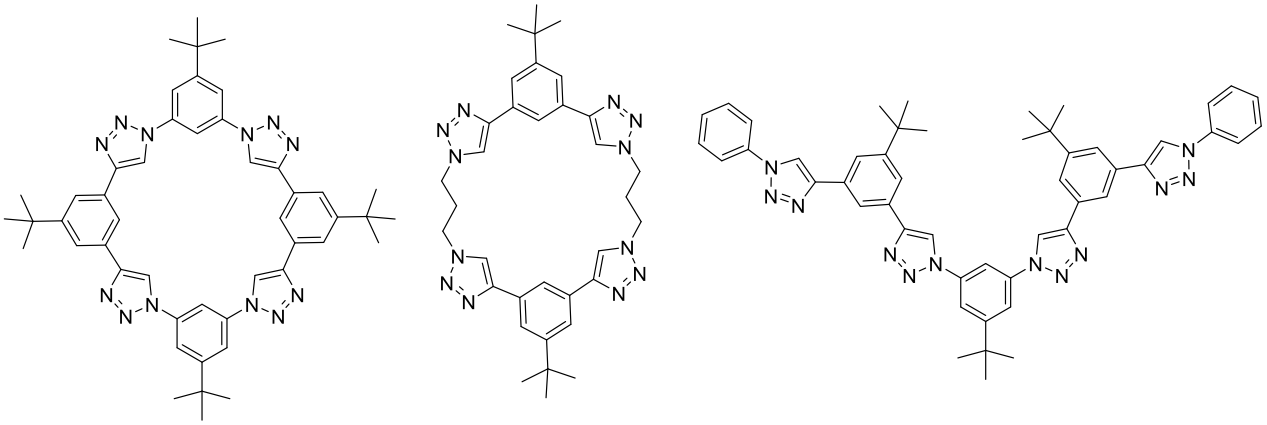


Figure 1.9. Structural rigidity and macrocyclic effect in the design of host molecules.[59]

1.2 Fundamental Aspects and Applications of Anion Recognition

1.2.1 The Importance and Challenges of Anion Recognition

Anions are ubiquitous and play important roles in many biological and environmental processes. In biology, carcinogenesis, aging and oxygen toxicity involves the biochemistry and reactivity of the superoxide ion (O_2^-).[61] Adenosine triphosphate (ATP), the "molecular unit of currency", is crucial to intracellular energy transfer in all organisms,[62] while I^- is one of the major components in the biosynthesis of thyroid hormones.[63] In addition, other halide imbalances can threaten human health. For example, the mis-regulation of Cl^- can lead to the life-threatening cystic fibrosis disease[64] while high F^- level in drinking water can cause skeletal fluorosis,[65] which is a major public health problem in some regions of the world. Environmentally, nitrates and phosphates from fertilizer and industrial waste water have resulted in eutrophication[66] in aquatic ecosystems; while highly-toxic anions such as N_3^- and CN^- from industrial pollution are lethal to the human respiration system.[67,68] In particular, radioactive $^{99}TcO_4^-$, a by-product of the nuclear reactors, has wide-ranging and long-lasting effects on the environment.[69]

Even though its importance has been recognised for a long time, the field of anion recognition remains highly challenging. First, in contrast with their isoelectronic cations (e.g. K^+, radius 1.37 Å), anions (e.g. Cl^-, radius 1.81 Å) are larger due to lower effective nuclear charge.[70] Consequently, anions have lower charge density resulting in weaker electrostatic interactions between anions and positively charged receptors. In addition, compared to the spherical shape of metal cations, anions exhibit a variety of geometries, as shown in Figure 1.10. Therefore, selective anion recognition requires careful design to achieve host-guest geometric and shape complementarity.

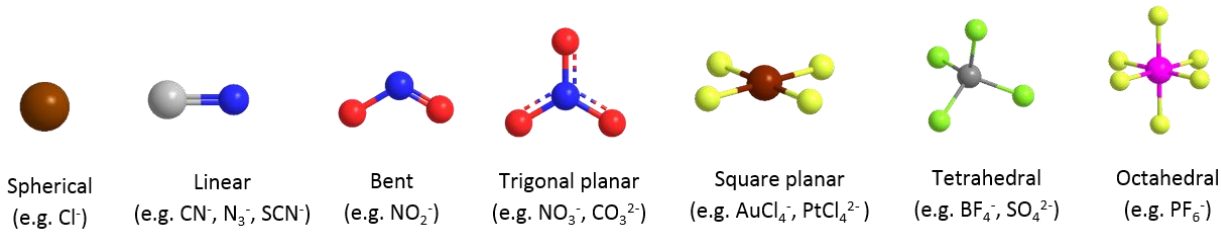


Figure 1.10. Anions with different geometries.

Many anions are also pH-sensitive and can be protonated at lower pH resulting in the loss of negative charge and electrostatic interaction with hosts. For example, phosphorylated anions can only be recognised by its receptors within a limited pH window.[71] Basic anions such as F^- and OAc^- can also abstract protons from acidic anion receptors.[72] Finally, anions exhibit a range of free energies of solvation. Protic solvents in particular strongly solvate anions due to favourable HB interactions, which is reflected in the Hofmeister series (Figure 1.11).[73] From left to right in the series, anions of decreasing charge density are less strongly hydrated. As a result, it is quite challenging to recognise highly solvated anions such as SO_4^{2-} in water.

$$SO_4^{2-} \approx F^- < H_2PO_4^- < OAc^- < Cl^- < Br^- < NO_3^- < I^- < ClO_4^- < SCN^-$$

Figure 1.11. Hofmeister series of anion solvation.

1.2.2 Biotic Anion Receptors

In nature, there are many biotic anion receptors which can bind specific anions in their three-dimensional cavities using non-covalent interactions, such as HB and electrostatic interactions. For example, sulphate, in the absence of its solvation shell, can be bound and stabilised by hydrogen bonds donated by specific parts of a sulphate binding protein (SBP) shown in Figure 1.12(a). Seven strong hydrogen bonds distributed in a three-dimensional fashion bind the anion tightly, rendering it completely inaccessible to the solvent molecules.[74] Another classic example is the phosphate-binding protein (PBP) in Figure 1.12(b), which can bind the hydrogen phosphate anion using electrostatics and twelve

hydrogen bonds. The negatively charged chain residue Asp-56 on the PBP repulses other similarly shaped anions such as sulphate, resulting in phosphate selectivity.[75] These outstandingly selective oxoanion biotic anion receptor examples have provided the inspiration for the design of artificial anion host molecules.

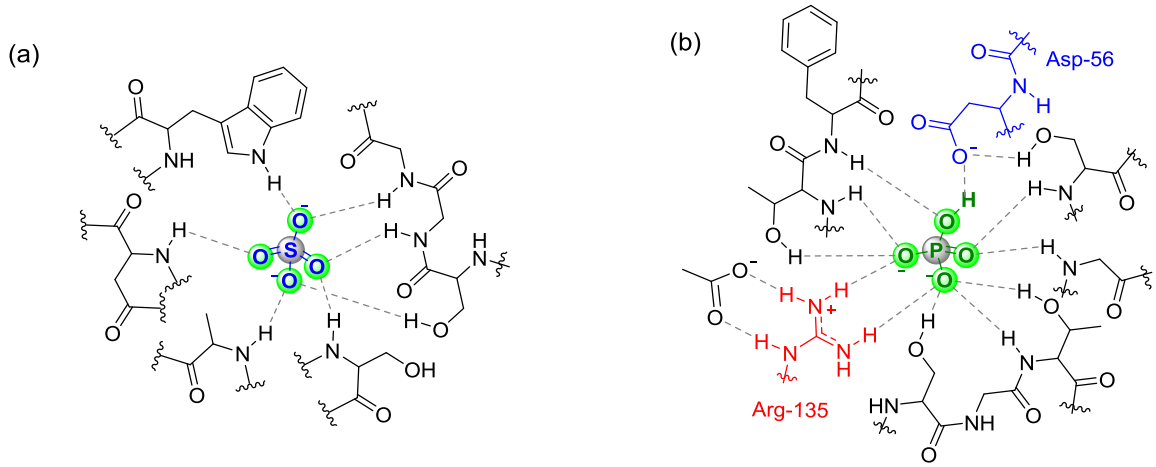


Figure 1.12. Binding pockets of proteins: (a) sulphate binding protein (b) phosphate binding protein.

1.2.3 Artificial Anion Receptors

1.2.3.1 Hydrogen Bonding Anion Receptors

Hydrogen bonding (HB) is widely used in anion recognition and a plethora of hydrogen bonding anion receptors incorporating C-H and N-H donor motifs, either neutral or cationic, have been synthesised and studied in the last few decades.[21]

Neutral HB Receptors

Amide, Thioamide and Sulfonamide Receptors

Amides are one of the most commonly used HB donor motifs for anion recognition. Incorporating amide units in a fixed geometric arrangement around a binding cavity can enhance binding selectivity. For example, Kubik's cyclic hexapeptide receptor containing four amide units exhibits impressive halide and sulphate binding affinities in D_2O/CD_3OD (4:1 *v/v*) (Figure 1.13(a)).[76,77] Compared to amides, thioamides are more acidic and exhibit stronger HB interactions with anions due to the increased resonant stability provided by the

sulphur atoms. An early example of a thioamide-containing receptor was Bowman-James' tetra-thioamide macrocycle, which showed increased binding affinities for $H_2PO_4^-$, HSO_4^- and F^- in DMSO over the corresponding amide analogues (Figure 1.13(b)).[78] Sulfonamides utilized for anion recognition can be found in Reinhoudt's tripodal receptor (Figure 1.13(c)) capable of selectively binding $H_2PO_4^-$ in CH_3CN. The receptor also shows stronger affinity towards $H_2PO_4^-$ than its amide counterparts.[79]

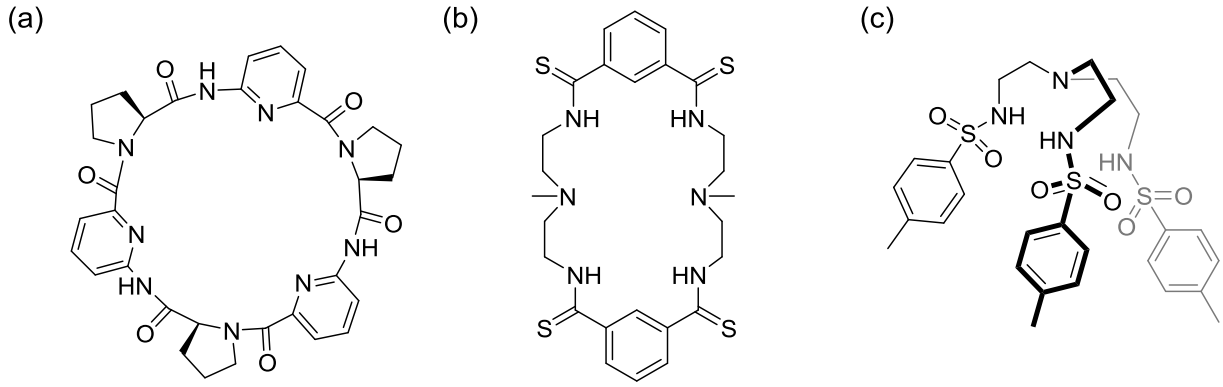


Figure 1.13. (a) Kubik's cyclic hexapeptide receptor;[76] (b) Bowman-James' thioamide-based macrocycle;[78] (c) Reinhoudt's sulfonamide tripod.[79]

Urea, Thiourea and Squaramide Receptors

Ureas have parallel HB donors which are optimal for binding Y-shaped anions such as carboxylates. As Figure 1.14(a) shows, a 32-membered macrocycle containing four rigid diphenyl ether units and four urea motifs, synthesised by Bohmer and co-workers,[80] selectively bound OAc^- and $H_2PO_4^-$ over halides in CH_3CN/THF (3:1 *v*/*v*) through convergent hydrogen bonds. Thiourea and squaramide motifs have also been incorporated into various anion receptor structural frameworks. For instance, a glycocluster thioureamethyl cavitand prepared by Reinhoudt and co-workers (Figure 1.14(b))[81] shows Cl^- selectivity in CH_3CN/H_2O (1:1 *v*/*v*) due to the complementarity between the halide anion and the tetra-thiourea binding pocket, while Jolliffe's macrocyclic squaramide-containing receptor (Figure 1.14(c)) was found to exhibit remarkable SO_4^{2-}, $H_2PO_4^-$ and OAc^- selectivity in $DMSO/H_2O$ (99.5:0.5 *v/v*) over Cl^-.[82]

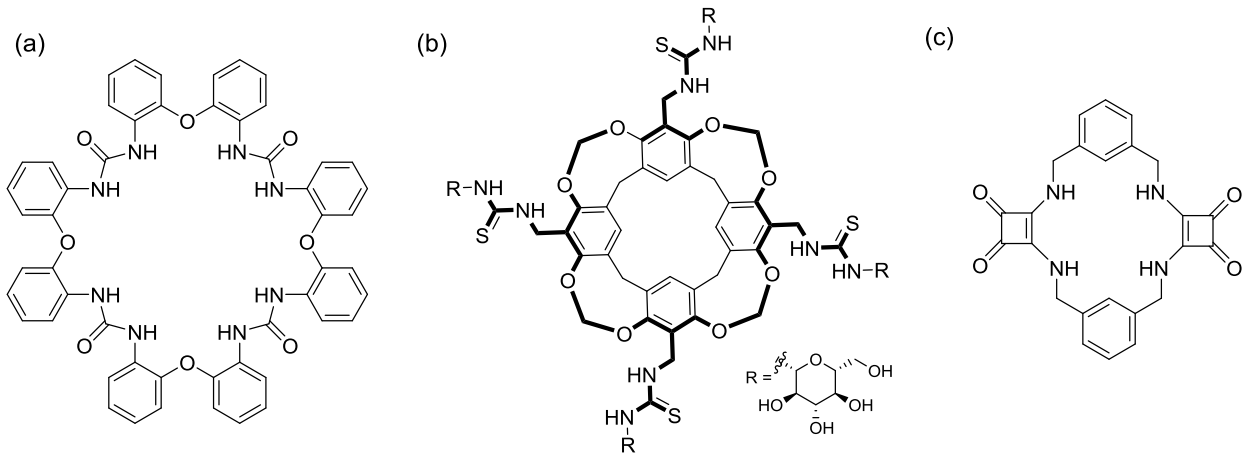


Figure 1.14. (a) Bohmer's tetra-urea macrocycle;[80] (b) Reinhoudt's thiourea cavitand;[81] (c) a bis-squaramide macrocyclic anion receptor.[82]

Heterocyclic HB Receptors

Heterocycles such as pyrroles, triazoles and imidazoles have proved to be efficient HB donors for anion binding applications. For example, Sessler's tetra-pyrrole macrocycle (Figure 1.15(a)) shows a marked selectivity for F^- over other anions (e.g. Cl^-, Br^-, I^-, $H_2PO_4^-$ and HSO_4^-), resulting from the proper arrangement in size and shape of the four pyrrole units in the macrocycle.[83] An example of triazole-containing receptors with HB donors is Flood's shape-persistent macrocycle (Figure 1.9) capable of strong Cl^- binding in CH_2Cl_2, which was presented in Section 1.1.3. Also, Lin and co-workers developed an imidazole-based anion receptor (Figure 1.15(b)) able to perform Cl^- binding in DMSO.[84]

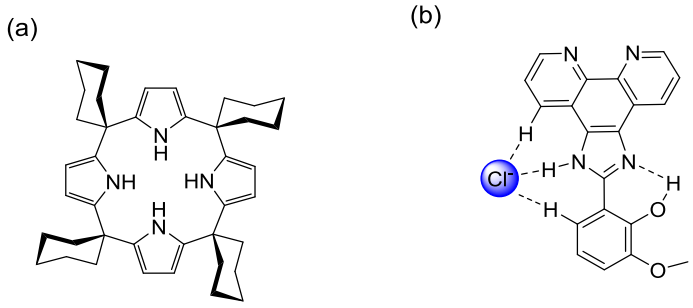


Figure 1.15. (a) Sessler's tetra-pyrrole receptor;[83] (b) Lin's imidazole-based anion receptor.[84]

Polarised C-H HB Motifs

Polarised C-H motifs have been demonstrated to be potent HB donors. The fluorinated macrocyclic compound in Figure 1.16(a) is an early example which binds F^- in a THF/Et_2O solvent mixture via four polarised methylene groups encircling the binding cavity.[85] Another interesting example is Flood's more recent cyanostar macrocycle (Figure 1.16(b)) capable of using five polarised C-H bonds to bind weakly-coordinating anions such as BF_4^-, ClO_4^- and PF_6^-, as 2:1 host/guest sandwich complexes in CH_3OH/CH_2Cl_2 (2:3 *v/v*).[86]

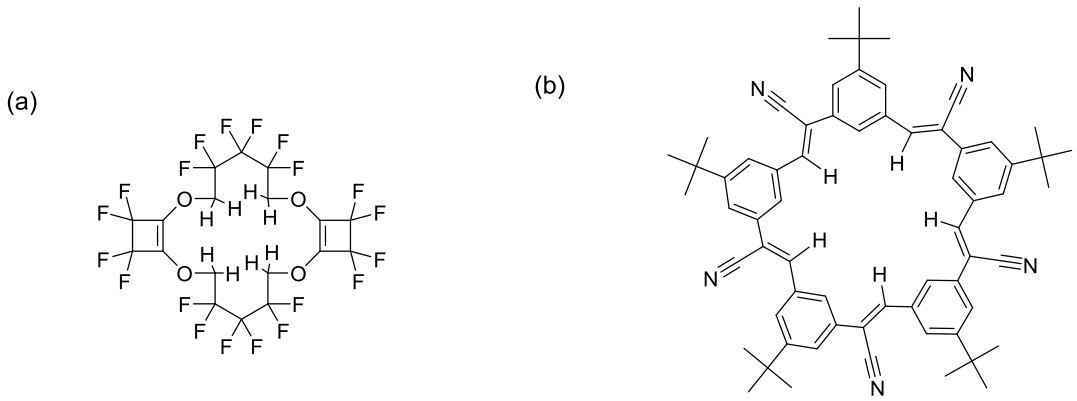


Figure 1.16. (a) A macrocyclic anion receptor using C-H···A^- interactions;[85] (b) Flood's cyanostar macrocycle.[86]

Cationic HB Receptors

In order to enhance anion binding affinities, especially to allow anion recognition in highly competitive aqueous media, many charge-assisted HB receptors have been synthesised and studied over many years, dating back to the first examples reported in the late 1960s – early 1970s.[87,88]

Polyammonium, Quaternary Ammonium and Guanidinium Receptors

Protonated polyammonium receptors can bind anions via HB and electrostatic interactions. A pioneering example is Lehn's hexa-cationic cryptand (Figure 1.17(a)), which exhibits selective recognition of linear triatomic species, such as azide, in an acidic aqueous solution (pH = 5) via two pyramidal arrays of three charge-assisted hydrogen bonds.[89]

However, despite their effectiveness in aqueous media, polyammonium receptors are highly dependent on an optimal pH window, where the polyammonium salts and anions coexist. In contrast, quaternary ammonium receptors are pH-independent utilising mainly electrostatic interactions to recognise anions. As shown in Figure 1.17(b), a tetrahedral cage receptor bearing four quaternary ammonium motifs was demonstrated by Schmidtchen to encapsulate Br^- and I^- in pure water.[90] The guanidinium motif is weakly acidic and hence can bind anions over a wide pH window.[91] Schmidtchen's preorganised guanidinium receptor (Figure 1.17(c)) can bind OAc^- strongly in CH_3CN or DMSO, driven by a combination of favourable enthalpy and entropy.[92]

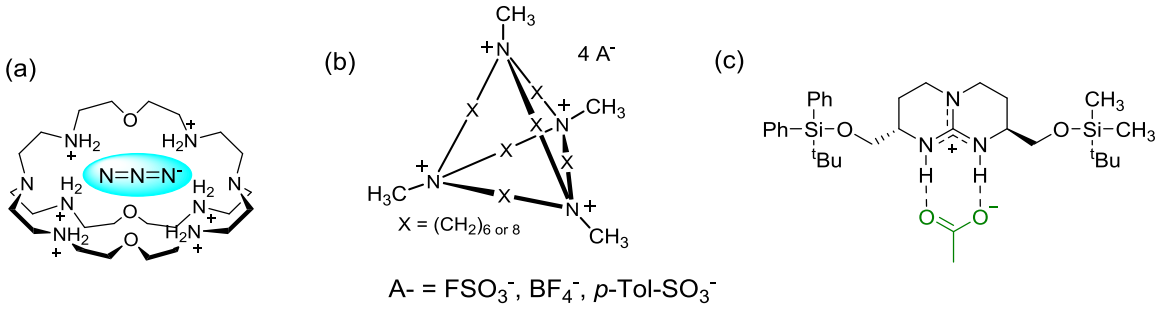


Figure 1.17. (a) Lehn's N_3^- binding cryptand;[89] (b) a tetra-quaternary-ammonium cage selective for Br^- and I^-;[90] (c) Schmidtchen's pre-organised guanidinium receptor binding Y-shaped OAc^-.[92]

Pyridinium Receptors

Multiple covalently linked pyridinium motifs are capable of binding anions via HB and electrostatic interactions. For example, a tetra-pyridinium macrocycle accessible by a one-step synthesis from 3-bromomethylpyridine (Figure 1.18(a)), reported by Shinada and co-workers, binds tri-carboxylate anions in neutral aqueous media,[93] while Ghosh's tweezer-like receptor containing two pyridinium and amide groups (Figure 1.18(b)) was found to selectively complex long-chain dicarboxylates such as pimelate in DMSO.[94]

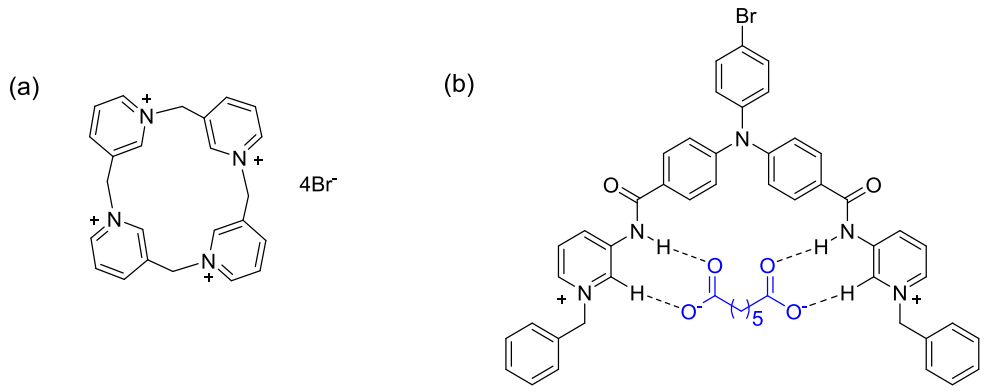


Figure 1.18. (a) Shinada's tetra-pydidinium macrocycle;[93] (b) Ghosh's di-carboxylate binding molecular tweezer.[94]

Triazolium and Imidazolium

Cationic heterocycles such as triazolium and imidazolium can function as strong HB donors. For instance, Beer's tetra-triazolium macrocycle shows a preference for the larger halides in DMSO/D_2O (1:1 *v/v*) (Figure 1.19(a))[95] while more recently a pyrene-appended triazolium receptor, explored by Cao and co-workers, acts as an efficient host for F^- in CH_3CN/H_2O (9:1 *v/v*) via HB interactions with triazolium C-H, sulfonamide N-H and pyrenyl C-H donors (Figure 1.19(b)).[96] In addition, Kim's water-soluble fluorescent imidazolium-based cyclophane (Figure 1.19(c)) exhibits effective recognition and sensing capability towards iodide in pure water at pH 7.4.[97]

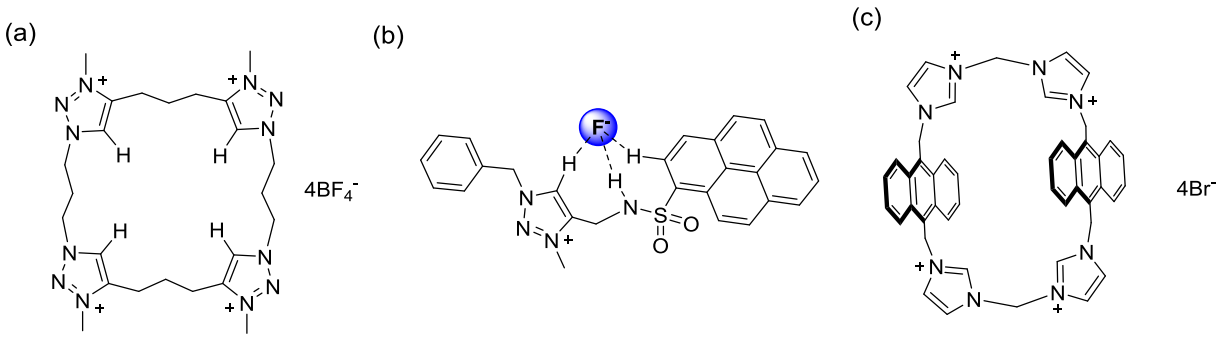


Figure 1.19. (a) Beer's tetra-triazolium macrocycle;[95] (b) Cao's triazolium fluorescent receptor binding F^-;[96] (c) Kim's water-soluble imidazolium cyclophane.[97]

1.2.3.2 Halogen Bonding Anion Receptors

While halogen bonding (XB) has been extensively utilised in crystal engineering and materials design, the application of this σ-hole interaction in solution-phase anion recognition has only begun to be exploited since 2005 onwards.[98] The first XB anion host was Resnati's heteroditopic receptor (Figure 1.20(a)) bearing 4-iodotetrafluorophenyl components which could bind the NaI ion-pair strongly in $CDCl_3$.[99] The solid state structure revealed the existence of a XB interaction between I^- and only one iodine donor atom due to the divergent nature of the iodoperfluoroarene groups. In contrast, a tripodal iodoperfluoroarene-containing anion receptor (Figure 1.20(b)), developed by Taylor and co-workers,[100,101] was able to selectively bind Cl^- in acetone via three convergent halogen bonds.[102] Importantly, compared to strong halide affinities, the tripodal receptor exhibited negligible binding to oxoanions TsO^-, HSO_4^- and NO_3^-, suggesting the intrinsic preference of the XB donors for 'softer' anions.

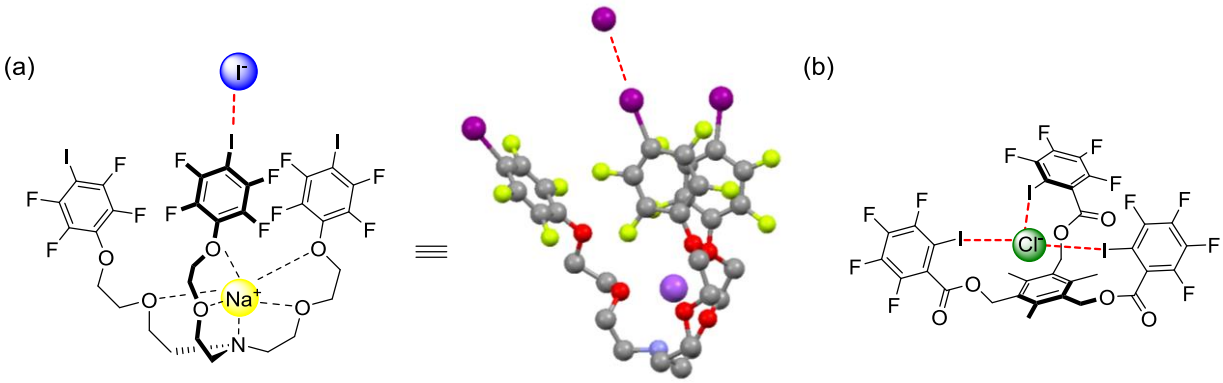


Figure 1.20. (a) Resnati's XB receptor and its crystal structure showing NaI ion pair binding;[99] (b) Taylor's XB tripodal receptor.[100]

Besides haloperfluoroarenes, iodotriazoles have proved to be potent neutral XB motifs for anion recognition. In Figure 1.21(a), a bidentate receptor bearing carbazole scaffolds and iodotriazoles was synthesised by Schubert and co-workers.[103] The intramolecular HB between the hydroxyl and adjacent iodotriazole groups preorganised the receptor into a rigid co-planar *syn-syn* conformation which resulted in stronger binding towards anions. ITC experiments in THF revealed a 2:1 host/guest stoichiometry for Cl^- and

Br^- binding driven by a combination of favourable enthalpy and entropy. Beer and co-workers developed a XB picket-fence zinc(II) metalloporphyrin scaffold containing four iodotriazole substituents (Figure 1.21(b)).[104] In $CHCl_3$, acetone and CH_3CN, the XB receptor displayed stronger halide binding affinities in comparison to the HB receptor analogue.

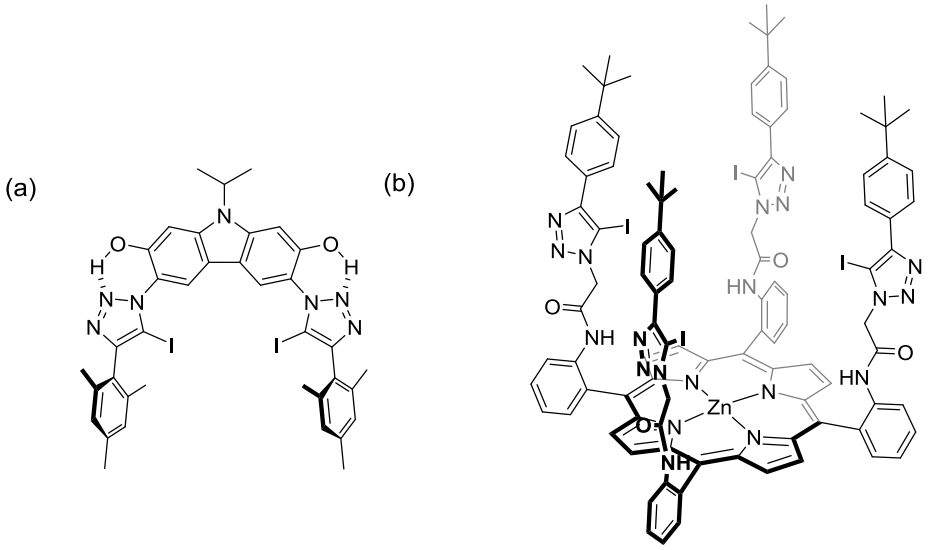


Figure 1.21. (a) Schubert's bidentate XB receptors[103] and (b) Beer's porphyrin-containing tetradentate XB receptor.[104]

Early examples of charge-assisted XB haloimidazolium-based cationic receptors were described by Beer and co-workers.[105] In Figure 1.22(a), the *syn* atropisomer of a cationic bromoimidazolium macrocycle was demonstrated to selectively bind Br^- in CD_3OD/D_2O (9:1 *v/v*) solvent mixture via convergent charge-assisted XB, while the *syn*-conformer of the iodoimidazolium naphthalene macrocycle (Figure 1.22(b)) acted as a fluorescent chemosensor sensing Br^- and I^- selectively over Cl^- and oxoanions in CH_3OH/H_2O (9:1, *v/v*).[106] Mono-, bis- and tripodal acyclic iodoimidazolium-based receptors were shown to exhibit contrasting anion selectivities. For example, Resnati, Metrangolo and co-workers synthesised an anthracene–appended iodoimidazolium receptor capable of strong XB interactions with $H_2PO_4^-$ in DMSO (Figure 1.22(c)).[107] Berryman's bipodal receptor (Figure 1.22(d))[107] shows a halide binding trend of $Cl^- > Br^- > I^-$ in CH_3CN/H_2O (99:1 *v/v*)

while Ghosh's tripodal receptor (Figure 1.22(e))[108] binds Br^- more strongly than Cl^- and I^- in pure CH_3CN presumably due to shape and size complementarity.

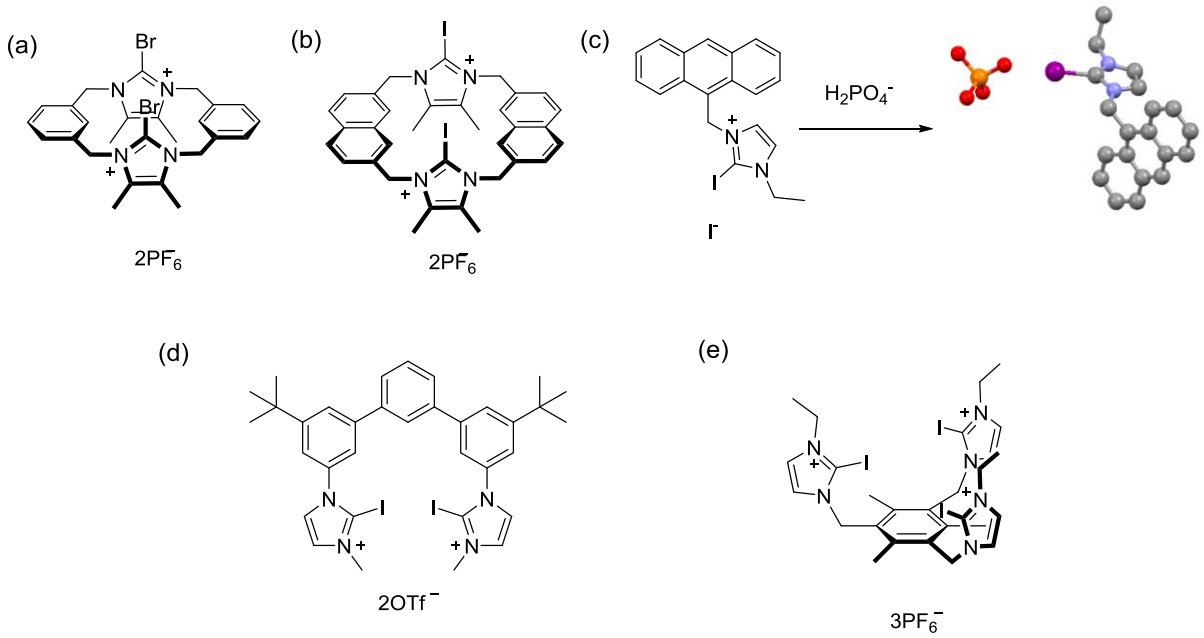


Figure 1.22. (a) Beer's bis-bromoimidazolium receptor;[105] (b) Beer's bis-iodoimidazolium receptor; [106] (c) Resnati and Metrangolo's anthracene-appended XB receptor and its solid state structure interacting with a $H_2PO_4^-$;[107] (d) Berryman's bipodal XB anion receptor;[108] (e) Ghosh's tripodal XB anion receptor.[109]

Related halotriazolium motifs have also been integrated into various acyclic anion receptor frameworks. For example, a water-soluble bis-iodotriazolium XB anion host, developed by Beer and co-workers, exhibits ReO_4^- binding in pure water through XB interactions (Figure 1.23(a)),[110] while by comparison, the HB analogue is incapable of binding the oxoanion species. A series of chiral XB (*S*)-BINOL-based receptors (Figure 1.23(b)) were demonstrated to enhance the enantioselective recognition of chiral anions compared to their HB analogues in CD_3CN/D_2O (99:1, *v*/*v*).[111] Computational studies indicated that the strict linearity of XB and sterics were the main reasons for the enhancement in enantioselectivity.

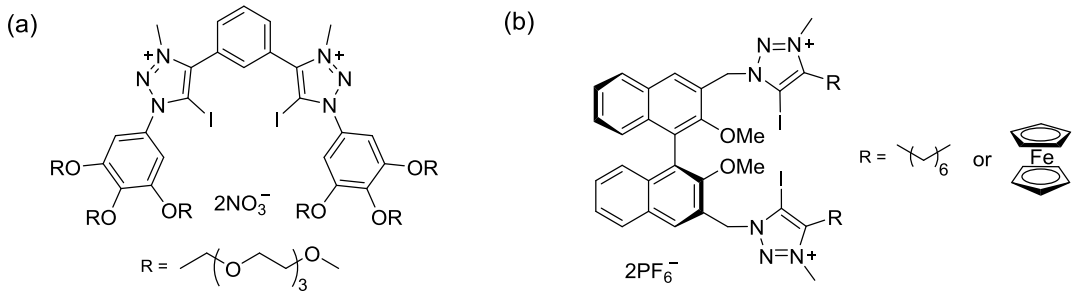


Figure 1.23. (a) A water-soluble XB ReO_4^- receptor[110] and (b) chiral XB (*S*)-BINOL-based receptors.[111]

Cationic pyridinium XB receptors have been utilised for anion recognition recently. A classic example is Beer's pyridinium-3,5-bis-iodotriazole-containing receptor (Figure 1.24(a)) which is able to selectively bind Cl^- over other halides and oxoanions in DMSO.[112] The solid state structure shows Cl^- is bound by two convergent halogen bonds. Also, Berryman's bis-pyridinium XB receptor (Figure 1.24(b)) was able to complex ReO_4^- strongly in $CHCl_3$/acetone (3:2 *v/v*).[113]

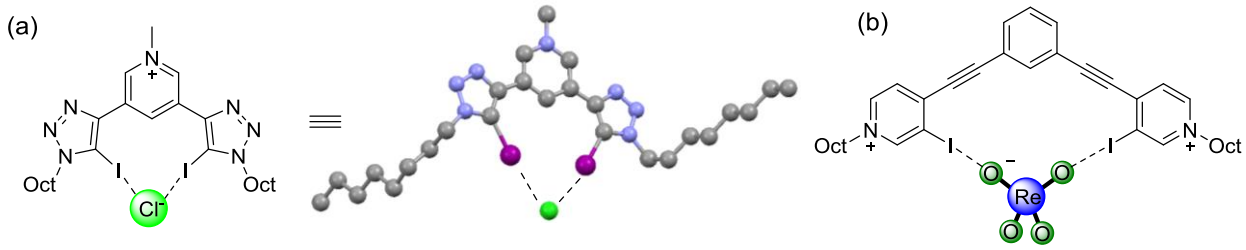


Figure 1.24. (a) Beer's pyridinium-3,5-bisiodotriazole receptor interacting with Cl^- and the corresponding solid state structure;[112] (b) Berryman's ReO_4^- pyridinium XB receptor.[113]

1.2.3.3 Anion Receptors Utilising Alternative Supramolecular Interactions

Receptors utilising anion-π interactions

Although anion-π interactions are quite weak amongst all the non-covalent interactions (see section 1.1.2), they have been incorporated in anion receptors.[114] For example, the multisite anion receptor $HAT(CN)_6$ (1,4,5,8,9,11-hexaazatriphenylene-hexacarbonitrile) is able to interact with hexacyanidometalates (M = Fe^{III}, Co^{III}) in CH_3CN by

multiple anion-π interactions between the CN^- ligands of the metal anions and its π-deficient areas (Figure 1.25(a)) as evidenced from UV-Vis absorption changes.[115] Besides anion recognition in organic solvents, anion-π interactions, supplemented by other stronger non-covalent interactions, can be utilised for anion recognition in water. The receptor shown in Figure 1.25(b) bound highly charged anions such as SO_4^{2-}, SeO_4^{2-}, $S_2O_3^{2-}$ and $Co(CN)_6^{3-}$ in aqueous media through a combination of salt-bridge and anion-π interactions.[116,117]

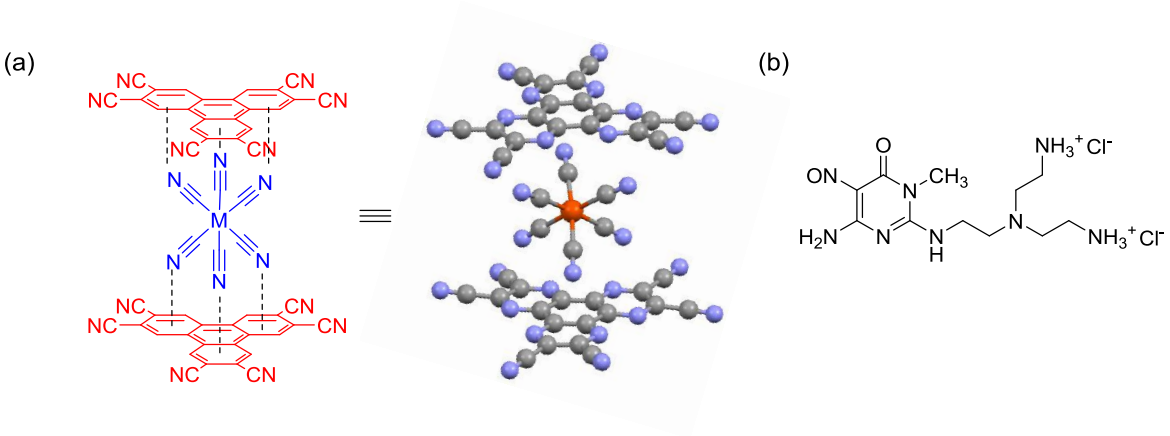


Figure 1.25. (a) The interaction between $M(CN)_6^{3-}$ with $HAT(CN)_6$ through anion-π interactions in the solid state structure;[115] (b) a water-soluble anion receptor using anion- π interactions.[116]

Receptors containing Lewis acidic centres

Over the years numerous boron, silicon, tin and transition metal Lewis acid centre based host systems have been explored in anion recognition. For example, Gabbaï and co-workers reported a boron-mercury receptor (Figure 1.26(a)) that was capable of sensing F^- selectively in THF/H_2O (9:1 *v/v*) by forming boron-fluoride and mercury-fluoride bonds.[118] More recently, a bis-nickel complexed cavitand (Figure 1.26(b)) also selectively bound F^- strongly in CH_3CN/CH_3OH (1:1 v/v) due to the highly preorganised receptor cavity enforcing optimal size complementarity for F^-.[119]

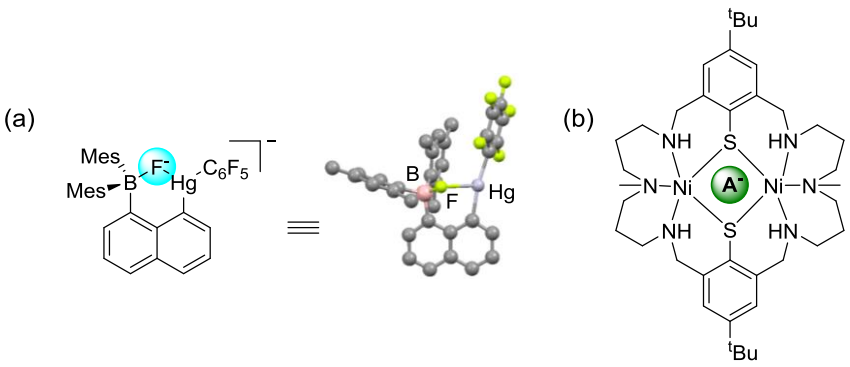


Figure 1.26. (a) GabbaÏ's bidentate Lewis acidic F^- receptor and its solid state structure;[118] (b) a cavitand incorporating Lewis acidic bis-nickel center.[119]

Chalcogen Bonding Receptors

Similar to XB, polarisable heavy chalogen atoms (Se/Te) that are covalently linked to electron-withdrawing substituents have been recently demonstrated to interact with anions via their σ-holes.[120] For instance, Taylor's monodentate and bidentate perfluoroaryl tellurophene-containing receptors (Figure 1.27) were shown to complex Cl^- in THF via chalcogen bonding interactions.[121]

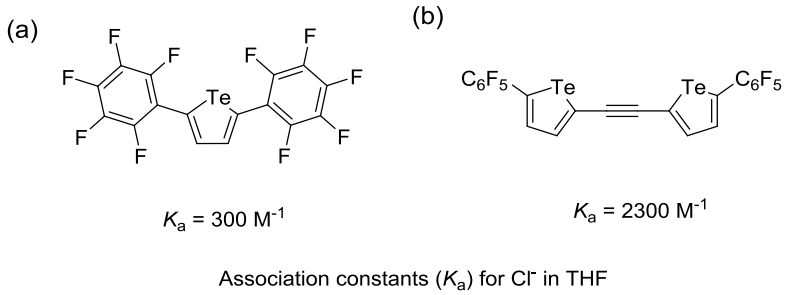


Figure 1.27. Taylor's (a) monodentate and (b) bidentate chalcogen bonding anion receptors.[121]

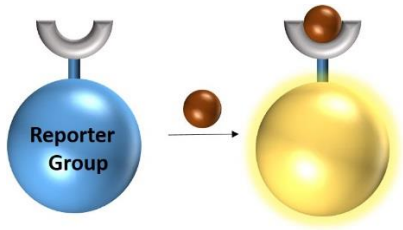
1.2.4 Applications of Anion Recognition

Advances in the fundamental understanding of anion recognition have led to a plethora of applications, such as anion sensing, extraction and separation of anions, transmembrane anion transport and anion-driven organocatalysis.[122]

1.2.4.1 Anion Sensing

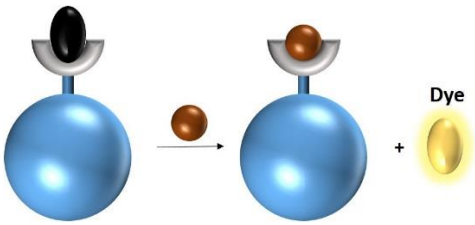
Anion sensing refers to the recognition of specific anions by a receptor resulting in an observable macroscopic response, which can be optical, electrochemical or rheological (e.g. sol-gel transition). The main principles of anion sensing are illustrated in Figure 1.28.

(a)



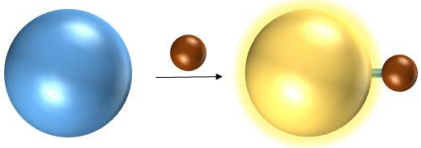
Anion binding through non-covalent interactions induces changes in redox and optical properties of the reporter group.

(b)



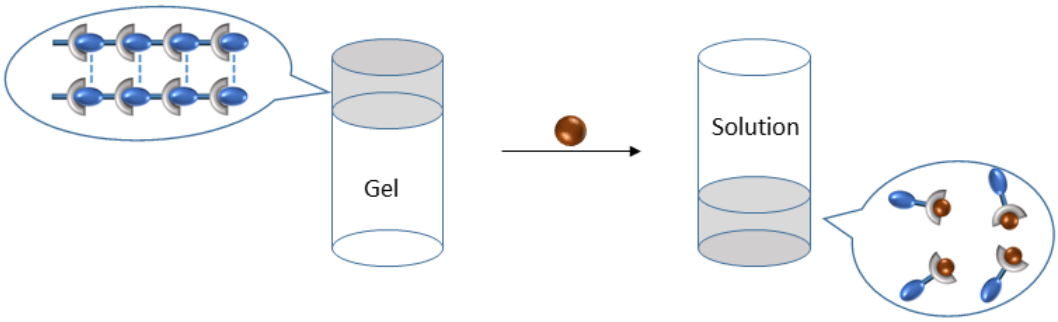
Through the indicator displacement assay (IDA) approach, an anion displaces a dye weakly associated with the receptor, resulting in detectable optical changes.

(c)



The chemodosimeter approach involves covalent bond formation between the anion and receptor, which changes the optical and electrochemical properties of the original receptor.

(d)



Anion-responsive gels function via cross-linked molecular networks that can form or break down in the presence of specific anions, inducing a visible change in the bulk viscosity of the sample.

Figure 1.28. Principles of anion sensing

Optical Anion Sensors

Optical anion sensors respond to specific anions with colorimetric or fluorescent changes. Colorimetric sensors allow naked-eye detection of anions while fluorescent sensors are highly sensitive. An example of the former type is the bis-thiourea-functionalised Tröger's base receptor (Figure 1.29(a)) which acts as a colorimetric sensor for F^-, undergoing a colour change from colorless to orange in DMSO due to deprotonation by the basic halide anion.[123] In Figure 1.29(b), a calix[4]pyrrole-anthraquinone conjugated system acts as an effective HB naked-eye sensor that permits discrimination between different anions such as F^-, Cl^- and $H_2PO_4^-$ in CH_2Cl_2.[124] An example of the IDA approach in colorimetric anion sensing involves the bis[zinc(II)dipicolylamine] peptide receptor-pyrocatechol violet complex (Figure 1.29(c)). Upon addition of stronger-binding pyrophosphate anion, the dye is released resulting in a color change from purple to green. In addition, the receptor shows remarkable selectivity towards pyrophosphate over ATP and ADP under physiological-like conditions.[125]

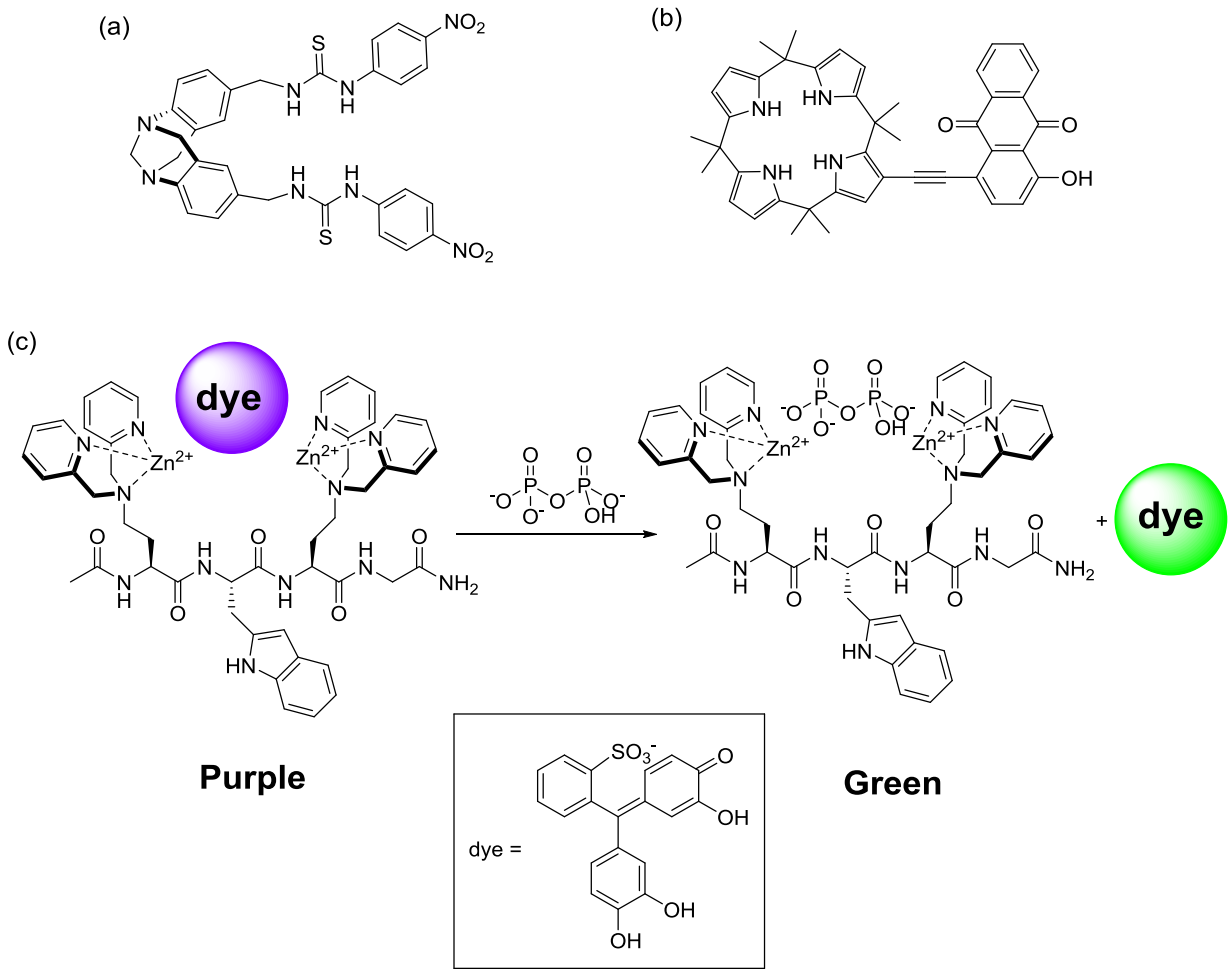


Figure 1.29. (a) A thiourea-functionalized Tröger's base F^- receptor;[123] (b) a calix[4]pyrrole-anthraquinone colourimetric sensor;[124] (c) an IDA approach for pyrophosphate recognition.[125]

More recently, XB optical anion sensors have been described. For example, Molina's iodotriazolium pyrene-based sensor (Figure 1.30(a)) can act as a fluorescent chemosensor for pyrophosphate anions undergoing an increase of the fluorescence intensity of the excimer band upon addition of the phosphate species.[126] Optical sensors utilising luminescent metal centres such as Re(I), Ru(II), Ir(III) and lanthanides have also been developed. An europium complex (Figure 1.30(b)) can be used to monitor hydroxide concentration in aqueous solution due to the reversible attack of hydroxide at the phenanthridinium chromophore.[127] In addition, a reduction of the lanthanide emission intensity of the same phenanthridinium europium complex was observed in the presence of

halides, which stemmed from the anion-induced collisional quenching of the singlet excited state of the ligand.

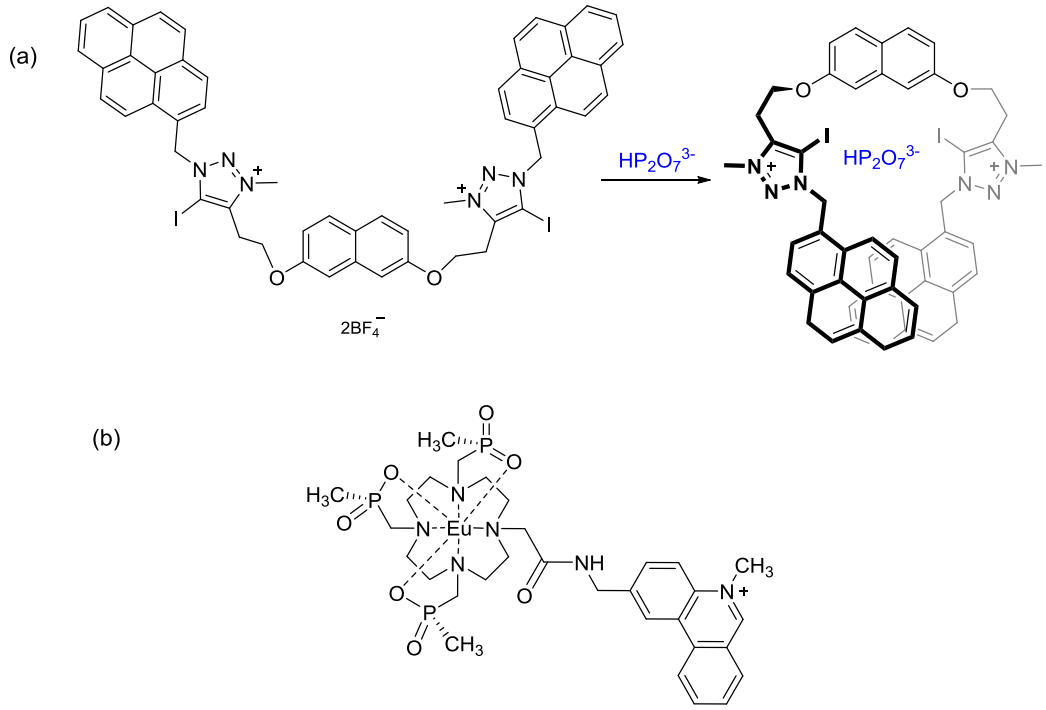


Figure 1.30. (a) Molina's XB pyrophosphate fluorescent sensor[126] and (b) a europium complex for hydroxide and halide sensing.[127]

Electrochemical Anion Sensors

Electrochemical anion sensors contain redox active reporter groups which typically sense anions via voltammetric shifts of their redox potentials. Ferrocene has been widely used as a stable, readily-functionalised redox-reporter unit. For example, Molina's ferrocene-containing electrochemical sensor (Figure 1.31(a)) senses F^-, OAc^-, $H_2PO_4^-$ and pyrophospate anions in CH_3CN via cathodic shifts of the ferrocene/ferrocenium redox couple.[128] Besides ferrocene-based anion sensors, a tetrathiafulvalene(TTF) calix[4]pyrrole sensor (Figure 1.31(b)) also allows the detection of halides (Cl^-, Br^-) through cathodic shifts (ΔE = -43 mV for Cl^- and ΔE = -34 mV for Br^-) of the first oxidation potential of the TTF unit in CH_3CN.[129] Recently, XB electrochemical anion sensors such as iodo-tetrathiafulvalene (Figure 1.32(c)) can recognise halides through cathodic shifts of the first TTF oxidation

potential (e.g. $\Delta E'$ = -53 mV for Cl^-) in DMF, much larger in magnitude than non-substituted tetrathiafulvalene analogue (e.g. $\Delta E'$ = -6 mV for Cl^-).[130]

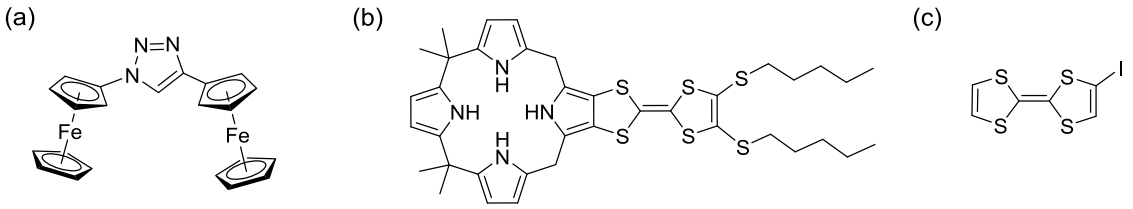


Figure 1.31. (a) A ferrocene-based electrochemical sensor;[128] (b) a redox-active tetrathiafulvalene(TTF) calix[4]pyrrole sensor for halide sensing;[129] (c) a XB electrochemical halide sensor.[130]

Anion-Responsive Gels

In recent years, anion-responsive gels have been widely studied as rheological anion sensors due to the possibility of naked-eye anion sensing via gel-solution phase changes. For example, a urea-based chiral BINOL molecule forms a gel in cyclohexane due to HB and π-π interactions (Figure 1.32(a)). However, the presence of F^- disrupts the intermolecular hydrogen bonds resulting in the breakdown of the gel network.[131] Similarly, the anthraquinone-derived oxalamide gelator (Figure 1.32(b)) undergoes a sol-gel transition in the presence of F^-.[132] More recently, a XB Cl^--responsive dendritic organogel (Figure 1.32(c)) developed by Feng and co-workers can form a gel via π-π stacking. The gel collapses upon addition of Cl^-, through the formation of XB interactions between the halide anion and receptor.[133]

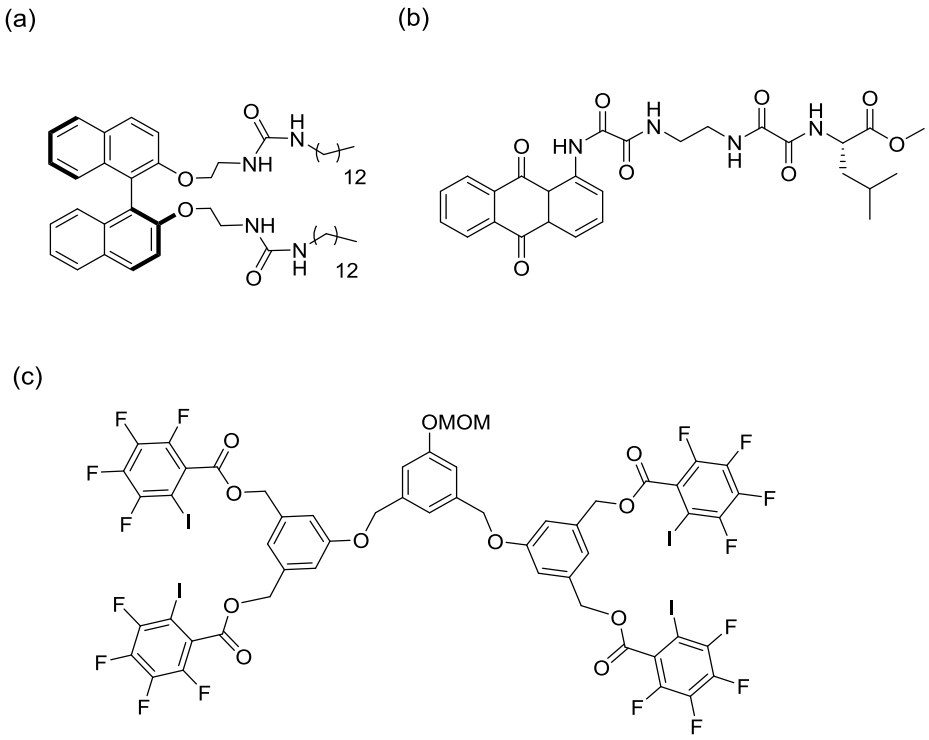


Figure 1.32. (a) A urea-based chiral BINOL gelator for F^- sensing;[131] (b) an anthraquinone derived oxalamide gelator for F^- sensing;[132] (c) Feng's Cl^--responsive XB dendrimer.[133]

1.2.4.2 Extraction and Separation of Anions

Another important application of anion supramolecular chemistry is the extraction and separation of precious metallic anions (e.g. $AuCl_4^-$) and removal of harmful anions (e.g. CN^-) from the environment. A calix[4]pyrrole-appended methyl methacrylate copolymer (Figure 1.33(a)) prepared by Sessler and co-workers extracts TBACl and TBAF from aqueous solution into an organic phase.[134] Compared to the copolymer, the calixpyrrole monomer is much more inefficient for the aqueous-organic anion extractions. Alternatively, gold nanoparticles decorated with functionalised double-armed calixpyrroles (Figure 1.33(b)) are effective extractants of F^- from an aqueous phase to an organic media while the momomeric calixpyrroles cannot perform the extractions under the same conditions.[135]

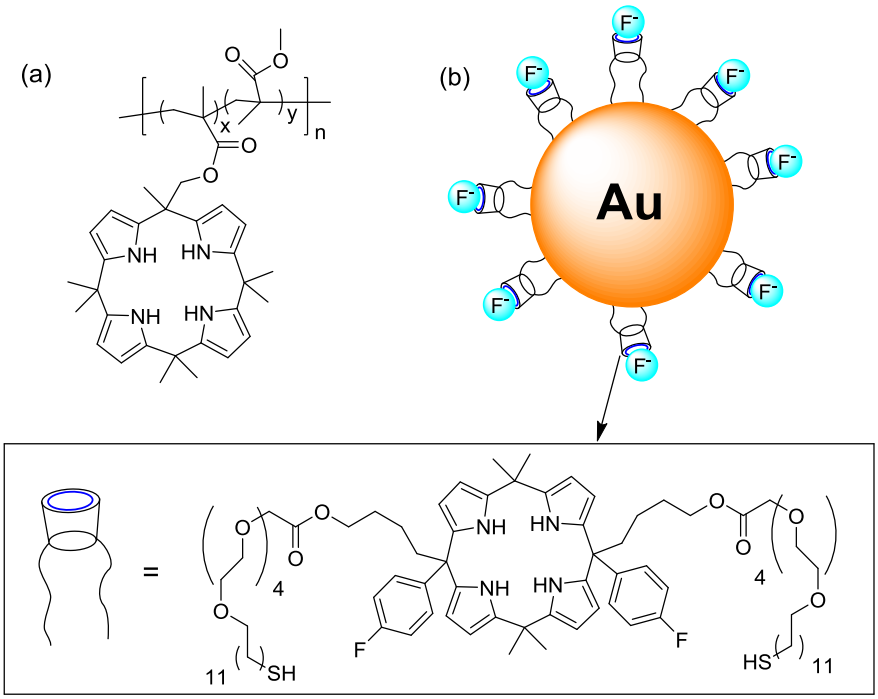


Figure 1.33. (a) Sessler's calixpyrrole-appended copolymer[134] and (b) gold nanoparticles decorated by with modified calixpyrroles for F^- extraction.[135]

1.2.4.3 Transmembrane Anion Transport

Anions are transported across the phospholipid membranes of cells via specialised proteins. Importantly, anion transport mis-regulation of anions caused by defects of these functional proteins can lead to a number of diseases, such as cystic fibrosis[136] and Dent's disease.[137] As a consequence, the design of abiotic receptors for transmembrane anion transport is an area of intense current interest. A potential anion transporter can function either as (a) a 'channel', which is a membrane-spanning structure that can provide an anion diffusion pathway; or (b) a 'mobile carrier', which can bind an anion on one side of membrane and transport it through a membrane to release it on the other side (Figure 1.34).

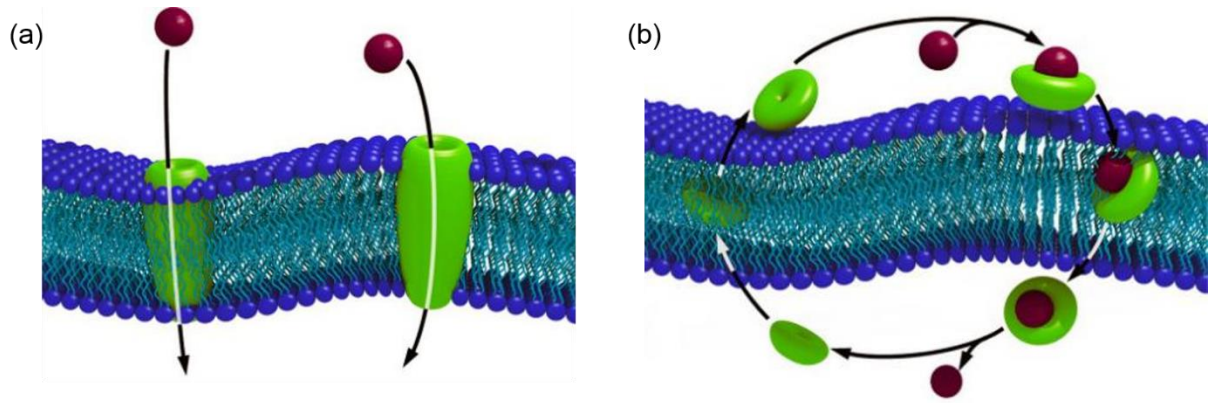


Figure 1.34. An anion transporter functioning as (a) a 'channel' or (b) a 'mobile carrier'. Reproduced from reference 122.

An imidazolium-functionalised BINOL cationic receptor (Figure 1.35(a)) was demonstrated to facilitate carbonate transport by unusually playing dual roles of being both a carrier and forming transmembrane pores,[138] while an exceptionally efficient synthetic mobile carrier, Obatoclax® (Figure 1.35(b)) transports Cl^- across lipid bilayers even at very low carrier concentrations.[139] Small perfluorinated molecules equipped with strong XB donors can act as efficient anion transporters as well (Figure 1.35(c)),[140] while a XB cascade bearing multiple iodoperfluoroaryl monomers can transport Cl^- via a hopping mechanism (Figure 1.35(d)).[141]

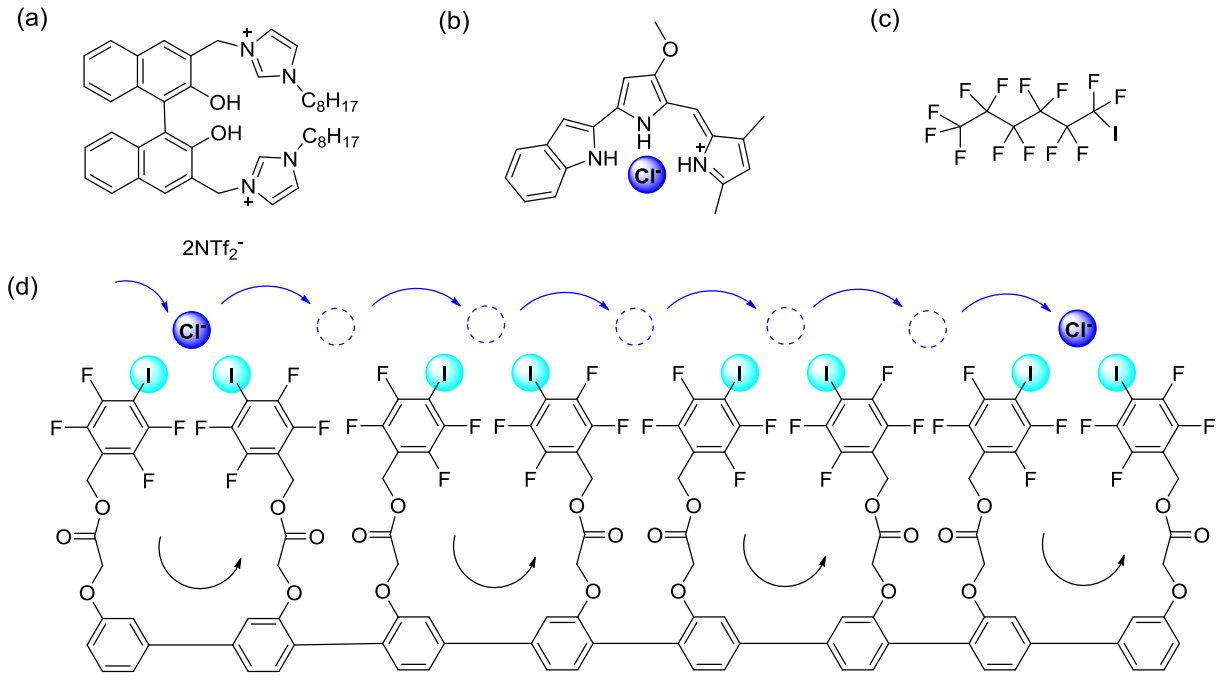


Figure 1.35. (a) An imidazolium-based anion transporter;[138] (b) Obatoclax®, an efficient Cl^- mobile carrier;[139] (c) a XB perfluorinated anion transporter;[140] (d) a XB oligomeric anion cascade.[141]

1.2.4.4 Anion-Driven Organocatalysis

Anions receptors have been developed as organocatalysts to avoid the use of polluting toxic metals typically used in the chemical industry. Ureas, thioureas and recently XB based catalysts can enhance reaction rates, regioselectivity and enantioselectivity.[142–145] For example, Schreiner and co-workers demonstrated a mild and efficient method for a regioselective epoxide ring opening reaction utilising mandelic acid and a fluorinated arylthiourea based catalyst (Figure 1.36).[143] The thiourea-based organocatalyst stabilises the mandelate ion through hydrogen bonds, promoting the alcoholysis of the styrene oxide producing an alkoxy alcohol in excellent yield and regioselectivity.

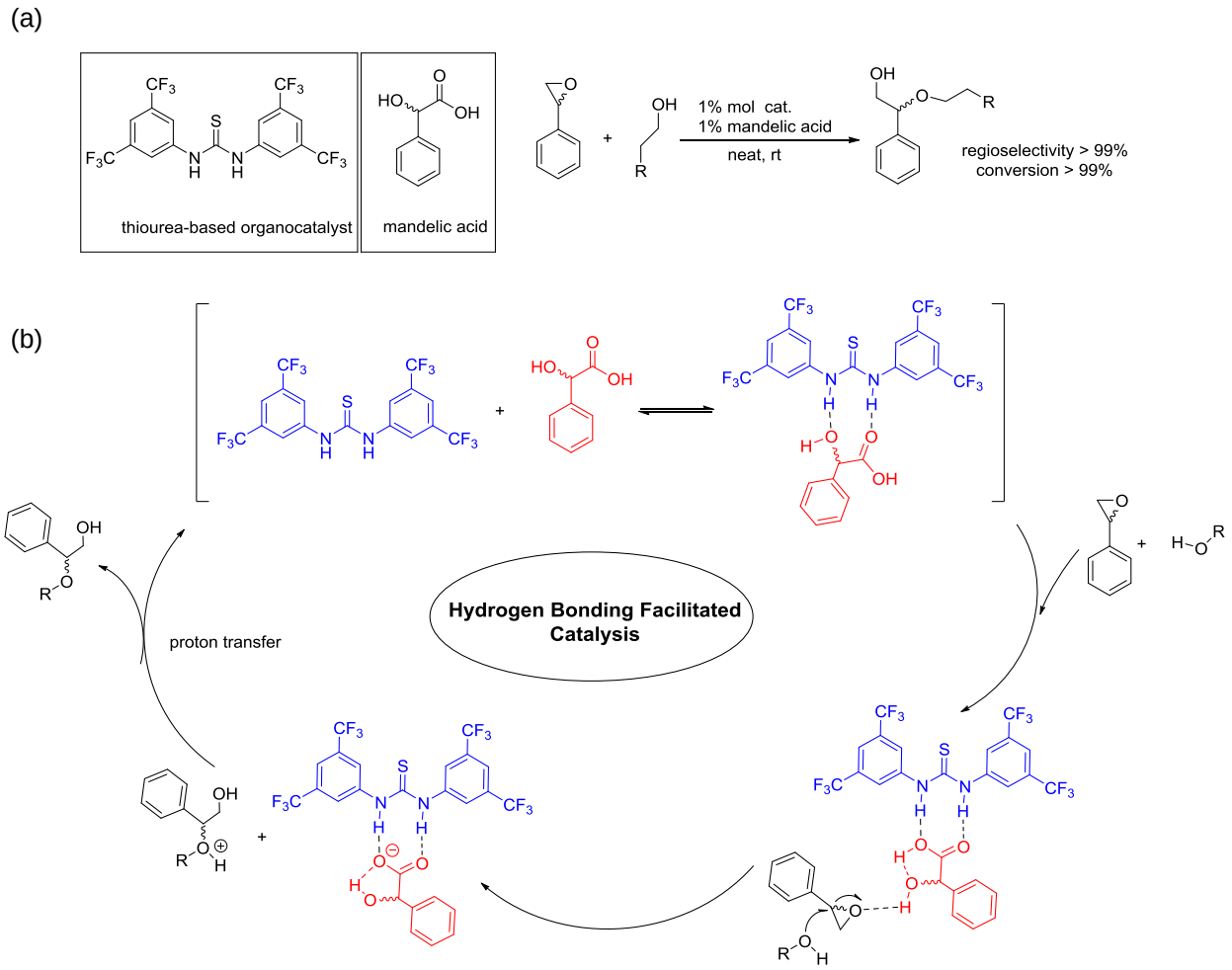


Figure 1.36. (a) Epoxide ring opening reaction using thiourea and mandelic acid as catalysts; (b) the proposed catalytic circle.[143]

1.3 Mechanically Interlocked Host Molecules for Guest Recognition

1.3.1 Strategies for Synthesis of Interlocked Molecules

1.3.1.1 The Mechanical Bond

A mechanical bond refers to a physical entanglement between two or more component parts, whereupon the mutually interlocked components cannot be separated without the cleavage of covalent bonds.[146] Molecules bearing mechanical bonds, termed mechanically-interlocked structures (MIMs), include [n]rotaxanes, [n]catenanes, where n refers to the number of molecular components interlocked together (Figure 1.37). Catenanes, Solomon knots and Borromean rings consist of inter-linked macrocycles which are topologically non-trivial indicating the actions such as rotation, distortion, bending and stretching cannot break the mechanical bond. Rotaxanes comprise of rings threaded by a dumbbell-shaped axle whose ends are too bulky for dethreading to occur. Unlike catenanes, a [2]rotaxane is topologically trivial as dethreading or slippage can result in the separation of the components through expansion of the ring or contraction of the stoppers, without breaking any covalent bonds.

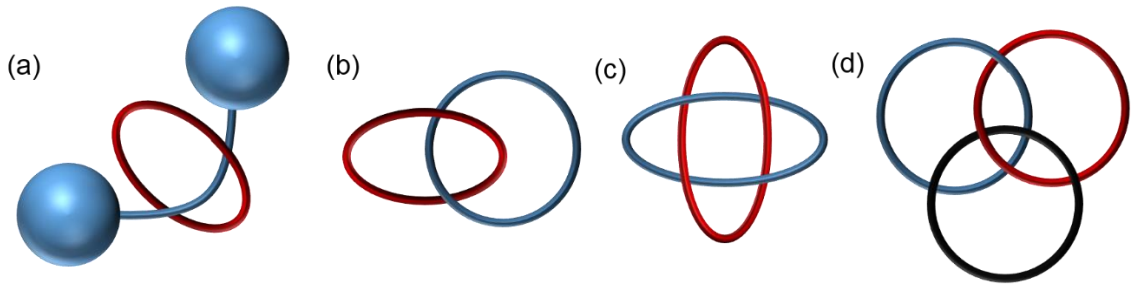


Figure 1.37. Schematic structures of MIMs: (a) [2]rotaxane; (b) [2]catenane; (c) Solomon knot; (d) Borromean ring.

Like normal chemical bonds, mechanical bonds can alter the physical and chemical properties of the sub-components of MIMs.[147] For example, due to the formation of a mechanical bond, the degrees of freedom of component parts decrease resulting in the amplification of non-covalent interactions. Metal complexes ligated by catenanes are more

stable and require harsher conditions to remove the metal, than their non-mechanically bonded analogues. This phenomenon is termed the 'catenand effect'.[148] In addition, the steric hindrance caused by the mechanical bond can increase the kinetic stability of the reactive functionalities.[149,150] These special characteristics of mechanical bonds have led to numerous, wide-ranging applications of MIMs in the areas of catalysis,[151–153] host-guest molecular recognition and sensing,[154,155] nanotechnology[156,157] and novel materials design[158].

1.3.1.2 Template-Directed Synthesis of Interlocked Molecules

Even though MIMs are attracting increasing attention in scientific research, their synthesis has until recent years been a challenge. The strategies for preparing interlocked molecules has sparked the imaginations of synthetic chemists for decades. Even though the idea of a 'mechanical bond' was first proposed in a publication by Frisch in 1953,[159] the first artificial interlocked structure, a catenane, was not successfully synthesised until 1960 by Wasserman and co-workers using a statistical approach.[160] Due to the lack of associative interactions between the components, catenane formation relied only on the statistically random penetration of a chain through the macrocycle, resulting in a very low yield (0.0001%). Subsequently, a template-directed synthesis approach led to a transformative breakthrough in the formation of interlocked structures in acceptable yields.

Template-directed synthesis provides many strategies for MIM formation. For example, as shown in Figure 1.38, a rotaxane can be made by (a) slippage - the slipping of a macrocycle onto the axle under elevated temperatures to form a kinetically-stable rotaxane;[161] (b) shrinkage – reduction in size of a large macrocycle around an axle with two stoppers;[162] (c) stoppering - the addition of two bulky stoppers to a pseudo-rotaxane to prevent dethreading;[163] (d) swelling - the expansion of stopper groups on the axle of a pseudo-rotaxane;[164] (e) snapping - the linkage of two half-axle precursors in the macrocycle

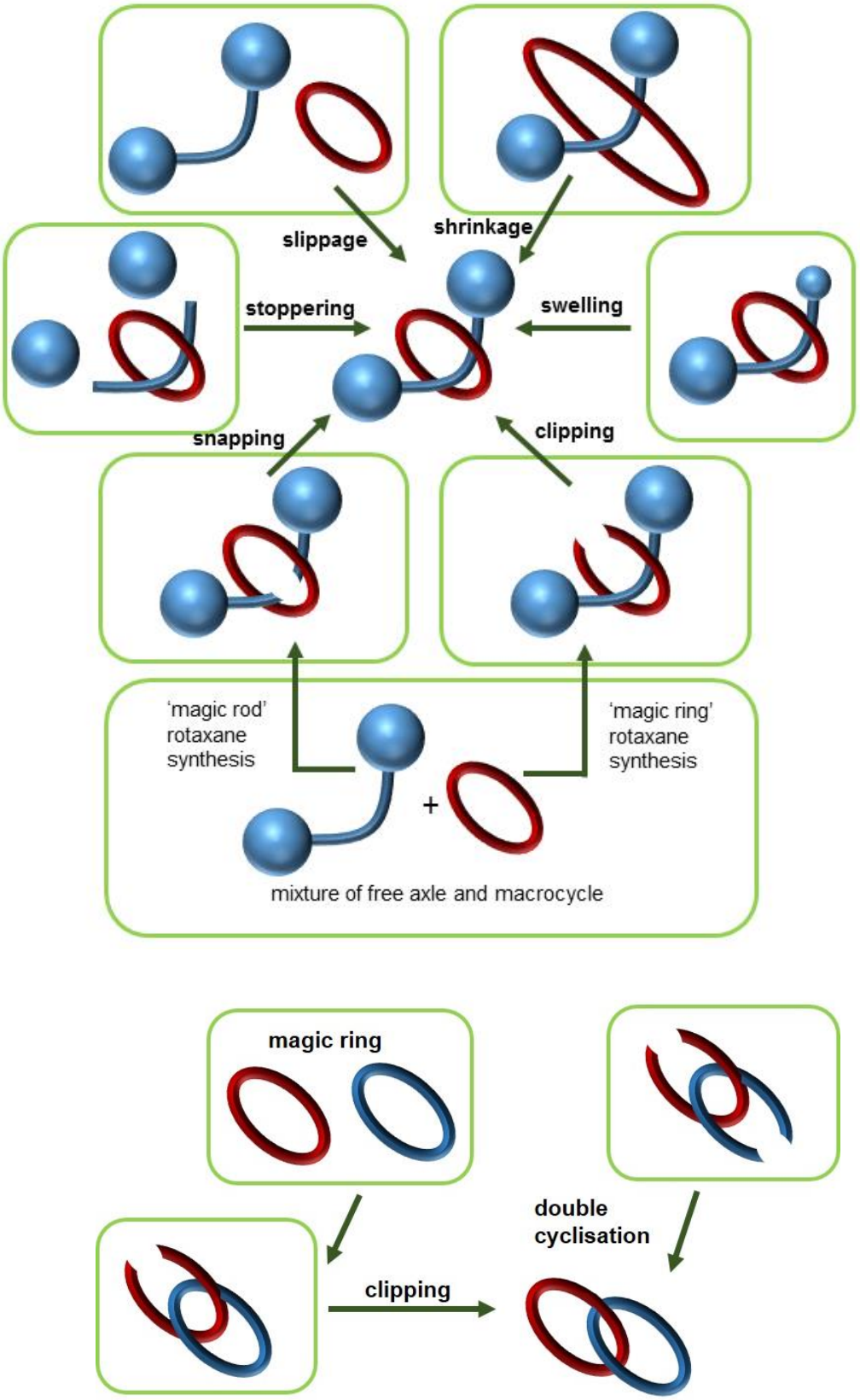


Figure 1.38. Schematic illustration of methodologies for rotaxane and catenane synthesis.

cavity;[165] or (f) clipping - the ring closure of a macrocycle precursor wrapping around a stopped axle.[166] Reversible reactions such as olefin metathesis[167,168] or sulfur-sulfur bond formation[169] can also facilitate the synthesis of rotaxanes. For example, 'magic rod' rotaxane synthesis refers to the snapping of two separated axle components which are broken from their corresponding complete axle,[168] while 'magic ring' rotaxane synthesis utilises the reversible ring-opening and ring-closing reactions for clipping methods.[167,169] Compared to rotaxanes, fewer synthetic methodologies exist for catenanes. Generally, a catenane synthesis involves the clipping of a pseudo-rotaxane molecule or double clipping of an orthogonal complex made by two macrocyclic precursors.[170] Similar to rotaxanations using reversible reactions, 'magic ring' approaches have also been utilised in catenane synthesis.[171]

The following sections will focus on the template-directed synthesis of MIMs using cation, neutral and anion templates.

Cation Templates

Metal cations are the most common templates used in the synthesis of MIMs. The seminal breakthrough was accomplished by Sauvage and co-workers in the early 1980s. A tetrahedral bis-phenanthroline Cu(I) complex consisting of a macrocycle and a thread was converted to a catenane by a clipping methodology (Figure 1.39).[172] The metal-free catenane could be obtained by removal of Cu(I) using KCN.

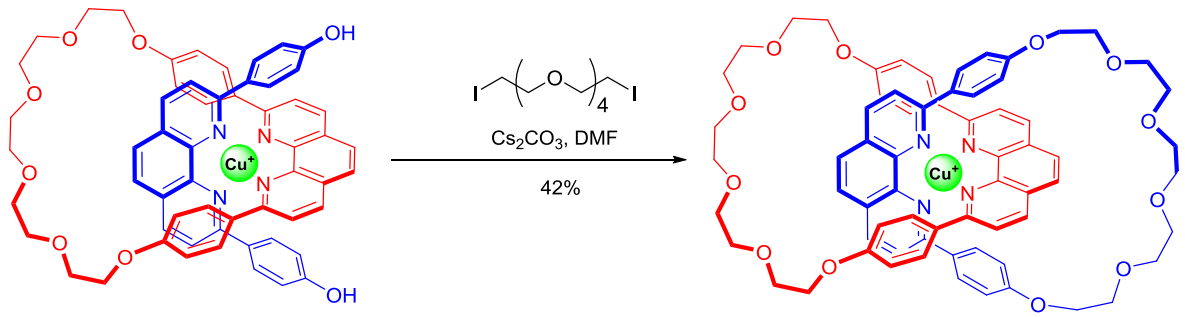


Figure 1.39. Sauvage's Cu(I) template [2]catenane.[172]

Since Sauvage's pioneering work, a wide range of transition metal templates with different stereochemical coordination preferences (e.g. Zn(II),[173] Au(I),[174] Pd(II)[175] and lanthanides[176–178]) have been utilised to construct MIMs (Figure 1.40(a)-(c)). Alkali and alkaline earth metal cations have also been used, despite their less well-defined coordination geometries. For example, sodium cation-polyether 'hard-hard' interactions were exploited by Chiu and co-workers to prepare a catenane via imine formation (Figure 1.40(d)).[179]

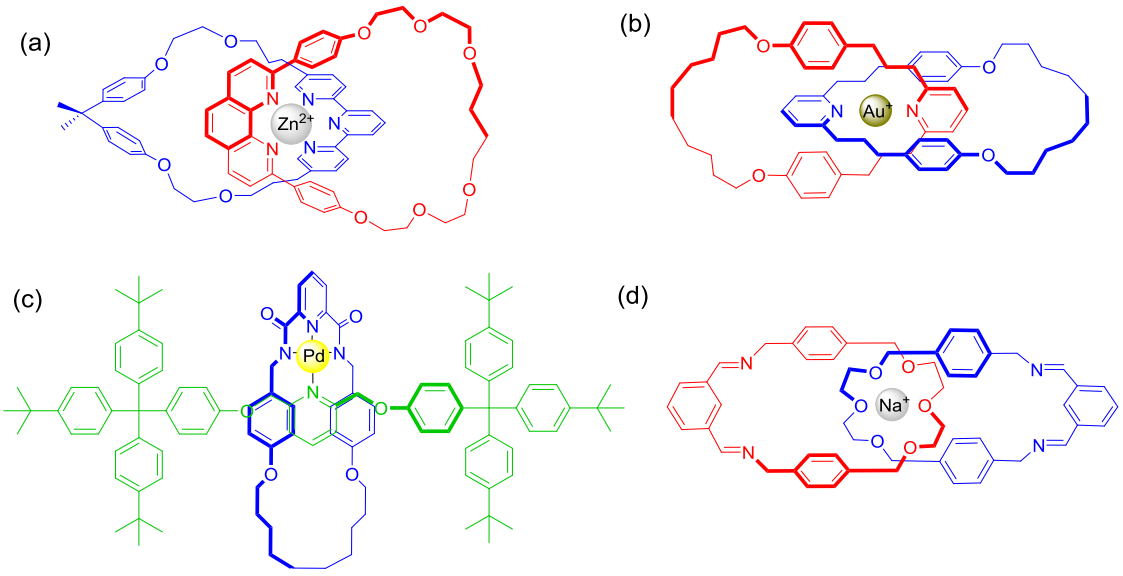


Figure 1.40. (a) Trigonal bipyrimidal Zn(II)-templated [2]catenane;[173] (b) linear Au(I)-templated [2]catenane;[174] (c) square-planar Pd(II)-templated [2]rotaxane;[175] (d) Na^+-templated [2]catenane.[179]

In the above examples, the metal is considered to act as a 'passive template' in assembling the MIM precursor sub-components. Leigh has pioneered the 'active metal template' (AMT) method for MIM synthesis where the metal plays a dual role of simultaneously preorganising the axle precursors and catalysing the formation of mechanical bonds (Figure 1.41).

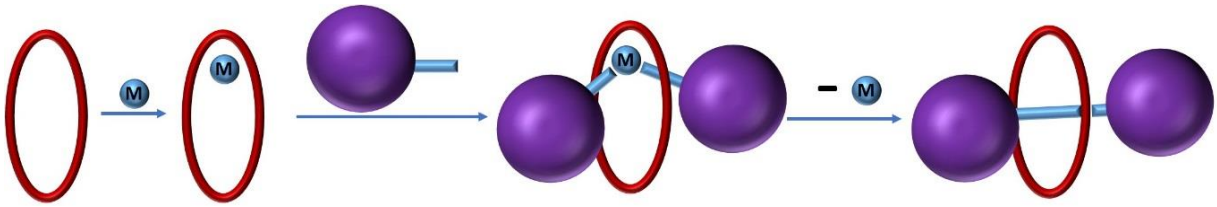


Figure 1.41. Schematic illustration of the ATM strategy for MIM synthesis

The AMT strategy was first demonstrated by Leigh and co-workers in 2007 with a series of [2]- and [3]rotaxanes formed using copper(I)-catalysed azide-alkyne cycloaddition occurring endotopically through the cavity of macrocycles (Figure 1.42(a)).[180] Since then, the AMT methodology has been expanded greatly to include a range of metals (e.g. Cu(I)[181–184], Pd(II),[185,186] Ni(II),[187] Zn(II)[188] and Co(II)[189]). For example, Anderson and co-workers utilised the Cu(I)-catalysed Cadiot-Chodiewicz alkyne cross-coupling reaction to form a polyyne-axle-containing [2]rotaxane (Figure 1.42(b))[184] while Goldup and Leigh used Pd(II)-mediated Michael addition reaction to synthesise a [2]rotaxane (Figure 1.42(c)).[186] More recently, Megiatto and co-workers exploited cobalt(II)/porphyrinate-containing macrocycles to promote olefin cyclopropanation through radical carbene transfer reactions facilitating the formation of a [2]rotaxane (Figure 1.42(d)).[189]

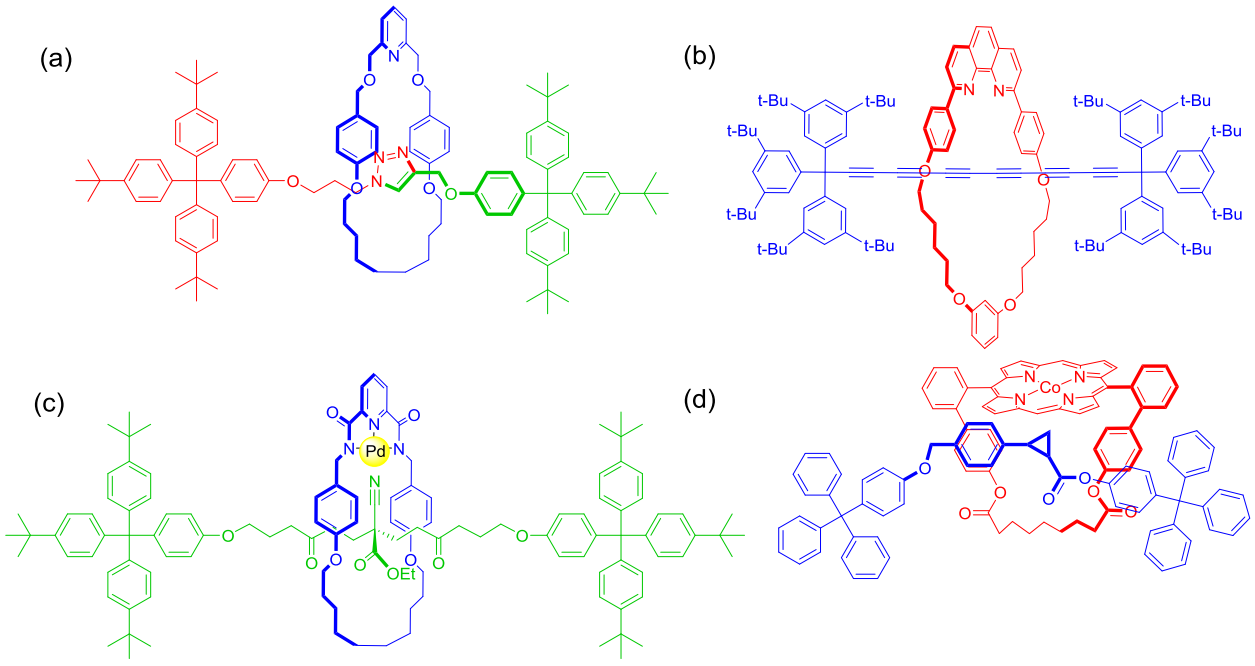


Figure 1.42. (a) Leigh's pioneering [2]rotaxane via AMT from Cu(I)-catalysed azide-alkyne cycloaddition;[180] (b) Anderson's polyyne [2]rotaxane from Cu(I)-catalysed Cadiot-Chodiewicz alkyne cross-coupling;[184] (c) a [2]rotaxane from Pd(II)-mediated Michael addition;[186] (d) Megiatto's [2]rotaxane from Co(II)-catalysed radical carbene transfer reactions.[189]

Organic cations have also been utilised as templates. Secondary ammonium functional groups, in conjunction with polyether-containing macrocycles, assemble

[n]rotaxanes,[190,191] [n]catenanes[192] and high-order interlocked structure via HB interactions.[193] A recent example is a hetero [4]rotaxane (Figure 1.43(a)) synthesised by Qu and co-workers. Exploiting charge-assisted aromatic donor-acceptor interactions, the electron-deficient 4,4'-bipyridinium motif in conjunction with electron-rich polyether hydroquinone (Figure 1.43(b))[194] or TTF-dihydroxynaphthalene derivatives[195] have been used in MIM construction, especially by Stoddart and co-workers.

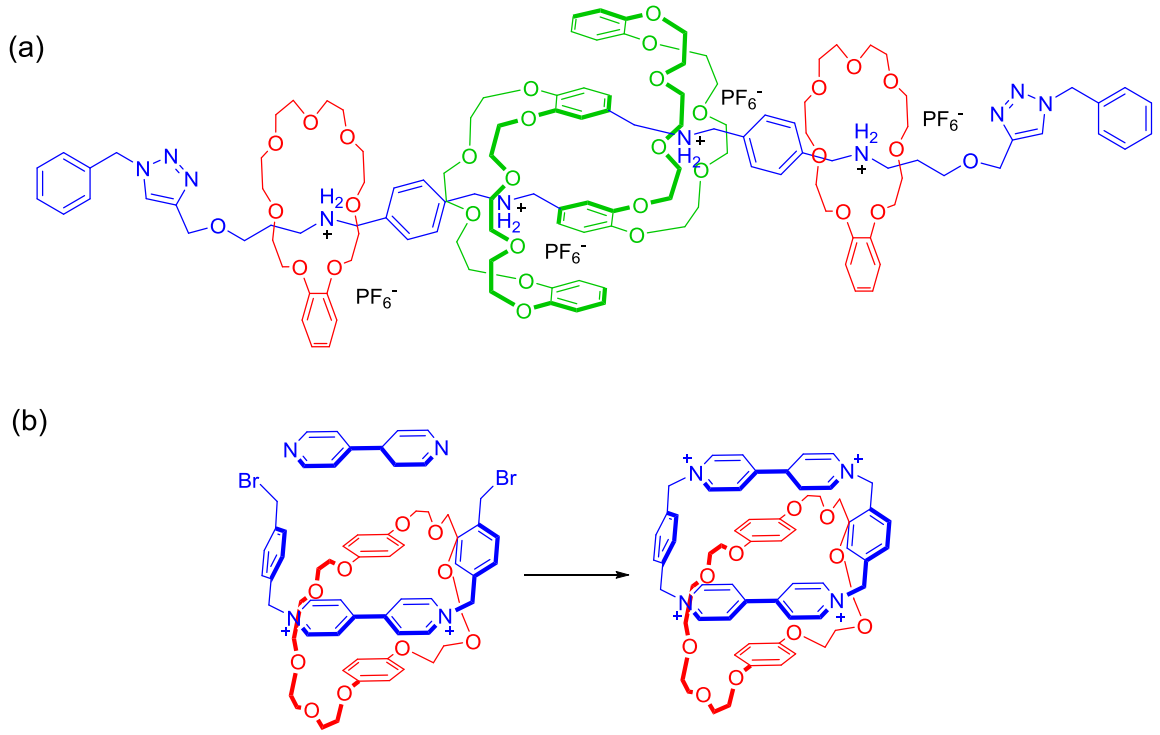


Figure 1.43. (a) Qu's hetero[4]rotaxane from secondary ammonium-polyether interactions;[191] (b) Stoddart's bipyridinium-hydroquinone catenane.[194]

Neutral Templates

Neutral molecules can be used to template MIM formation by utilising intermolecular interactions such as HB, aromatic donor-acceptor interactions, the hydrophobic effect, and C-H···π interactions. Pioneering work exploiting HB templation in the 1990s was presented by Hunter[196], Vögtle[197] and Leigh.[198,199] For example, Leigh and co-workers developed fumaramide axles to generate [2]rotaxanes (Figure 1.44(a)) in yields of up to 97% due to the preorganised HB template.[198] As an example of utilising aromatic donor-acceptor

interactions for MIM construction, a [2]catenane (Figure 1.44(b)) was assembled in aqueous solution via a dynamic combinational library approach by Sanders and co-workers.[200] Anderson and co-workers exploited the hydrophobic effect to form an inclusion complex between a γ-cyclodextrin and a stilbene diboronic acid organic thread in aqueous media, which can be converted to a [2]rotaxane by a Suzuki coupling reaction (Figure 1.44(c)).[201] More recently, C-H···π interactions have been used to synthesise rotaxanes such as pillar[5]arene-based [2]rotaxanes (Figure 1.44(d)), which were prepared from inclusion complexes formed between pillar[5]arene and acyl chains via a stoppering methodology.[202]

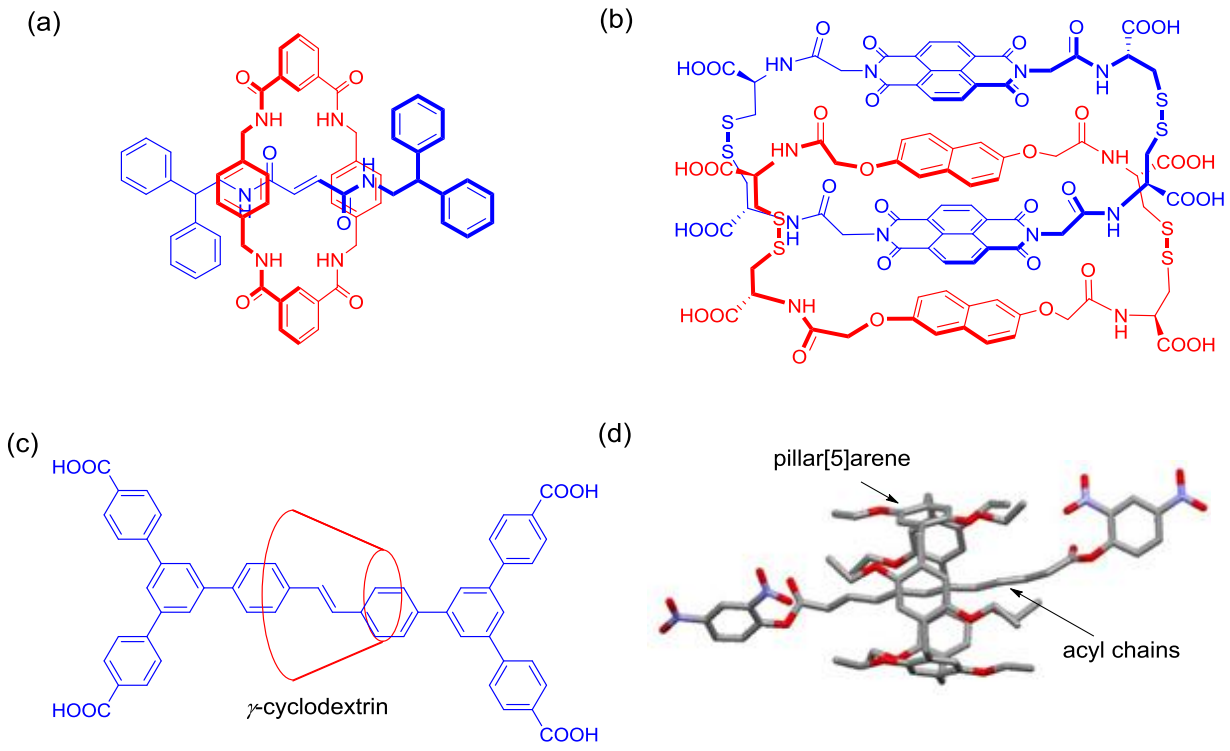


Figure 1.44. (a) Leigh's HB template [2]rotaxane;[198] (b) Sander's [2]catenane formed by donor-acceptor interactions;[200] (c) Anderson's [2]rotaxane assembled using the hydrophobic effect;[201] (d) crystal structure of a [2]rotaxane templated by C-H···π interactions.[202]

Anion Templates

The first example of anion templated MIM formation was reported by Vögtle and co-workers in 1999, where a bulky phenoxide anion half-axle and a bis-isophthalamide macrocycle formed a rotaxane in 95% yield by a S_N2 reaction with another bromo-benzyl

half-axle component in CH_2Cl_2 (Figure 1.45(a)).[165] A similar phenoxide templated method was subsequently exploited by Schalley and co-workers (Figure 1.45(b).[203]

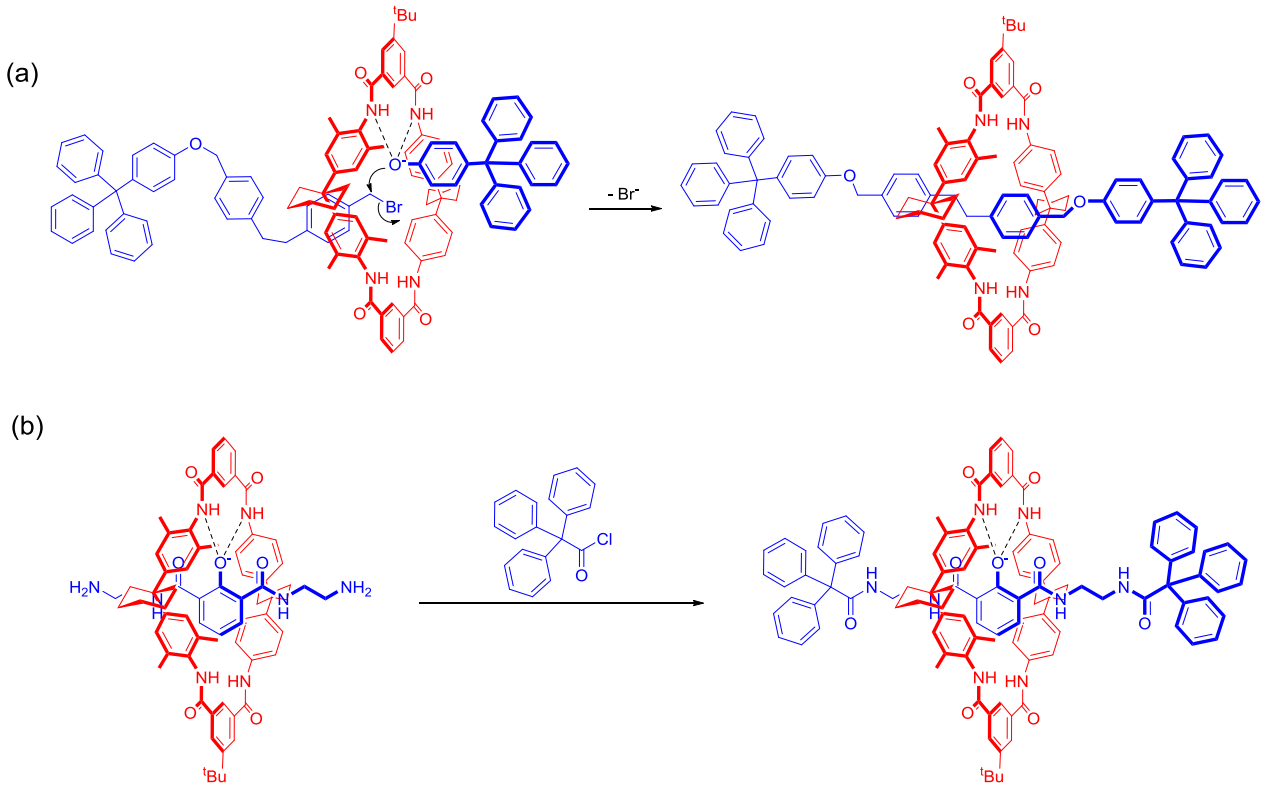


Figure 1.45. (a) Vögtle's pioneering [2]rotaxane via anion templation;[165] (b) Schalley's [2]rotaxane via a phenoxide template.[203]

In 2001, Beer and co-workers developed a discrete anion templation strategy. Chloride was found to template the formation of a pseudorotaxane between an isophthalamide macrocycle and a 3,5-bis-amide alkyl substituted pyridinium thread in acetone (Figure 1.46(a)),[204] which could be converted to rotaxanes[205] and catenanes[206] via a clipping methodology (Figure 1.46(b)). Other anion templates such as Br^-,[207] SO_4^{2-},[208] NO_3^- [209,210] and NO_2^- [211] in conjunction with various binding motifs (e.g. indolocarbazole,[212] prototriazolium[207] and imidazolium[213]) have also been successfully used for MIM construction. Upon anion template removal, the resulting three-dimensional cavities of the MIMs can be exploited for anion recognition, exhibiting a high degree of selectivity for the template anion (see next section). Using similar protocols, XB functionalities were utilised in

the anion templation methodology for preparing several interlocked anion receptors (Figure 1.46(c) and (d)). [112,214]

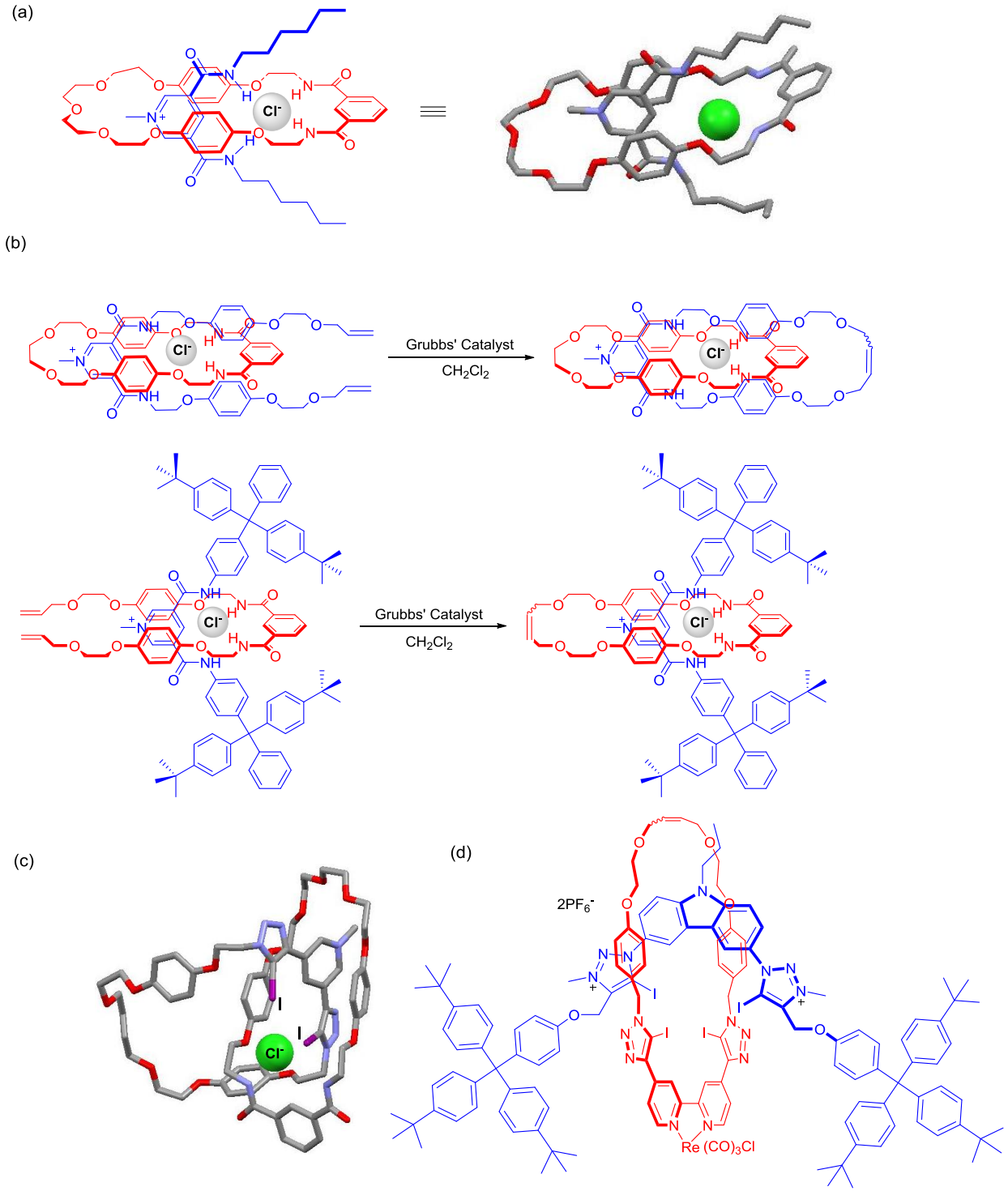


Figure 1.46. (a) A pseudorotaxane templated by Cl^- and corresponding crystal structure;[204] (b) a [2]catenane[206] and a [2]rotaxane[205] synthesised by Cl^- templation; (c) the crystal structure of a XB [2]catenane via anion templation;[112] (d) an all-XB [2]rotaxane via Cl^- templation.[214]

More recently, Flood and co-workers synthesised a [3]rotaxane by stoppering a 2:1 'sandwich' complex between a 'cyanostar' macrocycle and a bis-alkyne functionalised phosphate anion using a CuAAC reaction (Figure 1.47).[215]

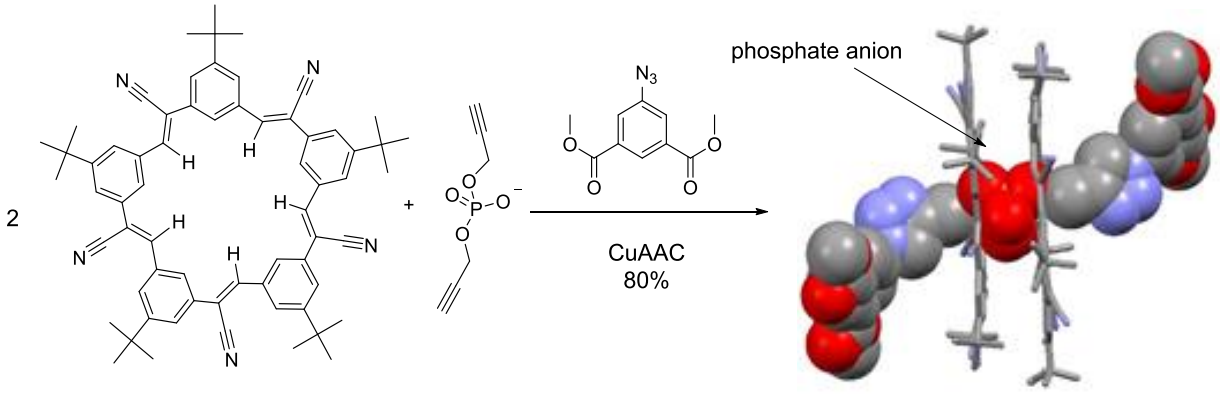


Figure 1.47. Flood's 'cyanostar'-based [3]rotaxane templated by a phosphate anion.[215]

1.3.2 Interlocked Host Molecules for Guest Recognition and Sensing

The unique three-dimensional host cavities of MIMs offer novel opportunities for the recognition of guest species.[216] Indeed, a variety of rotaxanes and catenanes have been shown to act as hosts for cations and anions. For example, a [1]rotaxane synthesised by Hiratani and co-workers showed a selective fluorescence response towards Li^+ over other alkali metals in CH_2Cl_2/CH_3CN (9:1, *v*/*v*) (Figure 1.48(a)), where the selectivity mainly stemmed from the size complementarity between Li^+ and the small three-dimensional cavity constructed by the ring and the chain.[217] Similarly, a [3]rotaxane prepared by the same group bound Cs^+ in a sandwich-type complex with a K_a = 6.3 X 10^5 M^{-1} in CD_2Cl_2/CD_3CN (9:1. *v*/*v*) (Figure 1.48(b)).[218] More recently, Goldup and co-workers developed a [2]rotaxane as a fluorescent chelating ligand (Figure 1.48(c)) which selectively bound Zn^{2+} in CH_3CN with a $K_a > 10^8$ M^{-1}.[219] A [2]rotaxane synthesised by Li and co-workers was shown to bind Li^+ and Zn^{2+} using different three-dimensional cavities, which could be monitored by fluorescence responses (Figure 1.48(d)).[155]

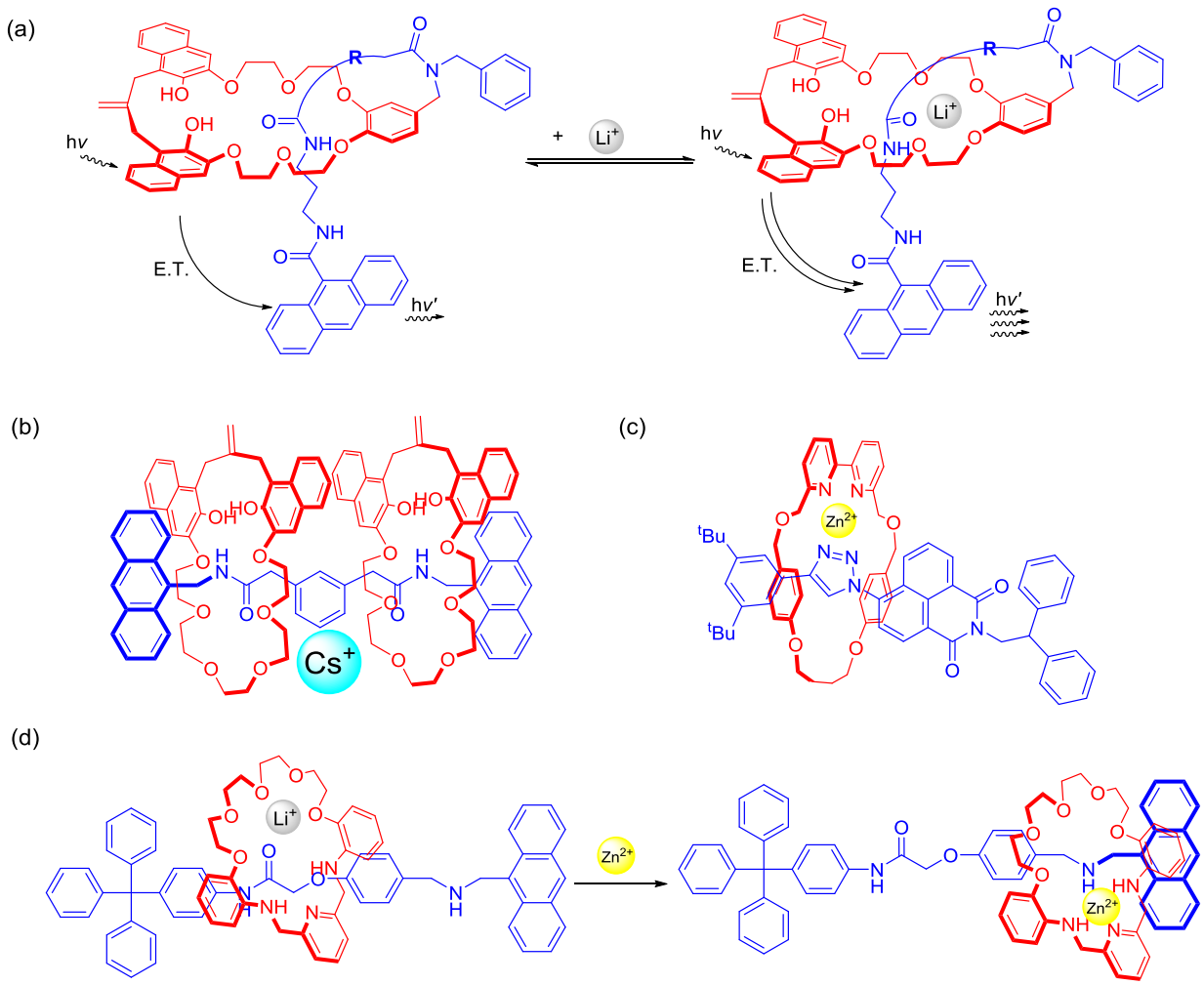


Figure 1.48. (a) Hiratani's lithium binding [1]rotaxane;[217] (b) a sandwich complex formed by a [3]rotaxane and Cs^+;[218] (c) Goldup's zinc-binding [2]rotaxane;[219] (d) a fluorescent molecular shuttle binding Li^+ and Zn^{2+}.[155]

Anion recognition by a MIM was first described by Sessler, Vögtle and co-workers who prepared a catenane (Figure 1.49(a)) that could bind F^- with a K_a = 1.48 x 10^5 M^{-1} in 1,1,2,2-tetrachloroethane-d_2.[220] An indolocarbazole-based catenane (Figure 1.49(b)), prepared by Jeong and co-workers, selectively bound Cl^- via strong HB interactions (K_a = 1.4 x 10^5 M^{-1}) in acetone/H_2O (99:1 *v*/*v*).[221] Beer and co-workers developed a plethora of interlocked anion receptors using discrete anion templation including a [2]catenane (Figure 1.46(b)) capable of selectively binding Cl^- in $CD_3OD/CDCl_3$ (1:1 v/v). More recently, XB interlocked anion hosts have been utilised for anion recognition such as Beer's Ru(II)-containing water-soluble XB rotaxane which could bind I^- in water with a K_a = 6300 M^{-1}

(Figure 1.49(c)). Upon I^- binding, an enhancement of the Ru-centred MLCT emission intensity was observed.[222] The same group also demonstrated that XB interlocked structures could be exploited for chiral anion discrimination. For example, a di-cationic [3]rotaxane (Figure 1.49(d)) could distinguish chiral dicarboxylate enantiomers via the formation of distinct 1:1 stoichiometric sandwich complexes through a combination of XB and HB interactions in $CDCl_3/CD_3OD/D_2O$ (60:39:1 *v*/*v*/*v*).[223]

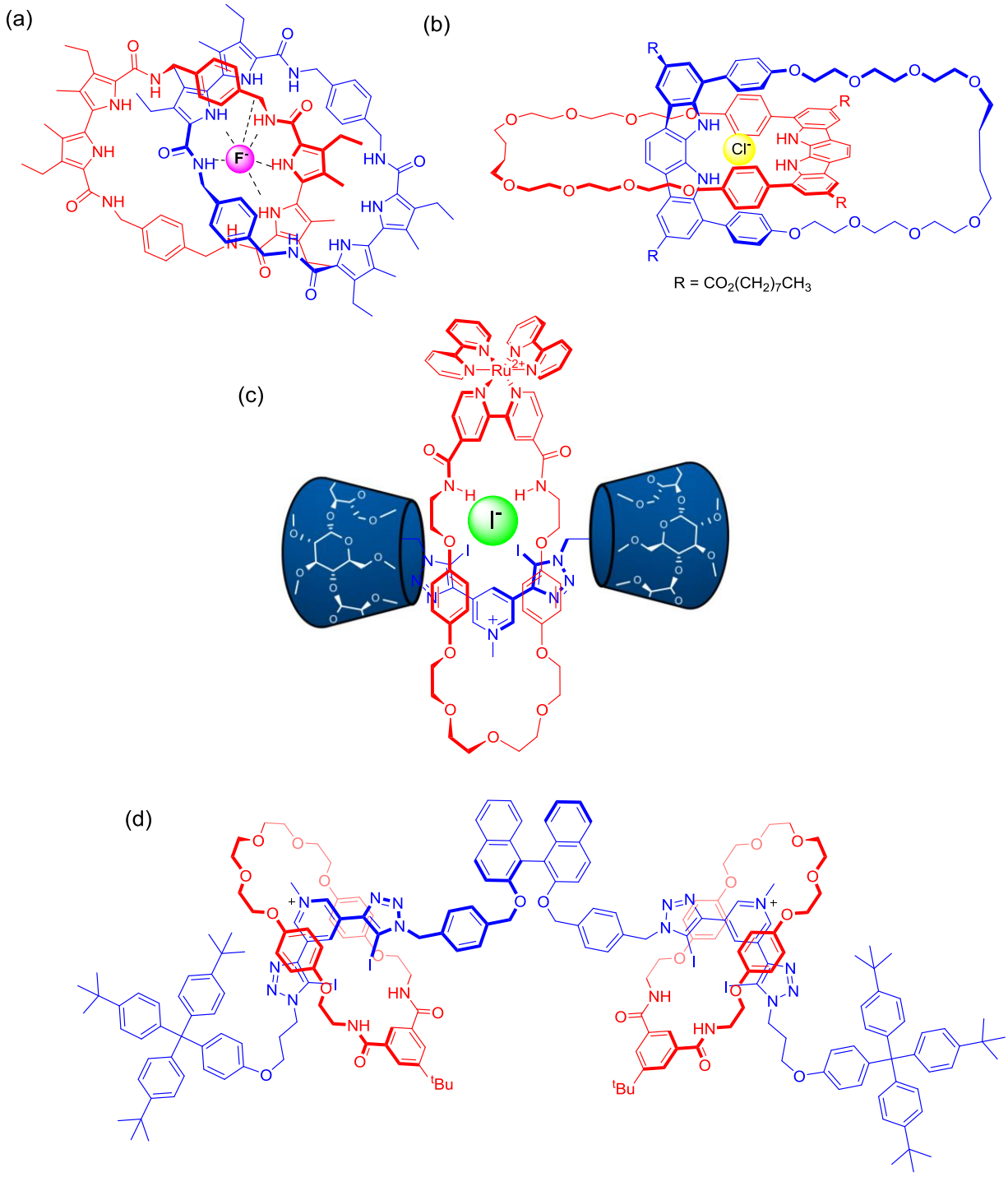


Figure 1.49. (a) Sessler and Vögtle's bipyrrole-based[2]catenane;[220] (b) Jeong's indolocarbazole-based chloride receptor;[221] (c) Beer's Ru(II)-containing water-soluble [2]rotaxane;[222] (d) Beer's [3]rotaxane for chiral dicarboxylate discrimination.[223]

1.4 Project Aims

The theme and aim of this project is to investigate the use of mechanically interlocked host structures for anion recognition and lanthanide complexation. In particular, halogen bonding (XB) will be mainly exploited as the intermolecular interaction of choice for anion guest recognition.

Chapter 2 focuses on the AMT preparation of a series of XB [2]rotaxane/catenane hosts which exploit Lewis basic N-donor triazoles for metal coordination and Lewis acidic iodotraizole motifs for anion binding. Importantly, protonation of the XB rotaxanes is demonstrated to enhance anion binding affinities

Chapter 3 investigates the synthesis and anion binding properties of XB cryptand anion hosts. Specifically, by incorporating naphthalene groups, the anion binding properties and fluorescent sensing capability of a novel XB cryptand are examined. The synthesis of interlocked structures containing XB cryptand structures is also attempted using a variety of template methodologies.

Chapter 4 details the synthesis of a series of [2]rotaxane hosts for lanthanide complexation. Their lanthanide binding properties are investigated using luminescence spectroscopy.

1.5 References

1 J.-M. Lehn, *Angew. Chem. Int. Ed. Engl.*, 1988, **27**, 89–112.
2 J. D. van der Waals, *Over de Continuiteit van den Gas-en Vloeistoftoestand*, Sijthoff, 1873, vol. 1.
3 R. U. Lemieux and U. Spohr, in *Advances in Carbohydrate Chemistry and Biochemistry*, ed. D. Horton, Academic Press, 1994, vol. 50, pp. 1–20.
4 W. M. Latimer and W. H. Rodebush, *J. Am. Chem. Soc.*, 1920, **42**, 1419–1433.
5 D. A. Smith, in *Modeling the Hydrogen Bond*, American Chemical Society, 1994, vol. 569, pp. 1–5.
6 C. J. Pedersen, *J. Am. Chem. Soc.*, 1967, **89**, 7017–7036.
7 C. J. Pedersen, *J. Am. Chem. Soc.*, 1967, **89**, 2495–2496.
8 G. M. Whitesides, J. P. Mathias and C. T. Seto, *Science*, 1991, **254**, 1312–1319.
9 J. Rebek, *Proc. Natl. Acad. Sci.*, 2009, **106**, 10423–10424.
10 L. Fang, M. A. Olson, D. Benítez, E. Tkatchouk, W. A. G. Iii and J. F. Stoddart, *Chem. Soc. Rev.*, 2009, **39**, 17–29.
11 S. Erbas-Cakmak, D. A. Leigh, C. T. McTernan and A. L. Nussbaumer, *Chem. Rev.*, 2015, **115**, 10081–10206.
12 J. M. Lehn, *Acc. Chem. Res.*, 1978, **11**, 49–57.
13 D. J. Cram, T. Kaneda, R. C. Helgeson and G. M. Lein, *J. Am. Chem. Soc.*, 1979, **101**, 6752–6754.
14 K. S. Chichak, S. J. Cantrill, A. R. Pease, S.-H. Chiu, G. W. V. Cave, J. L. Atwood and J. F. Stoddart, *Science*, 2004, **304**, 1308–1312.
15 D. Fujita, Y. Ueda, S. Sato, N. Mizuno, T. Kumasaka and M. Fujita, *Nature*, 2016, **540**, 563–566.
16 D. E. Koshland, *Proc. Natl. Acad. Sci.*, 1958, **44**, 98–104.
17 T. Steiner and G. R. Desiraju, *Chem. Commun.*, 1998, 891–892.
18 S. J. Grabowski, *Chem. Rev.*, 2011, **111**, 2597–2625.
19 J. A. K. Howard, V. J. Hoy, D. O'Hagan and G. T. Smith, *Tetrahedron*, 1996, **52**, 12613–12622.
20 J. Emsley, *Chem. Soc. Rev.*, 1980, **9**, 91–124.
21 P. A. Gale, E. N. W. Howe and X. Wu, *Chem*, 2016, **1**, 351–422.
22 G. R. Desiraju, P. S. Ho, L. Kloo, A. C. Legon, R. Marquardt, P. Metrangolo, P. Politzer, G. Resnati and K. Rissanen, *Pure Appl. Chem.*, 2013, **85**, 1711–1713.
23 T. Clark, M. Hennemann, J. S. Murray and P. Politzer, *J. Mol. Model.*, 2006, **13**, 291–296.
24 A. Brown and P. D. Beer, *Chem. Commun.*, 2016, **52**, 8645–8658.
25 G. Cavallo, P. Metrangolo, R. Milani, T. Pilati, A. Priimagi, G. Resnati and G. Terraneo, *Chem. Rev.*, 2016, **116**, 2478–2601.
26 M. H. Kolář, P. Deepa, H. Ajani, A. Pecina, P. Hobza, in *Halogen Bonding II*, *Topic in Current Chemistry*, Springer, Cham, 2014, vol, 359, pp 1-25.
27 P. Metrangolo, F. Meyer, T. Pilati, G. Resnati and G. Terraneo, *Angew. Chem. Int. Ed.*, 2008, **47**, 6114–6127.
28 P. Metrangolo, H. Neukirch, T. Pilati and G. Resnati, *Acc. Chem. Res.* 2005, **38**, 386–395.
29 L. C. Gilday, S. W. Robinson, T. A. Barendt, M. J. Langton, B. R. Mullaney and P. D. Beer, *Chem. Rev.*, 2015, **115**, 7118–7195.
30 J. Y. C. Lim and P. D. Beer, *Chem*, 2018, **4**, 731–783.
31 A. Bauzá, D. Quiñonero, P. M. Deyà and A. Frontera, *CrystEngComm*, 2013, **15**, 3137–3144.
32 J. Y. C. Lim, I. Marques, A. L. Thompson, K. E. Christensen, V. Félix and P. D. Beer, *J. Am. Chem. Soc.*, 2017, **139**, 3122–3133.
33 J. Sunner, K. Nishizawa and P. Kebarle, *J. Phys. Chem.*, 1981, **85**, 1814–1820.
34 D. Kim, E. C. Lee, K. S. Kim and P. Tarakeshwar, *J. Phys. Chem. A*, 2007, **111**, 7980–7986.
35 D. P. Weimann and C. A. Schalley, *Supramol. Chem.*, 2008, **20**, 117–128.
36 Kennedy C. Rose, Lin Song and Jacobsen Eric N., *Angew. Chem. Int. Ed.*, 2016, **55**, 12596–12624.
37 M. E. Weber, E. K. Elliott and G. W. Gokel, *Org. Biomol. Chem.*, 2006, **4**, 83–89.
38 M. Mascal, A. Armstrong and M. D. Bartberger, *J. Am. Chem. Soc.*, 2002, **124**, 6274–6276.
39 D. Kim, P. Tarakeshwar and K. S. Kim, *J. Phys. Chem. A*, 2004, **108**, 1250–1258.
40 D. Quiñonero, C. Garau, C. Rotger, A. Frontera, P. Ballester, A. Costa and P. M. Deyà, *Angew. Chem. Int. Ed.*, 2002, **41**, 3389–3392.
41 D.-X. Wang and M.-X. Wang, *J. Am. Chem. Soc.*, 2013, **135**, 892–897.
42 S. Li, S.-X. Fa, Q.-Q. Wang, D.-X. Wang and M.-X. Wang, *J. Org. Chem.*, 2012, **77**, 1860–1867.
43 T. J. Mooibroek, C. A. Black, P. Gamez and J. Reedijk, *Cryst. Growth Des.*, 2008, **8**, 1082–1093.
44 S. Guha and S. Saha, *J. Am. Chem. Soc.*, 2010, **132**, 17674–17677.
45 R. E. Dawson, A. Hennig, D. P. Weimann, D. Emery, V. Ravikumar, J. Montenegro, T. Takeuchi, S. Gabutti, M. Mayor, J. Mareda, C. A. Schalley and S. Matile, *Nat. Chem.*, 2010, **2**, 533–538.
46 N. Sakai, J. Mareda, E. Vauthey and S. Matile, *Chem. Commun.*, 2010, **46**, 4225–4237.
47 J. Mareda and S. Matile, *Chem. – Eur. J.*, 2009, **15**, 28–37.
48 C. R. Martinez and B. L. Iverson, *Chem. Sci.*, 2012, **3**, 2191–2201.
49 S. Grimme, *Angew. Chem. Int. Ed.*, 2008, **47**, 3430–3434.
50 J. W. G. Bloom and S. E. Wheeler, *Angew. Chem. Int. Ed.*, 2011, **50**, 7847–7849.
51 C. A. Hunter and J. K. M. Sanders, *J. Am. Chem. Soc.*, 1990, **112**, 5525–5534.

52 M. S. Cubberley and B. L. Iverson, *J. Am. Chem. Soc.*, 2001, **123**, 7560–7563.
53 J. Seelig and P. Ganz, *Biochemistry*, 1991, **30**, 9354–9359.
54 M. Fernández-Vidal, S. H. White and A. S. Ladokhin, *J. Membr. Biol.*, 2011, **239**, 5–14.
55 S. Mukherjee and S. Talukder, *J. Fluoresc.*, 2017, **27**, 1567–1572.
56 L. Fabbrizzi, M. Licchelli, L. Parodi, A. Poggi and A. Taglietti, *Eur. J. Inorg. Chem.*, 1999, **1999**, 35–39.
57 A. E. Martell, in *Werner Centennial*, ed. G. B. Kauffman, American Chemical Society, 1967, vol. 62, pp. 272–294.
58 R. D. Hancock and A. E. Martell, *Comments Inorg. Chem.*, 1988, **6**, 237–284.
59 Y. Hua, R. O. Ramabhadran, J. A. Karty, K. Raghavachari and A. H. Flood, *Chem. Commun.*, 2011, **47**, 5979–5981.
60 D. J. Cram, *Angew. Chem. Int. Ed. Engl.*, 1988, **27**, 1009–1020.
61 M. Hayyan, M. A. Hashim and I. M. AlNashef, *Chem. Rev.*, 2016, **116**, 3029–3085.
62 J. R. Knowles, *Annu. Rev. Biochem.*, 1980, **49**, 877–919.
63 M. Santanu, R. Karuppusamy, S. Ulrich and M. Govindasamy, *Angew. Chem. Int. Ed.*, 2016, **55**, 7606–7630.
64 A. Vankeerberghen, H. Cuppens and J.-J. Cassiman, *J. Cyst. Fibros.*, 2002, **1**, 13–29.
65 A. A. Mohammadi, M. Yousefi, M. Yaseri, M. Jalilzadeh and A. H. Mahvi, *Sci. Rep.*, 2017, **7**, 17300.
66 D. J. Conley, H. W. Paerl, R. W. Howarth, D. F. Boesch, S. P. Seitzinger, K. E. Havens, C. Lancelot and G. E. Likens, *Science*, 2009, **323**, 1014–1015.
67 M. W. Bowler, M. G. Montgomery, A. G. W. Leslie and J. E. Walker, *Proc. Natl. Acad. Sci.*, 2006, **103**, 8646–8649.
68 H. B. Leavesley, L. Li, K. Prabhakaran, J. L. Borowitz and G. E. Isom, *Toxicol. Sci.*, 2008, **101**, 101–111.
69 J. G. Darab, A. B. Amonette, D. S. D. Burke, R. D. Orr, S. M. Ponder, B. Schrick, T. E. Mallouk, W. W. Lukens, D. L. Caulder and D. K. Shuh, *Chem. Mater.*, 2007, **19**, 5703–5713.
70 R. D. Shannon, *Acta Crystallogr. A*, 1976, **32**, 751–767.
71 A. E. Hargrove, S. Nieto, T. Zhang, J. L. Sessler and E. V. Anslyn, *Chem. Rev.*, 2011, **111**, 6603–6782.
72 N. Busschaert, C. Caltagirone, W. Van Rossom and P. A. Gale, *Chem. Rev.*, 2015, **115**, 8038–8155.
73 F. Hofmeister, *Arch. Exp. Pathol. Pharmakol.*, 1888, **24**, 274–260.
74 J. W. Pflugrath and F. A. Quiocho, *Nature*, 1985, **314**, 257–260.
75 H. Luecke and F. A. Quiocho, *Nature*, 1990, **347**, 402–406.
76 S. Kubik, R. Goddard, R. Kirchner, D. Nolting and J. Seidel, *Angew. Chem. Int. Ed.*, 2001, **40**, 2648–2651.
77 S. Kubik and R. Goddard, *Proc. Natl. Acad. Sci.*, 2002, **99**, 5127–5132.
78 M. A. Hossain, S. O. Kang, J. M. Llinares, D. Powell and K. Bowman-James, *Inorg. Chem.*, 2003, **42**, 5043–5045.
79 S. Valiyaveettil, J. F. J. Engbersen, W. Verboom and D. N. Reinhoudt, *Angew. Chem. Int. Ed. Engl.*, 1993, **32**, 900–901.
80 D. Meshcheryakov, F. Arnaud-Neu, V. Böhmer, M. Bolte, J. Cavaleri, V. Hubscher-Bruder, I. Thondorf and S. Werner, *Org. Biomol. Chem.*, 2008, **6**, 3244–3255.
81 G. V. Oshovsky, W. Verboom, R. H. Fokkens and D. N. Reinhoudt, *Chem. – Eur. J.*, 2004, **10**, 2739–2748.
82 L. Qin, A. Hartley, P. Turner, R. B. P. Elmes and K. A. Jolliffe, *Chem. Sci.*, 2016, **7**, 4563–4572.
83 P. A. Gale, J. L. Sessler, V. Král and V. Lynch, *J. Am. Chem. Soc.*, 1996, **118**, 5140–5141.
84 H. Chen, H. Lin, Z. Cai and H. Lin, *IJCA Vol46A5 May 2007*.
85 W. B. Farnham, D. C. Roe, D. A. Dixon, J. C. Calabrese and R. L. Harlow, *J. Am. Chem. Soc.*, 1990, **112**, 7707–7718.
86 S. Lee, C.-H. Chen and A. H. Flood, *Nat. Chem.*, 2013, **5**, 704–710.
87 C. H. Park and H. E. Simmons, *J. Am. Chem. Soc.*, 1968, **90**, 2429–2431.
88 C. H. Park and H. E. Simmons, *J. Am. Chem. Soc.*, 1968, **90**, 2431–2432.
89 J. M. Lehn, E. Sonveaux and A. K. Willard, *J. Am. Chem. Soc.*, 1978, **100**, 4914–4916.
90 F. P. Schmidtchen, *Angew. Chem. Int. Ed. Engl.*, 1977, **16**, 720–721.
91 B. Dietrich, D. L. Fyles, T. M. Fyles and J.-M. Lehn, *Helv. Chim. Acta*, 1979, **62**, 2763–2787.
92 M. Berger and F. P. Schmidtchen, *J. Am. Chem. Soc.*, 1999, **121**, 9986–9993.
93 S. Shinoda, M. Tadokoro, H. Tsukube, S. Shinoda and R. Arakawa, *Chem. Commun.*, 1998, 181–182.
94 K. Ghosh, G. Masanta and A. P. Chattopadhyay, *Eur. J. Org. Chem.*, 2009, **2009**, 4515–4524.
95 N. G. White, S. Carvalho, V. Félix and P. D. Beer, *Org. Biomol. Chem.*, 2012, **10**, 6951–6959.
96 B.-Y. Wang, Z.-Q. Chen, H. Huang and Q.-Y. Cao, *RSC Adv.*, 2017, **7**, 43950–43956.
97 N. Ahmed, B. Shirinfar, I. Geronimo and K. S. Kim, *Org. Lett.*, 2011, **13**, 5476–5479.
98 A. Brown and P. D. Beer, *Chem. Commun.*, 2016, **52**, 8645–8658.
99 A. Mele, P. Metrangolo, H. Neukirch, T. Pilati and G. Resnati, *J. Am. Chem. Soc.*, 2005, **127**, 14972–14973.
100 M. G. Sarwar, B. Dragisic, S. Sagoo and M. S. Taylor, *Angew. Chem. Int. Ed.*, 2010, **49**, 1674–1677.
101 E. Dimitrijević, O. Kvak and M. S. Taylor, *Chem. Commun.*, 2010, **46**, 9025–9027.
102 M. G. Sarwar, B. Dragisić, E. Dimitrijević and M. S. Taylor, *Chem. – Eur. J.*, 2013, **19**, 2050–2058.
103 R. Tepper, B. Schulze, H. Görls, P. Bellstedt, M. Jäger and U. S. Schubert, *Org. Lett.*, 2015, **17**, 5740–5743.
104 L. C. Gilday, N. G. White and P. D. Beer, *Dalton Trans.*, 2013, **42**, 15766–15773.

105 A. Caballero, N. G. White and P. D. Beer, *Angew. Chem. Int. Ed.*, 2011, **50**, 1845–1848.
106 F. Zapata, A. Caballero, N. G. White, T. D. W. Claridge, P. J. Costa, V. Félix and P. D. Beer, *J. Am. Chem. Soc.*, 2012, **134**, 11533–11541.
107 M. Cametti, K. Raatikainen, P. Metrangolo, T. Pilati, G. Terraneo and G. Resnati, *Org. Biomol. Chem.*, 2012, **10**, 1329–1333.
108 N. B. Wageling, G. F. Neuhaus, A. M. Rose, D. A. Decato and O. B. Berryman, *Supramol. Chem.*, 2016, **28**, 665–672.
109 S. Chakraborty, R. Dutta and P. Ghosh, *Chem. Commun.*, 2015, **51**, 14793–14796.
110 J. Y. C. Lim and P. D. Beer, *Chem. Commun.*, 2015, **51**, 3686–3688.
111 J. Y. C. Lim, I. Marques, L. Ferreira, V. Félix and P. D. Beer, *Chem. Commun.*, 2016, **52**, 5527–5530.
112 S. W. Robinson, C. L. Mustoe, N. G. White, A. Brown, A. L. Thompson, P. Kennepohl and P. D. Beer, *J. Am. Chem. Soc.*, 2015, **137**, 499–507.
113 C. J. Massena, A. M. S. Riel, G. F. Neuhaus, D. A. Decato and O. B. Berryman, *Chem. Commun.*, 2015, **51**, 1417–1420.
114 P. Ballester, *Acc. Chem. Res.*, 2013, **46**, 874–884.
115 J. Kobylarczyk, D. Pinkowicz, M. Srebro-Hooper, J. Hooper and R. Podgajny, *Dalton Trans.*, 2017, **46**, 3482–3491.
116 P. Arranz-Mascarós, C. Bazzicalupi, A. Bianchi, C. Giorgi, M.-L. Godino-Salido, M.-D. Gutiérrez-Valero, R. Lopez-Garzón and M. Savastano, *J. Am. Chem. Soc.*, 2013, **135**, 102–105.
117 P. Arranz, A. Bianchi, R. Cuesta, C. Giorgi, M. L. Godino, M. D. Gutiérrez, R. López and A. Santiago, *Inorg. Chem.*, 2010, **49**, 9321–9332.
118 M. Melaimi and F. P. Gabbaï, *J. Am. Chem. Soc.*, 2005, **127**, 9680–9681.
119 A. Jeremies, U. Lehmann, S. Gruschinski, F. Schleife, M. Meyer, V. Matulis, O. A. Ivashkevich, M. Handke, K. Stein and B. Kersting, *Inorg. Chem.*, 2015, **54**, 3937–3950.
120 J. Y. C. Lim and P. D. Beer, *Chem*, 2018, **4**, 731–783.
121 G. E. Garrett, E. I. Carrera, D. S. Seferos and M. S. Taylor, *Chem. Commun.*, 2016, **52**, 9881–9884.
122 N. Busschaert, C. Caltagirone, W. Van Rossom and P. A. Gale, *Chem. Rev.*, 2015, **115**, 8038–8155.
123 E. M. Boyle, S. Comby, J. K. Molloy and T. Gunnlaugsson, *J. Org. Chem.*, 2013, **78**, 8312–8319.
124 H. Miyaji, W. Sato and J. L. Sessler, *Angew. Chem. Int. Ed.*, 2000, **39**, 1777–1780.
125 K. K. Y. Yuen and K. A. Jolliffe, *Chem. Commun.*, 2013, **49**, 4824–4826.
126 F. Zapata, A. Caballero, P. Molina, I. Alkorta and J. Elguero, *J. Org. Chem.*, 2014, **79**, 6959–6969.
127 D. Parker, P. K. Senanayake and J. A. G. Williams, *J. Chem. Soc. Perkin Trans. 2*, 1998, 2129–2140.
128 T. Romero, R. A. Orenes, A. Tárraga and P. Molina, *Organometallics*, 2013, **32**, 5740–5753.
129 K. A. Nielsen, J. O. Jeppesen, E. Levillain and J. Becher, *Angew. Chem. Int. Ed.*, 2003, **42**, 187–191.
130 R. Oliveira, S. Groni, C. Fave, M. Branca, F. Mavré, D. Lorcy, M. Fourmigué and B. Schöllhorn, *Phys. Chem. Chem. Phys.*, 2016, **18**, 15867–15873.
131 C. Wang, D. Zhang and D. Zhu, *Langmuir*, 2007, **23**, 1478–1482.
132 Z. Džolić, M. Cametti, A. D. Cort, L. Mandolini and M. Žinić, *Chem. Commun.*, 2007, 3535–3537.
133 Z.-X. Liu, Y. Sun, Y. Feng, H. Chen, Y.-M. He and Q.-H. Fan, *Chem. Commun.*, 2016, **52**, 2269–2272.
134 A. Aydogan, D. J. Coady, V. M. Lynch, A. Akar, M. Marquez, C. W. Bielawski and J. L. Sessler, *Chem. Commun.*, 2008, 1455–1457.
135 P. Sokkalingam, S.-J. Hong, A. Aydogan, J. L. Sessler and C.-H. Lee, *Chem. – Eur. J.*, 2013, **19**, 5860–5867.
136 M. J. Welsh and A. E. Smith, *Cell*, 1993, **73**, 1251–1254.
137 S. E. Lloyd, S. H. S. Pearce, S. E. Fisher, K. Steinmeyer, B. Schwappach, S. J. Scheinman, B. Harding, A. Bolino, M. Devoto, P. Goodyer, S. P. A. Rigden, O. Wrong, T. J. Jentsch, I. W. Craig and R. V. Thakker, *Nature*, 1996, **379**, 445–449.
138 M. Vidal and A. Schmitzer, *Chem. – Eur. J.*, 2014, **20**, 9998–10004.
139 B. Díaz de Greñu, P. I. Hernández, M. Espona, D. Quiñonero, M. E. Light, T. Torroba, R. Pérez-Tomás and R. Quesada, *Chem. – Eur. J.*, 2011, **17**, 14074–14083.
140 A. V. Jentzsch, D. Emery, J. Mareda, S. K. Nayak, P. Metrangolo, G. Resnati, N. Sakai and S. Matile, *Nat. Commun.*, 2012, **3**, 905.
141 A. Vargas Jentzsch and S. Matile, *J. Am. Chem. Soc.*, 2013, **135**, 5302–5303.
142 S. J. Connon, *Chem. – Eur. J.*, 2006, **12**, 5418–5427.
143 T. Weil, M. Kotke, C. M. Kleiner and P. R. Schreiner, *Org. Lett.*, 2008, **10**, 1513–1516.
144 D. Bulfield and S. M. Huber, *Chem. – Eur. J.*, 2016, **22**, 14434–14450.
145 J.-P. Gliese, S. H. Jungbauer and S. M. Huber, *Chem. Commun.*, 2017, **53**, 12052–12055.
146 C. J. Bruns and J. F. Stoddart, *The Nature of the Mechanical Bond: From Molecules to Machines*, John Wiley & Sons, Inc., 2016
147 J. E. M. Lewis, M. Galli and S. M. Goldup, *Chem. Commun.*, 2017, **53**, 298–312.
148 A. M. Albrecht-Gary, Z. Saad, C. O. Dietrich-Buchecker and J. P. Sauvage, *J. Am. Chem. Soc.*, 1985, **107**, 3205–3209.
149 L. D. Movsisyan, D. V. Kondratuk, M. Franz, A. L. Thompson, R. R. Tykwinski and H. L. Anderson, *Org. Lett.*, 2012, **14**, 3424–3426.
150 N. Weisbach, Z. Baranová, S. Gauthier, J. H. Reibenspies and J. A. Gladysz, *Chem. Commun.*, 2012, **48**, 7562–7564.
151 P. Thordarson, E. J. A. Bijsterveld, A. E. Rowan and R. J. M. Nolte, *Nature*, 2003, **424**, 915–918.

152 Y. Matsuoka, Y. Mutoh, I. Azumaya, S. Kikkawa, T. Kasama and S. Saito, *J. Org. Chem.*, 2016, **81**, 3479–3487.
153 G. De Bo, S. Kuschel, D. A. Leigh, B. Lewandowski, M. Papmeyer and J. W. Ward, *J. Am. Chem. Soc.*, 2014, **136**, 5811–5814.
154 A. Caballero, F. Zapata and P. D. Beer, *Coord. Chem. Rev.*, 2013, **257**, 2434–2455.
155 W. Zhou, J. Li, X. He, C. Li, J. Lv, Y. Li, S. Wang, H. Liu and D. Zhu, *Chem. – Eur. J.*, **14**, 754–763.
156 S. Erbas-Cakmak, D. A. Leigh, C. T. McTernan and A. L. Nussbaumer, *Chem. Rev.*, 2015, **115**, 10081–10206.
157 A. Coskun, J. M. Spruell, G. Barin, W. R. Dichtel, A. H. Flood, Y. Y. Botros and J. Fraser Stoddart, *Chem. Soc. Rev.*, 2012, **41**, 4827–4859.
158 X. Yan, F. Wang, B. Zheng and F. Huang, *Chem. Soc. Rev.*, 2012, **41**, 6042–6065.
159 H. Frisch, I. Martin and H. Mark, *Monatshefte Für Chem. Verwandte Teile Anderer Wiss.*, 1953, **84**, 250–256.
160 E. Wasserman, *J. Am. Chem. Soc.*, 1960, **82**, 4433–4434.
161 X. Huang, S. Huang, B. Zhai, Y. Zhang, Y. Xu and Q. Wang, *Tetrahedron Lett.*, 2012, **53**, 6414–6417.
162 S.-Y. Hsueh, J.-L. Ko, C.-C. Lai, Y.-H. Liu, S.-M. Peng and S.-H. Chiu, *Angew. Chem.*, 2011, **123**, 6773–6776.
163 P. R. Aston, P. T. Glink, J. F. Stoddart, P. A. Tasker, A. J. P. White and D. J. Williams, *Chem. – Eur. J.*, 1996, **2**, 729–736.
164 C.-W. Chiu, C.-C. Lai and S.-H. Chiu, *J. Am. Chem. Soc.*, 2007, **129**, 3500–3501.
165 G. M. Hübner, J. Gläser, C. Seel and F. Vögtle, *Angew. Chem. Int. Ed.*, 1999, **38**, 383–386.
166 J. Yin, S. Dasgupta and J. Wu, *Org. Lett.*, 2010, **12**, 1712–1715.
167 A. F. M. Kilbinger, S. J. Cantrill, A. W. Waltman, M. W. Day and R. H. Grubbs, *Angew. Chem. Int. Ed.*, 2003, **42**, 3281–3285.
168 J. S. Hannam, T. J. Kidd, D. A. Leigh and A. J. Wilson, *Org. Lett.*, 2003, **5**, 1907–1910.
169 H. Zheng, Y. Li, C. Zhou, Y. Li, W. Yang, W. Zhou, Z. Zuo and H. Liu, *Chem. – Eur. J.*, 2011, **17**, 2160–2167.
170 C. O. Dietrich-Buchecker and J. P. Sauvage, *Chem. Rev.*, 1987, **87**, 795–810.
171 E. N. Guidry, S. J. Cantrill, J. F. Stoddart and R. H. Grubbs, *Org. Lett.*, 2005, **7**, 2129–2132.
172 C. O. Dietrich-Buchecker, J. P. Sauvage and J. P. Kintzinger, *Tetrahedron Lett.*, 1983, **24**, 5095–5098.
173 C. Hamann, J.-M. Kern and J.-P. Sauvage, *Inorg. Chem.*, 2003, **42**, 1877–1883.
174 S. M. Goldup, D. A. Leigh, P. J. Lusby, R. T. McBurney and A. M. Z. Slawin, *Angew. Chem. Int. Ed.*, 2008, **47**, 6999–7003.
175 A.-M. Fuller, D. A. Leigh, P. J. Lusby, I. D. H. Oswald, S. Parsons and D. B. Walker, *Angew. Chem. Int. Ed.*, 2004, **43**, 3914–3918.
176 C. Lincheneau, B. Jean-Denis and T. Gunnlaugsson, *Chem. Commun.*, 2014, **50**, 2857–2860.
177 G. Zhang, G. Gil-Ramírez, A. Markevicius, C. Browne, I. J. Vitorica-Yrezabal and D. A. Leigh, *J. Am. Chem. Soc.*, 2015, **137**, 10437–10442.
178 G. Gil-Ramírez, S. Hoekman, M. O. Kitching, D. A. Leigh, I. J. Vitorica-Yrezabal and G. Zhang, *J. Am. Chem. Soc.*, 2016, **138**, 13159–13162.
179 S.-T. Tung, C.-C. Lai, Y.-H. Liu, S.-M. Peng and S.-H. Chiu, *Angew. Chem. Int. Ed.*, 2013, **52**, 13269–13272.
180 V. Aucagne, J. Berná, J. D. Crowley, S. M. Goldup, K. D. Hänni, D. A. Leigh, P. J. Lusby, V. E. Ronaldson, A. M. Z. Slawin, A. Viterisi and D. B. Walker, *J. Am. Chem. Soc.*, 2007, **129**, 11950–11963.
181 S. M. Goldup, D. A. Leigh, T. Long, P. R. McGonigal, M. D. Symes and J. Wu, *J. Am. Chem. Soc.*, 2009, **131**, 15924–15929.
182 P. E. Barran, H. L. Cole, S. M. Goldup, D. A. Leigh, P. R. McGonigal, M. D. Symes, J. Wu and M. Zengerle, *Angew. Chem. Int. Ed.*, 2011, **50**, 12280–12284.
183 J. E. M. Lewis, J. Winn and S. M. Goldup, *Molecules*, 2017, **22**, 89.
184 L. D. Movsisyan, M. Franz, F. Hampel, A. L. Thompson, R. R. Tykwinski and H. L. Anderson, *J. Am. Chem. Soc.*, 2016, **138**, 1366–1376.
185 J. Berná, J. D. Crowley, S. M. Goldup, K. D. Hänni, A.-L. Lee and D. A. Leigh, *Angew. Chem. Int. Ed.*, 2007, **46**, 5709–5713.
186 S. M. Goldup, D. A. Leigh, P. J. Lusby, R. T. McBurney and A. M. Z. Slawin, *Angew. Chem. Int. Ed.*, 2008, **47**, 3381–3384.
187 S. M. Goldup, D. A. Leigh, R. T. McBurney, P. R. McGonigal and A. Plant, *Chem. Sci.*, 2010, **1**, 383–386.
188 J. D. Crowley, K. D. Hänni, D. A. Leigh and A. M. Z. Slawin, *J. Am. Chem. Soc.*, 2010, **132**, 5309–5314.
189 A. F. P. Alcântara, L. A. Fontana, V. H. Rigolin, Y. F. S. Andrade, M. A. Ribeiro, W. P. Barros, C. Ornelas and J. D. Megiatto, *Angew. Chem. Int. Ed.*, 2018, **57**, 8979–8983.
190 Y. Tokunaga, M. Kimura, M. Ueda, S. Miyagawa, T. Kawasaki and K. Hisada, *Tetrahedron Lett.*, 2016, **57**, 1120–1123.
191 S.-J. Rao, Q. Zhang, X.-H. Ye, C. Gao and D.-H. Qu, *Chem. – Asian J.*, **13**, 815–821.
192 M. C. T. Fyfe and J. F. Stoddart, *Acc. Chem. Res.*, 1997, **30**, 393–401.
193 A. R. Williams, B. H. Northrop, T. Chang, J. F. Stoddart, A. J. P. White and D. J. Williams, *Angew. Chem. Int. Ed.*, 2006, **45**, 6665–6669.

194 P. R. Ashton, T. T. Goodnow, A. E. Kaifer, M. V. Reddington, A. M. Z. Slawin, N. Spencer, J. F. Stoddart, C. Vicent and D. J. Williams, *Angew. Chem. Int. Ed. Engl.*, 1989, **28**, 1396–1399.

195 M. Asakawa, P. R. Ashton, V. Balzani, A. Credi, C. Hamers, G. Mattersteig, M. Montalti, A. N. Shipway, N. Spencer, J. F. Stoddart, M. S. Tolley, M. Venturi, A. J. P. White and D. J. Williams, *Angew. Chem. Int. Ed.*, 1998, **37**, 333–337.

196 C. A. Hunter, *J. Am. Chem. Soc.*, 1992, **114**, 5303–5311.

197 F. Vögtle, S. Meier and R. Hoss, *Angew. Chem. Int. Ed. Engl.*, 1992, **31**, 1619–1622.

198 F. G. Gatti, D. A. Leigh, S. A. Nepogodiev, A. M. Z. Slawin, S. J. Teat and J. K. Y. Wong, *J. Am. Chem. Soc.*, 2001, **123**, 5983–5989.

199 D. A. Leigh, A. Venturini, A. J. Wilson, J. K. Y. Wong and F. Zerbetto, *Chem. – Eur. J.*, 2004, **10**, 4960–4969.

200 F. B. L. Cougnon, H. Y. Au-Yeung, G. D. Pantoş and J. K. M. Sanders, *J. Am. Chem. Soc.*, 2011, **133**, 3198–3207.

201 E. J. F. Klotz, T. D. W. Claridge and H. L. Anderson, *J. Am. Chem. Soc.*, 2006, **128**, 15374–15375.

202 I. Nierengarten, E. Meichsner, M. Holler, P. Pieper, R. Deschenaux, B. Delavaux-Nicot and J.-F. Nierengarten, *Chem. – Eur. J.*, 2018, **24**, 169–177.

203 P. Ghosh, O. Mermagen and C. A. Schalley, *Chem. Commun.*, 2002, 2628–2629.

204 J. A. Wisner, P. D. Beer and M. G. B. Drew, *Angew. Chem. Int. Ed.*, 2001, **40**, 3606–3609.

205 J. A. Wisner, P. D. Beer, M. G. B. Drew and M. R. Sambrook, *J. Am. Chem. Soc.*, 2002, **124**, 12469–12476.

206 M. R. Sambrook, P. D. Beer, J. A. Wisner, R. L. Paul and A. R. Cowley, *J. Am. Chem. Soc.*, 2004, **126**, 15364–15365.

207 K. M. Mullen, J. Mercurio, C. J. Serpell and P. D. Beer, *Angew. Chem. Int. Ed.*, **48**, 4781–4784.

208 Y. Li, K. M. Mullen, T. D. W. Claridge, P. J. Costa, V. Felix and P. D. Beer, *Chem. Commun.*, 2009, 7134–7136.

209 V. Martí-Centelles and P. D. Beer, *Chem. – Eur. J.*, 2015, **21**, 9397–9404.

210 M. J. Langton and P. D. Beer, *Chem. Commun.*, 2014, **50**, 8124–8127.

211 M. J. Langton, O. A. Blackburn, T. Lang, S. Faulkner and P. D. Beer, *Angew. Chem. Int. Ed.*, 2014, **53**, 11463–11466.

212 A. Brown, K. M. Mullen, J. Ryu, M. J. Chmielewski, S. M. Santos, V. Felix, A. L. Thompson, J. E. Warren, S. I. Pascu and P. D. Beer, *J. Am. Chem. Soc.*, 2009, **131**, 4937–4952.

213 G. T. Spence, N. G. White and P. D. Beer, *Org. Biomol. Chem.*, 2012, **10**, 7282–7291.

214 B. R. Mullaney, A. L. Thompson and P. D. Beer, *Angew. Chem. Int. Ed.*, 2014, **53**, 11458–11462.

215 B. Qiao, Y. Liu, S. Lee, M. Pink and A. H. Flood, *Chem. Commun.*, 2016, **52**, 13675–13678.

216 J. E. M. Lewis, M. Galli and S. M. Goldup, *Chem. Commun.*, 2016, **53**, 298–312.

217 K. Hiratani, M. Kaneyama, Y. Nagawa, E. Koyama and M. Kanesato, *J. Am. Chem. Soc.*, 2004, **126**, 13568–13569.

218 Y. Nagawa, J. Suga, K. Hiratani, E. Koyama and M. Kanesato, *Chem. Commun.*, 2005, 749–751.

219 M. Denis, J. Pancholi, K. Jobe, M. Watkinson and S. M. Goldup, *Angew. Chem. Int. Ed.*, 2018, **57**, 5310–5314.

220 A. Andrievsky, F. Ahuis, J. L. Sessler, F. Vögtle, D. Gudat and M. Moini, *J. Am. Chem. Soc.*, 1998, **120**, 9712–9713.

221 M. K. Chae, J. Suk and K.-S. Jeong, *Tetrahedron Lett.*, 2010, **51**, 4240–4242.

222 M. J. Langton, I. Marques, S. W. Robinson, V. Félix and P. D. Beer, *Chem. – Eur. J.*, 2016, **22**, 185–192.

223 J. Y. C. Lim, I. Marques, V. Félix and P. D. Beer, *Angew. Chem. Int. Ed.*, 2018, **57**, 584–588.

Chapter 2: Halogen Bonding Interlocked Structures for Anion Recognition using Bifunctional Bis-iodotriazole Motifs

2.1 Introduction

In the area of anion supramolecular chemistry there are still relatively few halogen bonding (XB) anion receptors in the literature and fewer still XB interlocked host systems. This chapter aims to investigate novel XB interlocked host systems for anion recognition. Herein, 1,2,3-iodotriazole motifs are utilised for anion binding due to their ease of synthesis, aromatic stability and potent XB interactions with anions.[1] Also, 1,2,3-triazole derivatives are able to perform metal complexation via their N-donors, resulting in the ability to enhance anion binding affinities and generate optical/electrochemical responses as well as facilitate the construction of MIMs via active metal templation. Furthermore, incorporating XB and HB 1,2,3-triazole motifs into different acyclic, cyclic and interlocked structures can potentially generate novel anion hosts with impressive selectivities and affinities.

2.1.1 Bifunctional Properties of 1,2,3-Triazole Derivatives

The 1,2,3-triazole motif is a five-membered heterocycle consisting of two carbon atoms and three nitrogen atoms. Its bifunctional character results from the heterocycle's Lewis basic N-donors for coordination of metals and Lewis acidic HB C-H/ XB C-I donors for anion recognition. Triazole metal chelation can further polarise the HB/XB donor capability towards anion guest species (Figure 2.1).[2]

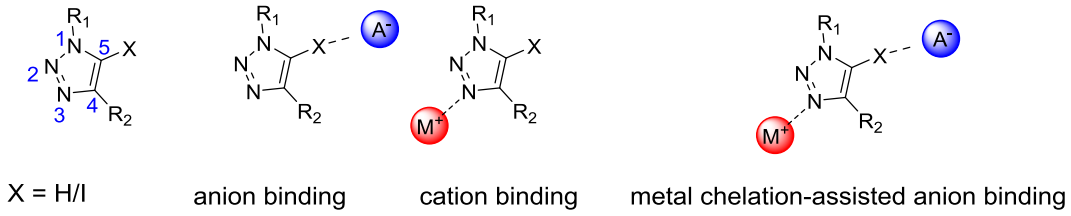


Figure 2.1. Structure and guest binding properties of 1,2,3-triazoles.

The synthesis of 1,2,3-triazoles, the prime example of 'click' reactions,[3,4] can be achieved efficiently through Cu(I)-catalyzed azide–alkyne cycloaddition (CuAAC) under mild conditions. Structurally diverse azide and alkyne functionalised molecules can be used to prepare various triazole derivatives. Importantly, iodotriazoles, which are potent XB donors, can be synthesised through a similar CuAAC reaction to the HB triazole motif by either using an azide and an iodoalkyne, or a straightforward 'one-pot' reaction of an azide and a protoalkyne with an iodine source.[5]

Utilising the lone pair electrons of N^2 and N^3 atoms, triazoles have been widely exploited in transition and lanthanide metal complexation. Compared to the N^2 atom, the N^3 atom is generally considered to have higher electron density, which increases the stability of metal complexation.[6,7] Examples of triazole ligands binding metals are shown in Figure 2.2. An anthracene-appended triazole-containing ligand (Figure 2.2(a)) displays nanomolar affinity for Zn^{2+} under physiological conditions with a turn-on fluorescent response[8] while a 2,6-bis-triazole-pyridine tridentate ligand (Figure 2.2(b)) developed by Flood and co-workers forms metal complexes with Fe(II), Ru(II) and Eu(III) centers.[9] In addition, the tripodal-triazole TBTA ligand (tris(benzyltriazolylmethyl)amine) generates stable complexes with Cu^+ and Cu^{2+} (Figure 2.2(c) and (d)) which facilitates the CuAAC reaction.[10]

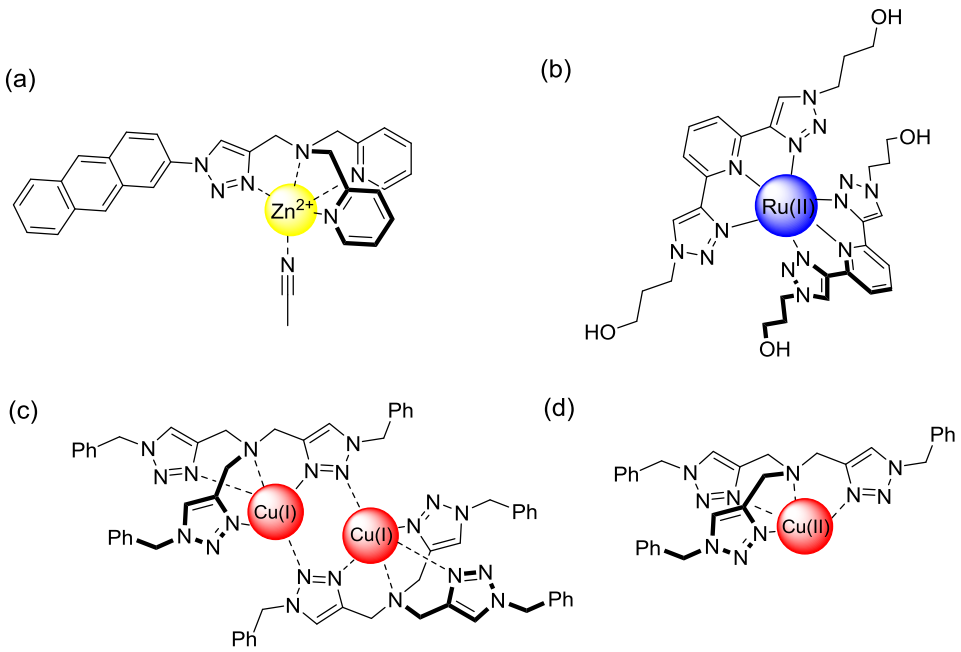


Figure 2.2. (a) A triazole-containing ligand for Zn^{2+} binding;[8] (b) Flood's bis-tridentate pyridyl triazole – Ru(II) complex;[9] (c) Cu(I)-TBTA complex;[10] (d) Cu(II)-TBTA complex.[10]

Anion HB/XB triazole based receptor examples have been discussed in Chapter 1.2, section 1. More recent examples include Beer's XB foldamer capable of selective iodide recognition in $CDCl_3$ (Figure 2.3(a))[11] and Ghosh's XB heteroleptic Ru(II)-containing anion receptor (Figure 2.3(b)) which selectively sensed $H_2PO_4^-$ in CH_3CN with a considerable amplification of the Ru(II) center-based MLCT emission through metal-assisted halogen bonds.[12] In addition, a bimetallic Re(I) bis-iodotriazole pyrimidine derivative (Figure 2.3(c)), synthesised by Beer and co-workers was able to sense halides and sulfate via UV-Vis and MLCT luminescence responses in CH_3CN solution.[13] Schubert and co-workers developed a heteroditopic crown ether-containing iodotriazole macrocycle which was capable of simultaneously binding a sodium cation and iodide anion via crown ether complexed metal assisted XB.[14]

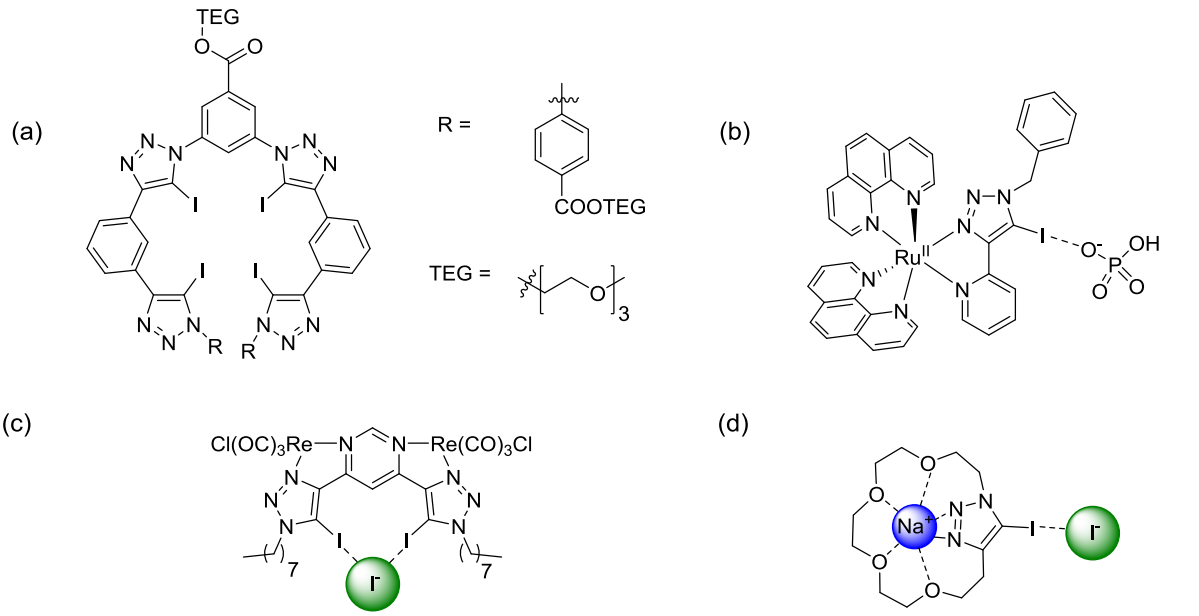


Figure 2.3. (a) Beer's iodotriazole-based XB foldamer for anion recognition;[11] (b) Ghosh's metal-assisted XB receptor for phosphate recognition;[12] (c) Beer's bis-Re(I) bidentate XB receptor;[13] (d) Schubert's XB receptor for cooperative ion-pair recognition.[14]

2.1.2 Active Metal Template Synthesis using Triazole Motifs

The triazole motif has been recently used in the construction of XB interlocked anion receptors via active metal template synthetic methodology.[15,16] Beer and co-workers described a bis-iodotriazole-containing macrocycle component with endo/exo-conformational metal binding capability.[17] The macrocycle was shown to bind Cu(I) endotopically to facilitate rotaxane synthesis via CuAAC iodotriazole axle formation. After removal of the copper catalyst and subsequent coordination to a larger metal, an exotopic Re(I) rotaxane host was isolated which bound halide anions using XB interactions (Figure 2.4).

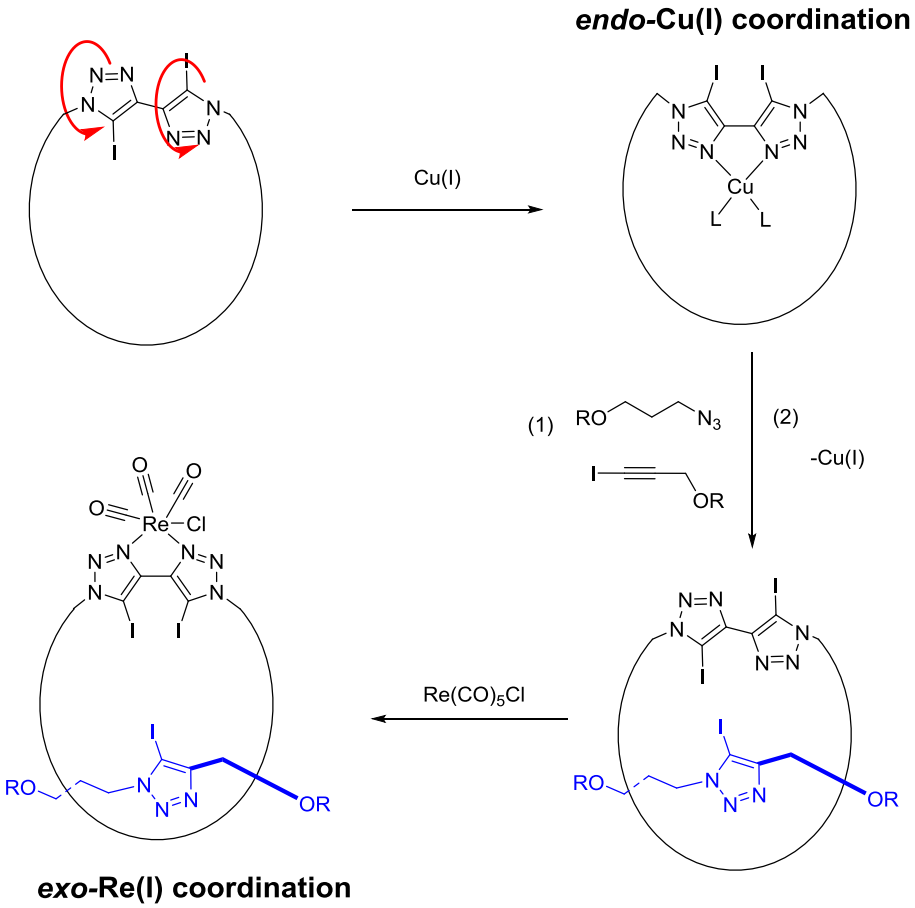


Figure 2.4. Schematic illustration for a XB [2]rotaxane formed by the active metal templation method.[17]

2.1.3 Chapter Aims

The project described in this Chapter focuses on the synthesis and anion binding studies of XB interlocked structures that contain bifunctional bis-iodotriazole motifs. Two research avenues are undertaken:

(1) Building on previous work in the Beer Group, a series of cationic Re(I)-containing XB rotaxane hosts are synthesised using active metal templation and their anion binding properties are investigated by ^{1}H NMR titration experiments.

(2) Switchable XB interlocked hosts capable of metal cation and anion guest binding are constructed whereby the addition of acid attenuates metal coordination to favour strong anion recognition.

2.2 Cationic All-XB Re(I)-Containing Rotaxanes for Anion Recognition†

2.2.1 Design of Target Rotaxanes

In preliminary work, Beer and co-workers reported a neutral Re(I)-containing all-XB rotaxane which showed modest halide binding affinities in $CHCl_3$.[17] In an effort to enhance anion binding strength, the integration of a positively charged moiety into the rotaxane host structure was undertaken. Two approaches were investigated: (a) post-rotaxane alkylation and (b) the AMT synthesis of a novel rotaxane containing a 3,5-bis-iodotriazole-pyridinium axle component (Figure 2.5).

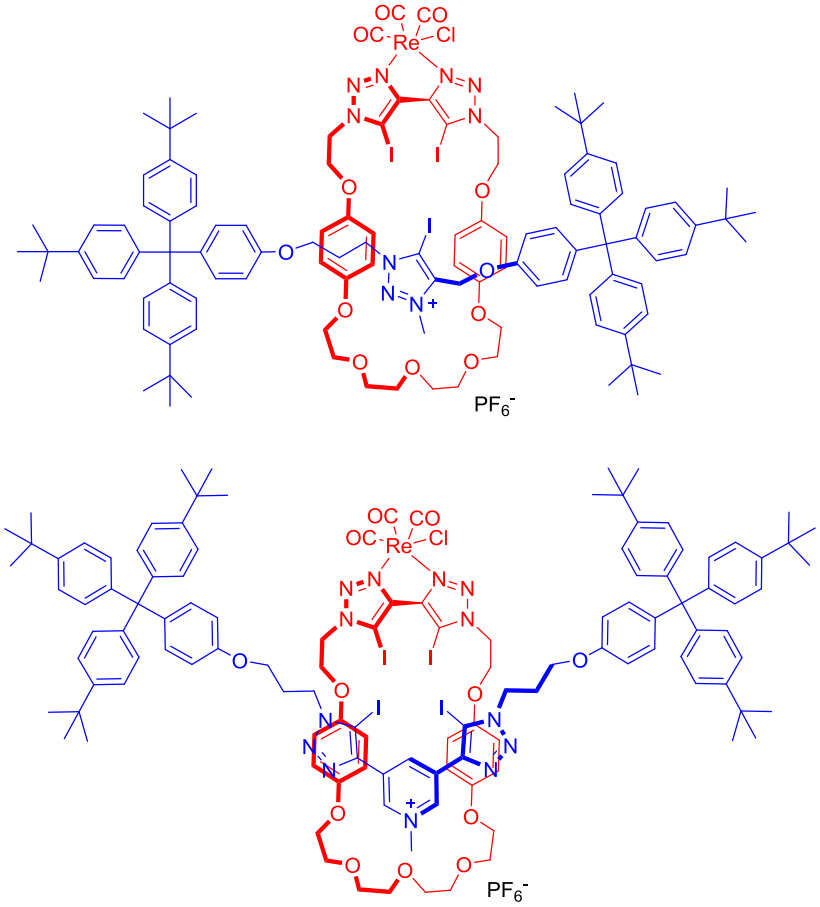


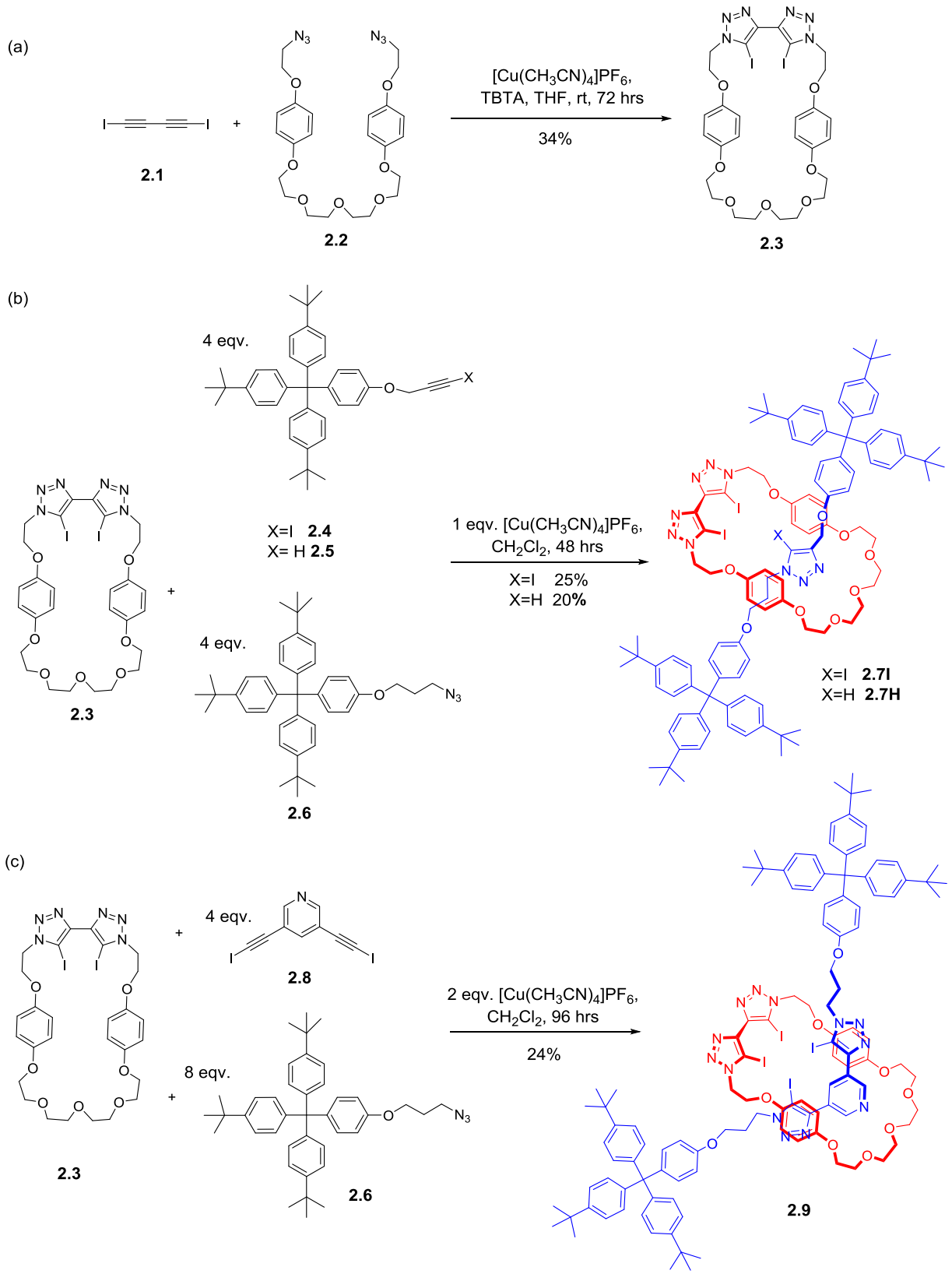
Figure 2.5. Design of target rotaxanes.

2.2.2 Synthesis of Target Rotaxanes

Rotaxane precursor bis-iodotriazole macrocycle **2.3** was synthesised in 34% yield following a literature procedure[17] in which 1,3-bis-iodoalkyne **2.1**[17] was reacted with bis-

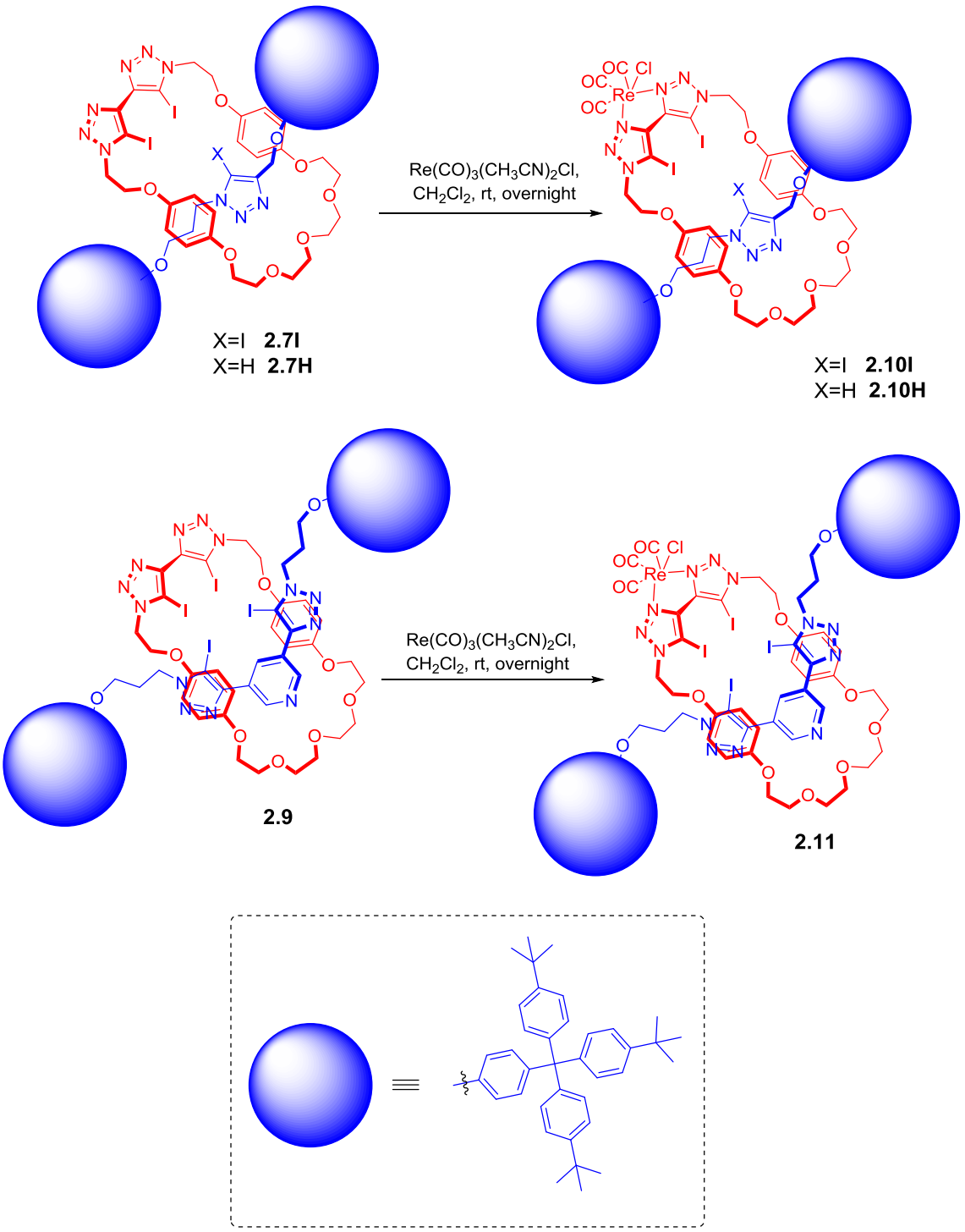
†This work was published as a full paper in Faraday Discussions.
'Cationic all-halogen bonding rotaxanes for halide anion recognition'
X. Li, J. Y. C. Lim and P. D. Beer, *Faraday Discuss.*, **2017**, *203*, 245–255.

azide **2.2**[18] via a click CuAAC ring-closing reaction under high dilution conditions (Scheme 2.1(a)). Following the AMT CuAAC method for MIM formation the macrocycle **2.3** was reacted with four equivalents of stopper iodoalkyne **2.4**[19] or protoalkyne **2.5**[19] and four equivalents of stopper azide **2.6**[20] using one equivalent of $[Cu(CH_3CN)_4]PF_6$ to obtain [2]rotaxanes **2.7I** and **2.7H** in 25% and 20% yield, respectively (Scheme 2.1(b)). Beer and co-workers have previously incorporated the XB 3,5-bis-iodotriazole pyridinium group into the axle component of [2]rotaxanes via an anion templation protocol.[21] Ambitiously, attempts were made to investigate whether the AMT procedure could also be used for axle integration of this potent XB motif. The CuAAC click reaction of reacting one equivalent of macrocycle **2.3** and $[Cu(CH_3CN)_4]PF_6$, four equivalents of 3,5-bis-iodoalkyne pyridine **2.8** [22] and eight equivalents of stopper azide **2.6** in dry degassed CH_2Cl_2, provided the target rotaxane **2.9** in a low yield of 5% which was thought to arise from the large excess of the pyridine-alkyne **2.8** inhibiting the AMT rotaxane forming reaction. An analogous procedure using two equivalents of $[Cu(CH_3CN)_4]PF_6$ increased the yield of rotaxane **2.9** significantly to 24% (Scheme 2.1(c)).



Scheme 2.1. Synthesis of (a) macrocycle **2.3**; (b) rotaxanes **2.7I** and **2.7H**; (c) rotaxane **2.9**.

To achieve Re(I) complexation, a solution of $Re(CO)_5Cl$ in dry CH_3CN was heated under reflux for 3 hrs to obtain $Re(CO_3)_3(CH_3CN)_2Cl$,[23] which was then reacted with rotaxanes **2.7I, 2.7H** and **2.9** in dry CH_2Cl_2 to afford the corresponding Re(I) rotaxanes **2.10I**, **2.10H** and **2.11** (Scheme 2.2). Unfortunately, pure samples of rotaxanes **2.10H** and **2.11** could not be isolated after several attempts by preparative TLC chromatography. The attempted purification of rotaxane **2.10I** by preparative TLC chromatography revealed two distinct products. Mass spectrometry analysis indicated both corresponded to the target rotaxane (m/z = 2380, $[M+H]^+$) as well as a rotaxane with loss of a Cl^- ligand (m/z = 2343, $[M-Cl]^+$). ^1H NMR analysis confirmed the two compounds' different structures as well as an apparent interconversion equilibrium between them. Kinetic studies performed using ^1H NMR spectroscopy in $CDCl_3$ at 298 K revealed that an initially pure solution of either product equilibrated in 20 hrs to give a final equilibrium ratio of [**2.10I**]/[**2.10I-Cl**] = 1:0.4 (Figure 2.6(a)). It is hypothesized that the interconversion may arise from the axle triazole nitrogen atoms displacing Cl^- from the Re(I) centre (Figure 2.6(b)). It is well-known that various *fac*-$[Re^I(L)(CO)_3(phen)]^+$ complexes can be prepared by reacting *fac*-$[Re^I(CO)_3Cl(phen)]$ and nitrogen donor aromatic compounds such as pyridine upon heating (Figure 2.6(c)).[24–26] A similar mechanical bond induced reaction may occur in rotaxane **2.10I** at room temperature due to the proximal nature of the interlocked axle within the macrocycle increasing the axle's triazole effective local concentration to facilitate Cl^- displacement.



Scheme 2.2. Synthesis of Re(I) XB rotaxanes **2.10I**, **2.10H** and **2.11.**

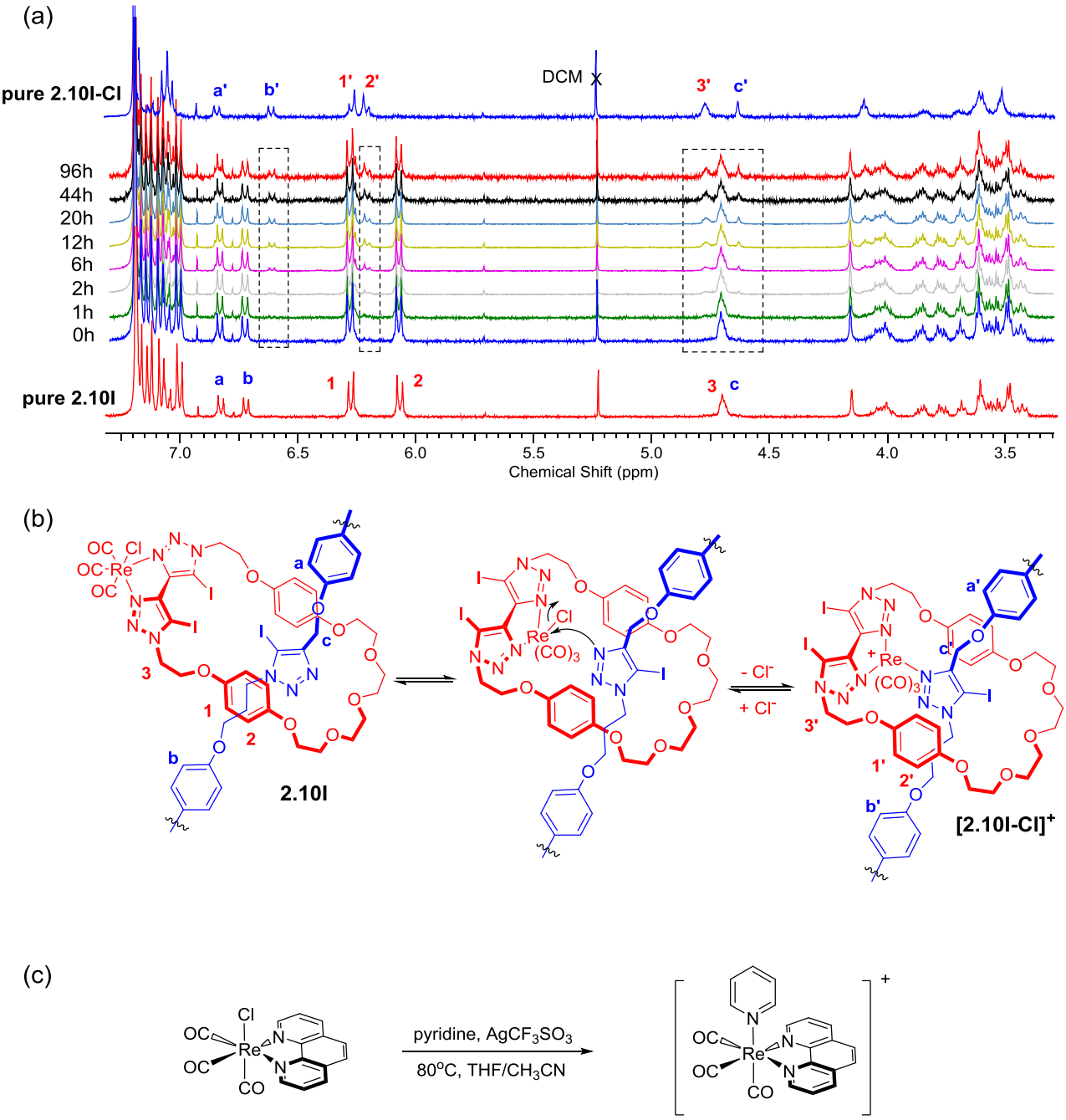
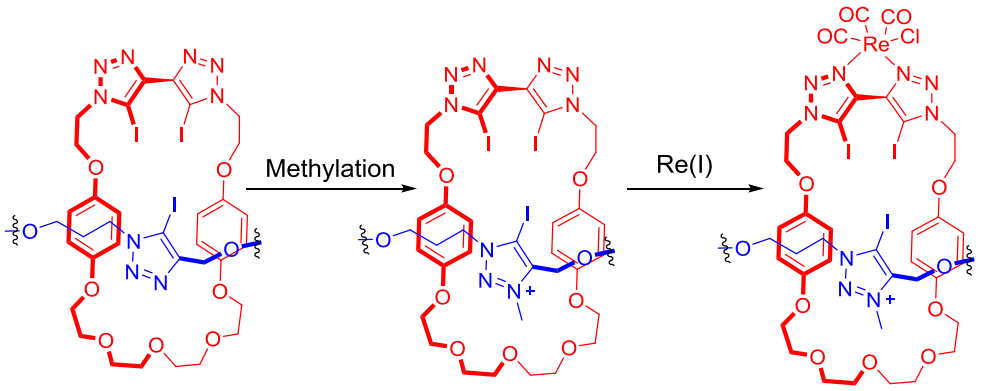


Figure 2.6. (a) Changes in the ^{1}H NMR spectrum of an initial pure solution of **2.10I** in $CDCl_3$ over time. Proton labels in (b) (T = 298 K, [rotaxane] = 3 mM); (b) proposed interconversion mechanism of **2.10I** and [**2.10I**-Cl]; (c) an analogous examples of Re(I) complex reaction.

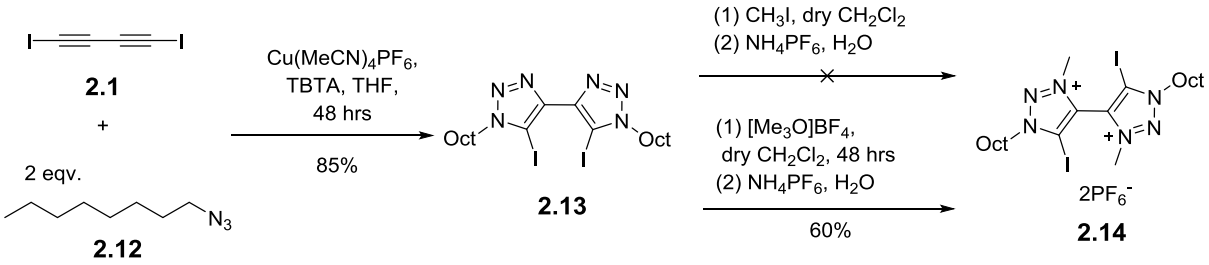
Due to the inherent interconversion equilibrium of Re(I) rotaxane **2.10I** and the difficulties in isolating pure samples of Re(I) rotaxanes **2.10H** and **2.11**, the synthesis of the target interlocked hosts was then attempted by first preparing the monocationic metal-free

rotaxanes before performing Re(I) coordination (Scheme 2.3). It was envisaged that methylation of the axle triazole moiety would negate its coordinating ability.



Scheme 2.3. Alternative synthetic strategy to target monocationic Re(I) XB rotaxanes

Before performing an alkylation reaction on the rotaxane, different methylation agents of varying reactivities were tested to identify one which would selectively methylate the axle's iodotriazole/pyridine motifs but not the macrocycle's bis-triazole group. Test reactions were first conducted on an acyclic compound. The acyclic bis-iodotriazole derivative **2.13** was synthesised using a CuAAC reaction between two equivalents of octyl azide **2.12** [27] and one equivalent of **2.1**. Subsequent methylation was first attempted by stirring **2.13** with excess iodomethane at room temperature. However, no methylated product was observed after a few days. However, when a stronger methylation reagent trimethyloxonium tetrafluoroborate ($[Me_3O]BF_4$) was used, the dicationic bis-iodotriazolium compound **2.14** was obtained in 60% yield after anion exchange to the hexafluorophosphate (PF_6^-) salt (Scheme 2.4).



Scheme 2.4. Synthesis of dicationic bis-iodotriazolium receptor **2.14**.

The addition of one equivalent of TBACl to a $CHCl_3$ solution of **2.14** led to the isolation of crystals of suitable quality for X-ray diffraction structural analysis.[‡] The structure shows Cl^- is binding in a monodentate fashion via XB with one of the two iodotriazolium groups (Figure 2.7). The two iodotriazolium groups are arranged in a divergent anti-parallel conformation and twisted out of the plane relative to each other, possibly as a result of steric hindrance. The bond angle of (C-I)-Cl^- is 179° and the I-Cl^- bond length is 78% of the sum of the van der Waals radii of the two atoms, indicating a strong XB interaction with Cl^-. In contrast, PF_6^- does not show any evidence of coordination to **2.14** in the solid state.

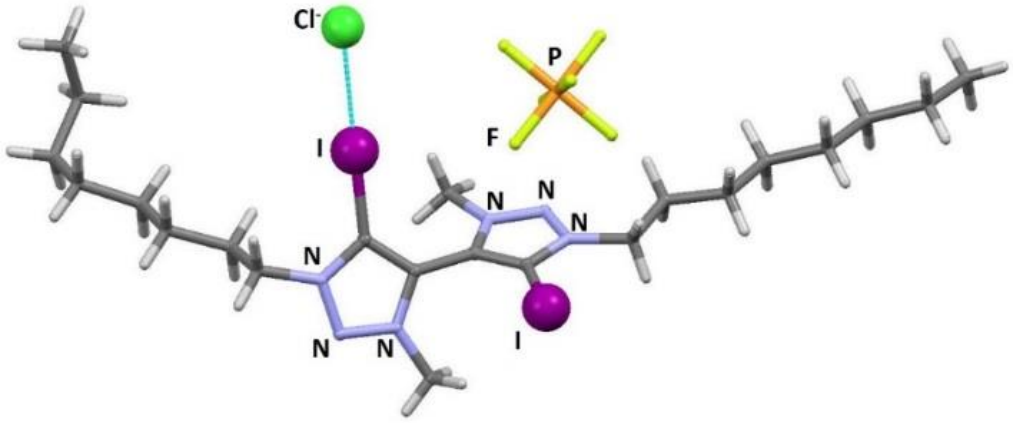
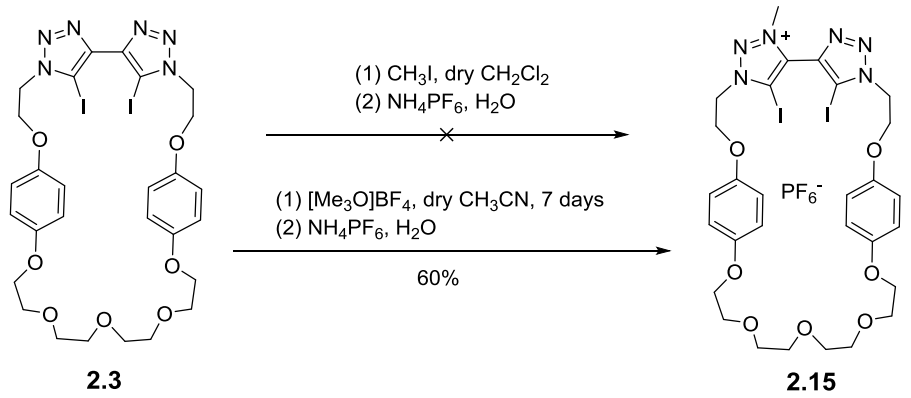


Figure 2.7. Crystal structure of Cl^- bounded **2.14**. XB interaction is shown by the blue dash line.

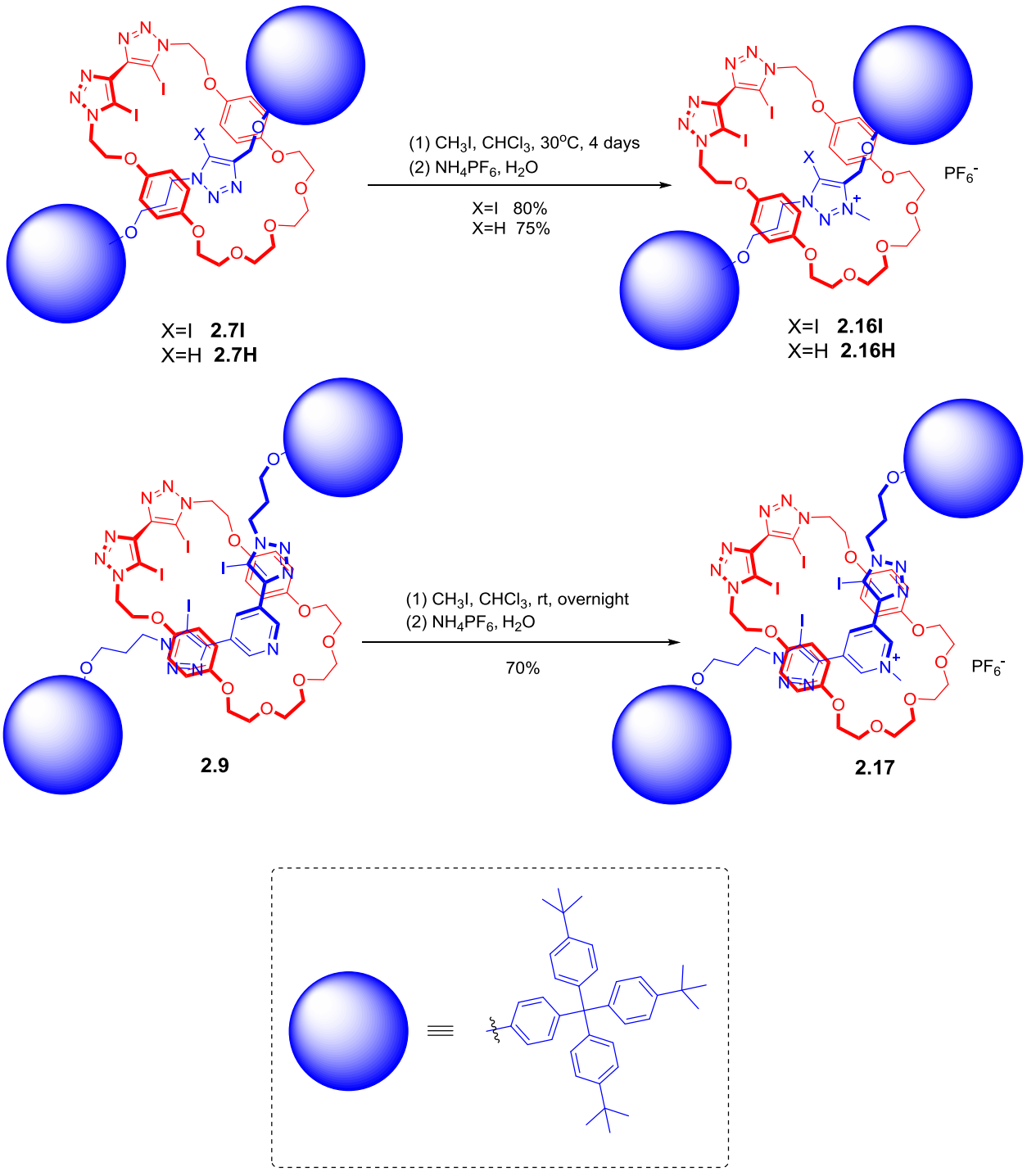
When incorporated into a macrocycle, the bis-iodotriazole motif of **2.3** proved even more unreactive and difficult to methylate. An attempt to alkylate macrocycle **2.3** using $[Me_3O]BF_4$ only afforded the monocationic macrocycle **2.15** (Scheme 2.5) after a continuous reflux over seven days. Compared to the relative ease of formation of the bis-iodotriazolium derivative **2.14**, conformational restrictions in the macrocycle may prevent both triazoles from twisting out of the plane as shown in the crystal structure of **2.14**, with the resulting steric hindrance disfavouring bis-methylation. It is noteworthy that like acyclic compound **2.13**, the macrocycle **2.3** could not be methylated with iodomethane.

[‡] Corresponding crystal data was collected and solved by Dr. Jason Lim.



Scheme 2.5. Synthesis of monocationic macrocycle **2.15**.

Taking into account the above, an attempt to selectively methylate the axle triazole or pyridine group of the respective rotaxane using iodomethane was undertaken (Scheme 2.6). Rotaxanes **2.7I** and **2.7H** were each stirred with excess iodomethane in $CHCl_3$ at 40^oC for 4 days, followed by purification by preparative TLC, and anion exchange to the PF_6^- salt to afford monocationic rotaxanes **2.16I** and **2.16H** in 80% and 75% yield respectively. Using a similar method, monocationic rotaxane **2.17** was obtained in 70% isolated yield by stirring rotaxane **2.9** with an excess of iodomethane in $CHCl_3$ at room temperature overnight. Mass spectrometry confirmed that the products were the desired monocationic species and additional evidence proving selective alkylation of the axles was also observed in the ^1H NMR spectra of the rotaxanes. As shown in Figure 2.8(a), the signal of axle triazolium proton H_a of rotaxane **2.16H** exhibited a large downfield shift from 7.79 ppm (before alkylation) to 8.38 ppm. Also, the signals of adjacent protons H_d and H_e moved downfield, while macrocycle protons H_3 and H_4 scarcely moved, indicating that the axle and not the macrocycle was alkylated. For rotaxane **2.17**, alkylation of the pyridine moiety caused an upfield signal shift of the internal proton H_b, while the iodotriazole proximal methylene proton H_d moved downfield (Figure 2.8(b)).



Scheme 2.6. Synthesis of monocationic rotaxane **2.9I.PF$_6$**, **2.9H.PF$_6$** and **2.17**

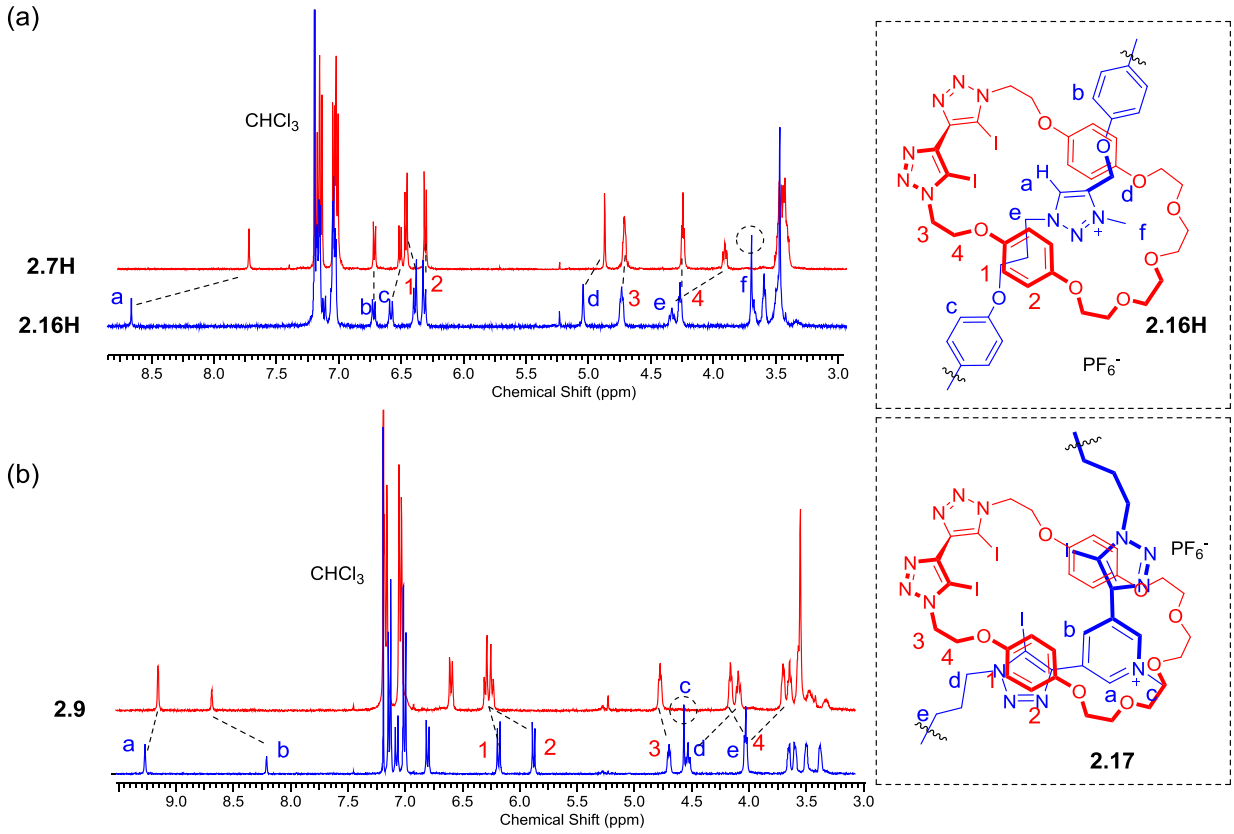
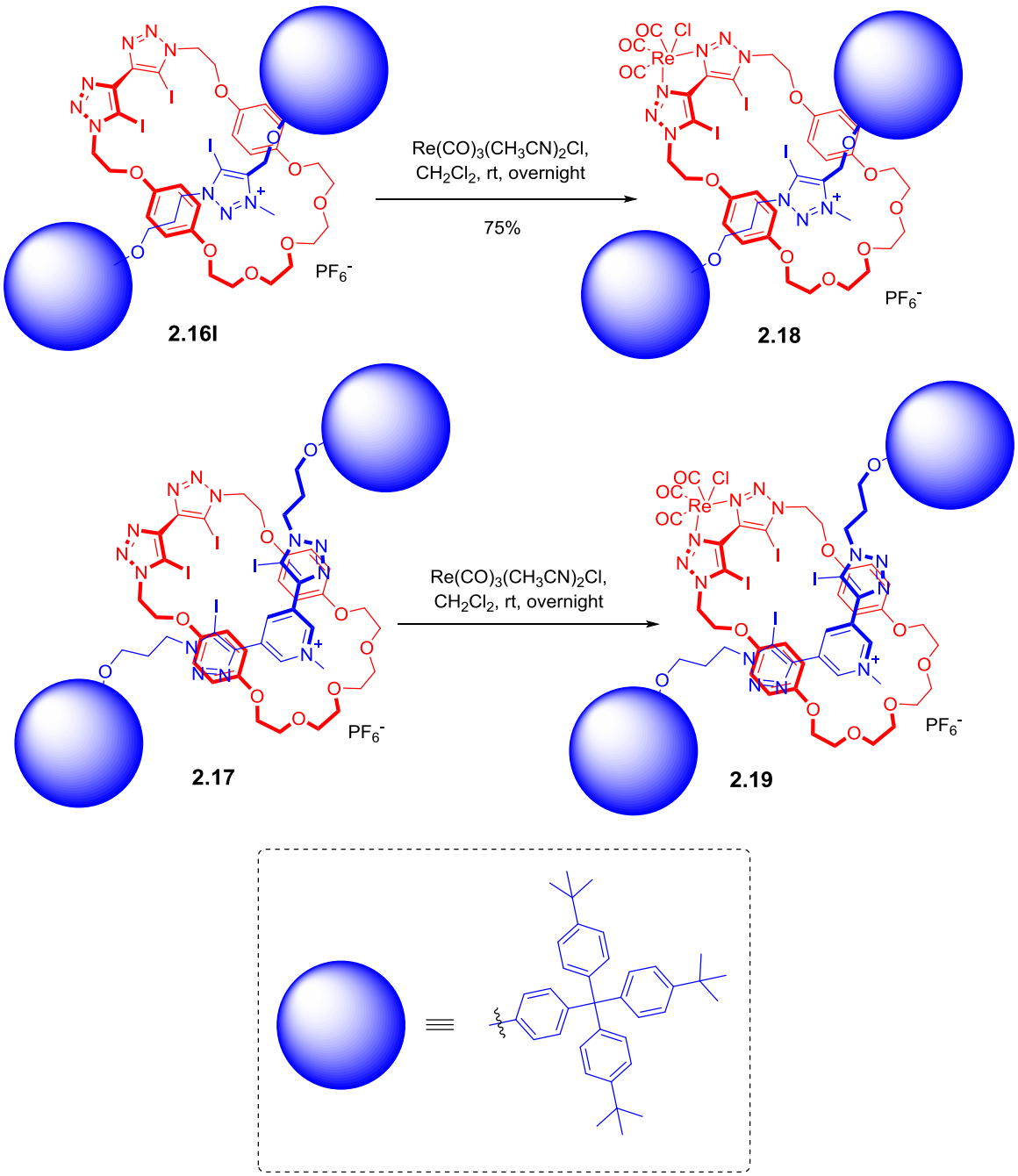


Figure 2.8. (a) Partial ^{1}H NMR spectra of neutral rotaxane **2.7H** and monocationic rotaxane **2.16H**; (b) partial ^{1}H NMR spectra of neutral rotaxane **2.9** and monocationic rotaxane **2.17**.

After the successful selective methylation of the axles of the rotaxanes, reaction with one equivalent of $Re(CO_3)_3(CH_3CN)_2Cl$ in CH_2Cl_2 afforded the corresponding Re(I)-complexed XB rotaxanes **2.18** and **2.19**, respectively (Scheme 2.7). Rotaxane **2.19** however was found to be unstable in solution at room temperature, decomposing to several unknown species in 24 hrs, which could not be identified by ESI-MS and ^{1}H NMR spectroscopy. In contrast, **2.18** was found to be stable in solution for over a week with no decomposition observed.



Scheme 2.7. Synthesis of monocationic Re(I)-containing all XB rotaxanes **2.18** and **2.19**.

A comparison of the ^{1}H NMR spectra of the Re-complexed rotaxane **2.18** with metal free rotaxane (Figure 2.9) reveals the H_3 signal to move downfield while H_4, which is not directly bonded to the bis-iodotriazole motif, only showed slight shifts. In addition, signals arising from macrocycle hydroquinone protons H_1 and H_2 exhibited larger splittings and axle protons H_a, H_b, H_c and H_d moved downfield indicating that the conformation of the rotaxane was perturbed upon Re(I) complexation.

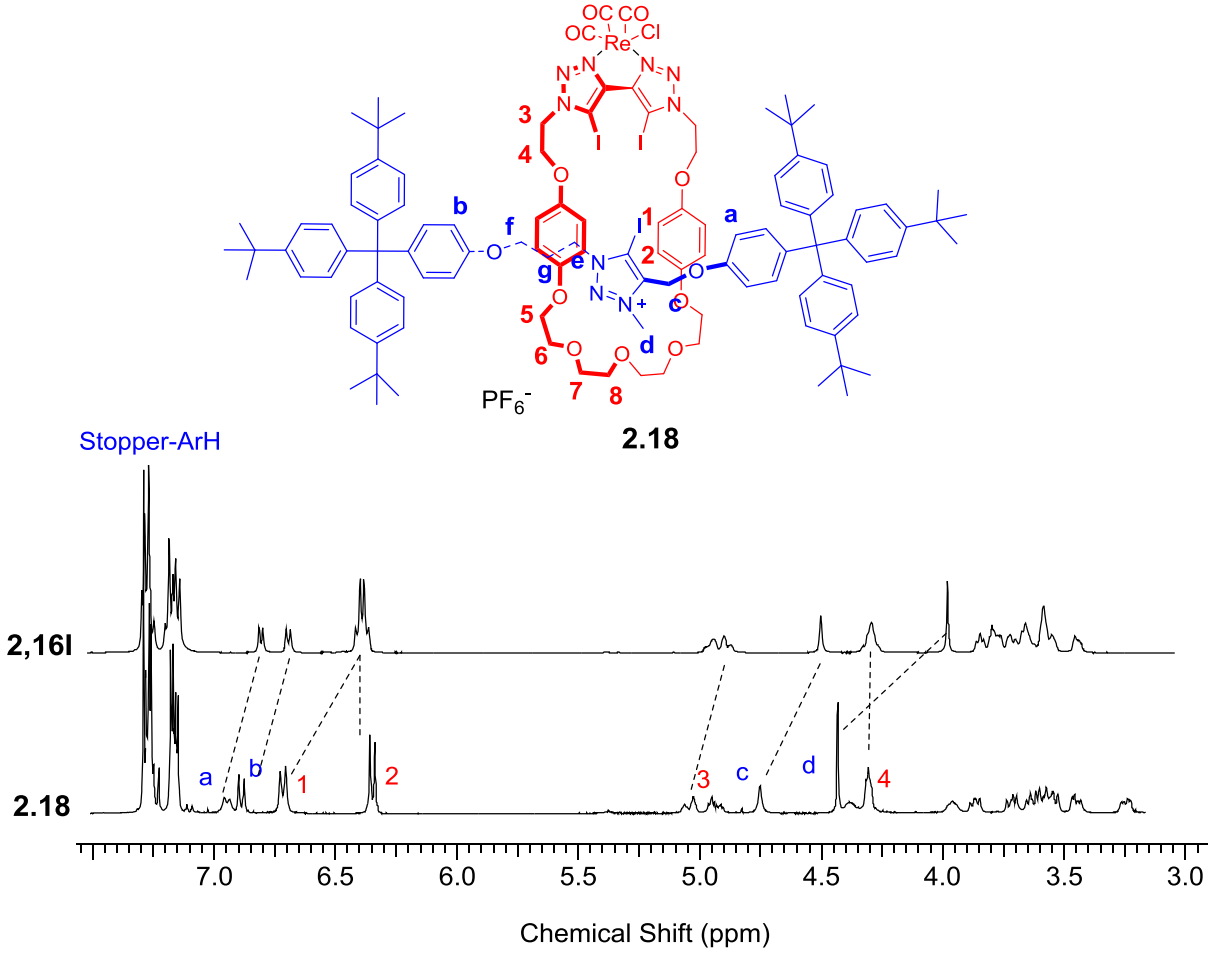


Figure 2.9. ^{1}H NMR comparison between rotaxane **2.16I** and **2.18**.

2.2.3 Anion Binding Studies

Halide and oxoanion binding studies were performed using ^{1}H NMR titration experiments by adding increasing quantities of anions, as their tetrabutylammonium (TBA) salts, to separate solutions of the host rotaxanes **2.16I**, **2.17** and **2.18** in d_6-acetone/D_2O (9:1 *v/v*), whereupon notable proton signal pertubations were observed with the heavier halides. For example, during the I^- titration with rotaxane **2.16I**, the axle triazolium methyl protons (H_d) and macrocycle methylene proton H_3 moved upfield, together with stopper protons H_a and H_b proximal to the interlocked anion binding cavity. In contrast, downfield shifts were observed for H_c on the axle immediately adjacent to the iodotriazolium group (Figure 2.10(a)). This suggests that halide anion binding may be occurring slightly above the plane of the macrocycle. Analogous titrations with Br^- elicited similar perturbations of the

rotaxane's proton signals, although they were of smaller magnitude. In contrast, no significant shifts were observed on addition of Cl^-, SO_4^{2-} and acetate indicating that these anions are not bound by the rotaxane, presumably due to their stronger hydration energy, and in the case of the oxoanions being too large to be encapsulated within the interlocked host cavity. As for the cationic Re(I)-rotaxane **2.18**, the addition of Br^- induced similar proton signal perturbations to **2.16I**, however, very small shifts were noted on addition of I^-, Cl^- and the oxoanions indicative of very weak association. When rotaxane **2.17** was titrated with TBAI, significant downfield shifts were seen for the internal pyridinium proton H_b, while the external proton H_a showed negligible shifts (Figure 2.10(b)), implying that the I^- is bound predominantly in the space flanked by both iodotriazole groups on the axle. Br^- and Cl^- elicited smaller shifts, while acetate and SO_4^{2-} showed no evidence of binding, presumably due to their poor size and shape complementarity with the interlocked cavity of the rotaxane. Monitoring ^{1}H NMR shifts of the iodotriazolium *N*-methyl proton H_d on the axle for rotaxanes **2.16I** and **2.18**, and pyridinium axle proton H_b of **2.17**, non-linear regression analysis of the titration data (Figure 2.11) using the WinEQNMR2 [28] software, determined 1:1 host/guest stoichiometric association constants (Table 2.1).

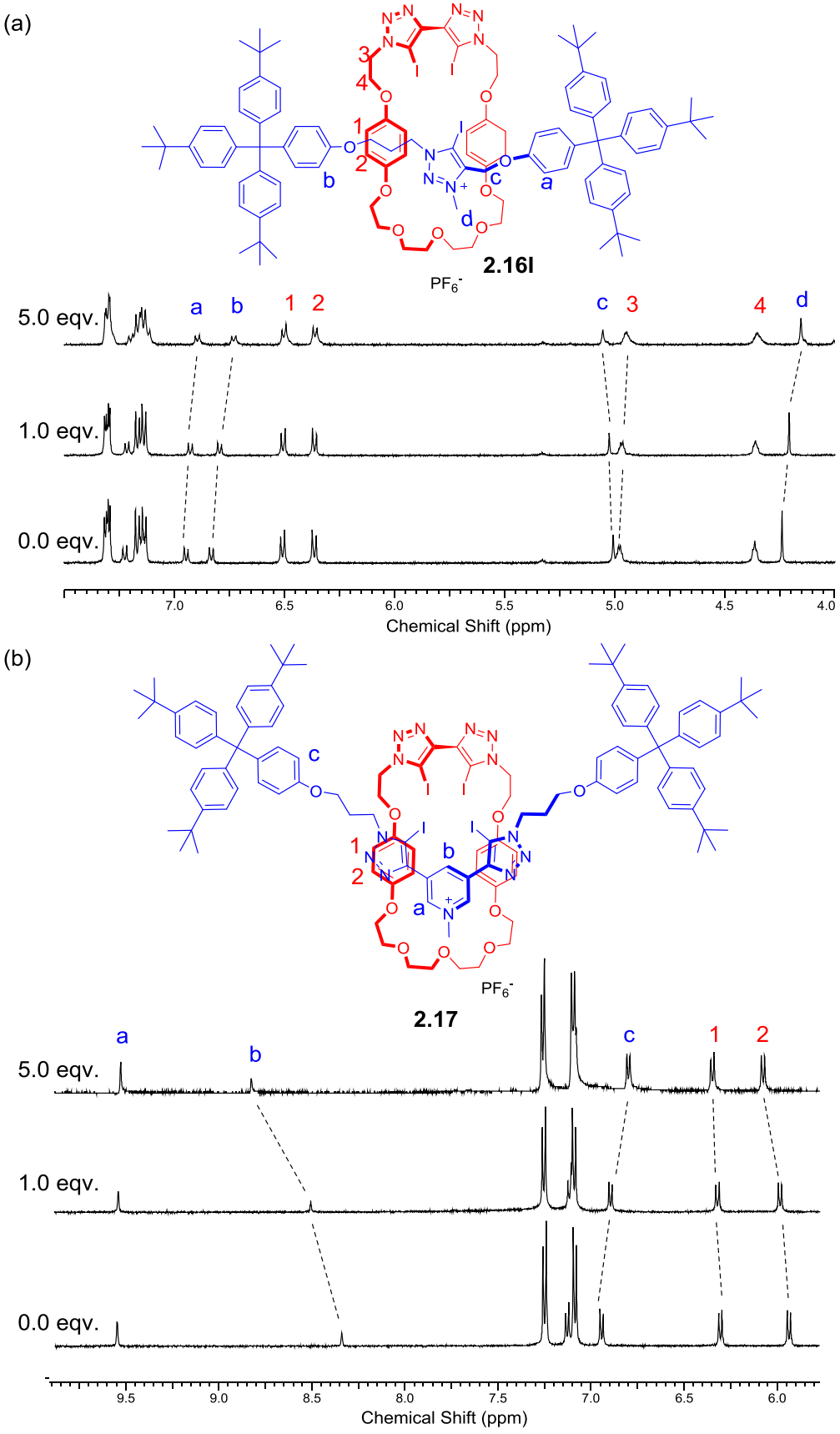


Figure 2.10. ^{1}H NMR of cationic rotaxane (a) **2.16I**; (b) **2.17** with 5.0, 1.0, 0.0 equivalents of TBAI present. (d_6-acetone/D_2O = 9:1 *v*/*v*, *T* = 298 K, [host] = 1.0 mM).

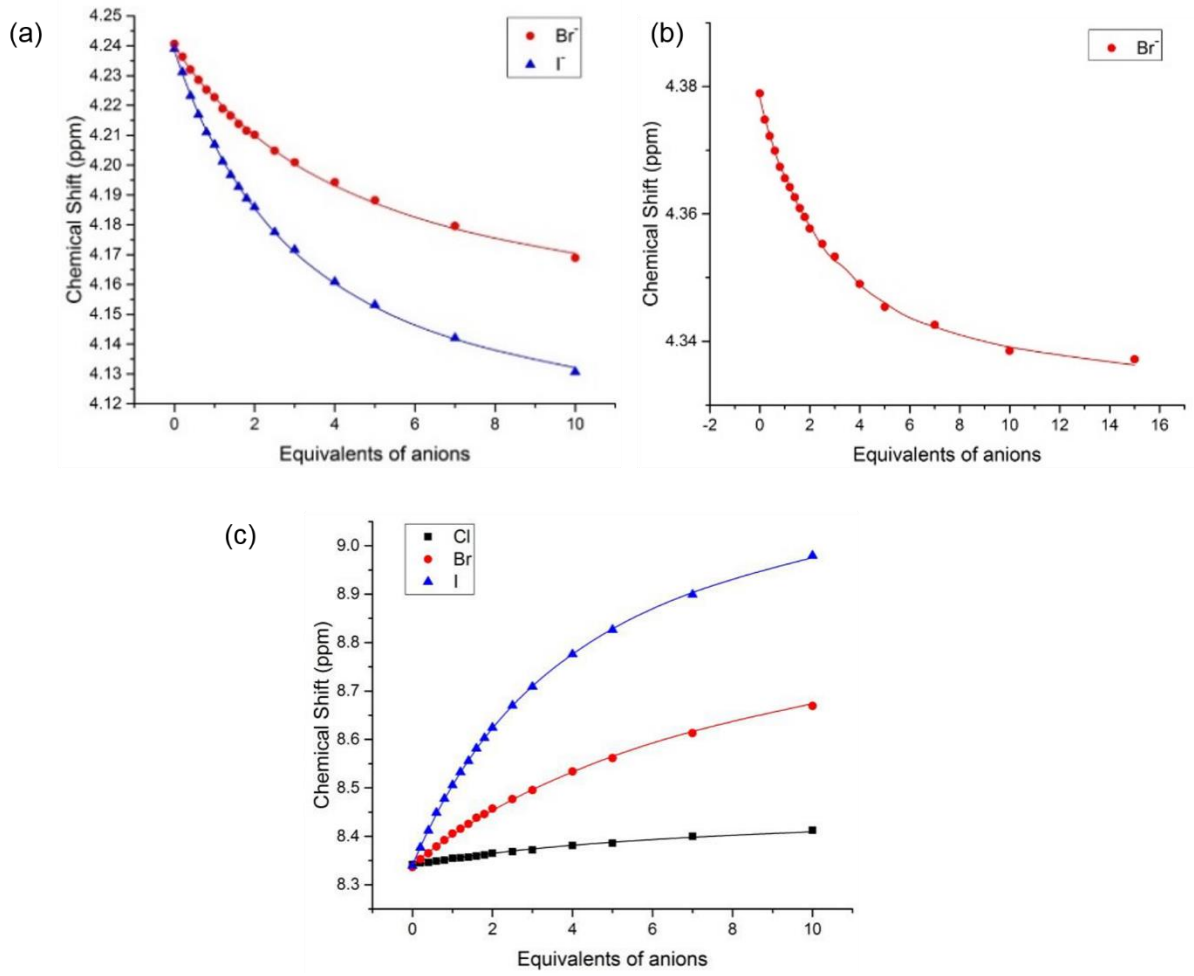


Figure 2.11. Binding isotherms of anion titrations for cationic rotaxane (a) **2.16I**, (b) **2.18** and (c) **2.17** with different halide anions. The chemical shifts of corresponding protons in different rotaxanes (H_d in rotaxane **2.16I** and **2.18**, H_b in rotaxane **2.17**) were plotted as a function of equivalents of TBA salts added. (d_6-acteone/D_2O = 9:1 *v*/*v*, *T* = 298 K, [host] = 1.0 mM).

Table 2.1. Association constants, K_a (M^{-1}), for cationic **2.16I**, **2.18** and **2.17** with various halide anions[a]

Rotaxane	K_a/M^{-1}		
	Cl^-	Br^-	I^-
2.16I	-[b]	236(16)	377(3)
2.18	-[b]	436(25)	-[b]
2.17	112(4)	94(4)	256(5)

[a] Anions added as their TBA salts, solvent: d_6-acteone/D_2O = 9:1 *v*/*v*, *T* = 298 K. The errors associated with each (< 10%) are quoted in parentheses. SO_4^{2-} and acetate did not bind to any of the rotaxanes investigated.
[b]Signal shifts too small for association constant determination suggesting very weak binding.

In the aqueous solvent mixture of d_6-acetone/D_2O 9:1 v/v, rotaxane **2.16I** exhibits the largest binding affinity towards I^-, which is the least hydrated halide. In stark contrast, Re(I)-rotaxane **2.18** exclusively recognises Br^- while exhibiting no binding of Cl^- and I^-. Importantly, this result indicates that a preorganised interlocked XB host cavity of complementary size for Br^- in rotaxane **2.18** was achieved due to exotopic Re(I) metal complexation of the macrocycle component of the metal-free rotaxane **2.16I**. Also, metal complexation results in greater metal-chelated iodotriazole polarisation, leading to a notably enhanced Br^- association constant value of K_a = 436 M^{-1} with Re(I)-rotaxane **2.18** compared to K_a = 236 M^{-1} with **2.16I**. Rotaxane **2.17** shows weaker Br^- and I^- binding affinities compared to **2.16I** in spite of the presence of its greater number of XB-donor iodotriazole groups. This may be attributed to additional steric hindrance of a more spatially restricted binding site due to greater numbers of bulky iodine atoms. Also, compared to the iodotriazolium functionalised axle component of **2.16I**, the pyridinium-3,5-bis(iodotriazole) motif on the axle of **2.17** potentially reduces electrophilicity, resulting in weaker XB donor ability.

Nevertheless, from the contrasting halide selectivity trend of **2.17** ($I^- > Cl^- > Br^-$) with the Hofmeister halide selectivity preference of **2.16I**, the importance of host-guest geometric complementarity can be clearly seen. In particular, the influence of complementarity is demonstrated by comparing the Cl^- binding behaviours of rotaxanes **2.16I** and **2.17**. In spite of the tightly-bound hydration shell of Cl^-, the interlocked XB binding site cavity of **2.17** is able to compete and bind Cl^- more strongly than Br^-. It is noteworthy that Re(I)-rotaxane **2.18** displays no Cl^- binding affinity which suggests that in order to effectively bind highly-hydrated anions, binding site structural preorganisation needs to be allied to an optimal host-guest geometric complementarity.

2.3 Re(I)-bis-iodotriazole-amine based XB Anion Receptor

2.3.1 Design of Target Receptors

In the previous section, 2.2, bidentate bis-triazole Re(I) metal coordination was shown to enhance the anion binding affinities of XB rotaxanes by preorganization and polarization. As a continuation of this work, a novel bis-iodotriazole secondary amine motif was designed for coordination to Re(I) in a tridentate fashion and subsequent XB anion recognition studies (Figure 2.12).

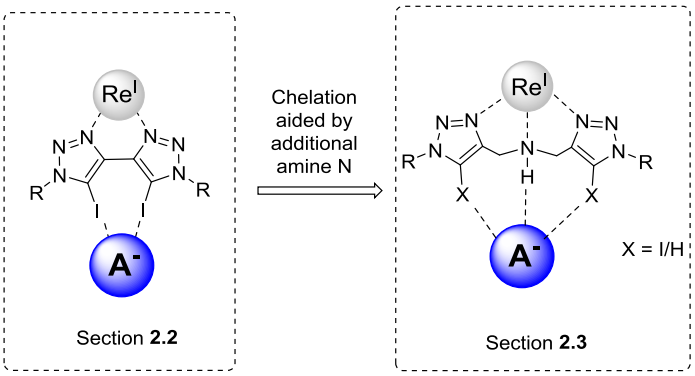
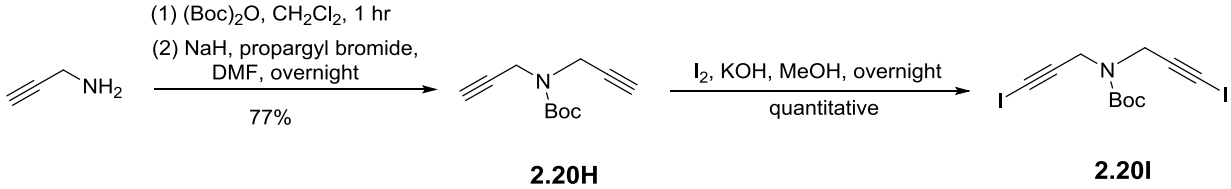


Figure 2.12. Design of the Re(I)-containing bis-triazole-amine anion receptors.

2.3.2 Synthesis and Anion Recognition Properties of Acyclic Systems

2.3.2.1 Synthesis and Characterisation

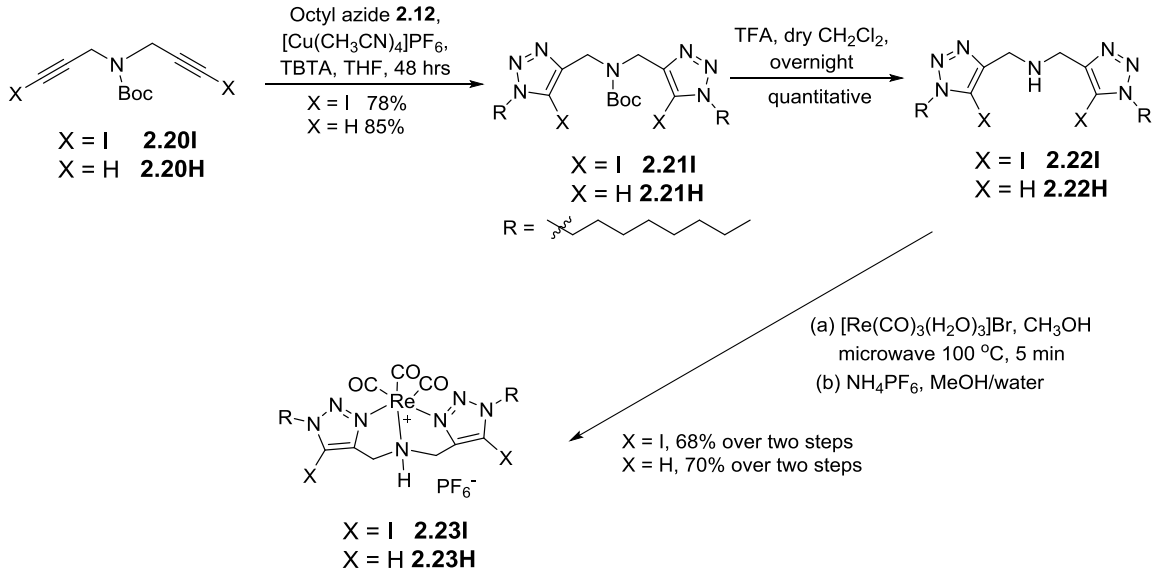
Initially acyclic systems were synthesised and investigated for their anion binding properties. Propargyl amine was protected using $(Boc)_2O$ and then reacted with propargyl bromide under basic conditions to afford *N*-Boc-protected bis-alkyne **2.20H** in 77% yield.[29] Iodination of **2.20H** using I_2 and KOH in MeOH afforded *N*-Boc-protected bis-iodoalkyne **2.20I** in quantitative yield (Scheme 2.8).



2.20H **2.20I**

Scheme 2.8. Synthesis of *N*-Boc-protected bis-iodoalkyne **2.20I**.

2.20H and **2.20I** were then reacted with two equivalents of octyl azide **2.12** under CuAAC conditions to afford the *N*-Boc-protected bis-triazole **2.21H** and bis-iodotriazole **2.21I** in 85% and 78% yield, respectively. Quantitative deprotection using trifluoroacetic acid (TFA) in CH_2Cl_2 gave bis-triazole-amine **2.22H** and bis-iodotriazole-amine **2.22I**. Complexation reactions with $[Re(CO)_3(H_2O)_3]Br$ [30,31] in CH_3OH under microwave reaction conditions followed by anion exchange to the PF_6^- salts afforded the Re(I) monocationic receptors **2.23H** in 70% yield and **2.23I** in 68% yield (Scheme 2.9).



Scheme 2.9. Synthesis of Re(I) monocationic receptor **2.23I** and **2.23H**

Both Re(I) receptors were characterised by ^1H and ^{13}C NMR and high-resolution mass spectrometry (HRMS). The ^1H NMR spectrum and HRMS spectrum of **2.23I** are shown in Figure 2.13(a)-(b). Facial complexation with Re(I) is evident from the desymmetrisation and signal splitting observed for diastereotopic protons H_a and H_b.[32] In addition, the coordination geometry is conclusively proven by the solid state structure of **2.23I** (Figure 2.13(c)). Slow evaporation of a methanol solution of **2.23I** afforded colourless single crystals of suitable quality for X-ray structure determination.[¥] The structure exhibits a facial metal coordination pattern via two N^3 donor atoms of the iodotriazole heterocycles, one N atom of the secondary amine and three carbonyl groups, resulting in different chemical environments for H_a and H_b.

[¥] X-ray structural data was collected and solved by Dr. Jason Lim.

In addition, strong XB interactions between **2.23I$^+$** and PF_6^- are shown: the bond angle of (C-I)-F is 172^o and the bond length is 86% of the sum of van der Waals radii. Also, HB interactions between the secondary amine protons and PF_6^- are observed. Due to the facial coordination geometry, the two bulky iodine atoms of the iodotriazoles and the acidic amine proton all point in different directions, preventing **2.23I$^+$** from interacting with the same PF_6^- using convergent XB and HB interactions, whilst allowing adjacent **2.23I$^+$** molecules to be linked by PF_6^- anions using various XB and HB interactions. Compared to the solid state structure of bis-iodotriazolium compound **2.14** which shows no PF_6^- coordination, the strong XB interactions between **2.23I$^+$** and PF_6^- indicate that Re(I) complexation is able to enhance the potency of XB for anion binding by strongly polarising the coordinating iodotriazoles. Unfortunately, compound **2.23I$^+$** did not exhibit any luminescence and obvious MLCT bands in its UV-Vis spectrum.

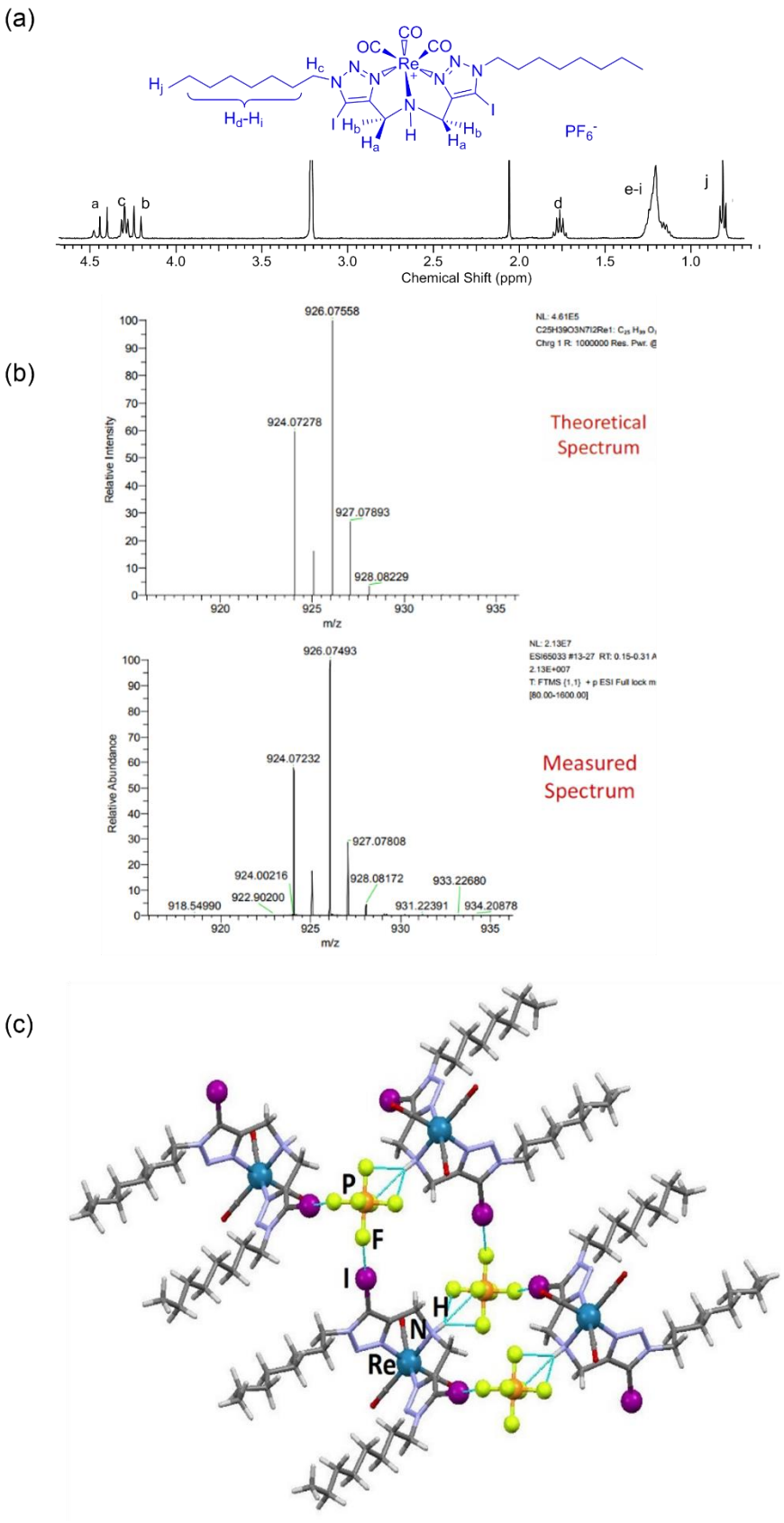


Figure 2.13. Characterisation of **2.23I**: (a) ^{1}H NMR spectrum in CD_3OD; (b) high-resolution mass spectrometry (up: theoretical spectrum and down: measured spectrum); (c) solid state structure (XB interactions between I atoms and F atoms are shown as purple dash lines; HB interactions between amine H atoms and F atoms are shown as blue dash lines.)

2.3.2.2 Anion Binding Studies

Preliminary anion binding studies of **2.23I** and **2.23H** were performed by ^{1}H NMR titrations in CD_3CN. For **2.23I**, upon addition of TBA acetate, the amine proton H_a signal exhibited a large downfield shift (Figure 2.14(a)) while other anions such as Cl^-, Br^-, HSO_4^- caused smaller Δδppm perturbations. Similar downfield shifts of amine proton H_b of **2.23H** were displayed upon anion addition while triazole proton H_a exhibited negligible movement indicating that anion binding was predominantly occurring via HB interactions with the amine proton (Figure 2.14(b)). This may stem from the facial Re(I) coordination geometry which prevents the triazole protons and amine proton of **2.23H** binding anions in a cooperative manner. Monitoring the receptors' amine proton, the anion titration binding isotherm data (Figure 2.15) was subjected to WinEQNMR2[28] software analysis and 1:1 host/guest stoichiometric association constants are reported in Table 2.2. The XB receptor **2.23I** binds acetate strongly, followed by $Br^- > I^- > HSO_4^-$ while **2.23H** shows binding affinities following the trend of anion basicity ($Cl^- > Br^- > HSO_4^- > I^-$). Notably, compared to **2.23H**, the XB analogue **2.23I** exhibits stronger I^-, comparable Br^- binding affinity and weaker binding of HSO_4^-. The combination of Re(I)-assisted XB as well as HB interactions between the acidic amine proton and anions, accounts for the contrasting anion binding properties compared to **2.23H**.

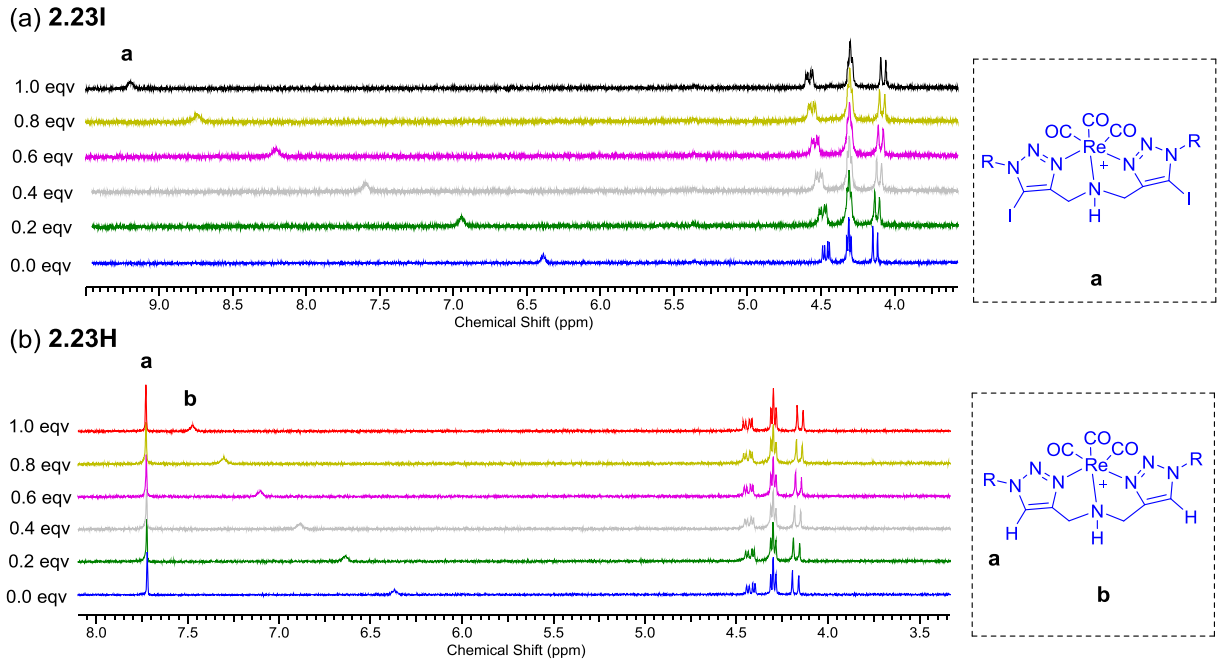


Figure 2.14. ^{1}H NMR titration of (a) **2.23I**; (b) **2.23H** with increasing amount of acetate anion (CD_3CN, *T* = 298 K, [host] = 1.0 mM).

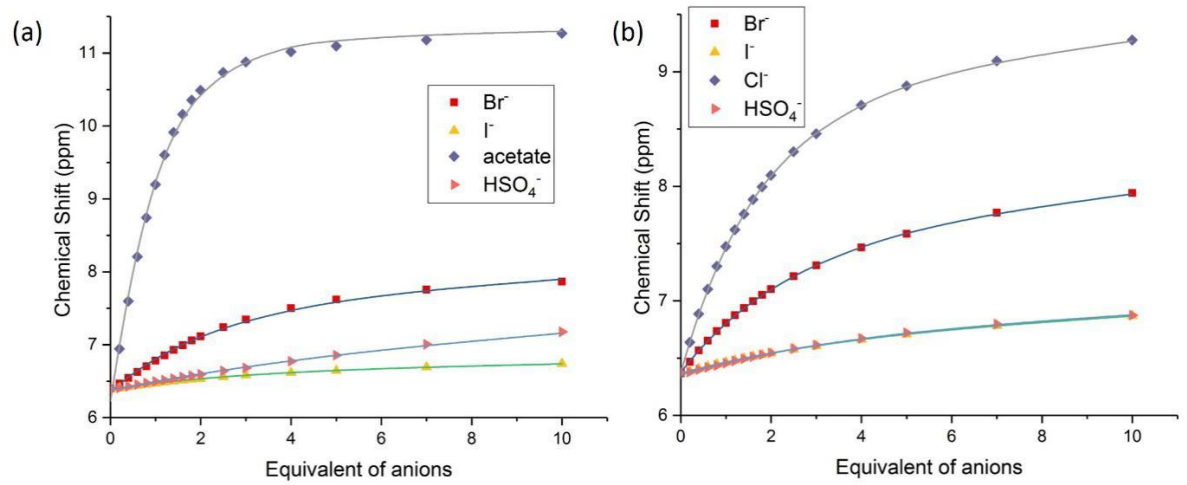


Figure 2.15. Binding isotherms of anion titrations for monocationic Re(I)-containing receptor (a) **2.23I** and (b) **2.23H** with different anions. The chemical shift of the amine proton is plotted as a function of equivalents of TBA salts added (CD_3CN, *T* = 298 K, [host] = 1.0 mM).

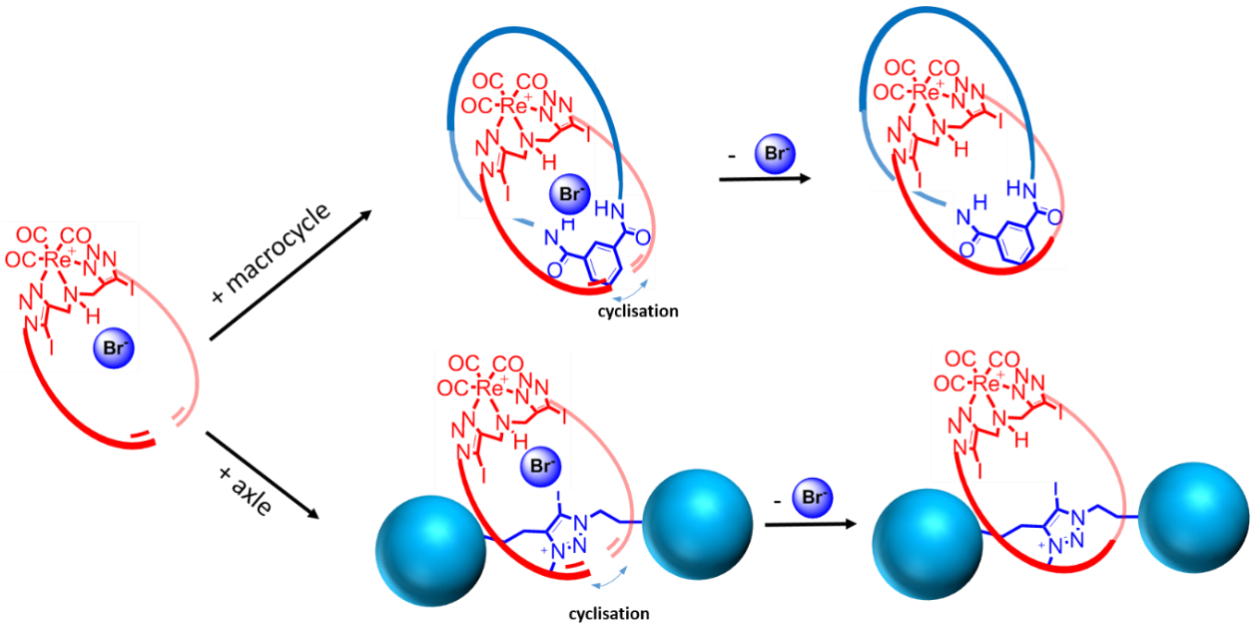
Table 2.2. Association constants, K_a (M^{-1}), for monocationic Re(I)-containing receptor **2.23I** and **2.23H** with various anions.[a]

Receptor	Cl^-	Br^-	I^-	acetate	HSO_4^-
2.23I	-[b]	355(27)	203(6)	2769(32)	43(3)
2.23H	694(7)	298(5)	112(2)	-[b]	120(8)

[a] Anions added as their TBA salts, T = 298 K, solvent = CD_3CN, values quoted have units of M^{-1}. The errors associated with each (< 10%) are quoted in parentheses. [b]Titration data could not be fitted to a 1:1 stoichiometric binding model suggesting complex equilibria.

2.3.3 Attempted Synthesis of Interlocked Systems

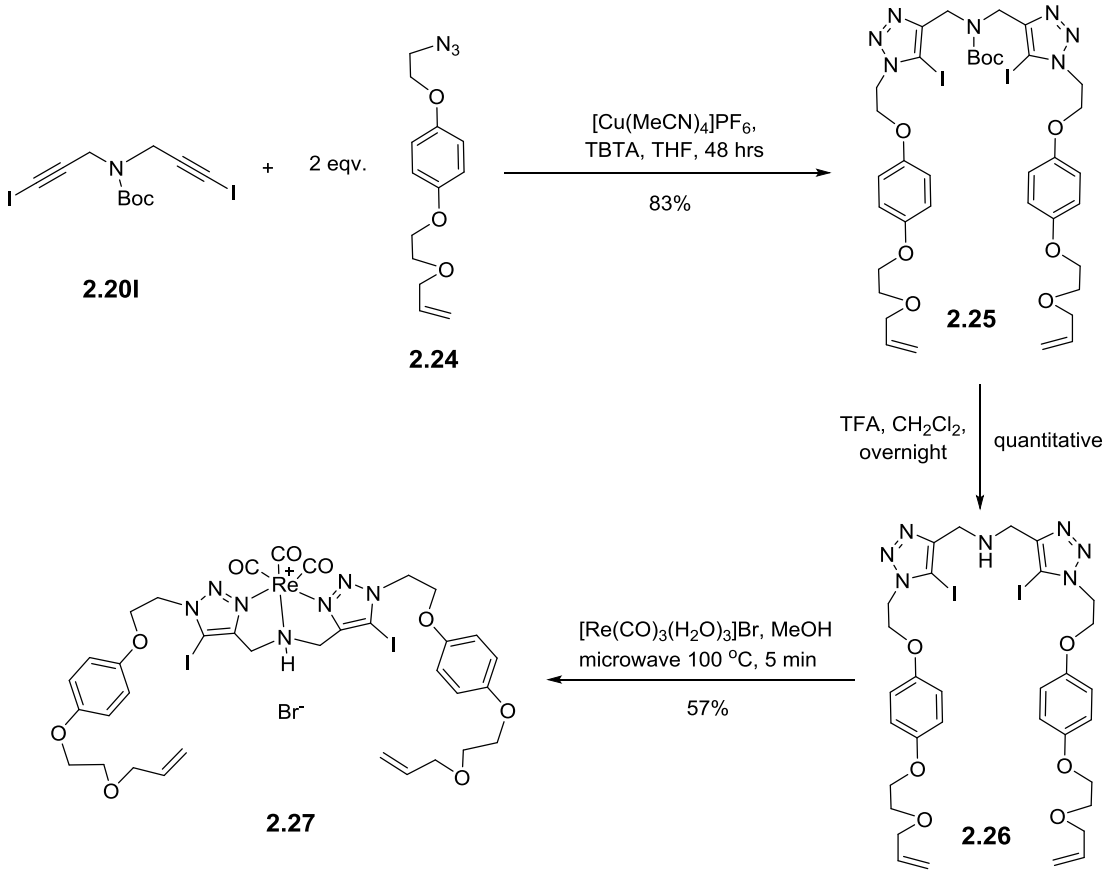
After demonstrating the capability of acyclic Re(I)-bis-iodotriazole-amine receptor to bind anions, the synthesis of interlocked rotaxane and catenane structures that contain this Re(I)-bis-iodotriazole-amine motif was attempted initially by anion templated ring closing methathesis (Scheme 2.10).



Scheme 2.10. Synthetic strategy towards interlocked molecules using anion templation.

Precursor bis-alkene **2.27** was prepared following the multi-step procedure summarised in Scheme 2.11. Bis-iodoalkyne **2.20I** was reacted with two equivalents of vinyl appended azide **2.24** [33] to give *N*-Boc-protected bis-alkene **2.25** in 83% yield. After

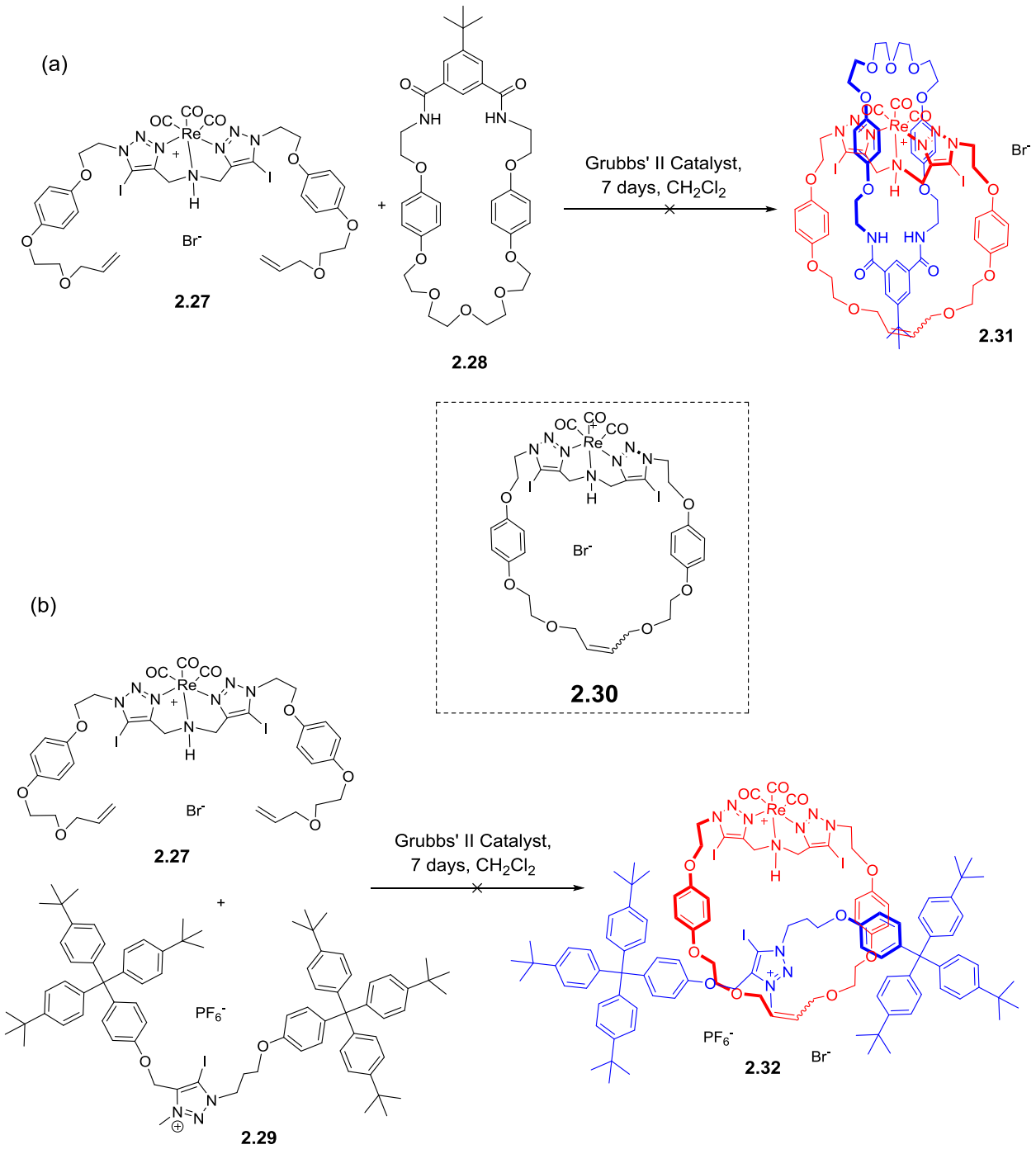
quantitative deprotection using TFA, the bis-iodotriazole-amine motif compound **2.26** was reacted with $[Re(CO)_3(H_2O)_3]Br$ to give monocationic Re(I) complex **2.27** in 57% yield.



Scheme 2.11. Synthesis of Re(I)-containing monocationic bis-alkene **2.27**.

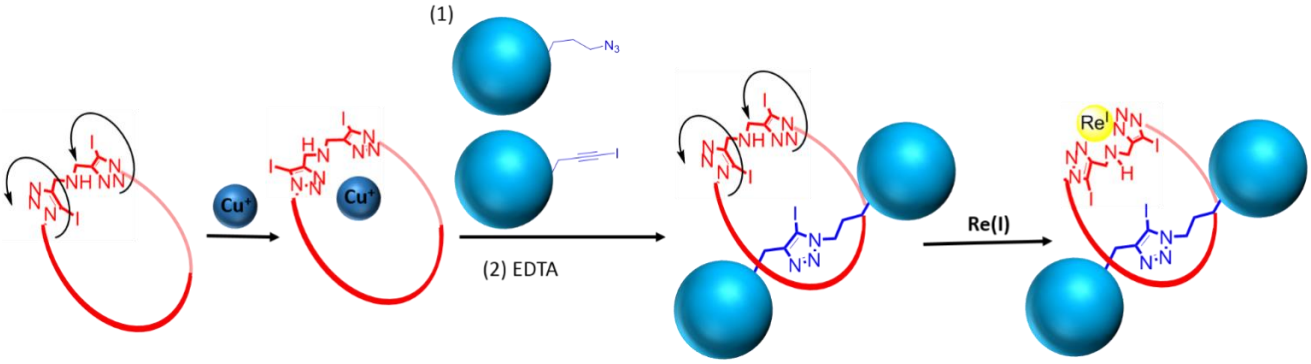
Catenane synthesis was attempted by stirring **2.27** with one equivalent of isophthalamide macrocycle **2.28**,[34] which is known to be able to bind anions via HB interactions,[35] in dry CH_2Cl_2 followed by adding 10% (by weight) Grubbs' II catalyst (Scheme 2.12(a)). However, no evidence of catenane **2.31** formation was observed by mass spectrometry after a week; only the ring-closed macrocycle **2.30** and isophthalamide macrocycle **2.28** were isolated. Similarly, the synthesis of target rotaxane **2.32** was also attempted by reacting **2.27** and XB axle **2.29**[19] under the same Grubbs' catalysed RCM conditions (Scheme 2.12(b)). However, again only the ring-closed macrocycle **2.30** was formed after a week. The unsuccessful formation of target catenane or rotaxane may result from the unfavourable geometries between **2.27** and halide anion binding macrocycle or the

axle preventing successful formation of the anion templated orthogonally assembled intermediates. Indeed, qualitative ^{1}H NMR pseudorotaxane studies performed by mixing equimolar quantities of **2.27** and **2.28** in CD_2Cl_2 showed only small perturbations of hydroquinone protons of macrocycle **2.28**, giving inconclusive evidence for interpenetration.



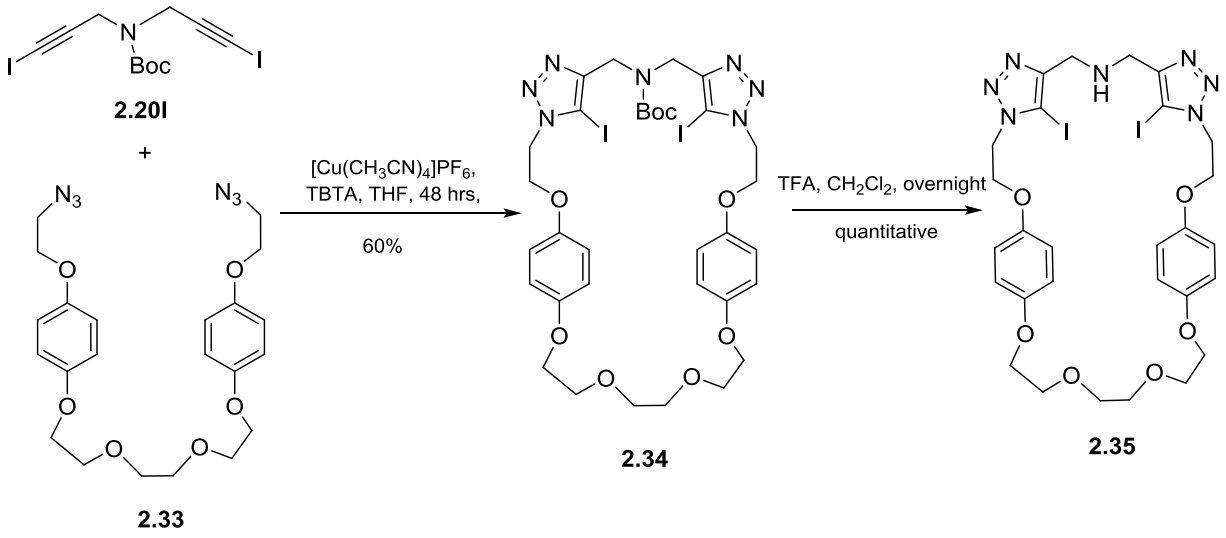
Scheme 2.12. Attempted synthesis of (a) catenane **2.31** and (b) rotaxane **2.32**.

After the unsuccessful synthesis of interlocked structures by anion templation, an AMT synthetic strategy used in Section 2.2, was investigated. In this case, a bis-iodotriazole-amine-containing macrocycle component with endo/exo-conformational metal binding capability was used to initially bind Cu(I) endotopically to facilitate active metal template rotaxane synthesis (Scheme 2.13). After removal of the metal catalyst, coordinating the bulky Re(I) functionality would afford the target exotopical Re(I) rotaxane.



Scheme 2.13. Schematic illustration of the Re(I)-rotaxane formation strategy.

The preparation of the key XB bis-iodotriazole-amine macrocycle component **2.35** is summarised in Scheme 2.14. CuAAC macrocycle ring-closing of equimolar amounts of **2.20I** with bis-azide **2.33**[18] under high-dilution conditions afforded *N*-Boc-protected macrocycle **2.34** in 60% yield. The high yield of the XB macrocycle synthesis reaction is especially noteworthy, given the lack of a template used to facilitate macrocyclisation over non-productive formation of acyclic oligomers. Quantitative *N*-Boc-deprotection with trifluoroacetic acid (TFA) afforded the target XB macrocycle **2.35**.



Scheme 2.14. Synthesis of macrocycle **2.35**.

Colourless crystals of *N*-Boc-protected macrocycle **2.34**, obtained by slow evaporation of a hexane/CH_2Cl_2 solution (1:1 *v*/*v*), were subjected by X-ray diffraction structure determination.[&] The solid state structure (Figure 2.16(a)) shows the iodotriazole groups of the macrocycle are almost antiparallel in the same plane which is nearly perpendicular to the *N*-Boc group. Also, half a molecule of CH_2Cl_2 from crystallisation is encapsulated in the macrocyclic cavity.[#] Strong XB interactions between iodine atoms and nitrogen atoms from adjacent macrocycles' iodotriazole moieties are shown: the bond angle of (C-I)-N is 174^o and the bond length is 85% of the sum of van der Waals radii (Figure 2.16(b)). The arrangement of antiparallel iodotriazoles, which have XB interactions with two adjacent macrocycles, results in face to face linear stacking in the crystal structure of **2.34**.

[&] X-ray structural data was collected and the structure was determined by Dr. Antonio Martinez.
[#] The electron density for the encapsulated CH_2Cl_2 solvent is diffuse and only allowed partial localisation of the solvent.

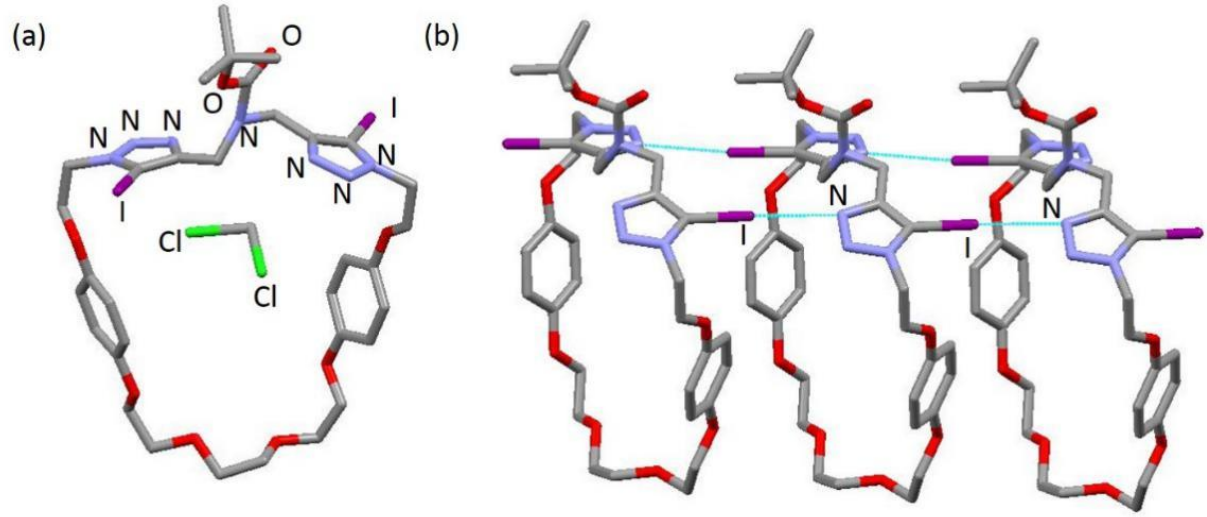
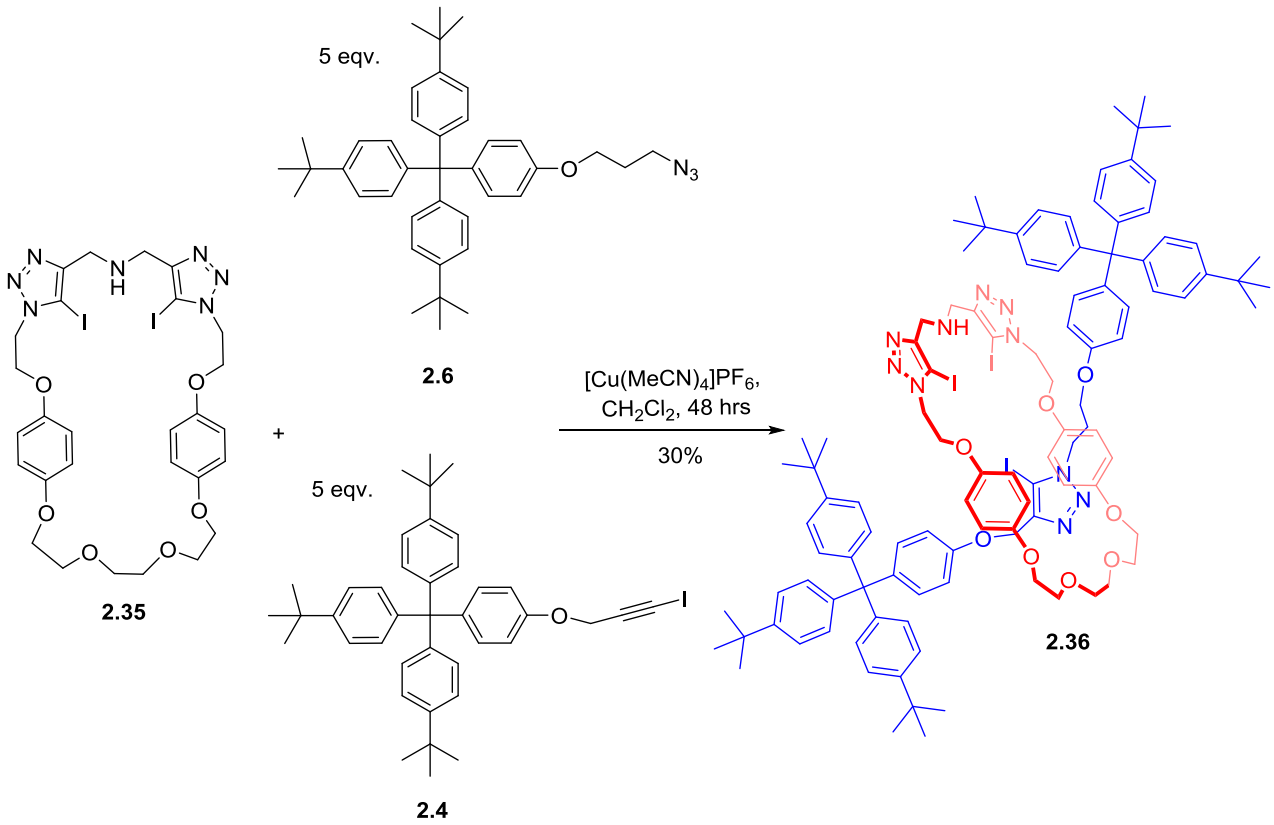


Figure 2.16. Crystal structure of XB macrocycle **2.34**: (a) single macrocycle with an encapsulated CH_2Cl_2 molecule; (b) the solid-state packing structure in the crystal lattice. Short contacts between the iodine atoms and nitrogen atoms are shown by the blue dash lines. H atoms, solvent molecules and all minor components of the disorder are omitted for clarity.

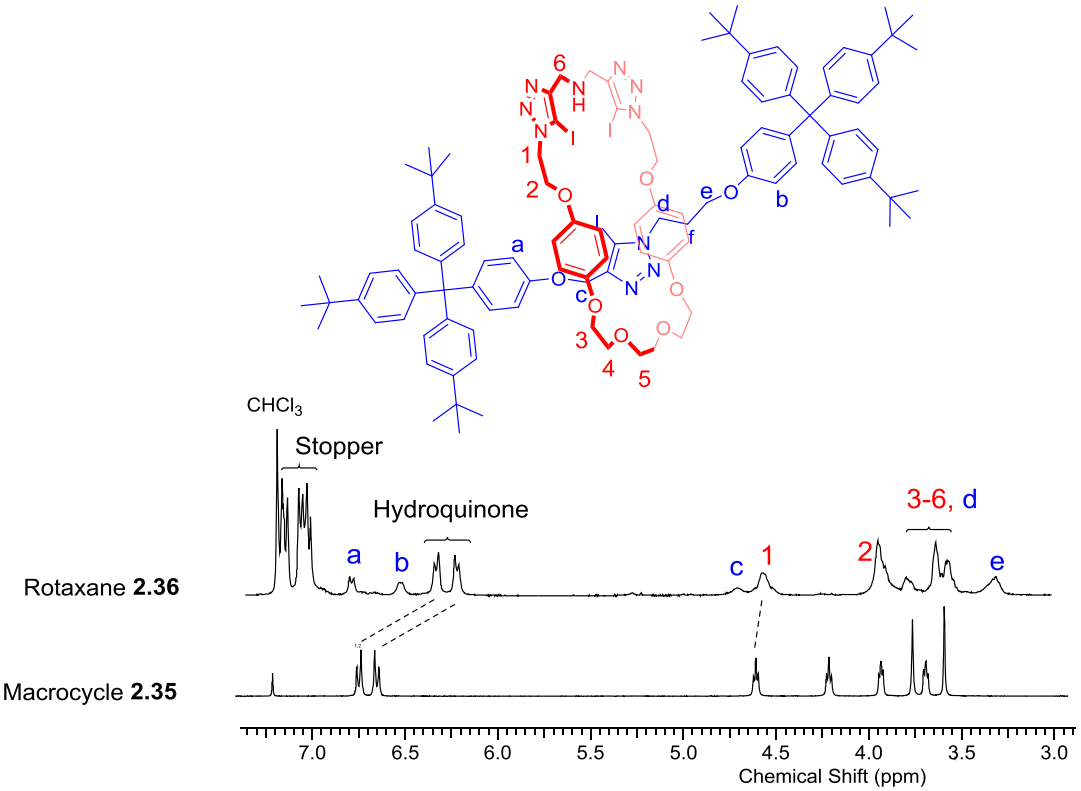
With macrocycle **2.35** (1.0 equiv.), CuAAC-AMT rotaxane formation was performed using a stoichiometric quantity of $[Cu(CH_3CN)_4]PF_6$ in CH_2Cl_2 with stopper azide **2.6** (5.0 eqv.) and stopper iodoalkyne **2.4** (5.0 eqv.), affording the neutral rotaxane **2.36** in 30% isolated yield after chromatographic purification (Scheme 2.15). The interlocked nature of rotaxane **2.36** was evident from the diagnostic upfield shifts of the macrocycle component's hydroquinone protons resulting from aromatic donor-acceptor π-π stacking interactions with the axle iodotriazole motif (Figure 2.17(a)) and conclusively demonstrated by ^{1}H-^{1}H ROESY spectroscopy (Figures 2.17(b)). The XB rotaxane **2.36** was then reacted with one equivalent of $[Re(CO)_3(H_2O)_3]Br$ to produce Re(I) rotaxane **2.37** (Scheme 2.16). The successful complexation of Re(I) was confirmed by ESI-MS (m/z = 2344, [**2.37**-Br]$^+$). However unfortunately, ^{1}H NMR spectroscopy revealed that after purification the isolated Re(I) rotaxane **2.37** was not stable in $CDCl_3$ solution and rapidly decomposed to several species which could not be identified by ^{1}H NMR and mass spectrometry (Figure 2.18). Given the stability of acyclic Re(I) anion receptor **2.23I**, the decomposition of rotaxane **2.36** may arise from the Re(I) centre being attacked by the N donor atoms of the proximal iodotriazole from axle component, in the same manner observed with rotaxane **2.10I** in Section 2.2. Due to

the instability of Re(I)-complexed rotaxane **2.37**, no anion binding studies could be undertaken.



Scheme 2.15. Synthesis of rotaxane **2.36**.

(a)



(b)

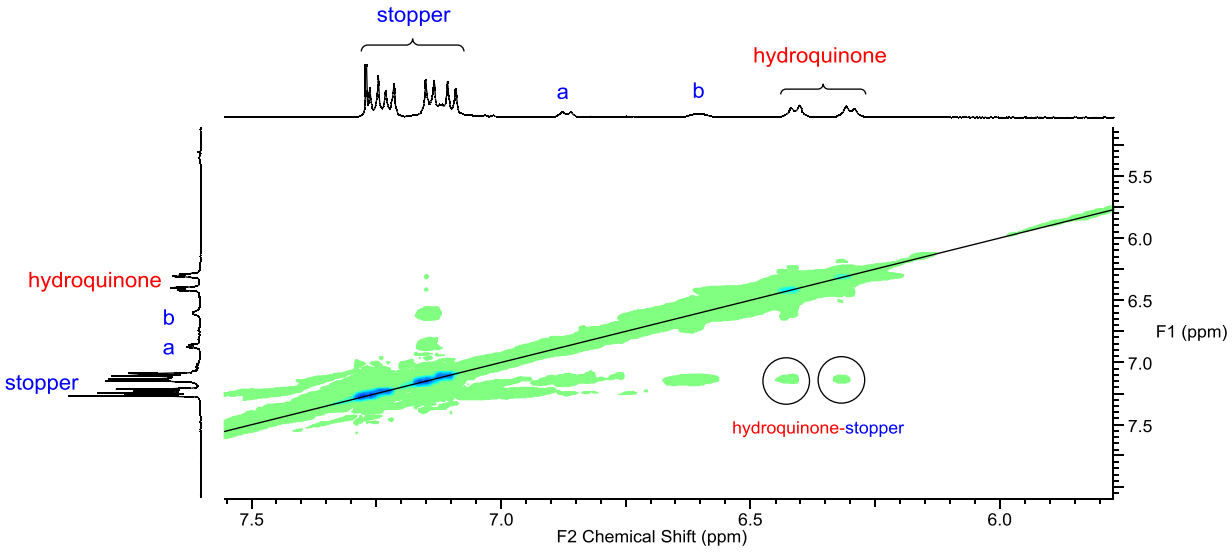
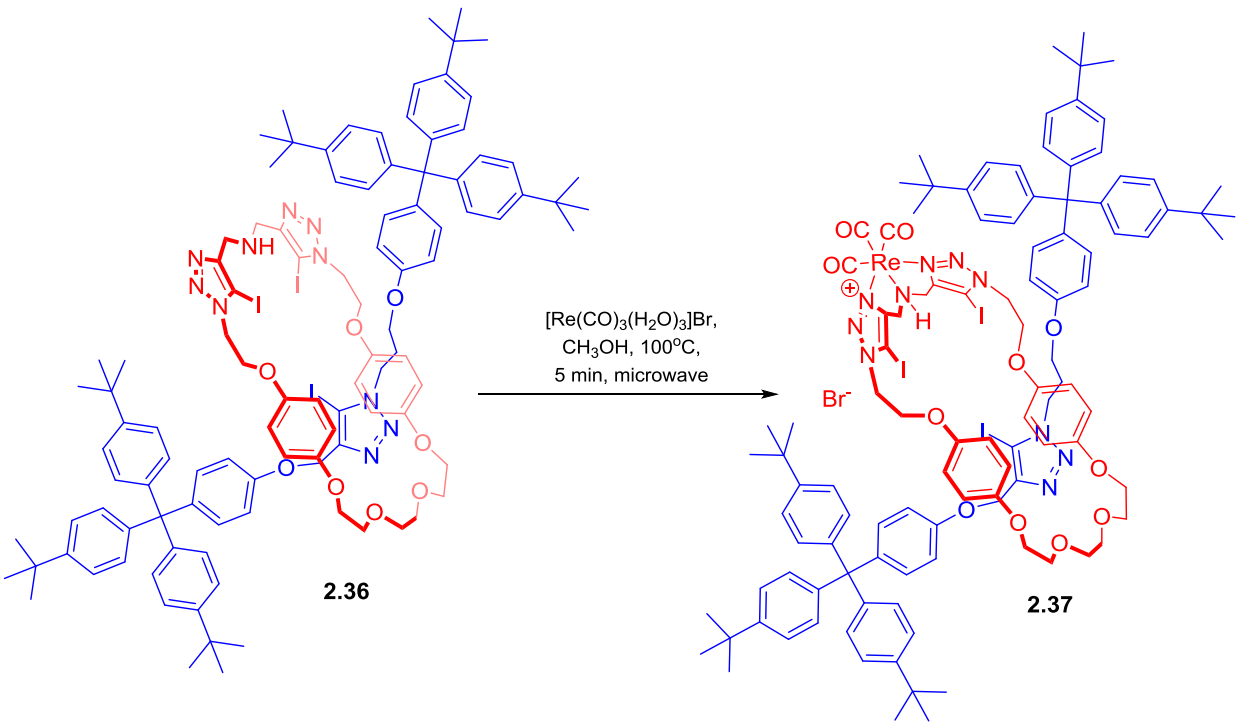


Fig 2.17. (a) Partial ^{1}H NMR spectra of macrocycle **2.35** and rotaxane **2.36**; (b) ^{1}H-^{1}H ROESY NMR spectrum rotaxane **2.36** in $CDCl_3$ at 298 K. Selected cross-peaks indicating through-space interactions between the macrocycle and axle component are circled.



Scheme 2.16. Synthesis of Re(I)-rotaxane **2.37**.

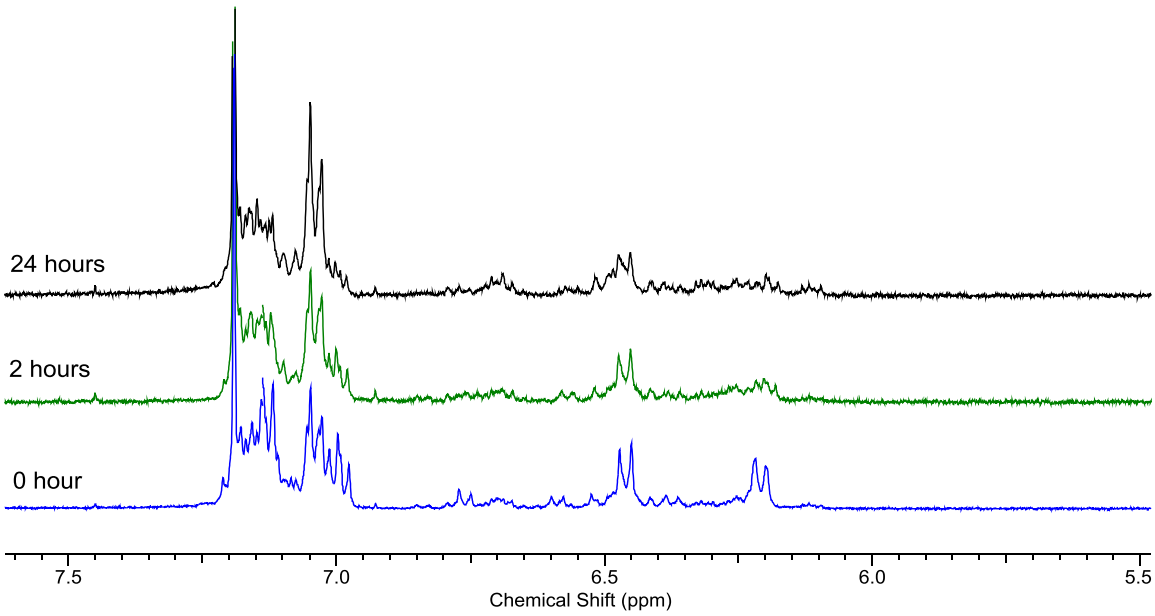


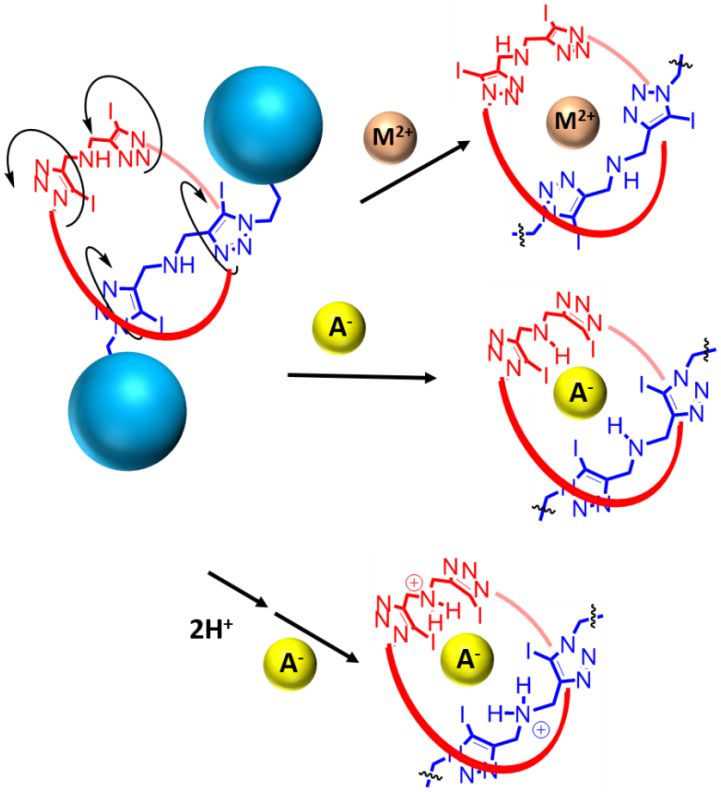
Figure 2.18. ^{1}H NMR changes of rotaxane **2.37** in $CDCl_3$ over time.

2.4 Acid-regulated Switching of Metal Cation and Anion Guest Binding in XB Rotaxanes[‡‡]

2.4.1 Design and Synthesis of Target Rotaxanes

In the previous Section 2.3, the success of constructing rotaxane **2.36** via AMT methodology demonstrated the ability of macrocycle **2.35** to coordinate Cu(I) endotopically. The macrocycle's conformationally flexible bis-iodotriazole-amine motif is capable of performing both metal complexation and XB anion binding. Incorporating this motif into the axle component as well as the macrocycle would produce a novel rotaxane host with the potential to facilitate metal cation and anion guest binding in its unique three-dimensional cavity (Scheme 2.17). Specifically, the target rotaxane contains multiple iodotriazole motifs flanking its three-dimensional interlocked cavity, which is capable of multi-dentate anion binding interactions via their Lewis acidic XB-donor iodine atoms. In addition, the presence of methylene spacers immediately adjacent to the iodotriazole units provides sufficient flexibility for endo/exo-dentate flipping of the iodotriazoles such that their Lewis basic nitrogen atoms can also coordinate to metal cations within the interlocked cavity, aided by the proximal secondary amine donor units. Importantly, the secondary amine residues can also be protonated upon addition of acid which can enhance anion recognition and switch off metal coordination.

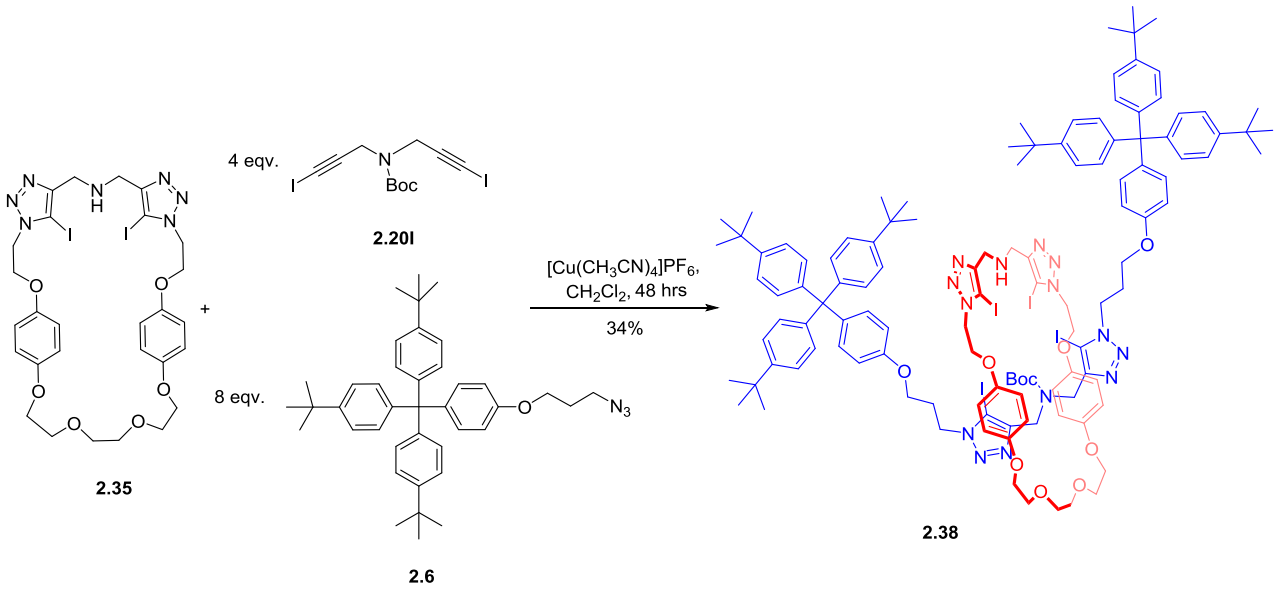
[‡‡]This work was published as an full paper in *Chemistry - An European Journal*.
"Acid-regulated Switching of Metal Cation and Anion Guest Binding in Halogen Bonding Rotaxanes"
X. Li, J. Y. C. Lim and P. D. Beer, *Chem. – Eur. J.* **2018**, *24*, 17788 – 17795



Scheme 2.17. Design of the target rotaxane for binding metal cations and anions.

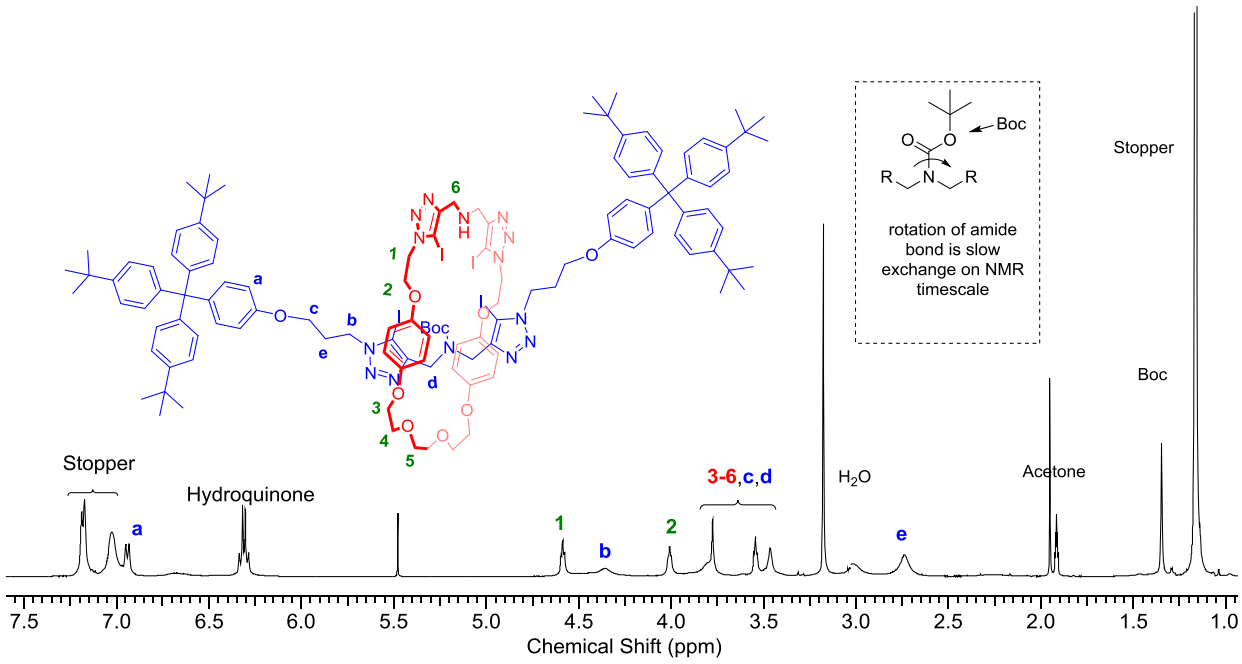
With one equivalent of macrocycle **2.35** and one equivalent of $[Cu(CH_3CN)_4]PF_6$, CuAAC-AMT rotaxane formation was performed in CH_2Cl_2 with bis-iodoalkyne **2.20I** (4 eqv.) and stoppered azide **2.6** (8 eqv.), affording rotaxane **2.38** in 34% isolated yield after chromatographic purification (Scheme 2.18). Due to the rotation barrier caused by the bulky tert-butyl group of Boc,[36] the methylene proton NMR signals of the rotaxane axle component exhibited slow exchange on the NMR timescale, making the signals broader than expected (Figure 2.19(a)). The ^{1}H-^{1}H ROESY spectrum proved the interlocked nature of rotaxane **2.38**, evident from the through-space interactions between hydroquinone protons on the macrocycle and stopper aromatic protons on the axle (Figure 2.19(b)). The target XB rotaxane **2.39** was then produced by *N*-Boc-deprotection of the axle component of rotaxane **2.38** using TFA (Scheme 2.19). An anthracene appended rotaxane host **2.40** with the potential of sensing guest binding via a fluorescence response was also prepared through the reaction of rotaxane **2.36** with 9-(chloromethyl)anthracene under basic conditions.

Anthracene appended acyclic receptors **2.41I** and **2.41H** were also prepared for comparison of anion binding properties to the interlocked structures (Scheme 2.19).



Scheme 2.18. Synthesis of rotaxane **2.38**.

(a)



(b)

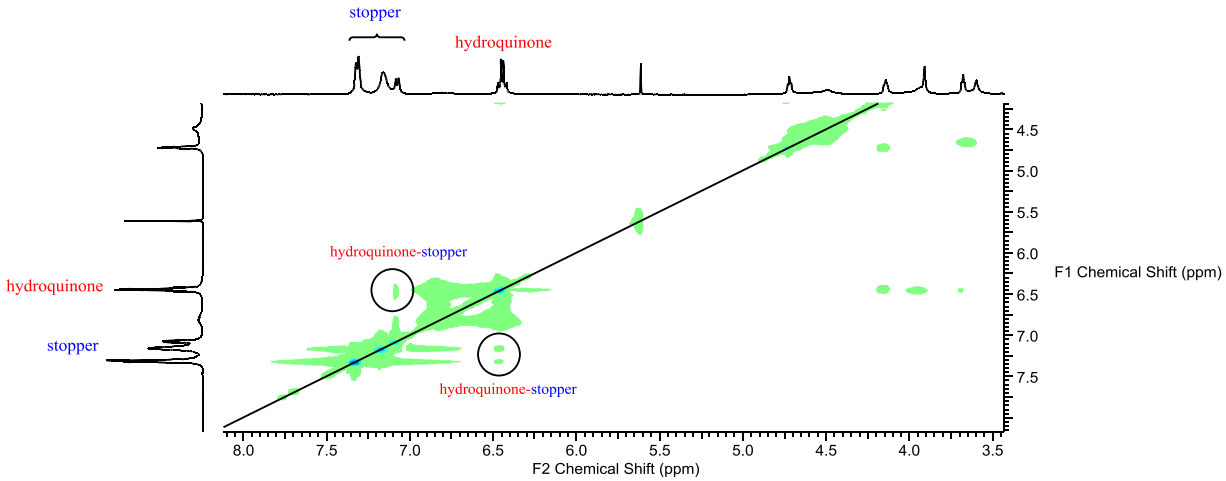
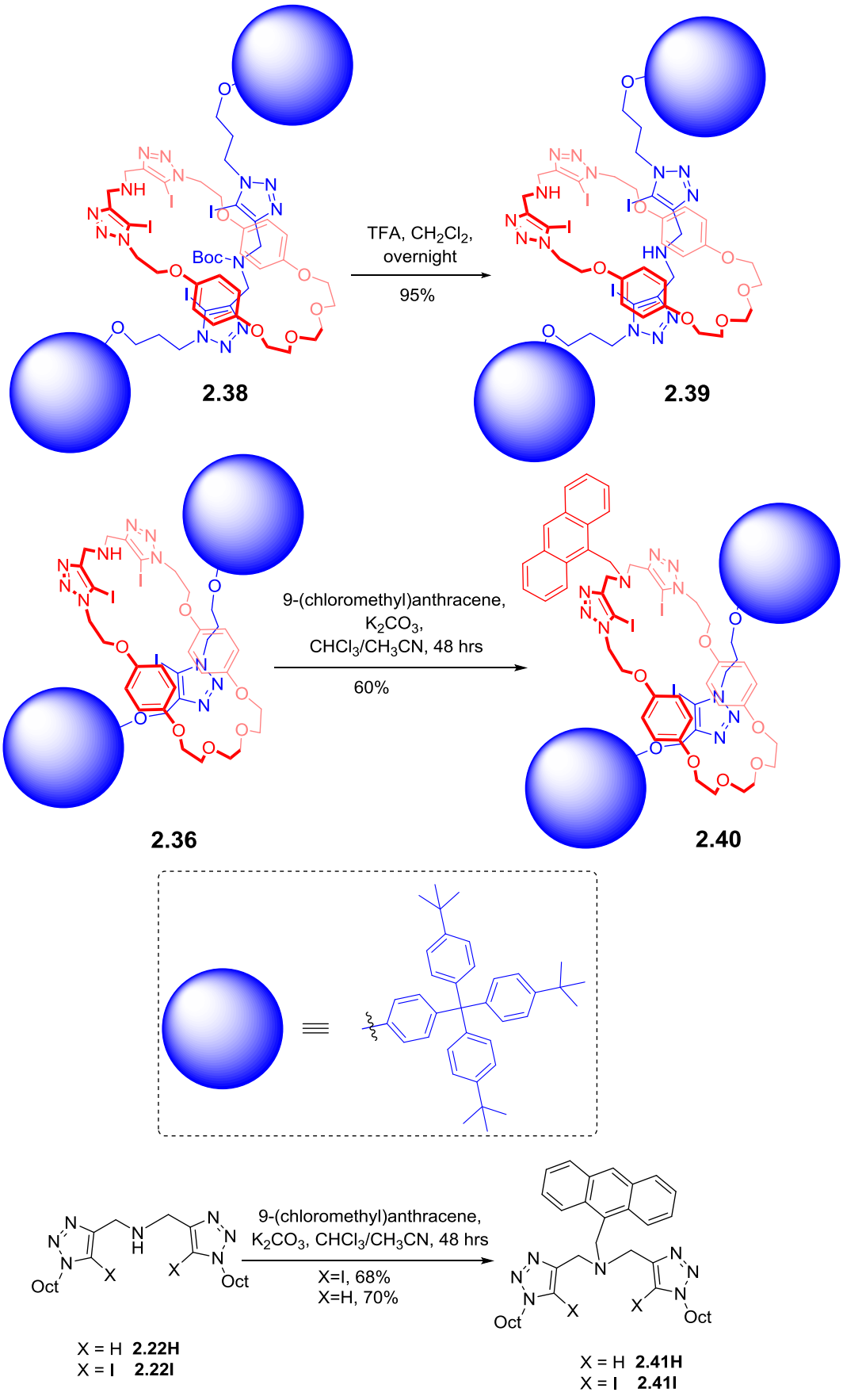


Figure 2.19. (a) ^{1}H NMR spectrum of rotaxane **2.38** in d_6-acetone (T = 298 K); (b) ^{1}H-^{1}H ROESY NMR spectrum of rotaxane **2.38**. The through-space interactions between macrocycle hydroquinone and stopper aromatic protons are circled (d_6-acetone, T = 298K).

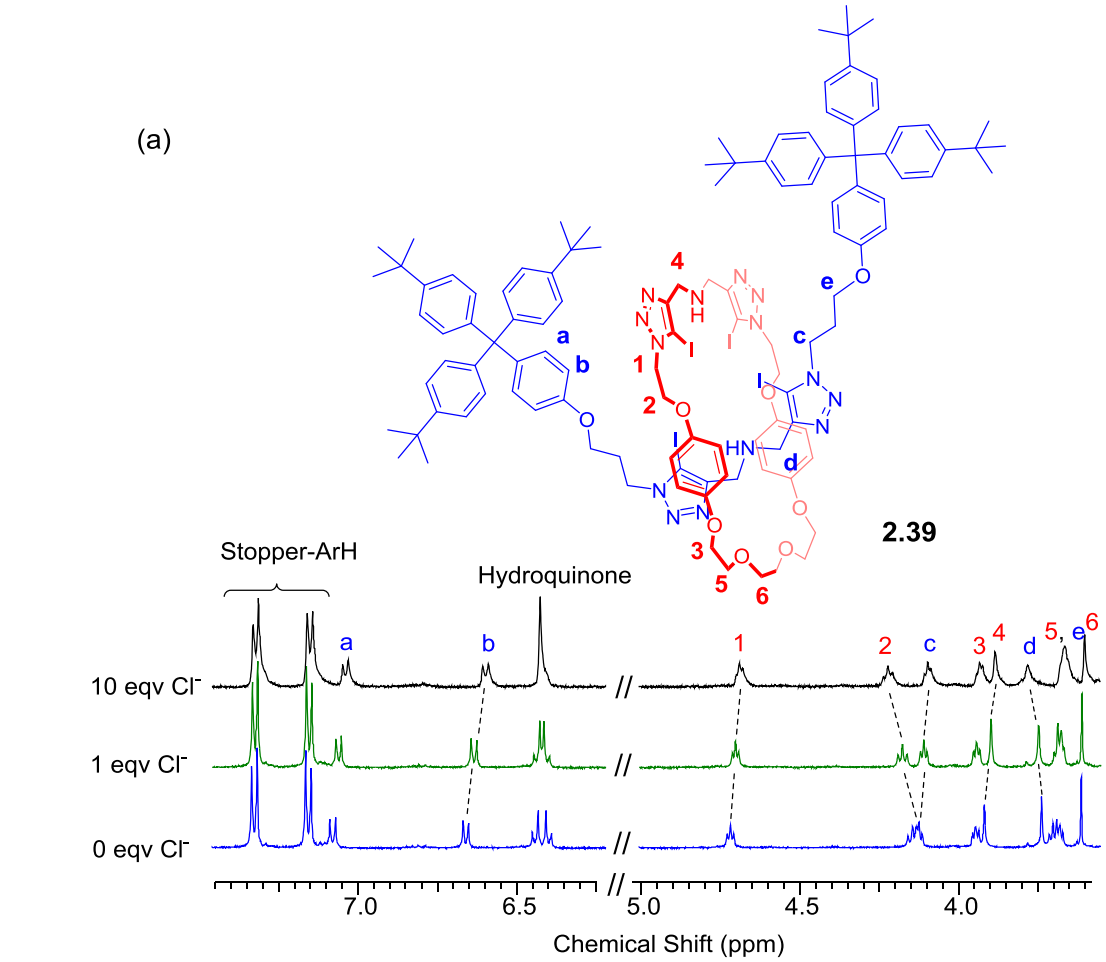


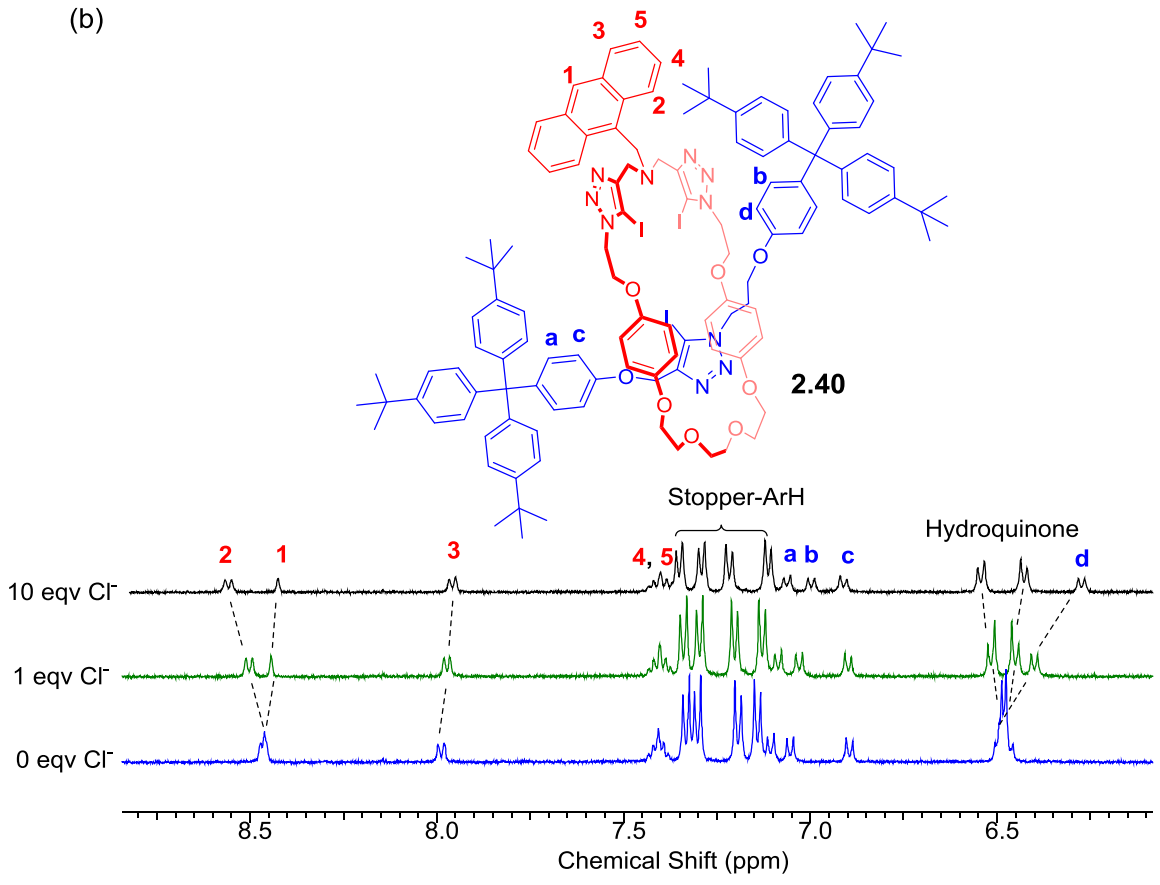
Scheme 2.19. Synthesis of neutral rotaxanes and acyclic receptors.

2.4.2 Guest Binding Properties of Neutral Rotaxanes

2.4.3.1 Anion Binding Studies

The anion binding properties of interlocked and acyclic compounds were first studied by ^{1}H NMR titration experiments, where increasing quantities of anions, as their tetrabutylammonium (TBA) salts, were added to separate d_6-acetone solutions of **2.39**, **2.40** and **2.41I/H**. As shown in Figure 2.20(a), upon addition of Cl^-, downfield shifts of signals arising from H_2 and H_d as well as significant upfield shifts of H_c, H_1, and H_4 of rotaxane **2.39** were observed. Notably, the perturbations of these signals, arising from protons flanking the interlocked binding cavity containing the iodotriazole units, reveal that Cl^- was binding in its vicinity. At the same time, the shifts of hydroquinone proton signals of the macrocycle component and those from the proximal stopper protons H_b of the axle suggest that anion binding resulted in conformational changes to the rotaxane framework. In contrast, negligible perturbations were exhibited in the analogous NO_3^- titration indicating no obvious association between **2.39** and NO_3^-. With rotaxane **2.40**, upon Cl^- addition, the ^{1}H NMR spectrum changed considerably (Figure 2.20(b)), most notably the downfield shift of H_2 of the macrocycle's anthracene unit and a large upfield shift of axle proton H_d, suggesting that Cl^- was binding just above the interlocked cavity. Analogous titrations with Br^- elicited similar signal perturbations of smaller magnitude while no significant perturbations occurred when adding I^-, NO_3^- and ReO_4^-. In the case of the acyclic compounds, the addition of Cl^- caused the downfield shift of H_2 on the anthracene component of **2.41I** while the signals of triazole protons H_6 of **2.41H** exhibited obvious downfield shifts due to the HB interactions with anions. However, addition of other anions such as Br^-, I^-, NO_3^- and ReO_4^- caused negligible influence to the proton signals of **2.41I** and **2.41H**. WinEQNMR2[28] analysis of the ^{1}H NMR titration data, monitoring the shifts of protons H_b of rotaxane **2.39**, H_2 of rotaxane **2.40**, H_2 of **2.41I** and H_6 of **2.41H** (Figure 2.21) respectively as a function of anion concentration, determined 1:1 host-guest stoichiometric association constants (K_a/M^{-1}) summarised in Table 2.3.


(a)
2.39
Stopper-ArH
Hydroquinone
10 eqv Cl⁻
1 eqv Cl⁻
0 eqv Cl⁻
7.0
6.5
5.0
4.5
4.0
Chemical Shift (ppm)


(b)
2.40
Stopper-ArH
Hydroquinone
10 eqv Cl⁻
1 eqv Cl⁻
0 eqv Cl⁻
8.5
8.0
7.5
7.0
6.5
Chemical Shift (ppm)

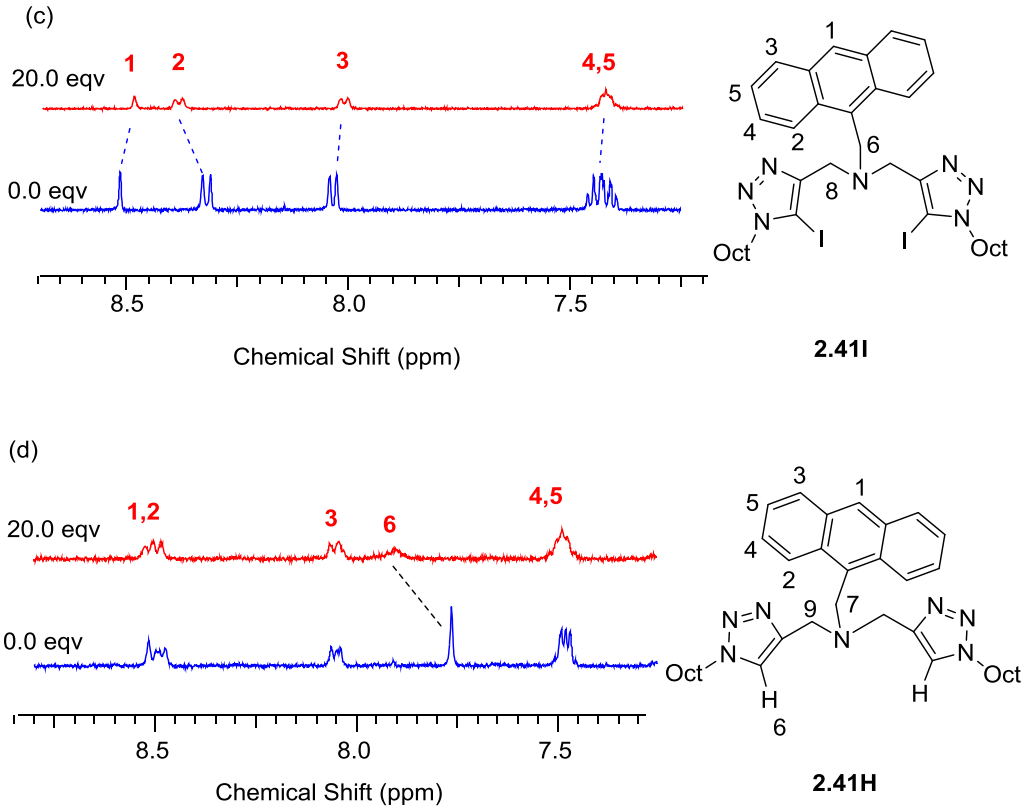


Figure 2.20. Partial ^{1}H NMR spectra of neutral rotaxanes (a) **2.39** and (b) **2.40** in the presence of 0.0, 1.0 and 10.0 equivalents of Cl^- ; (c) **2.41I** and (d) **2.41H** in the presence of 0.0, 1.0 and 20.0 equivalents of Cl^- in d_6-acetone ([host] = 1.0 mM, *T* = 298 K).

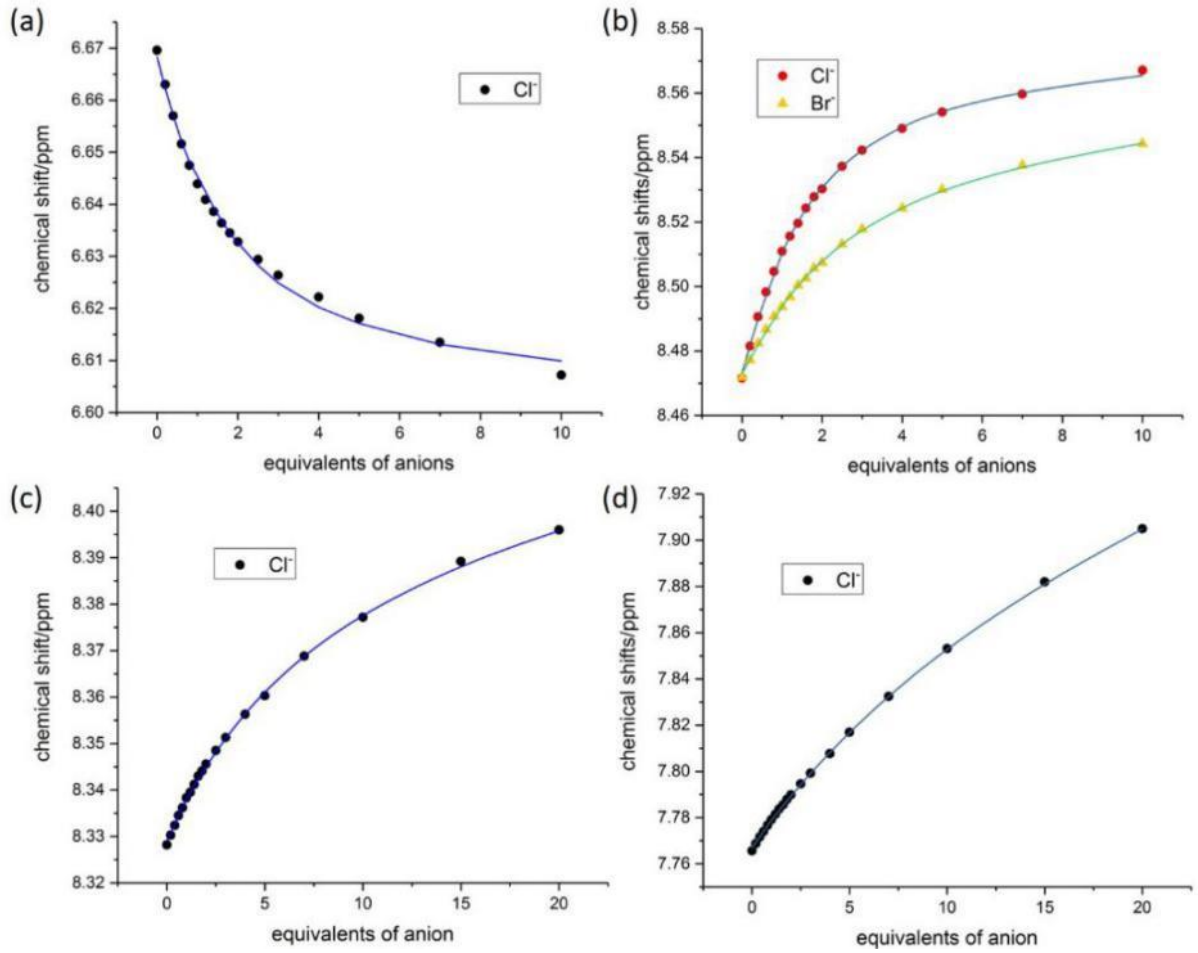


Figure 2.21. Binding isotherms showing the changes in the chemical shift of proton (a) H_b in rotaxane **2.39**; (b) H_2 in rotaxane **2.40**; (c) H_2 in **2.41I**; (d) H_6 in **2.41H** with increasing equivalents of anions added in pure d_6-acetone ([host] = 1.0 mM, *T* = 298 K).

Table 2.3. Association constants (K_a [M^{-1}]) of halides with neutral rotaxanes **2.39** and **2.40**, as well as acyclic receptors **2.41I** and **2.41H** in d_6-acetone. [a]

	Rotaxane **2.39**	Rotaxane **2.40**	Receptor **2.41I**	Receptor **2.41H**
Cl^-	800(5)	823(3)	72(3)	15(0.5)
Br^-	-[c]	342(12)	-[b]	-[b]

[a] Values of K_a are calculated by the WinEQNMR2[28] software using a 1:1 host-guest stoichiometric binding model. Errors (±) are in parentheses (<10%). No binding observed for NO_3^- to rotaxane **2.39**. No binding observed for I^-, NO_3^- and ReO_4^- to **2.40**, **2.41I** and **2.42H**.
[b] No binding.
[c] Not conducted.

From Table 2.3, both rotaxanes **2.39** and **2.40** show comparable affinities for Cl^- in d_6-acetone despite the greater number of XB-donor iodotriazole units of the former. This may be a consequence of rotaxane **2.40**'s more preorganised cavity due to a lower number

of conformationally-flexible methylene units, and the bulky anthracene unit favouring endo-orientation of the XB donor iodine atoms on the macrocycle component for convergent anion coordination. Compared with Cl^-, rotaxane **2.40** forms a weaker association with Br^-, likely arising from its lower charge density. Interestingly, no significant interactions of rotaxane **2.40** with I^-, NO_3^- and ReO_4^- were observed, presumably due to their poor shape/size-complementarity with the rotaxane's binding cavity. Similarly, rotaxane **2.39** did not show any binding to NO_3^-. Nonetheless, both rotaxanes were found to bind Cl^- with K_a values more than an order-of-magnitude larger than acyclic receptor **2.41I**, which highlights the importance of the preorganised rotaxane interlocked cavity and convergent XB interactions for anion binding. Furthermore, compared to the acyclic HB receptor analogue **2.41H**, the greatly enhanced Cl^- affinity of **2.41I** emphasises the superiority of XB over HB for anion binding. When the ^{1}H NMR titration experiments of rotaxanes **2.39** and **2.40** with Cl^- were repeated in the more competitive solvent mixture of $CDCl_3/CD_3OD$ (1:1 v/v), no evidence of anion binding was found.

Utilising the anthracene reporter group, the anion binding properties of rotaxane **2.40** were also investigated via fluorescence spectroscopy. In CH_3CN, rotaxane **2.40** exhibits typical anthracene fluorescence emission between 370 and 530 nm (Figure 2.22).[37] In the presence of Cl^-, significant fluorescence enhancement was observed, likely due to rigidification of the rotaxane framework upon anion binding which reduces the likelihood of non-radiative decay pathways.[11,38,39] Similar enhancement of fluorescence intensity was observed for acyclic receptors **2.41I** and **2.41H** upon chloride addition in acetonitrile.

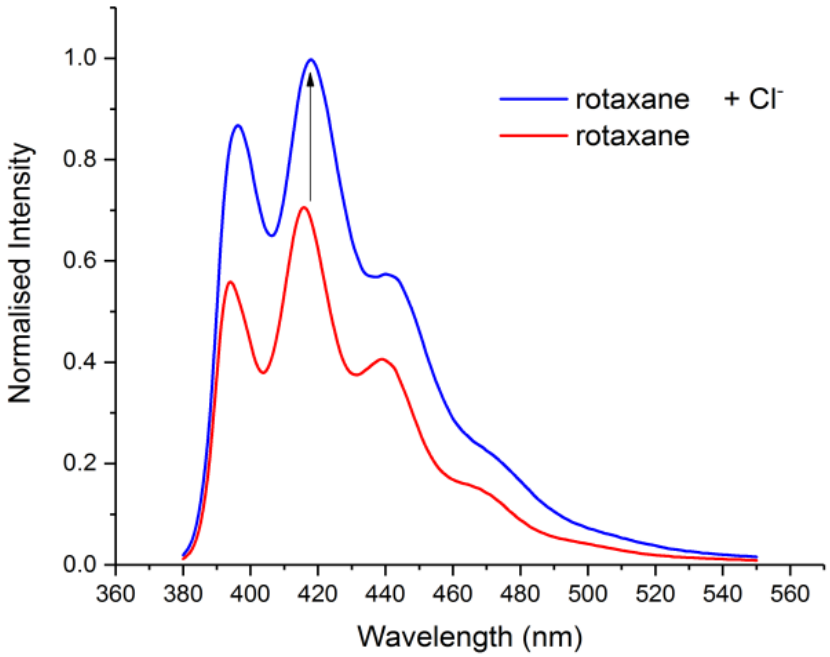


Figure 2.22. Fluorescence spectra of rotaxane **2.40** in the presence of 200 equivalents of Cl^- ([host] = 5 μM, T = 293 K, solvent = CH_3CN, λ_{ex} = 368 nm).

2.4.3.2 Metal Cation Binding Studies

Having demonstrated the anion binding abilities of rotaxane **2.39** and **2.40**, the possibility of using the rotaxanes as multidentate ligands for metal cation guest binding was investigated. The complexation reaction of **2.39** with Zn^{2+} was performed under ambient conditions by stirring a solution of the neutral rotaxane with equimolar $Zn(ClO_4)_2{\cdot}6H_2O$ in CH_2Cl_2/CH_3OH (1:1 v/v) to afford the Zn^{2+}-bound rotaxane in quantitative yield. A comparison of the ^1H NMR spectra of free rotaxane **2.39** and its Zn^{2+} complex revealed clear evidence of metal cation coordination (Figure 2.23).* Signals from protons H_2, H_4, H_c and H_d displayed large downfield shifts, while those of the polyether portion of the macrocycle component (H_3, H_5, H_6) exhibited very small perturbations, indicating that Zn^{2+} was coordinating in the rotaxane cavity flanked by the two tridentate triazole-secondary amine N-donors of the MIM's axle and macrocycle components, and not interacting with the polyether group of the macrocycle. Simultaneously, increased splitting of the macrocycle component's hydroquinone signals revealed that Zn^{2+} coordination further amplified the differences

*Due to their paramagnetic nature, binding of Ni^{2+} and Cu^{2+} to rotaxane **2.39** could not be investigated using ^1H NMR spectroscopy.

between both hydroquinone proton environments as a result of its interlocked cavity binding location.

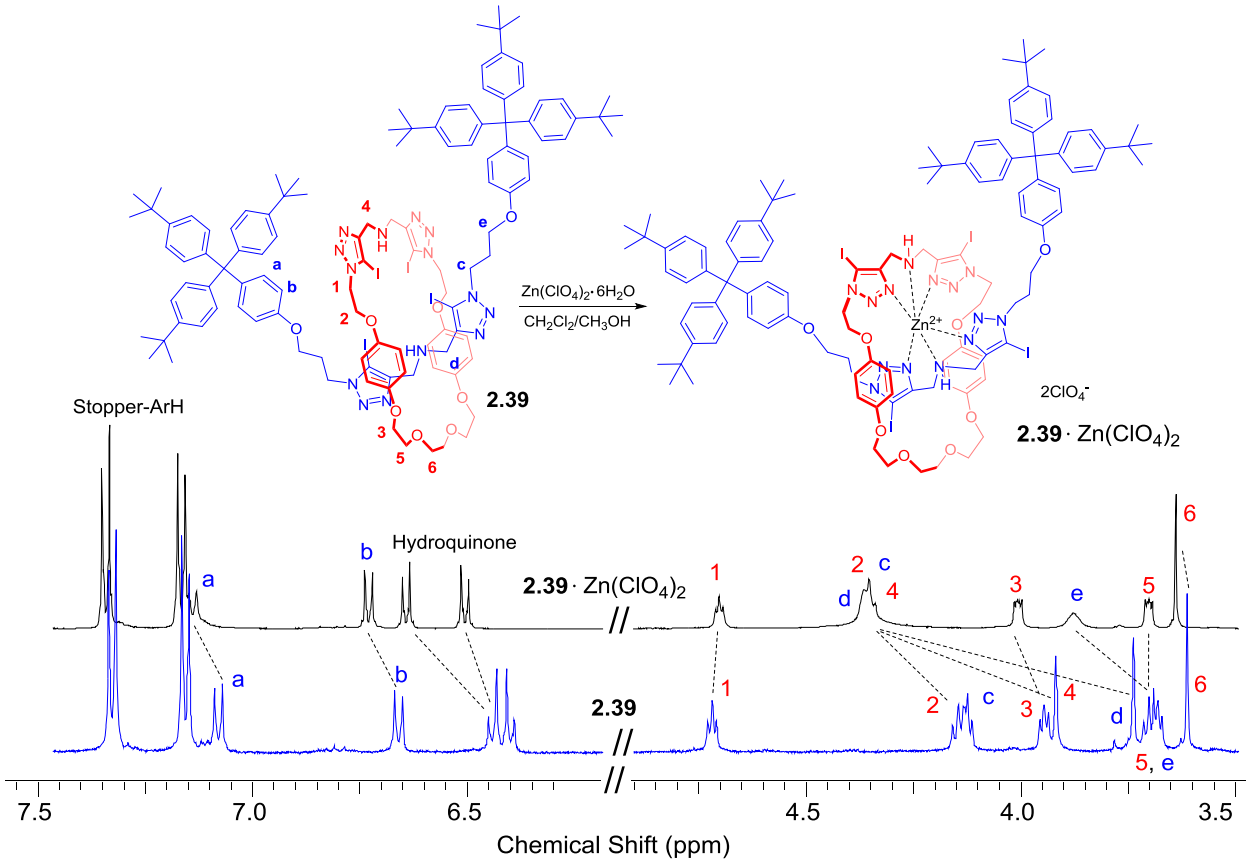


Figure 2.23. ^{1}H NMR spectra of free rotaxane **2.39** and its Zn^{2+} complex in d_6-acetone showing the effects of cation association ([rotaxane **2.39**] = 2 mM, *T* = 298 K).

To confirm the participation of the iodotriazole N-donors in Zn^{2+} coordination, a qualitative UV-Vis experiment was performed. One equivalent of $Zn(ClO_4)_2{\cdot}6H_2O$ was added to an acetonitrile solution of rotaxane **2.39**, resulting in an intensity decrease of the 290 nm absorbance peak (Figure 2.24(a)). These observations are consistent with those observed during triazole N-coordination to transition metal cations such as Cu^{+} [40,41] and Zn^{2+} [42] due to perturbations of the energy levels of the heterocycle's frontier molecular orbitals. Further evidence of Zn^{2+} coordination within the rotaxane structure was obtained from high-resolution electrospray ionisation mass spectrometry (Figure 2.24(b)). It is noteworthy that the presence of methanol in the CH_2Cl_2/CH_3OH (1:1 v/v) solvent mixture used to prepare the zinc(II) complex with **2.39**, was found to negate the rotaxane's ability to bind anions (*vide*

supra), demonstrating that the neutral interlocked host **2.39** favours metal cation binding over anions.

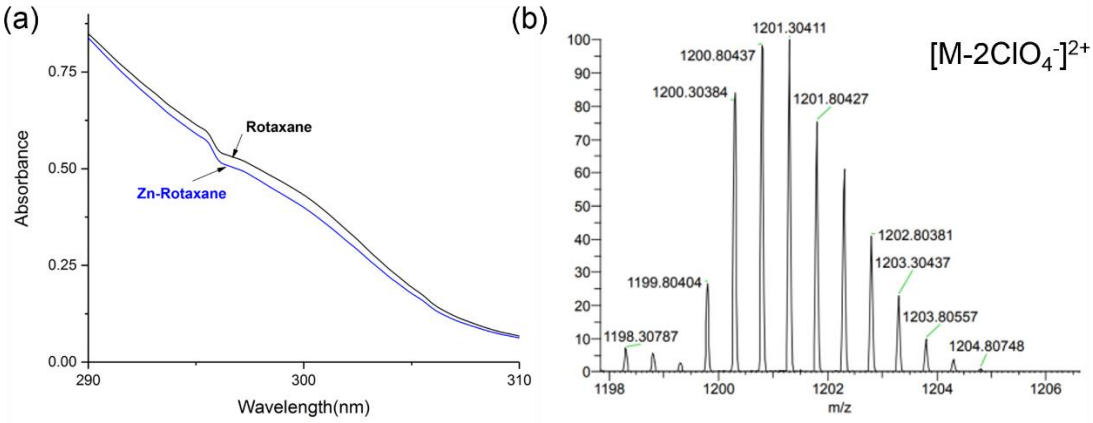


Figure 2.24. (a) UV spectrum of rotaxane **2.39**·$Zn(ClO_4)_2$. (concentration = 0.1 mM, solvent = CH_3CN); (b) high-resolution ESI mass spectrum of rotaxane **2.39**·$Zn(ClO_4)_2$.

The metal cation guest binding properties of rotaxane **2.40** were explored via fluorescence titrations upon addition of transition metal cations, as their perchlorate salts, in CH_3CN. The binding of closed-shell Zn^{2+} resulted in a dramatic increase in the rotaxane's fluorescence intensity (Figure 2.25(a)), which was likely primarily due to metal coordination of the Lewis basic lone pair on the macrocycle component's tertiary amine functionality responsible for photoinduced electron transfer (PET) quenching of the anthracene's fluorescence.[38,43] In stark contrast, the binding of redox-active Cu^{2+} and Ni^{2+} to rotaxane **2.40** elicited significant fluorescence quenching (Figure 2.25(b) and (c)) which probably results from an electron transfer quenching mechanism from the photoexcited anthracene moiety to the respective transition metal centre.[44,45]

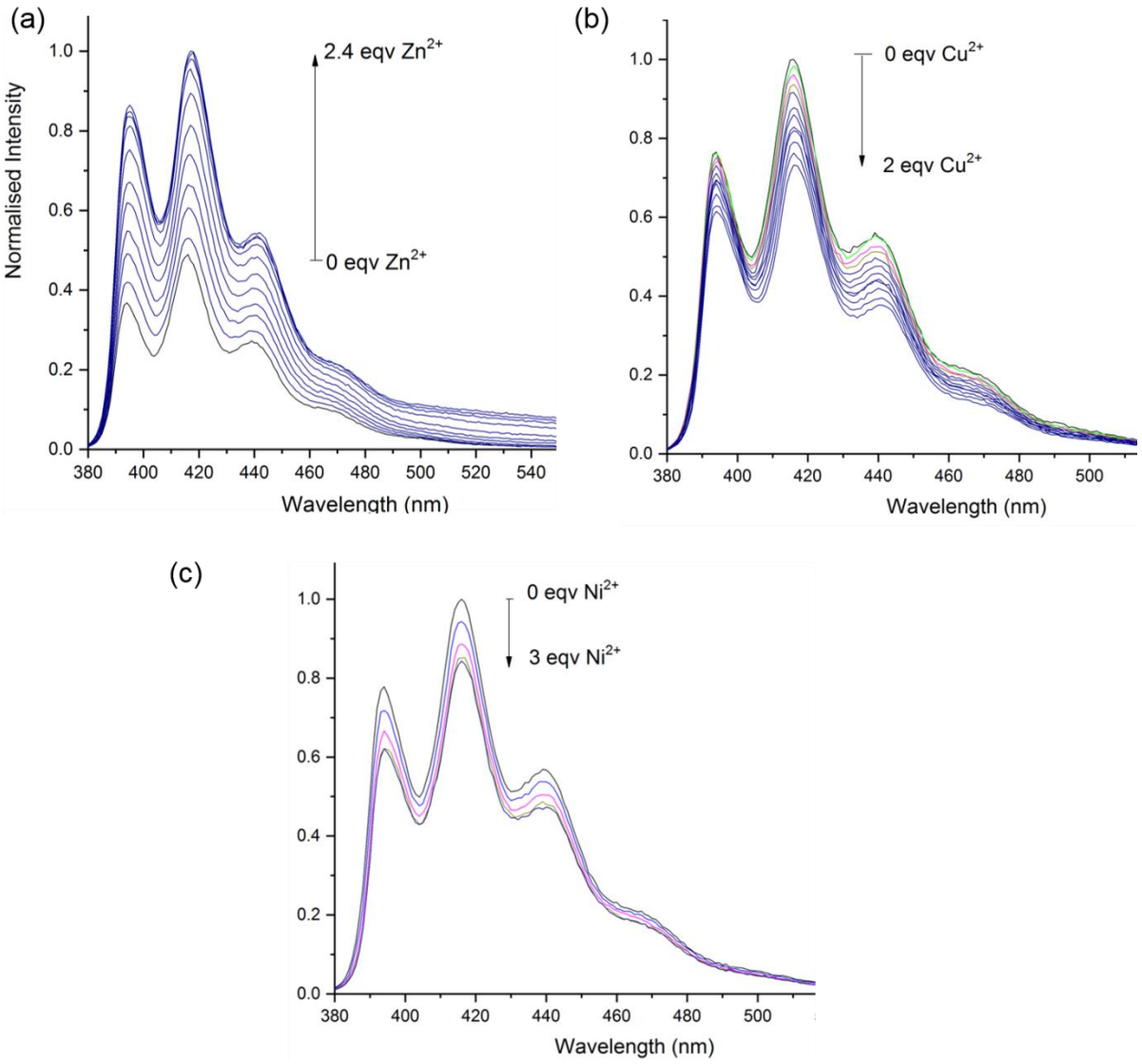


Figure 2.25. Fluorescence spectra of rotaxane **2.40** before and after addition of (a) Zn^{2+}; (b) Cu^{2+}; (c) Ni^{2+}. ([host] = 5 μM, T = 293 K, solvent = CH_3CN, λ_{ex} = 368 nm)

2.4.3 Acid-triggered Regulations in Rotaxane's Guest Binding Behaviour

After demonstrating the predisposition of the neutral binding cavities of both rotaxanes **2.39** and **2.40** for metal cation coordination over Cl^- recognition in methanol-containing solvent media, the regulation of their binding properties upon protonation was investigated. The effects of protonation on the structure of the neutral [2]rotaxanes and the anion binding properties of their protonated forms were initially investigated using ^{1}H NMR spectroscopy. As shown in Figure 2.26, upon the addition of two equivalents of HBF_4 to a solution of rotaxane **2.39** in $CDCl_3/CD_3OD/D_2O$ (45:45:10 v/v/v), the largest downfield shift

was observed for the signal arising from proton H_4, which was immediately adjacent to the secondary amine moiety on the macrocycle ($\Delta\delta$ = +0.4 ppm). This observation was consistent with increased electron-deficiency arising from protonation of the adjacent amine unit, indicating that despite the presence of Lewis basic nitrogen atoms on the iodotriazoles, the amine unit is preferentially protonated. At the same time, perturbations of the signals arising from the macrocycle component's polyether unit (H_3, H_5, H_6) may stem from HB interactions between the protonated ammonium moiety on the axle and the oxygen atoms. This is also likely to restrict the rotational freedom of the macrocycle unit around the axle, resulting in observed greater desymmetrisation of the macrocycle hydroquinone protons. Notable conformational changes of the rotaxane framework occur upon protonation as well, as evident from the dramatic upfield signal shift of axle proton H_d ($\Delta\delta$ = -0.2 ppm), possibly as a result of increased shielding from the macrocycle hydroquinone motifs. These structural changes, as well as being in close proximity to a dicationic bis-protonated rotaxane cavity, result in significant deshielding and downfield shifts of axle proton signals H_b, H_c and H_e.

Compared to neutral rotaxane **2.39**, the dicationic binding cavity of rotaxane [**2.39**·$2H^+$]$(BF_4^-)_2$ was now expected to bind anions strongly in competitive solvent media. Indeed, upon Cl^- addition in the competitive organic-aqueous solvent mixture $CDCl_3/CD_3OD/D_2O$ (45:45:10 v/v/v), numerous changes to the ^1H NMR spectrum of rotaxane [**2.39**·$2H^+$]$(BF_4^-)_2$ were observed (Figure 2.26) . The most noteworthy perturbations were the downfield shifts of H_d and H_4, likely arising from anion binding in close vicinity to the interlocked cavity which results in further structural changes to the rotaxane. Analogous Br^- and NO_3^- titrations exhibited relatively smaller $\Delta\delta$ppm changes to the proton signals of [**2.39**·$2H^+$]$(BF_4^-)_2$ while addition of I^- and ReO_4^- showed negligible perturbations.

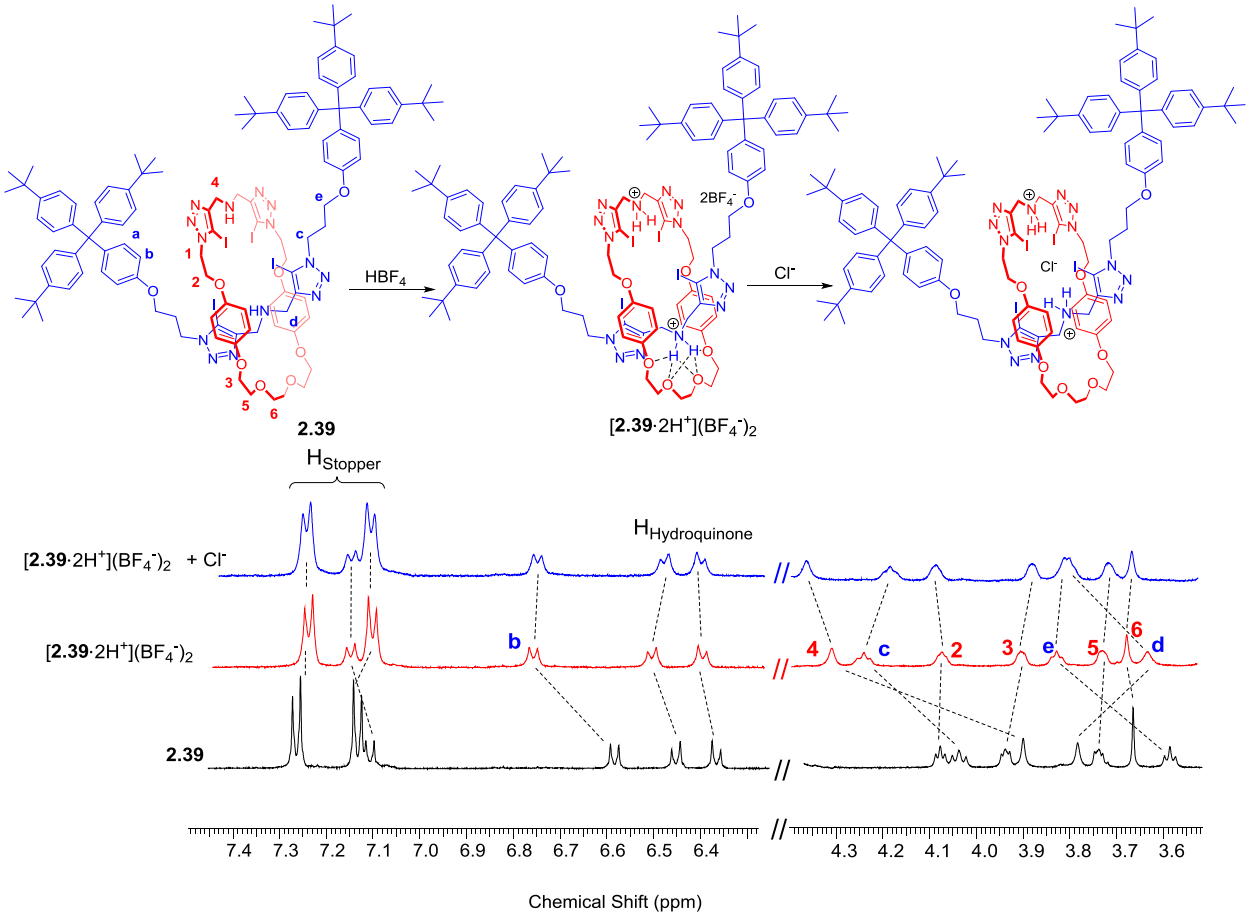


Figure 2.26. Partial ^{1}H NMR spectra of neutral rotaxane **2.39** and doubly-protonated [**2.39**·2H^{+}](BF$_4^{-}$)$_2$ in the presence of 0.0 and 10 equivalents of TBACl ([host] = 1.0 mM, $CDCl_3/CD_3OD/D_2O$ (45:45:10 *v*/*v*/*v*), *T* = 298 K).

Compared to rotaxane **2.39**, the changes upon addition of one equivalent of HBF_4 to rotaxane **2.40**'s ^{1}H NMR spectrum in $CDCl_3/CD_3OD$ (1:1 v/v) are more modest, owing to its single tertiary amine moiety available for protonation (Figure 2.27). Notably however, the largest downfield shift was also observed for the anthracene methylene protons H_6 adjacent to the ammonium unit (Δδ = +0.4 ppm), with the axle protons next to the iodotriazole moiety showing much smaller shifts. Signals arising from methylene protons H_{10} also exhibited a slight downfield shift, which were also seen in the case of acyclic motifs **2.41I** and **2.41H** with addition of one equivalent of HBF_4. For singly-protonated rotaxane [**2.40**·H^{+}]BF$_4^{-}$, an upfield shift was observed for the signal of macrocycle methylene protons H_{10} after addition of Cl^{-} in $CDCl_3/CD_3OD$ (1:1 v/v), indicative of HB interactions between Cl^{-} and the protonated tertiary ammonium unit. By contrast no significant changes were seen during the Br^{-} titration.

Addition of Cl^- to a $CDCl_3/CD_3OD$ (1:1 v/v) solution of [**2.41I**·H^+]BF_4 and [**2.41H**·H^+]BF_4 also caused perturbations of the methylene protons H_8 or H_9 respectively while other protons scarcely moved (Figure 2.28).

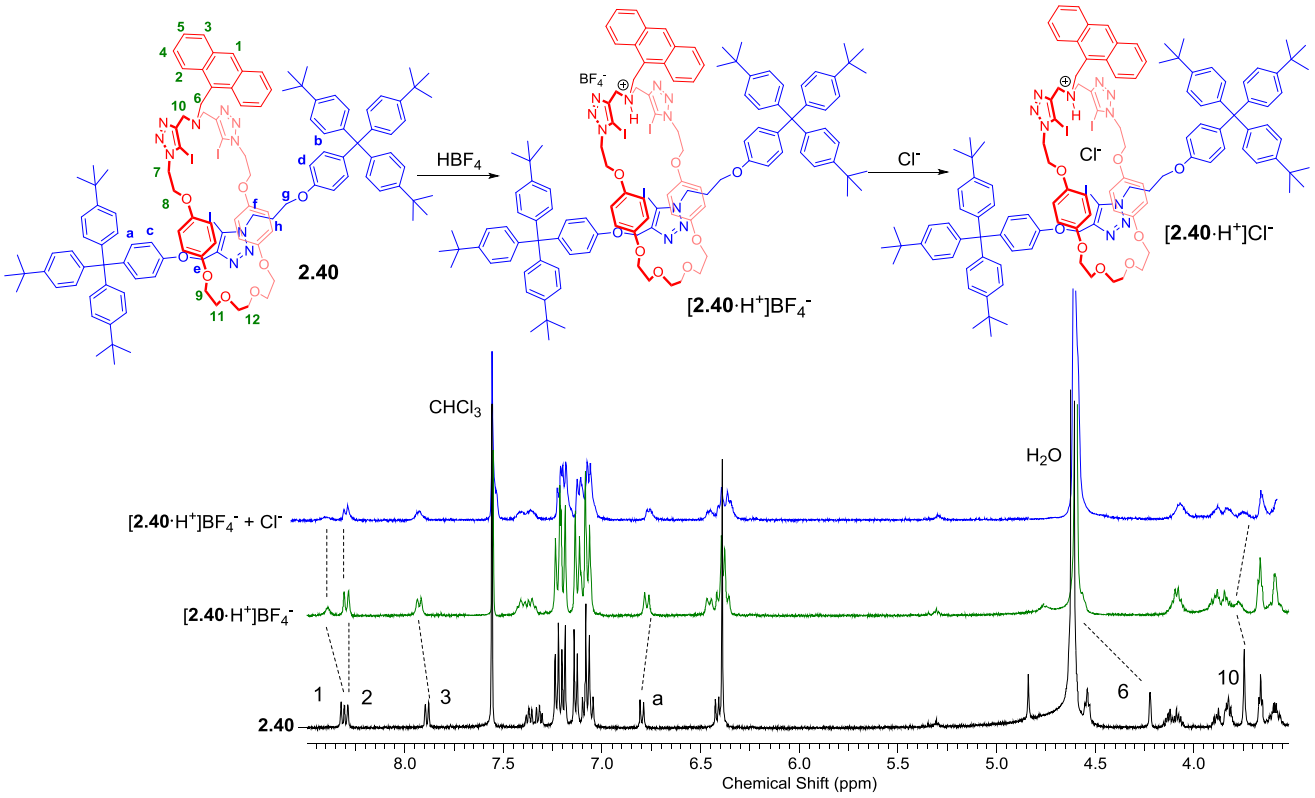


Figure 2.27. Partial ^{1}H NMR spectra of neutral rotaxane **2.40** and singly-protonated [**2.40**·H^+]BF_4^- in the presence of 0.0 and 10 equivalents of TBACl ([host] = 1.0 mM, $CDCl_3$/ CD_3OD (1:1 *v*/*v*), *T* = 298 K).

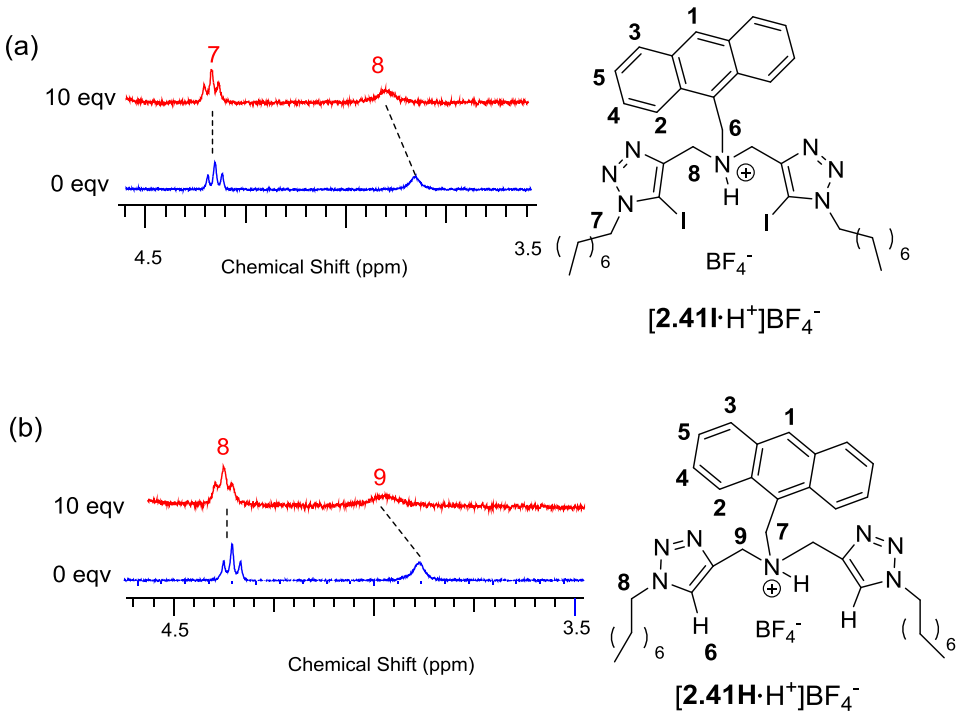


Figure 2.28. Partial ^{1}H NMR spectra showing the perturbations of the signals of compound (a) [**2.41I**·H^{+}]BF$_4$ and (b) [**2.41H**·H^{+}]BF$_4$ in the presence of 0.0 and 10 equivalents of TBACl. ([host]= 1.0 mM, $CDCl_3/CD_3OD$ (1:1 *v*/*v*), *T* = 298 K).

Further evidence of amine protonation was gained by fluorescence experiments, where HBF_4 addition to rotaxane **2.40** led to a large turn-on fluorescence response from the anthracene fluorophore due to the loss of PET fluorescence quenching pathways upon amine protonation (Figure 2.29(a)).[38,43,46,47] However, as shown in Figure 2.29(b), addition of 80 equivalents of Cl^- to rotaxane [**2.40**·H^{+}]BF_4^- in CH_3CN resulted in an approximately 60 % reduction in fluorescence intensity, attributable to strong ammonium-Cl^- HB interactions which partially restores the PET quenching properties of the macrocycle's amine moiety. A considerably smaller fluorescence 'turn-off' quenching response was recorded in the more competitive solvent mixture of $CHCl_3/CH_3OH$ (1:1 *v*/*v*) after adding the same amount of Cl^- anion (Figure 2.29(c)), consistent with greater competition from the protic solvent mixture for HB interactions with the highly charge-dense Cl^-.

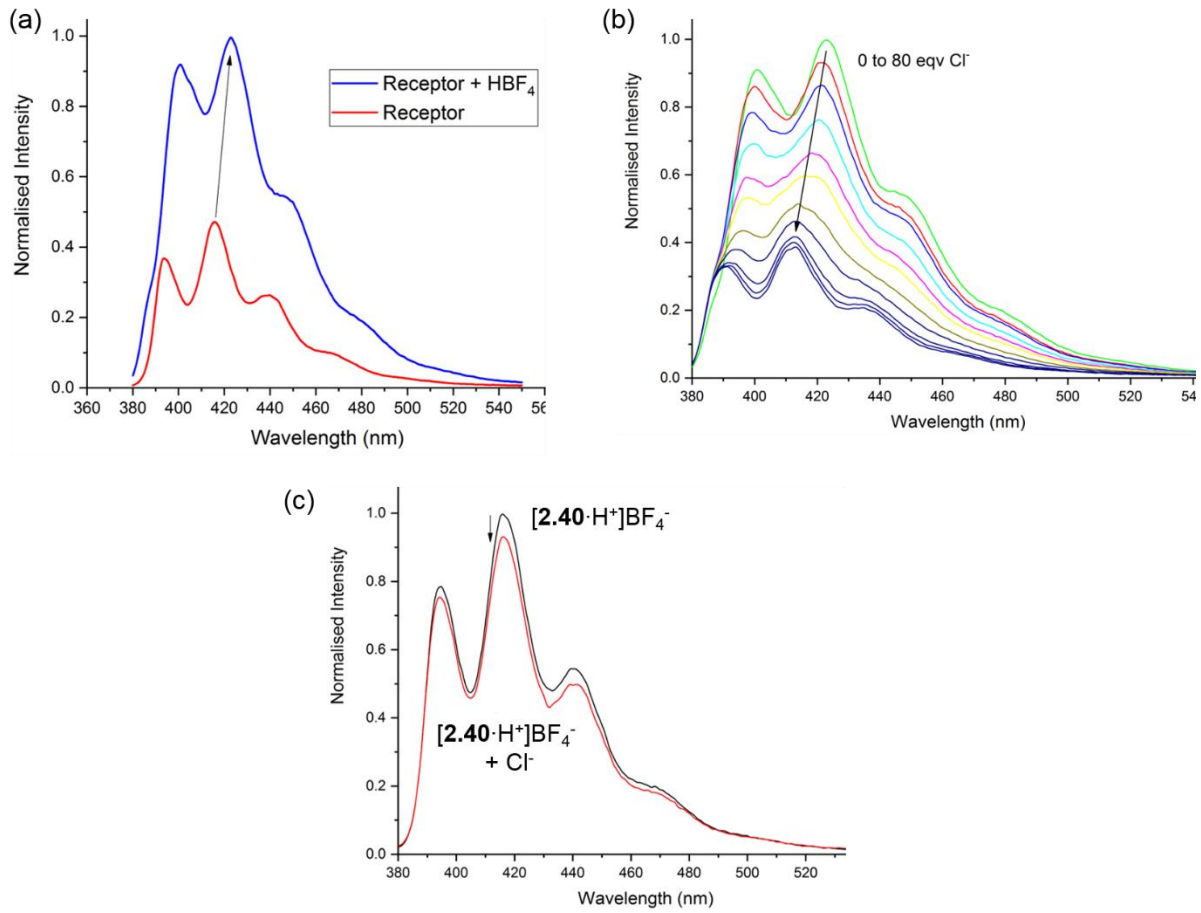


Figure 2.29. (a) Fluorescence spectra of neutral rotaxane **2.40** and [**2.40**·H^+]BF_4^-. (Red line: neutral rotaxane **2.40**; blue line: cationic rotaxane [**2.40**·H^+]BF_4^-); (b) fluorescence spectra showing the changes in anthracene fluorescence intensity of singly-protonated rotaxane [**2.40**·H^+]BF_4^- upon Cl^- addition in acetonitrile and (c) in $CHCl_3$/CH_3OH (1:1 *v*/*v*). ([host] = 5 μM , *T* = 298 K, λ_{ex} = 368 nm).

Given that the neutral rotaxanes **2.39** and **2.40** showed no evidence of interactions with anions in competitive methanolic solvent media, the corresponding cationic rotaxanes are now capable of recognising anions in protic media upon protonation. By monitoring the ^{1}H NMR shifts of protons H_{10} of the protonated rotaxanes [**2.39**·$2H^+$]$(BF_4^-)_2$ and [**2.40H**·H^+]BF_4 as a function of anion concentration (Figure 2.30), 1:1 host-guest stoichiometric association constants were determined using the WinEQNMR2[28] software, and compared with those of acyclic protonated receptors [**2.41I**·H^+]BF_4 and [**2.41H**·H^+]BF_4 (Table 2.4). Both protonated XB rotaxane hosts display notable affinities for Cl^- in the competitive protic solvent medium. Importantly, for [**2.39**·$2H^+$]$(BF_4^-)_2$ an anti-Hofmeister binding trend was observed for the anions tested, with the less strongly-hydrated anions Br^- and NO_3^- more weakly bound than Cl^-. No appreciable binding was observed for I^- and ReO_4^-

, which may stem from their poor size/geometric complementarity to the preorganised rotaxane cavity. Considering the inherent preference of XB donor host molecules to bind to the heavier and 'softer' halides in aqueous solvents due to their greater ease of dehydration,[40,48–50] this result is especially notable since it is the first example of a XB rotaxane preferentially binding the most strongly-hydrated Cl^- in the presence of water, and only the second XB receptor known to display an anti-Hofmeister binding bias.[51] While rotaxane [**2.39**·2H$^+$]$(BF_4^-)_2$ displays stronger Cl^- affinity compared to [**2.40**·H$^+$]BF_4^-, which is likely to be a consequence of its dicationic character, [**2.40**·H$^+$]BF_4^- displayed rare exclusive Cl^- selectivity. The importance of XB interactions for anion binding, even with the contribution of HB interactions from the ammonium group(s), can be seen from the significantly stronger Cl^- binding affinities of protonated XB acyclic receptor [**2.41I**·H$^+$]BF_4 compared with [**2.41H**·H$^+$]BF_4. Hence the observed Cl^- selectivity for both rotaxanes is likely to result from a combination of favourable ammonium HB- and XB-chloride interactions together with a preorganised interlocked binding cavity which is of complementary shape and size to the halide guest species.

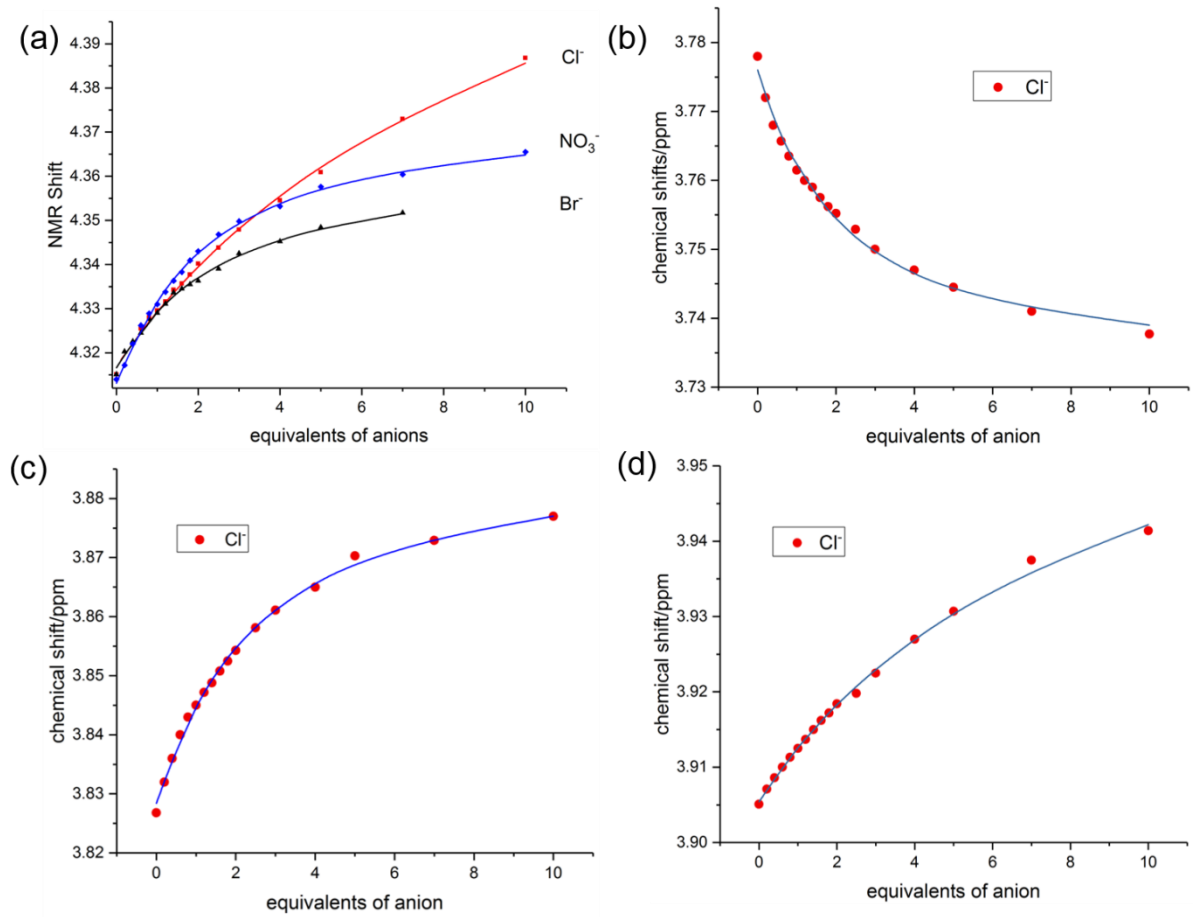


Figure 2.30. Binding isotherms showing the changes in the chemical shift of proton (a) H_4 in rotaxane [**2.39**·2H$^+$](BF$_4^-$)$_2$ in $CDCl_3/CD_3OD/D_2O$ (45:45:10 v/v/v); (b) H_{10} in rotaxane [**2.40**·H$^+$]BF$_4^-$; (c) H_8 in [**2.41I**·H$^+$]BF$_4$; (d) H_9 in [**2.41H**·H$^+$]BF$_4$ in $CHCl_3/CH_3OH$ (1:1 v/v) with increasing equivalents of anions added ([host] = 1.0 mM, 500 MHz, *T* = 298 K).

Table 2.4. Association constants (K_a [M^{-1}]) of anions with cationic rotaxanes [**2.39**·2H$^+$](BF$_4^-$)$_2$ and [**2.40**·H$^+$]BF$_4^-$, as well as acyclic receptors [**2.41I**·H$^+$]BF$_4^-$ and [**2.41H**·H$^+$]BF$_4^-$.[a]

	[**2.39**·2H$^+$](BF$_4^-$)$_2$ [b]	[**2.40**·H$^+$]BF$_4^-$ [c]	[**2.41I**·H$^+$]BF$_4$ [c]	[**2.41H**·H$^+$]BF$_4$ [c]
Cl$^-$	812(4)	662(7)	488(38)	102(3)
Br$^-$	476(47)	-[d]	-[e]	-[e]
NO_3^-	584(35)	-[d]	-[e]	-[e]

[a] Values of K_a are calculated by the WinEQNMR2[28] software using a 1:1 host-guest stoichiometric binding model. Errors (±) are in parentheses (<10%). No binding observed for I$^-$ and ReO_4^- with both [**2.39**·2H$^+$](BF$_4^-$)$_2$ and [**2.40**·H$^+$]BF$_4^-$;

[b] Performed in $CDCl_3$/ CD_3OD/ D_2O (45:45:10, *v/v/v*);

[c] Performed in $CDCl_3$/ CD_3OD (1:1 *v/v*);

[d] No binding;

[e] Not conducted.

In contrast to anion binding, as expected addition of acid proved highly detrimental to the rotaxanes' inherent metal cation affinity. Upon addition of two equivalents of HBF_4 to a solution of Zn^{2+}-complexed rotaxane **2.39** in d_6-acetone, considerable broadening of its ^1H NMR spectrum was observed, accompanied by the appearance of multiple additional peaks (Figure 2.31), revealing Zn^{2+} displacement from the rotaxane's binding cavity due to the protonation of the amine units. This hypothesis was also supported by fluorescence spectroscopy, where the addition of one equivalent of HBF_4 to separate CH_3CN solutions of Zn^{2+}, Cu^{2+} and Ni^{2+}-bound complexes of rotaxane **2.40** resulted in significant fluorescence 'turn-on' responses. This observation suggested the respective metal cation's displacement from the rotaxane cavity by protonation of the macrocycle component's tertiary amine unit (Figure 2.32).

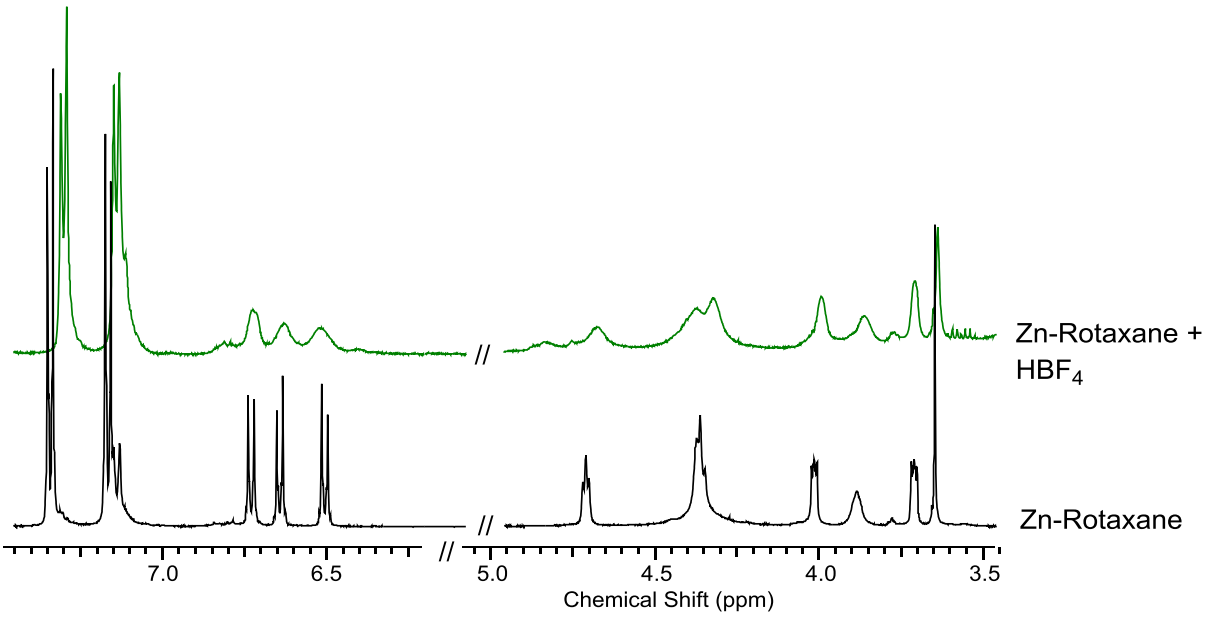


Figure 2.31. Partial ^1H NMR spectra of rotaxane **2.39**·$Zn(ClO_4)_2$ before and after addition of two equivalents of HBF_4 (solvent = d_6-acetone).

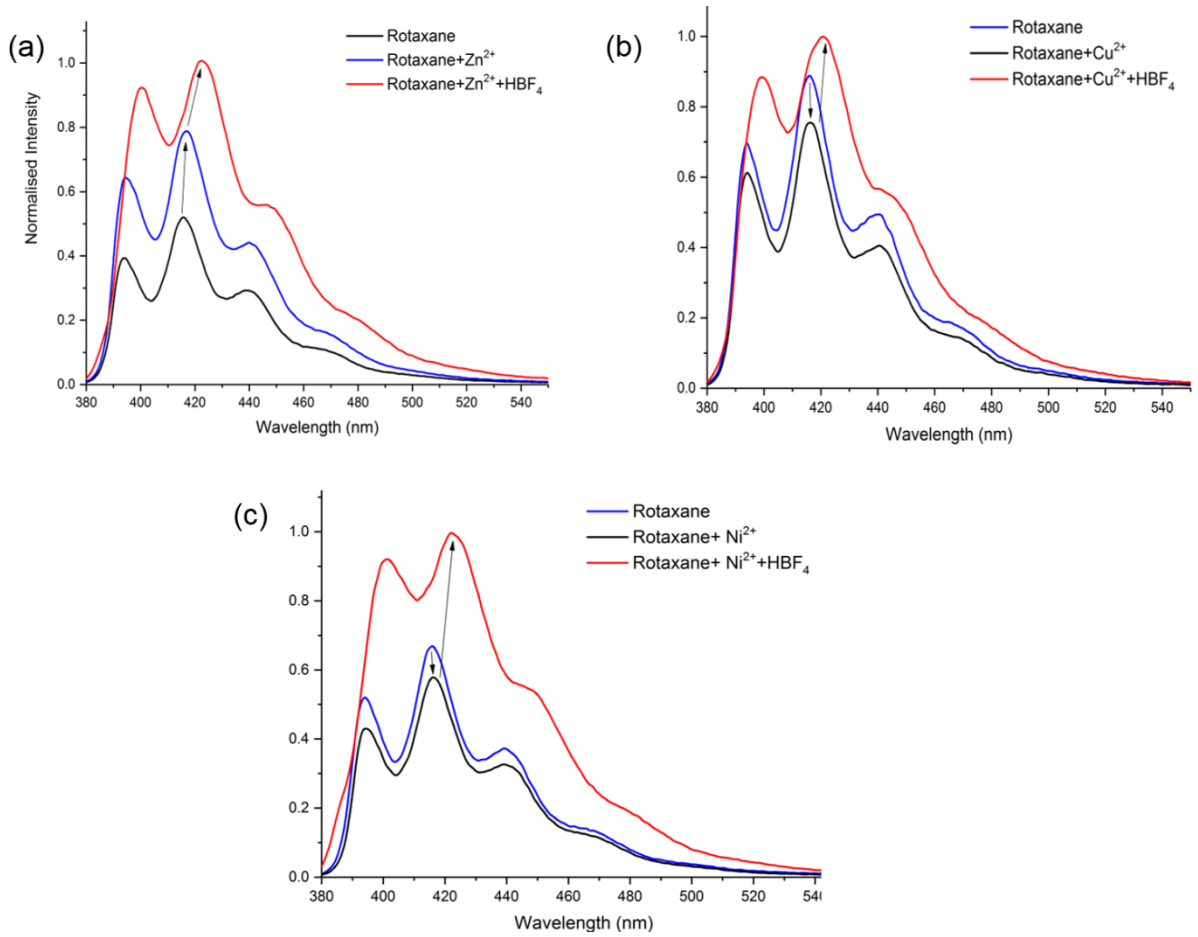


Figure 2.32. Fluorescence response of rotaxane **2.40** after addition of one equivalent of (a) Zn^{2+}; (b) Cu^{2+}; (c) Ni^{2+} and subsequent addition of one equivalent of HBF_4.

2.5 Towards XB Catenanes Capable of Acid-regulated Switching of Metal Cation and Anion Guest Binding

2.5.1 Design of Target Catenanes

Compared to rotaxanes, catenanes have special three-dimensional cavities potentially leading to different guest binding affinities and selectivities. After the successful construction of rotaxanes capable of acid-regulated switching of metal cation and anion guests, the attempted synthesis of corresponding XB catenanes were undertaken (Figure 2.33) via active and passive metal templation.

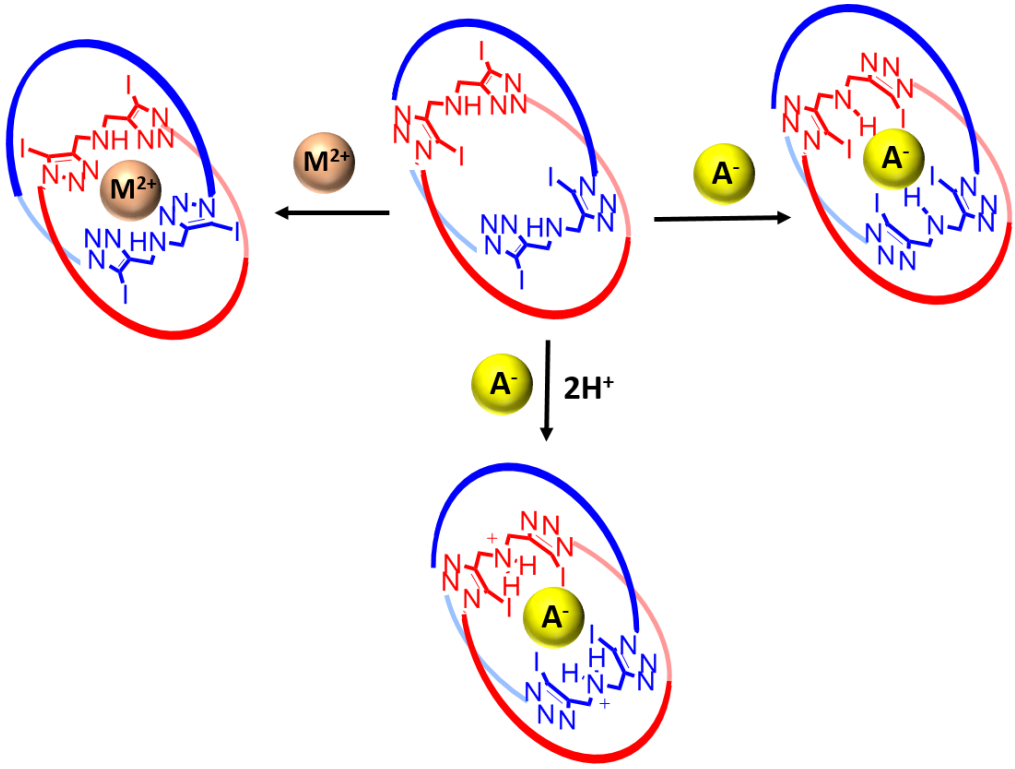
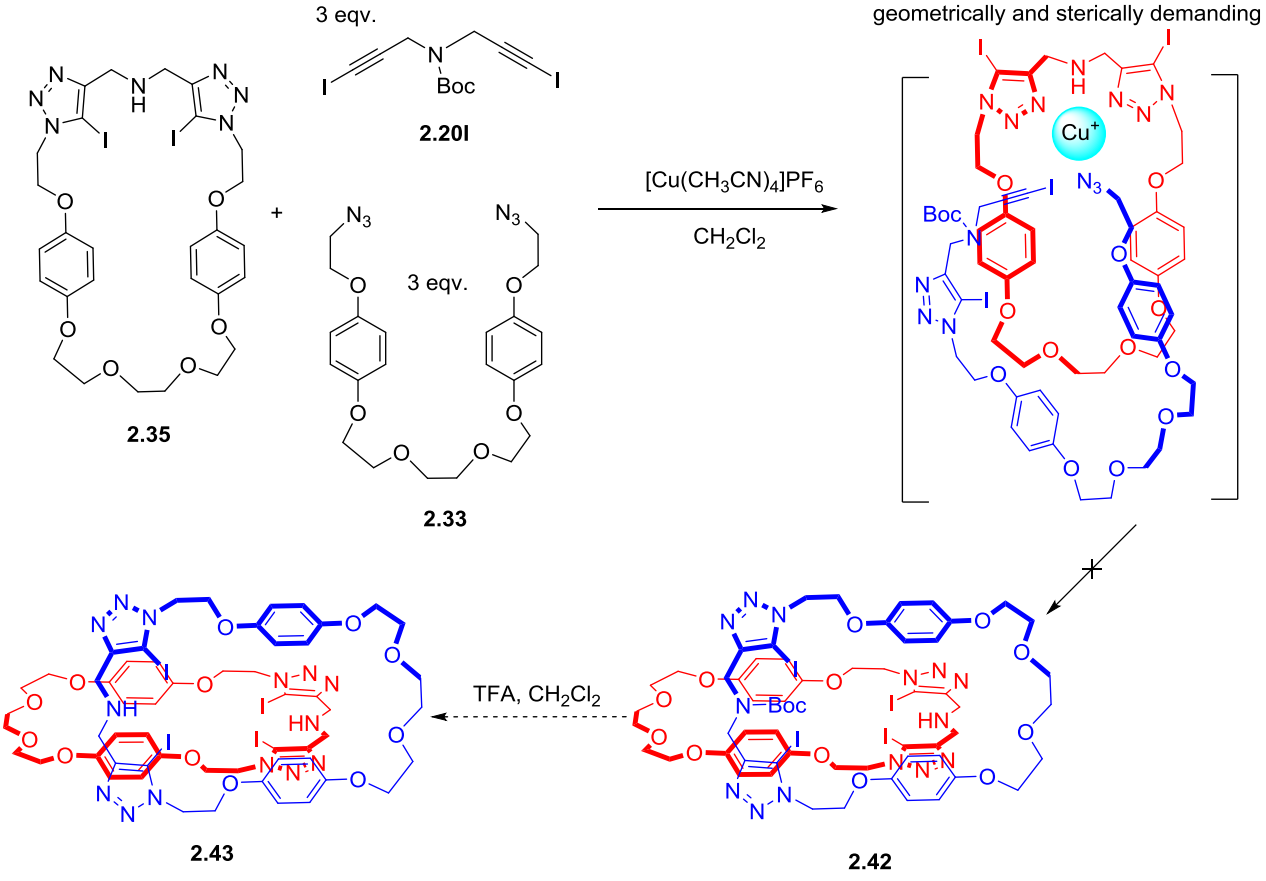


Figure 2.33. Target XB catenane for acid-regulated metal cation and anion guest binding.

2.5.2 Active Metal Templation

Given the success of AMT rotaxane synthesis, the attempted synthesis of the target catenane was initially performed by CuAAC-AMT reaction using similar protocols following previously reported procedures.[52] Three equivalents of bis-iodoalkyne **2.20I** and bis-azide **2.33** were added to an equimolar CH_2Cl_2 room temperature mixture of macrocycle **2.35** and

$[Cu(CH_3CN)_4]PF_6$ (Scheme 2.20). However, after monitoring the reaction mixture by ESI-MS for a week, no evidence of catenane **2.42** formation was observed while only the macrocycle was detected. Repeating the reaction at 40°C did not improve the outcome. Considering the comparable ease of synthesising rotaxane **2.39** under similar AMT conditions, the unsuccessful formation of the target catenane may arise from the more sterically demanding endotopic geometry that is required for the interlocked CuAAC ring-closure reaction (Scheme 2.20).[52,53]

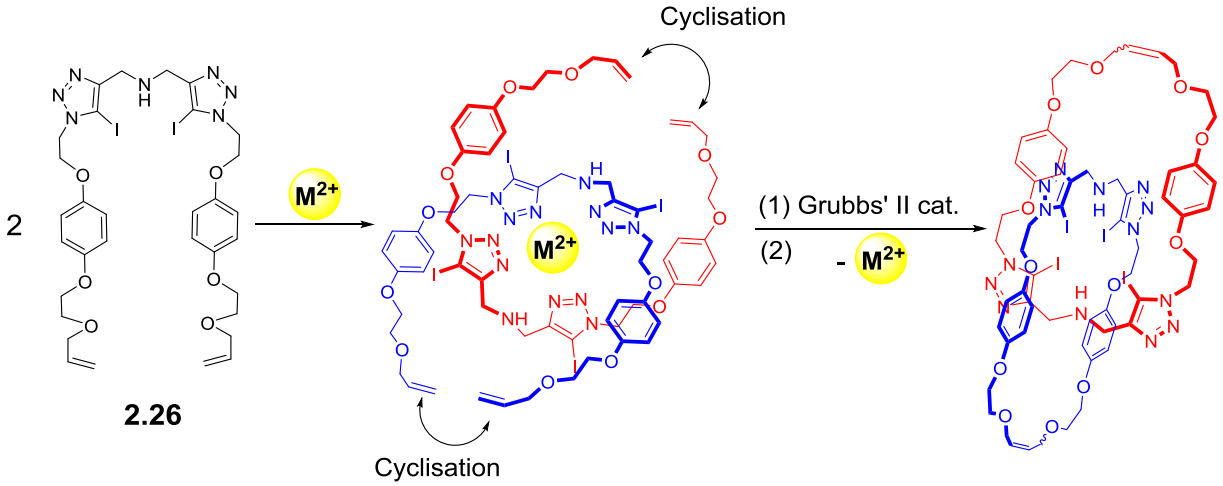


Scheme 2.20. Attempted synthesis of target catenane **2.43** via AMT synthesis.

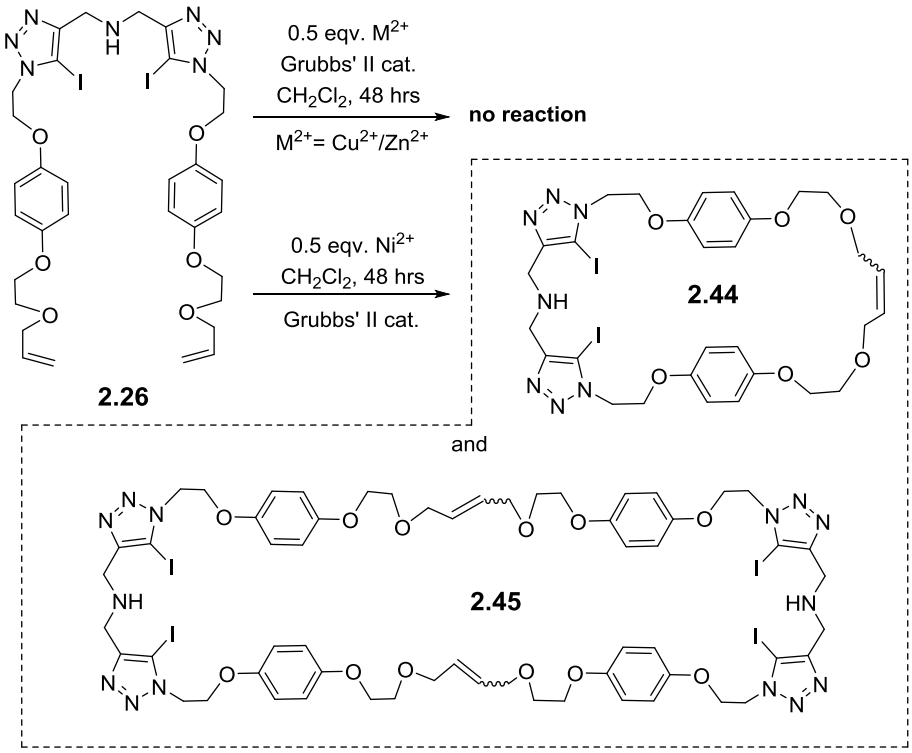
2.5.3 Passive Metal Templation

Passive metal templates such as Ni^{2+}, Cu^{2+} and Zn^{2+} have been successfully utilised in constructing interlocked structures (as introduced in Section 1.3). Taking into account the ability of the bis-iodotriazole-amine motif to bind metal cations (Ni^{2+}, Cu^{2+}, Zn^{2+}), as demonstrated in Section 2.4, the synthesis of the target catenane was then attempted via a

passive metal template approach (Scheme 2.21). Catenane synthesis was attempted by stirring one equivalent of **2.26** with 0.5 equivalents of the perchlorate salts of transition metal (Ni^{2+}, Cu^{2+}, Zn^{2+}) in CH_2Cl_2 for 5 mins respectively, followed by addition of 10% (by weight) Grubbs' II RCM catalyst. With Cu^{2+} and Zn^{2+}, as evidenced by ESI-MS after 48 hrs, no ring-closure reactions had occurred. However, when using Ni^{2+} all the starting materials had been consumed, and two products were separated by preparative TLC (Scheme 2.22). High-resolution mass spectrometry analysis revealed one to be the ring-closed macrocycle **2.44** (m/z = 844, $[M+H^+]$, yield = 41%) and the other (compound **2.45**) as either the desired homo-catenane or a macrocycle dimer (m/z = 1687, $[M+H^+]$, yield = 39%, Figure 2.34(a)). By comparing the ^1H NMR spectra of **2.44** and **2.45**, no obvious signal differences were observed. In particular, negligible perturbations of the hydroquinone protons were evident, indicating that **2.45** was not an interlocked catenane structure and was more likely to be the macrocycle dimer (Figure 2.34(b)). The preferential formation of the macrocycle dimer may stem from the bis-tridentate ligated geometry of the Ni^{2+}-complex template assembly facilitating the synthesis of the non-interlocked species (Scheme 2.23).



Scheme 2.21. Attempt synthesis of target catenane via passive metal templation.



Scheme 2.22. Products resulting from the RCM reactions.

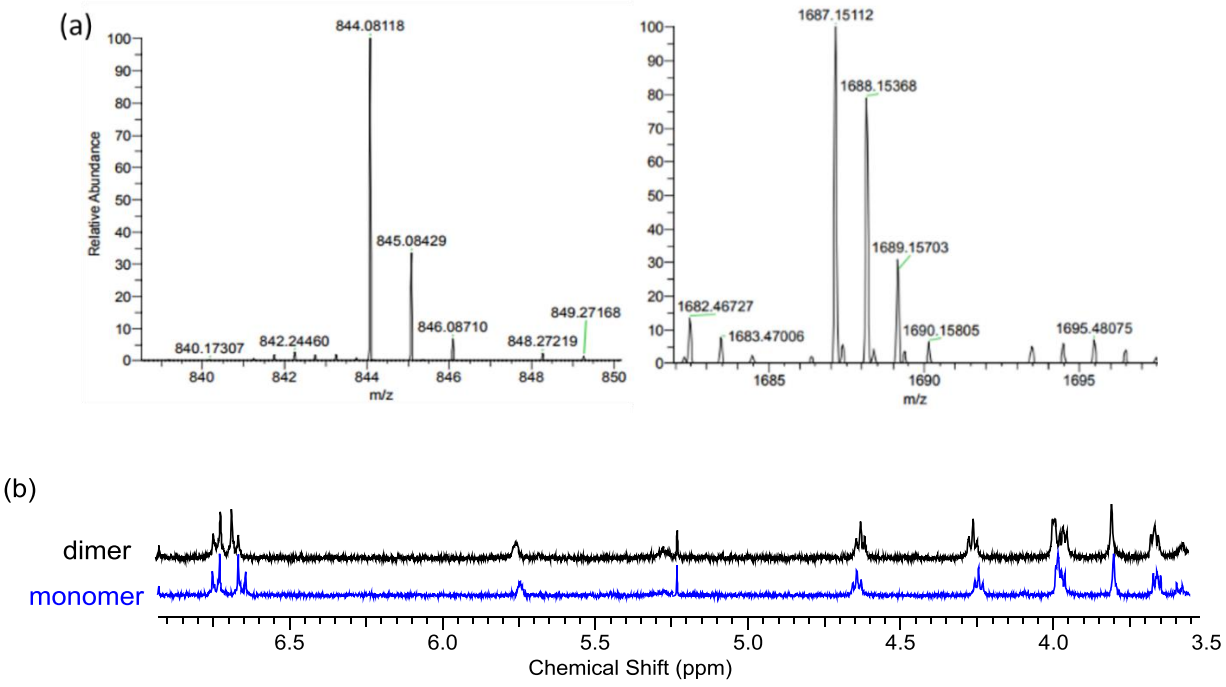
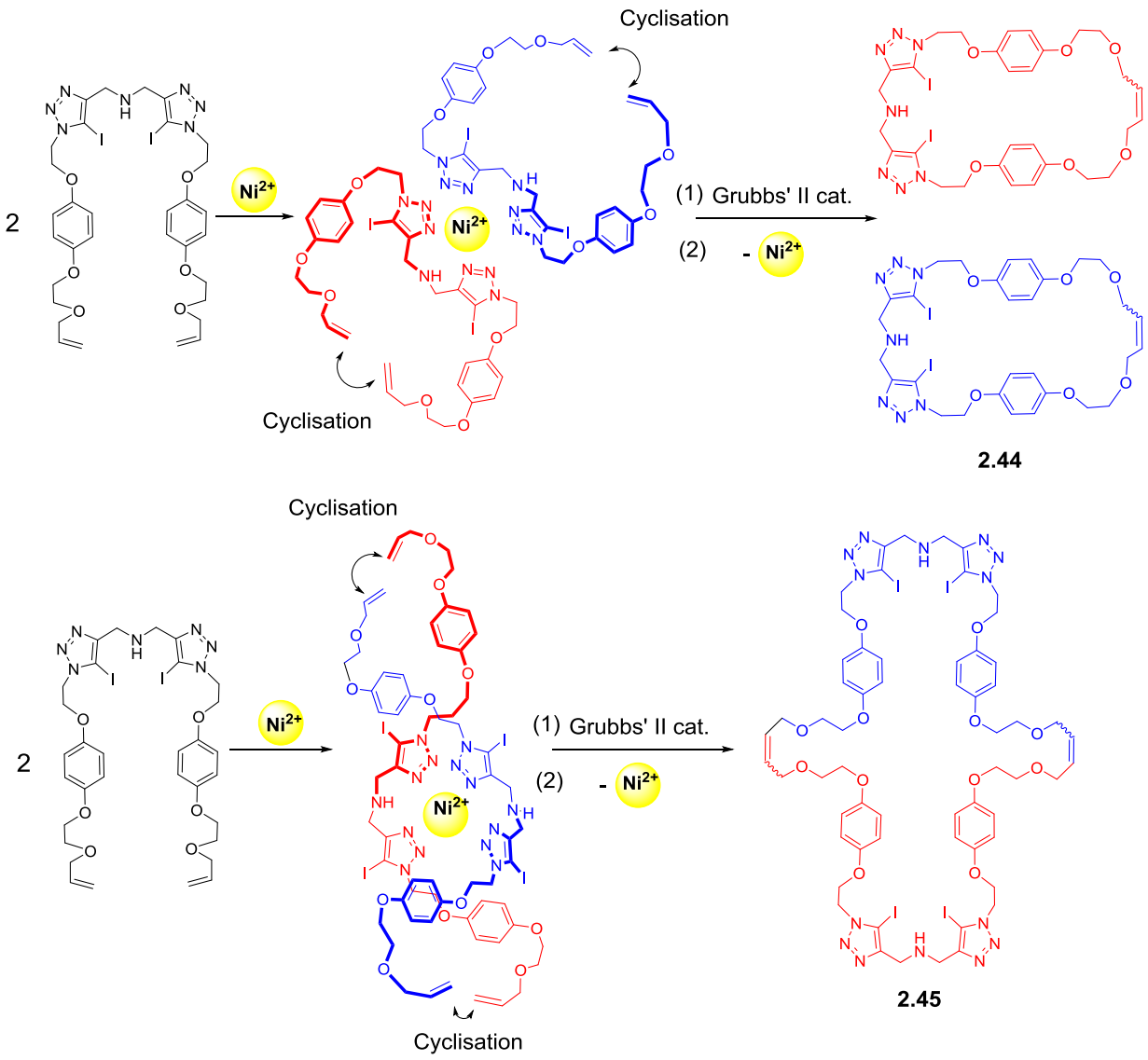


Figure 2.34. (a) High resolution mass spectrometry and (b) partial ^{1}H NMR spectra of macrocycle **2.44** and macrocycle dimer **2.45** (solvent = $CDCl_3$).

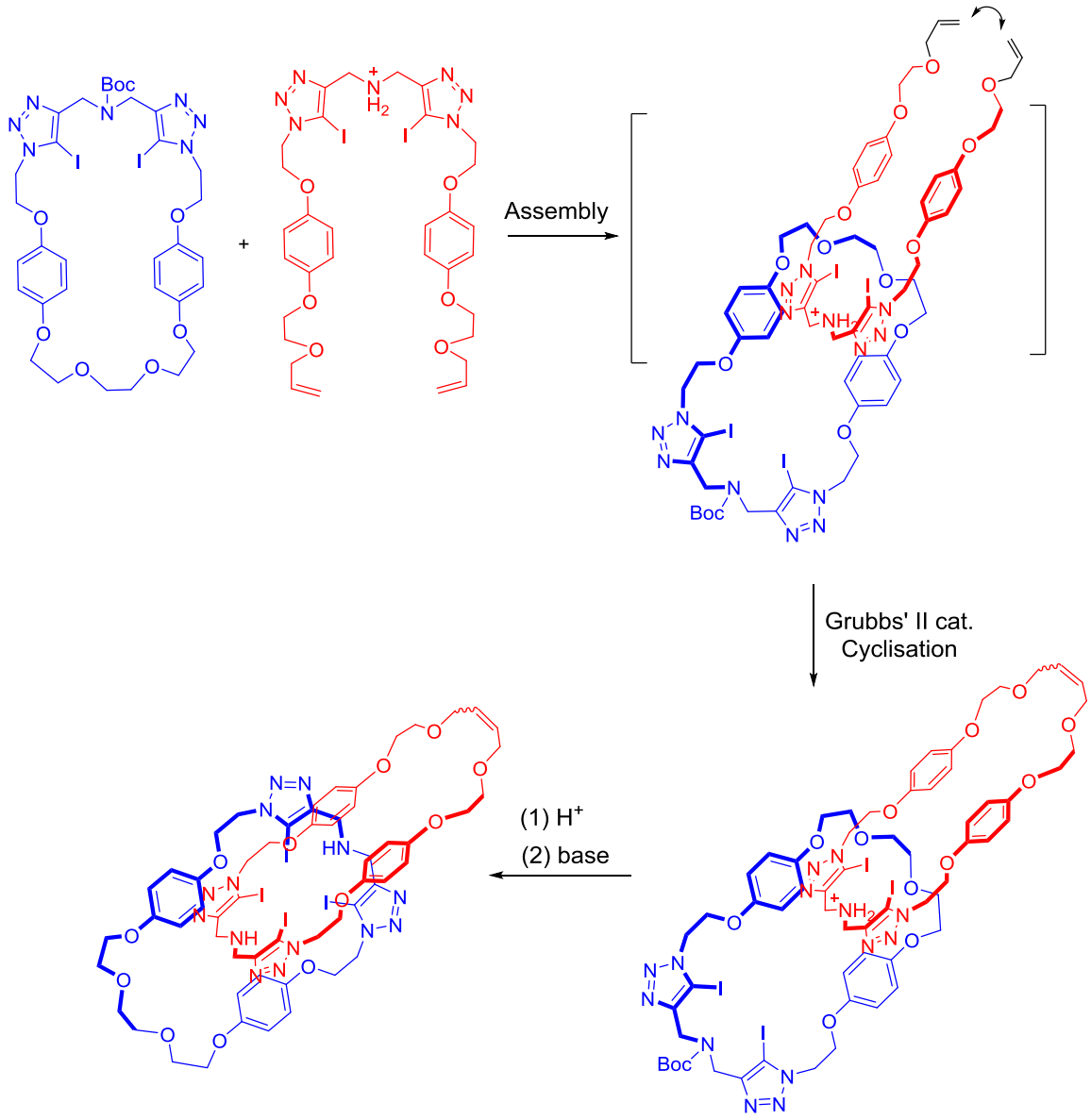


Scheme 2.23. Proposed mechanism to generate resulting products **2.44** and **2.45**.

2.6 Conclusion and Future Work

In conclusion, a series of XB interlocked rotaxanes were constructed using bifunctional bis-iodotriazole derivatives. Their Lewis basic N-donor atoms were able to perform metal complexation, which could facilitate active metal templation rotaxane synthesis, while polarised H/I atoms were capable of anion binding via HB/XB interactions. For instance, by coordinating to Re(I), anion affinity and selectivity of XB rotaxanes could be manipulated and tuned. In addition, by virtue of the antagonistic Lewis basic triazole-secondary amine and Lewis acidic XB bis-iodotriazole functional motifs, novel XB rotaxanes were demonstrated to be capable of acid-triggered switching of metal cation and anion guest binding behaviour.

Future work could focus on the synthesis of XB catenanes using hydrogen bonding templation (Scheme 2.24). By utilising the HB interactions between the macrocycle polyether groups and a protonated secondary ammonium XB motif functionalised with vinyl groups, a RCM reaction would produce the target XB catenane host for metal cation and anion guest recognition applications.



Scheme 2.24. Target XB catenane synthesis via HB templation.

2.7 Reference:

1 B. Schulze and U. S. Schubert, *Chem. Soc. Rev.*, 2014, **43**, 2522–2571.

2 A. J. McConnell and P. D. Beer, *Angew. Chem. Int. Ed.*, 2012, **51**, 5052–5061.

3 H. C. Kolb, M. G. Finn and K. B. Sharpless, *Angew. Chem. Int. Ed.*, 2001, **40**, 2004–2021.

4 J. E. Moses and A. D. Moorhouse, *Chem. Soc. Rev.*, 2007, **36**, 1249–1262.

5 D. N. Barsoum, N. Okashah, X. Zhang and L. Zhu, *J. Org. Chem.*, 2015, **80**, 9542–9551.

6 A. Bastero, D. Font and M. A. Pericàs, *J. Org. Chem.*, 2007, **72**, 2460–2468.

7 T. L. Mindt, H. Struthers, L. Brans, T. Anguelov, C. Schweinsberg, V. Maes, D. Tourwé and R. Schibli, *J. Am. Chem. Soc.*, 2006, **128**, 15096–15097.

8 S. Huang, R. J. Clark and L. Zhu, *Org. Lett.*, 2007, **9**, 4999–5002.

9 Y. Li, J. C. Huffman and A. H. Flood, *Chem. Commun.*, 2007, 2692–2694.

10 P. S. Donnelly, S. D. Zanatta, S. C. Zammit, J. M. White and S. J. Williams, *Chem. Commun.*, 2008, 2459–2461.

11 A. Borissov, J. Y. C. Lim, A. Brown, K. E. Christensen, A. L. Thompson, M. D. Smith and P. D. Beer, *Chem. Commun.*, 2017, **53**, 2483–2486.

12 B. Chowdhury, S. Sinha and P. Ghosh, *Chem. – Eur. J.*, 2016, **22**, 18051–18059.

13 T. K. Mole, W. E. Arter, I. Marques, V. Félix and P. D. Beer, *J. Organomet. Chem.*, 2015, **792**, 206–210.

14 R. Tepper, B. Schulze, P. Bellstedt, J. Heidler, H. Görls, M. Jäger and U. S. Schubert, *Chem. Commun.*, 2017, **53**, 2260–2263.

15 J. Y. C. Lim, I. Marques, V. Félix and P. D. Beer, *J. Am. Chem. Soc.*, 2017, **139**, 12228–12239.

16 J. Y. C. Lim, T. Bunchuay and P. D. Beer, *Chem. – Eur. J.*, 2017, **23**, 4700–4707.

17 M. J. Langton, Y. Xiong and P. D. Beer, *Chem. – Eur. J.*, 2015, **21**, 18910–18914.

18 J. Y. C. Lim, I. Marques, A. L. Thompson, K. E. Christensen, V. Félix and P. D. Beer, *J. Am. Chem. Soc.*, 2017, **139**, 3122–3133.

19 N. L. Kilah, M. D. Wise, C. J. Serpell, A. L. Thompson, N. G. White, K. E. Christensen and P. D. Beer, *J. Am. Chem. Soc.*, 2010, **132**, 11893–11895.

20 V. Aucagne, K. D. Hänni, D. A. Leigh, P. J. Lusby and D. B. Walker, *J. Am. Chem. Soc.*, 2006, **128**, 2186–2187.

21 S. W. Robinson, C. L. Mustoe, N. G. White, A. Brown, A. L. Thompson, P. Kennepohl and P. D. Beer, *J. Am. Chem. Soc.*, 2015, **137**, 499–507.

22 S. W. Robinson and P. D. Beer, *Org. Biomol. Chem.*, 2016, **15**, 153–159.

23 H. C. Zhao, B. Mello, B.-L. Fu, H. Chowdhury, D. J. Szalda, M.-K. Tsai, D. C. Grills and J. Rochford, *Organometallics*, 2013, **32**, 1832–1841.

24 M. Busby, A. Gabrielsson, P. Matousek, M. Towrie, A. J. Di Bilio, H. B. Gray and A. Vlček, *Inorg. Chem.*, 2004, **43**, 4994–5002.

25 A. E. Nahhas, A. Cannizzo, F. van Mourik, A. M. Blanco-Rodríguez, S. Záliš, J. Vlček Antonín and M. Chergui, *J. Phys. Chem. A*, 2010, **114**, 6361–6369.

26 S. M. Fredericks, J. C. Luong and M. S. Wrighton, *J. Am. Chem. Soc.*, 1979, **101**, 7415–7417.

27 S.-Y. Baek, Y.-W. Kim, S.-H. Yoo, K. Chung, N.-K. Kim and J.-S. Kim, *Ind. Eng. Chem. Res.*, 2012, **51**, 9669–9678.

28 M. J. Hynes, *J. Chem. Soc. Dalton Trans.*, 1993, 311.

29 P. Bonomi, M. D. Attieh, C. Gonzato and K. Haupt, *Chem. – Eur. J.*, 2016, **22**, 10150–10154.

30 N. Harada, H. Kimura, M. Ono, D. Mori, Y. Ohmomo, T. Kajimoto, H. Kawashima and H. Saji, *J. Organomet. Chem.*, 2011, **696**, 3745–3749.

31 N. Lazarova, S. James, J. Babich and J. Zubieta, *Inorg. Chem. Commun.*, 2004, **7**, 1023–1026.

32 T. L. Mindt, C. Schweinsberg, L. Brans, A. Hagenbach, U. Abram, D. Tourwé, E. Garcia-Garayoa and R. Schibli, *ChemMedChem*, 2009, **4**, 529–539.

33 N. G. White and P. D. Beer, *Chem. Commun.*, 2012, **48**, 8499–8501.

34 J. A. Wisner, P. D. Beer and M. G. B. Drew, *Angew. Chem. Int. Ed.*, 2001, **40**, 3606–3609.

35 N. G. White, C. J. Serpell and P. D. Beer, *Cryst. Growth Des.*, 2014, **14**, 3472–3479.

36 T. Drakenberg, K. I. Dahlqvist and S. Forsen, *J. Phys. Chem.*, 1972, **76**, 2178–2183.

37 B. Valeur and M. N. Berberan-Santos, *Molecular Fluorescence: Principles and Applications*, John Wiley & Sons, 2013.

38 R. Martínez-Máñez and F. Sancenón, *Chem. Rev.*, 2003, **103**, 4419–4476.

39 P. D. Beer, *Acc. Chem. Res.*, 1998, **31**, 71–80.

40 J. Y. C. Lim, T. Bunchuay and P. D. Beer, *Chem. – Eur. J.*, 2017, **23**, 4700–4707.

41 O. Fleischel, N. Wu and A. Petitjean, *Chem. Commun.*, 2010, **46**, 8454–8456.

42 F. Otón, M. del C. González, A. Espinosa, A. Tárraga and P. Molina, *Organometallics*, 2012, **31**, 2085–2096.

43 R. R. Mittapalli, S. S. R. Namashivaya, A. S. Oshchepkov, E. Kuczyńska and E. A. Kataev, *Chem. Commun.*, 2017, **53**, 4822–4825.

44 L. Fabbrizzi and A. Poggi, *Chem. Soc. Rev.*, 1995, **24**, 197–202.

45 P. V. Bernhardt, B. M. Flanagan and M. J. Riley, *J. Chem. Soc. Dalton Trans.*, 1999, 3579–3584.

46 D. H. Vance and A. W. Czarnik, *J. Am. Chem. Soc.*, 1994, **116**, 9397–9398.

47 F. Sancenón, A. Benito, J. M. Lloris, R. Martínez-Máñez, T. Pardo and J. Soto, *Helv. Chim. Acta*, 2002, **85**, 1505–1516.

48 M. J. Langton, L. C. Duckworth and P. D. Beer, *Chem. Commun.*, 2013, **49**, 8608–8610.

49 M. J. Langton and P. D. Beer, *Chem. Commun.*, 2014, **50**, 8124–8127.

50 A. Brown and P. D. Beer, *Chem. Commun.*, 2016, **52**, 8645–8658.

51 D. Mungalpara, S. Stegmüller and S. Kubik, *Chem. Commun.*, 2017, **53**, 5095–5098.

52 S. M. Goldup, D. A. Leigh, T. Long, P. R. McGonigal, M. D. Symes and J. Wu, *J. Am. Chem. Soc.*, 2009, **131**, 15924–15929.

53 J. D. Crowley, S. M. Goldup, A.-L. Lee, D. A. Leigh and R. T. McBurney, *Chem. Soc. Rev.*, 2009, **38**, 1530–1541.

54 P. R. Aston, P. T. Glink, J. F. Stoddart, P. A. Tasker, A. J. P. White and D. J. Williams, *Chem. – Eur. J.*, 1996, **2**, 729–736.

55 H. Liu, W.-J. Hu, Y. A. Liu, J.-S. Li, B. Jiang and K. Wen, *Eur. J. Org. Chem.*, 2015, **2015**, 6270–6277.

56 Z.-J. Zhang, H.-Y. Zhang, H. Wang and Y. Liu, *Angew. Chem. Int. Ed.*, 2011, **50**, 10834–10838.

57 P. R. Ashton, R. A. Bartsch, S. J. Cantrill, R. E. Hanes, S. K. Hickingbottom, J. N. Lowe, J. A. Preece, J. F. Stoddart, V. S. Talanov and Z.-H. Wang, *Tetrahedron Lett.*, 1999, **40**, 3661–3664.

58 H. Iwamoto, W. Takizawa, K. Itoh, T. Hagiwara, E. Tayama, E. Hasegawa and T. Haino, *J. Org. Chem.*, 2013, **78**, 5205–5217.

59 D. E. Phipps and P. D. Beer, *Tetrahedron Lett.*, 2009, **50**, 3454–3457.

Chapter 3: Halogen Bonding Cryptands and Cryptand-based Interlocked Structures for Anion Recognition

3.1 Introduction

A cryptand refers to a bicyclic host molecule which is able to bind guests in a crypt-like structure, interring them as in a burial. This term was first introduced by Lehn, Dietrich and Sauvage in 1968,[1] for these macrobicyclic molecules, as three-dimensional analogues of crown ethers, with better selectivity and strength when complexing alkali metal cations (see Chapter 1, section 1). Studies of cryptand host systems launched a novel flourishing field of supramolecular host-guest chemistry, in particular for anion receptor design. This introduction will focus mainly on anion cryptand host systems and the synthesis of cryptand-based interlocked structures whose unique three-dimensional cavities can provide potentially new possibilities for anion recognition.

3.1.1 Cryptands for Anion Recognition

The first examples of cryptands for anion recognition, known as *katapinands*, were reported by Park and Simmons in 1968.[2,3] The protonated forms of these hosts were able to bind halides (Cl^-, Br^- and I^-) in their cavities in 50% deuteriotrifluoroacetic acid aqueous solvent (Figure 3.1(a)). After this pioneering work, a range of polyammonium cryptands for binding various anions such as halides[4] and azide[5] was developed by Lehn and co-workers.[5] For example, in acidic aqueous media the hexa-protonated octa-aza macrobicyclic polyammonium cryptand (Figure 3.1(b)) was able to bind F^- via a quasi-trigonal prismatic array of six $F^-\cdots HN^+$ hydrogen bonds[4] while a more recent furan-containing cryptand developed by Nelson and co-workers could, after hexa-protonation, form a inclusion complex with SO_4^{2-} (Figure 3.1(c)).[6]

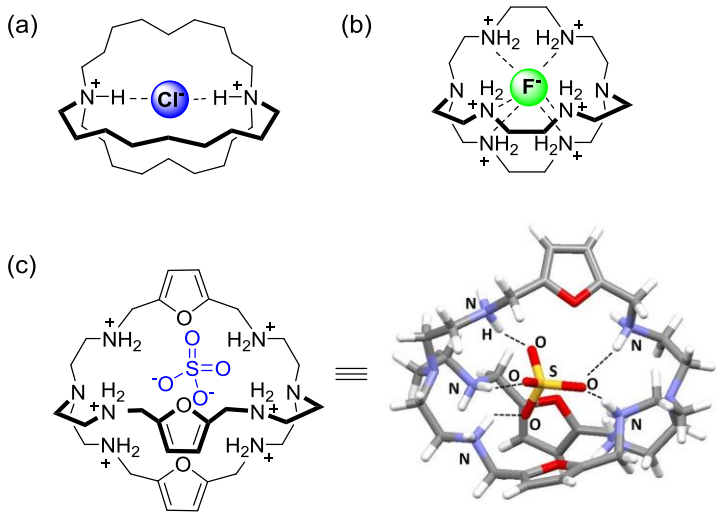


Figure 3.1. (a) An inclusion complex formed by a *katapinand* and Cl^-;[2,3] (b) Lehn's hexa-protonated aza-cryptand binding F^-;[4] (c) Nelson's sulphate binding hexa-protonated aza-cryptand and its crystal structure.[6]

Besides pH-dependent protonated secondary ammoniums, other HB-donating functionalities such as amide, thioamide, urea, thiourea and pyrrole have also been employed in cryptand hosts for anion recognition.[7] For example, a cryptand bearing six amide functional groups, developed by Bowman-James and co-workers, was able to selectively bind F^- over other halides (Cl^- and Br^-) and oxoanions (AcO^-, $H_2PO_4^{2-}$, NO_3^- and HSO_4^-) in d_6-DMSO.[8] The fluoride-complexed solid state structure shows the F^- is centred in the cryptand cavity, forming hydrogen bonds to all six amide protons (Figure 3.2(a)). A more recent example is Sessler's naphthobipyrrole-strapped calix[4]pyrrole which is capable of binding N_3^- in $CDCl_3$ (Figure 3.2(b)).[9] In addition, heteroditopic cryptand hosts bearing both cation and anion binding sites exhibit enhanced anion binding affinities in the presence of co-bound metal cations. For example, a pyrrole-containing cryptand developed by Gale and co-workers formed a stronger association with Cl^- in the presence of K^+ or Na^+ in d_6-DMSO.[10] The crystal structure of the NaCl-complexed cryptand revealed the halide hydrogen bonding with protons from two amides and pyrrole functional groups as well as a direct contact ion-pair interaction with the aza-crown ether complexed Na^+ (Figure 3.2(c)).

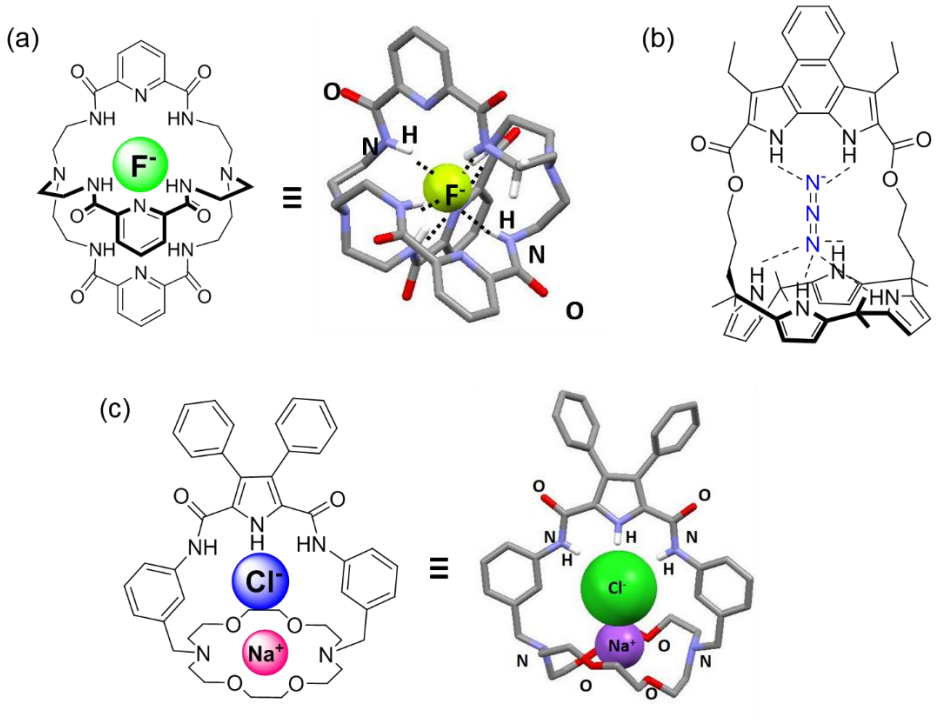


Figure 3.2. (a) Bowman-James' F^- selective binding cryptand and its crystal structure;[8] (b) Sessler's azide-complexed strapped calix[4]pyrrole;[9] (c) Gale's pyrrole-based cryptand with NaCl ion-pair and its crystal structure.[10]

3.1.2 Cryptand-based Interlocked Structures

Cryptands have also been utilised in the construction of interlocked structures. Inspired by the supramolecular complexes formed by dibenzo-crown ethers with N,N'-dimethyl-4,4'-bipyridinium salts (paraquats), crown ether-based cryptands have been used as wheel components to generate pseudorotaxanes with such dicationic derivatives. For example, an interpenetrated complex, studied by Gibson and co-workers, was formed by a crown ether-based cryptand and a paraquat via HB and aromatic donor-acceptor charge-transfer interactions (Figure 3.3).[11] Interlocked rotaxane and catenane analogues can be synthesised by stoppering or clipping approaches (Figure 3.4).[12–16] More recently, cryptand-based rotaxanes were synthesised using active metal templation by Leigh and co-workers. A pyridine-containing cryptand was able to facilitate active metal template one-pot synthesis of various [2]- and [3]rotaxanes, where the cryptand acted as a ligand for the Cu(I) catalyst to mediate triazole mechanical bond formation (Figure 3.5).[19]

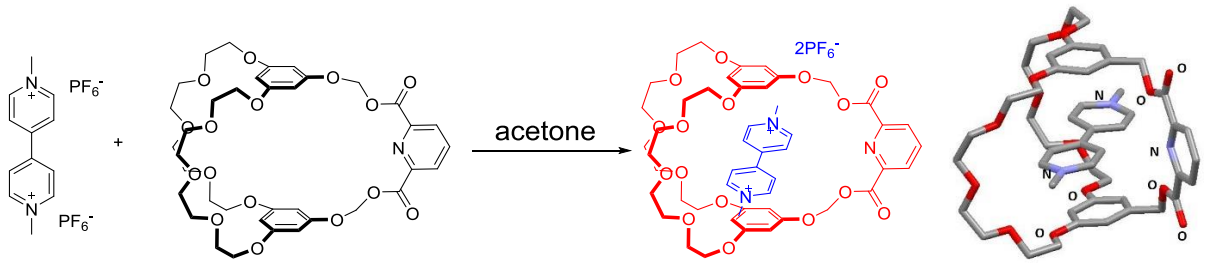


Figure 3.3. A pseudorotaxane (formed by a crown-ether based cryptand and a paraquat) and its solid state structure.[11]

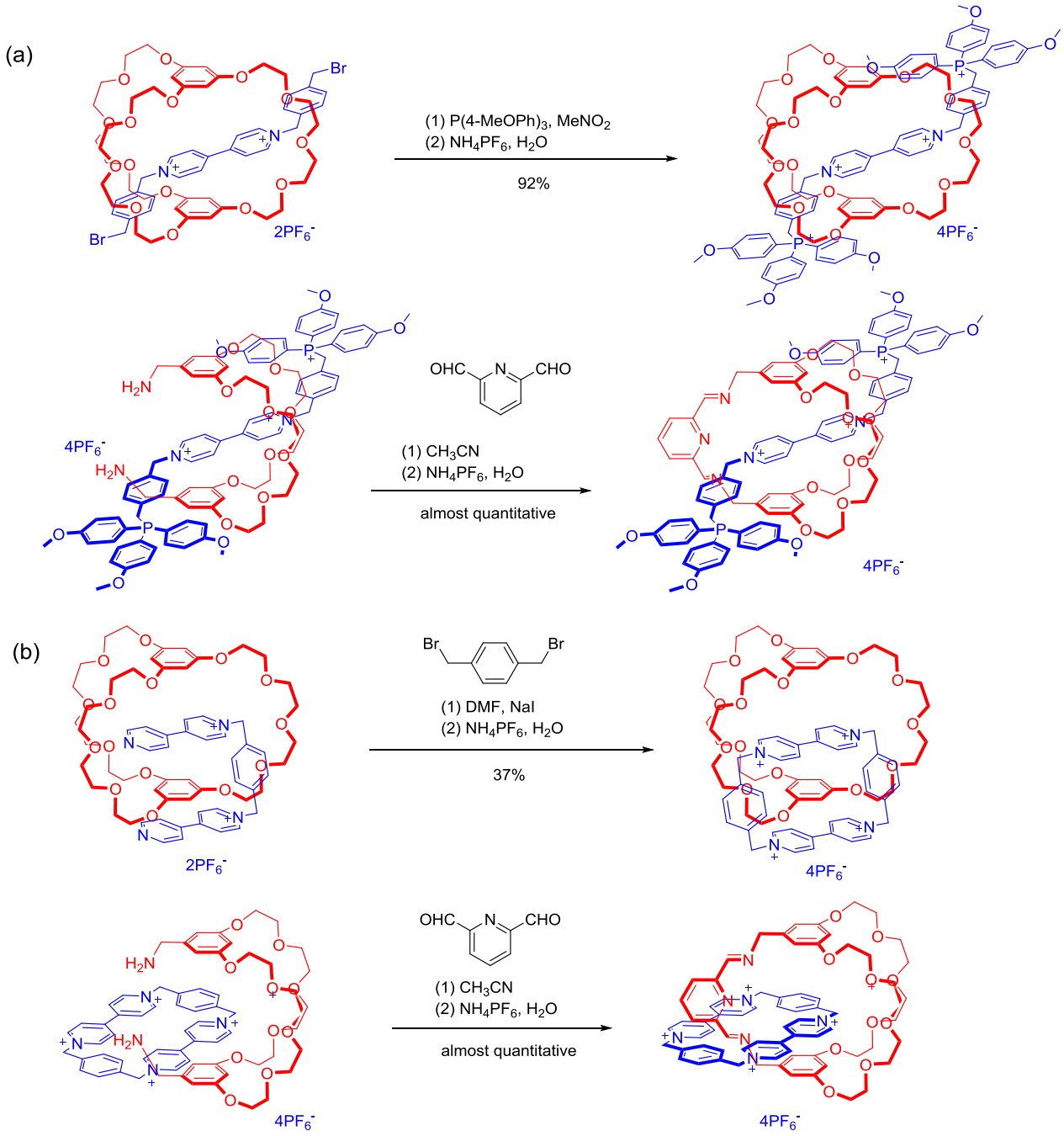


Figure 3.4. Synthesis of cryptand-based (a) rotaxanes and (b) catenanes.[12–16]

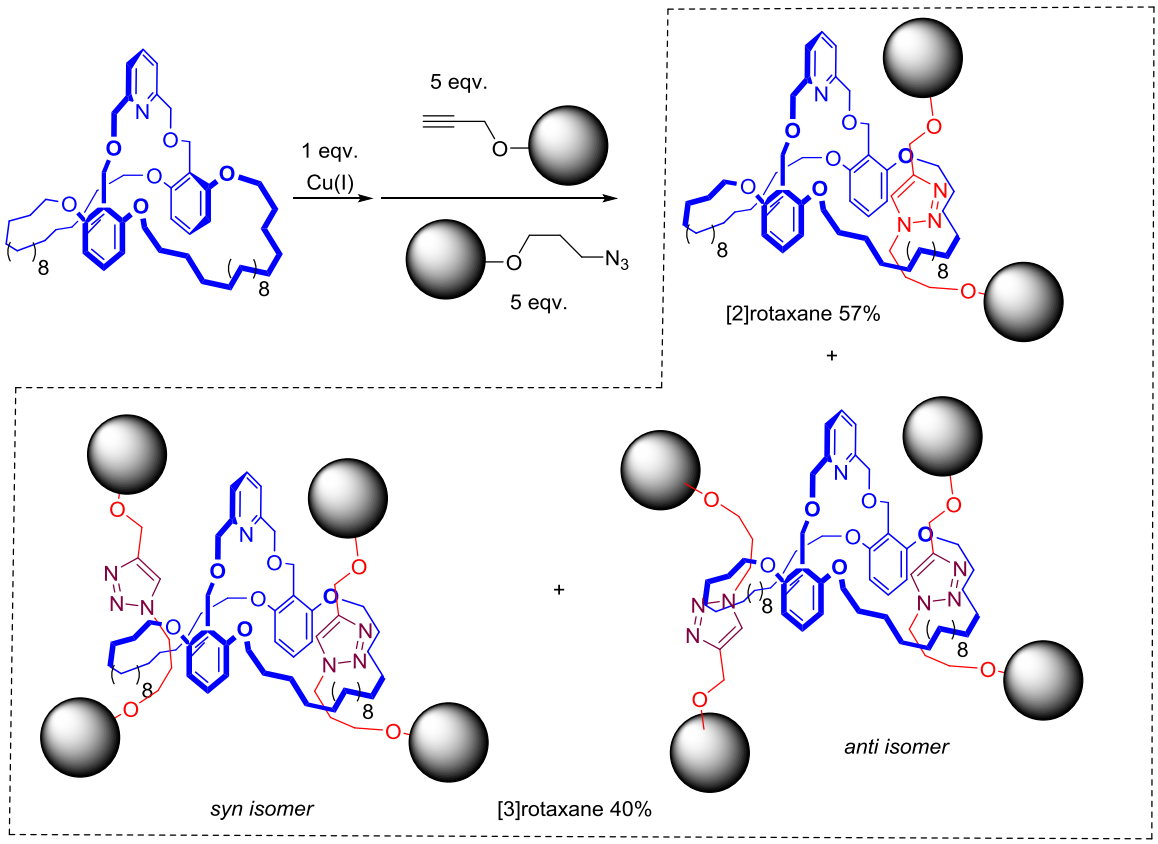


Figure 3.5. Synthesis of cryptand-based [2] and [3]rotaxanes via active metal templation.[19]

3.1.3 Chapter Aims

In spite of the well-established HB cryptand host systems in the field of anion supramolecular chemistry, XB cryptands for anion recognition are unprecedented. Also, the unique three-dimensional cavities of cryptand-based interlocked structures have remained overlooked for anion recognition. This chapter is concerned with the synthesis and anion binding studies of XB cryptands as well as attempts to construct cryptand-based interlocked anion hosts (Figure 3.6).

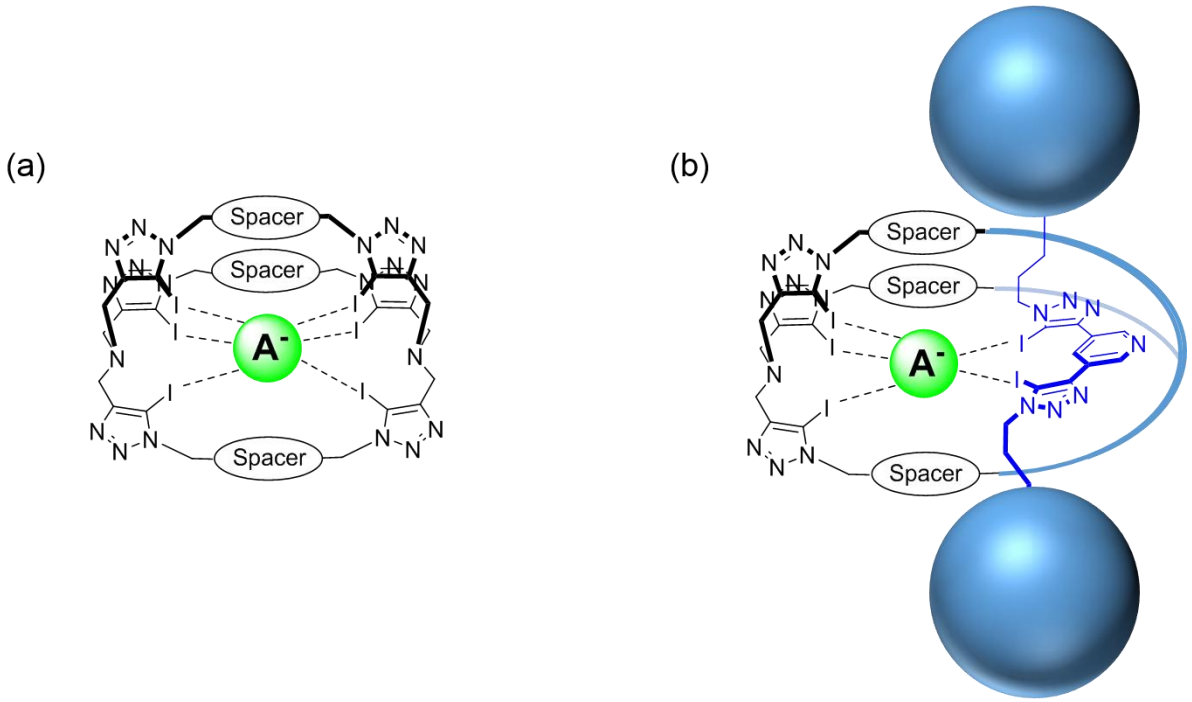


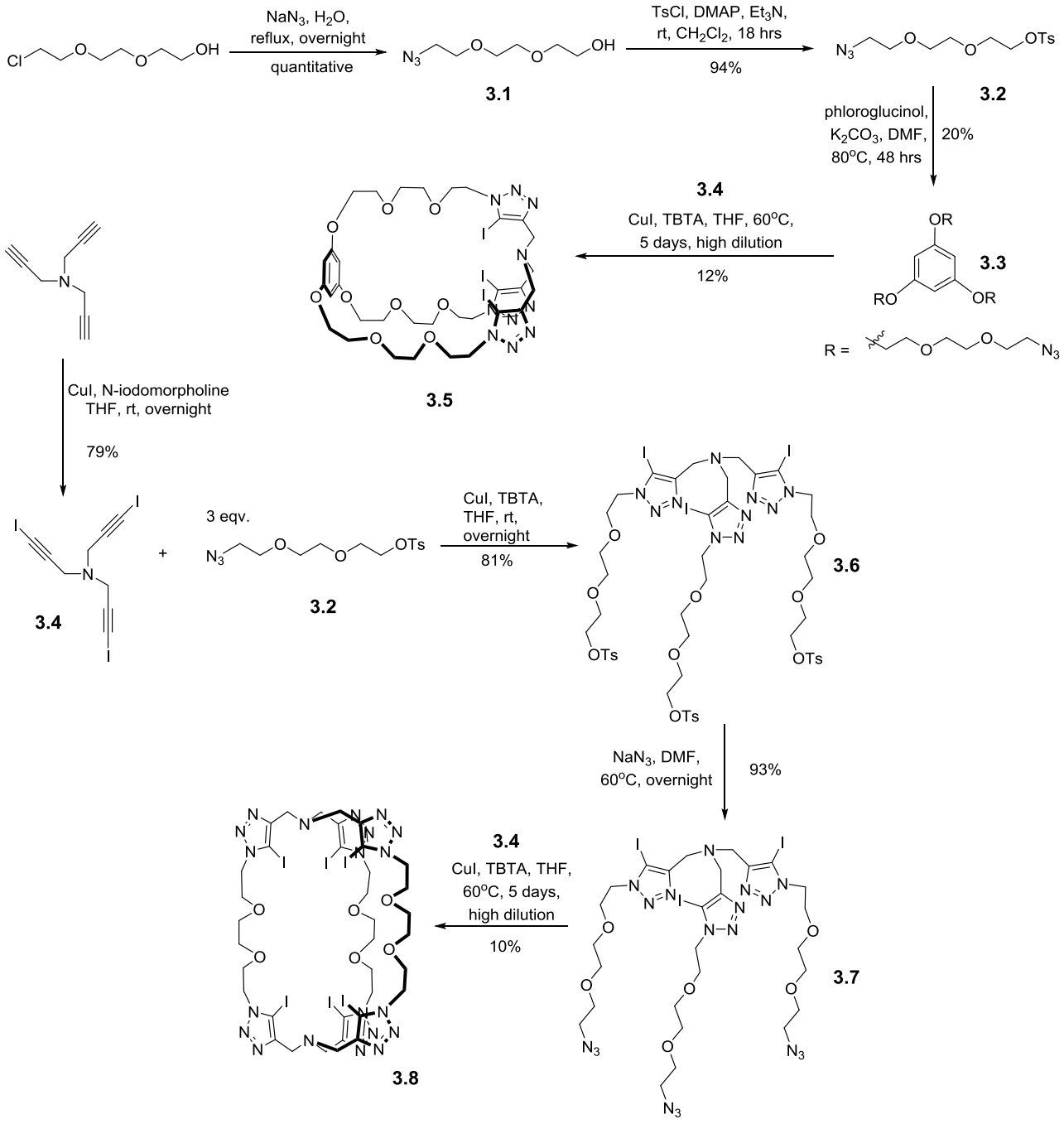
Figure 3.6. Target (a) XB cryptand and (b) XB cryptand-based interlocked structures for anion recognition.

3.2 Halogen Bonding Cryptands for Anion Recognition

3.2.1 Tripodal Capping Synthesis and Anion Binding Properties of XB Cryptands

XB cryptands were initially prepared through tripodal capping Cu(I)-catalysed CuAAC iodo-click reactions. XB cryptands **3.5** and **3.8** were synthesised following the procedure summarised in Scheme 3.1. Commercially available 2-(2-(2-chloroethoxy)ethoxy)ethan-1-ol was reacted with NaN_3 to afford azide **3.1** in quantitative yield,[20] followed by reaction with 4-toluenesulfonyl chloride (TsCl) in CH_2Cl_2 to give azide-tosylate precursor **3.2** in 94% yield.[21] Tris-azide **3.3** was prepared by reacting three equivalents of **3.2** with 1,3,5-trihydroxybenzene (phloroglucinol) under basic conditions in DMF. A tris-CuAAC reaction under high dilution conditions between an equimolar mixture of **3.3** and tris-iodoalkyne amine **3.4**, which was synthesised by iodination of tripropargyl amine using N-iodomorpholine,[22] afforded the target XB cryptand **3.5** in 12% isolated yield after preparative TLC purification. Tris-azide **3.7** was synthesised by reaction of NaN_3 with the tris-tosylate **3.6**, which was prepared in 81% yield by reacting tris-iodoalkyne amine **3.4** with three equivalents of tosyl azide **3.2** under CuAAC reaction conditions. The target XB cryptand **3.8** was prepared in 10% yield by reacting tris-azide **3.7** with equimolar quantities of **3.4** in THF under high dilution CuAAC conditions and preparative TLC purification. Both XB cryptands **3.5** and **3.8** were characterised by ^{1}H and ^{13}C NMR and high resolution ESI mass spectrometry.

Cryptand **3.5** exhibited good solubility in a variety of organic solvents (CH_2Cl_2, $CHCl_3$, acetone, THF, DMSO, DMF) and modest solubility in pure water while cryptand **3.8** only showed good solubility in DMSO and DMF. In the ^{1}H NMR spectra of cryptand **3.5** in $CDCl_3$ and D_2O (Figure 3.7(a) and (b)), the signals of the polyether protons from each bridging linker appeared identical due to C_{3v} symmetry of the cryptand **3.5** while the ^{1}H NMR spectrum of cryptand **3.8** (Figure 3.7(c)) was consistent with its D_{3h} symmetry.



Scheme 3.1. Synthesis of target XB cryptands **3.5** and **3.8**.

The anion binding properties of cryptand **3.5** were studied by ^{1}H NMR titrations in d_6-acetone, by adding increasing quantities of TBACl or TBABr. However, no significant proton signal shifts from the ^{1}H NMR spectra were observed, possibly due to the fact that no HB-donor protons around the binding site were available for monitoring the anion binding event.

The poor solubility of cryptand **3.8** in common organic solvents negated analogous ^{1}H NMR anion binding studies being performed.

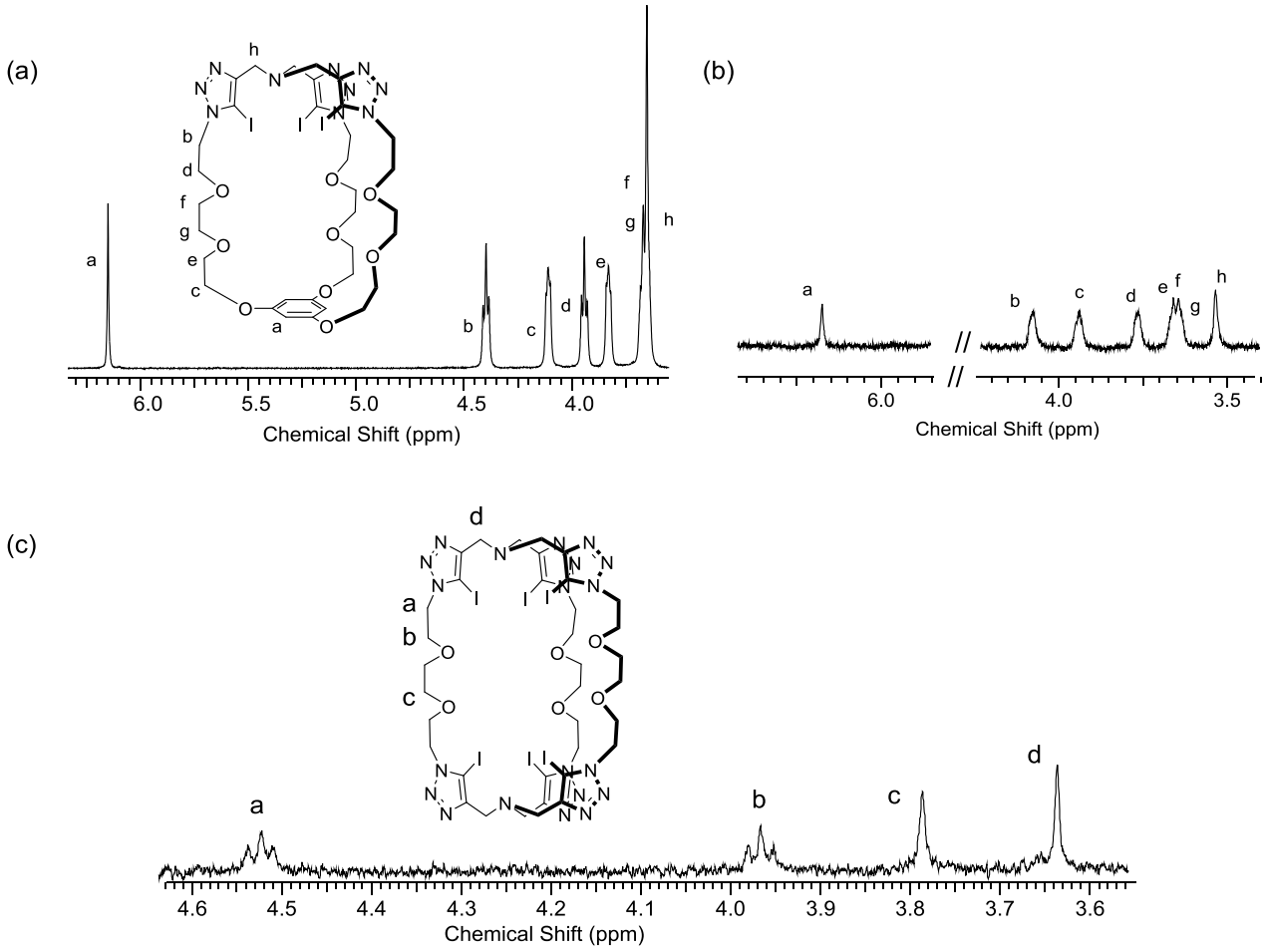


Figure 3.7. (a) Partial ^{1}H NMR spectra of cryptand **3.5** in $CDCl_3$ and (b) in D_2O; (c) partial ^{1}H NMR spectrum of cryptand **3.8** in $CDCl_3$.

3.2.2 Macrocyclic Bridging Synthesis and Anion Binding Properties of XB Cryptands

The drawbacks encountered with XB cryptands **3.5** and **3.8** led to the incorporation of rigid, fluorescent naphthalene motifs into the cryptand structural host framework, which could potentially enhance the solubility in organic solvents and sense anion binding. Additionally, in order to improve the synthetic yields and afford a series of cryptands with different anion binding cavities, the preparation of the target cryptands was achieved by a macrocyclic bridging synthetic approach, where a XB diaza-macrocycle was reacted with a variety of XB bridging linkers (Figure 3.8).

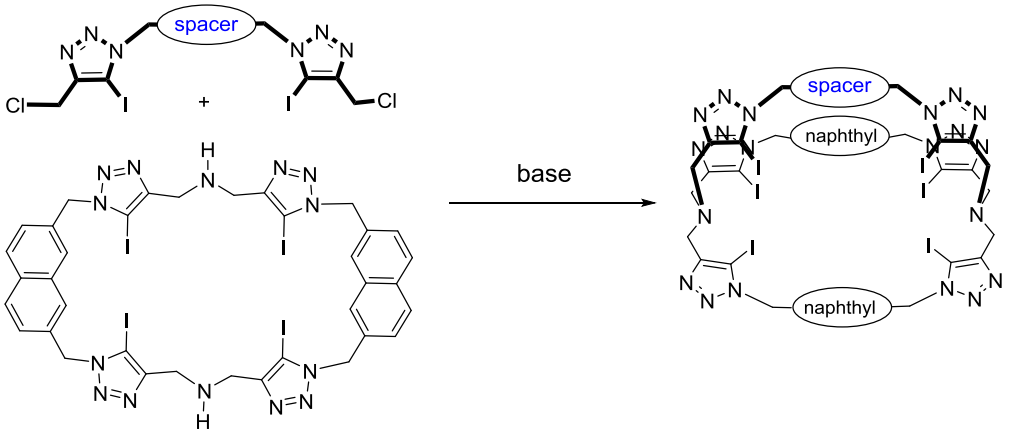
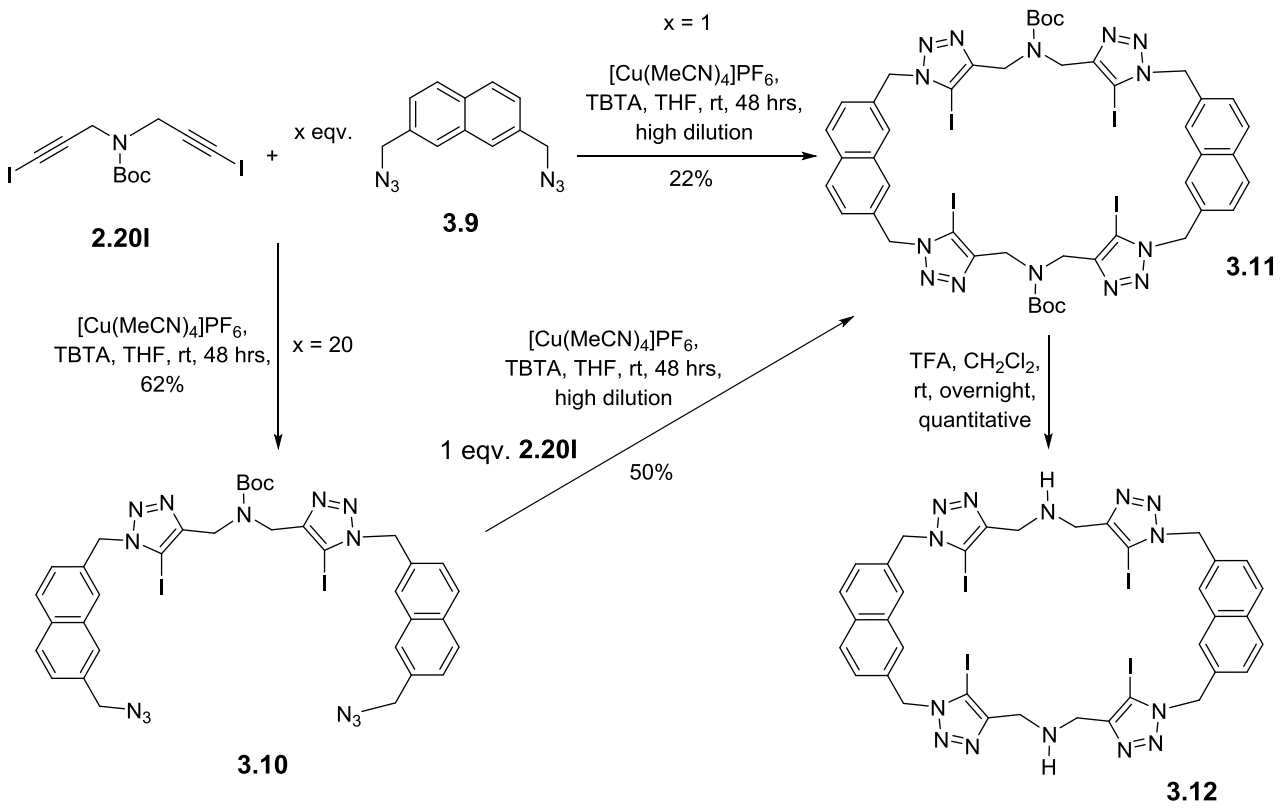


Figure 3.8. Macrocyclic bridging synthesis of a XB cryptand by reacting a XB macrocycle with a XB bridging linker.

3.2.2.1 Synthesis of Target XB Macrocycle

XB macrocycle **3.12** was synthesised following the procedure summarised in Scheme 3.2. *N*-Boc-protected macrocycle **3.11** was prepared in 22% yield through a '2+2' one step high dilution CuAAC macrocyclisation reaction between 2,7-bis(azidomethyl)naphthalene **3.9**[23] with equimolar quantities of *N*-Boc-protected bis-iodoalkyne **2.20I** under CuAAC conditions in THF. In order to improve the yield, **3.11** was also prepared in a stepwise manner. Bis-azide **3.10**, synthesised in 62% yield by reacting **2.20I** with twenty equivalents of **3.9**, was reacted with **2.20I** under high-dilution CuAAC conditions to afford macrocycle **3.11** in 50% yield (31% overall yield over two steps). Quantitative *N*-Boc-deprotection using trifluoroacetic acid in CH_2Cl_2 afforded XB macrocycle **3.12**.

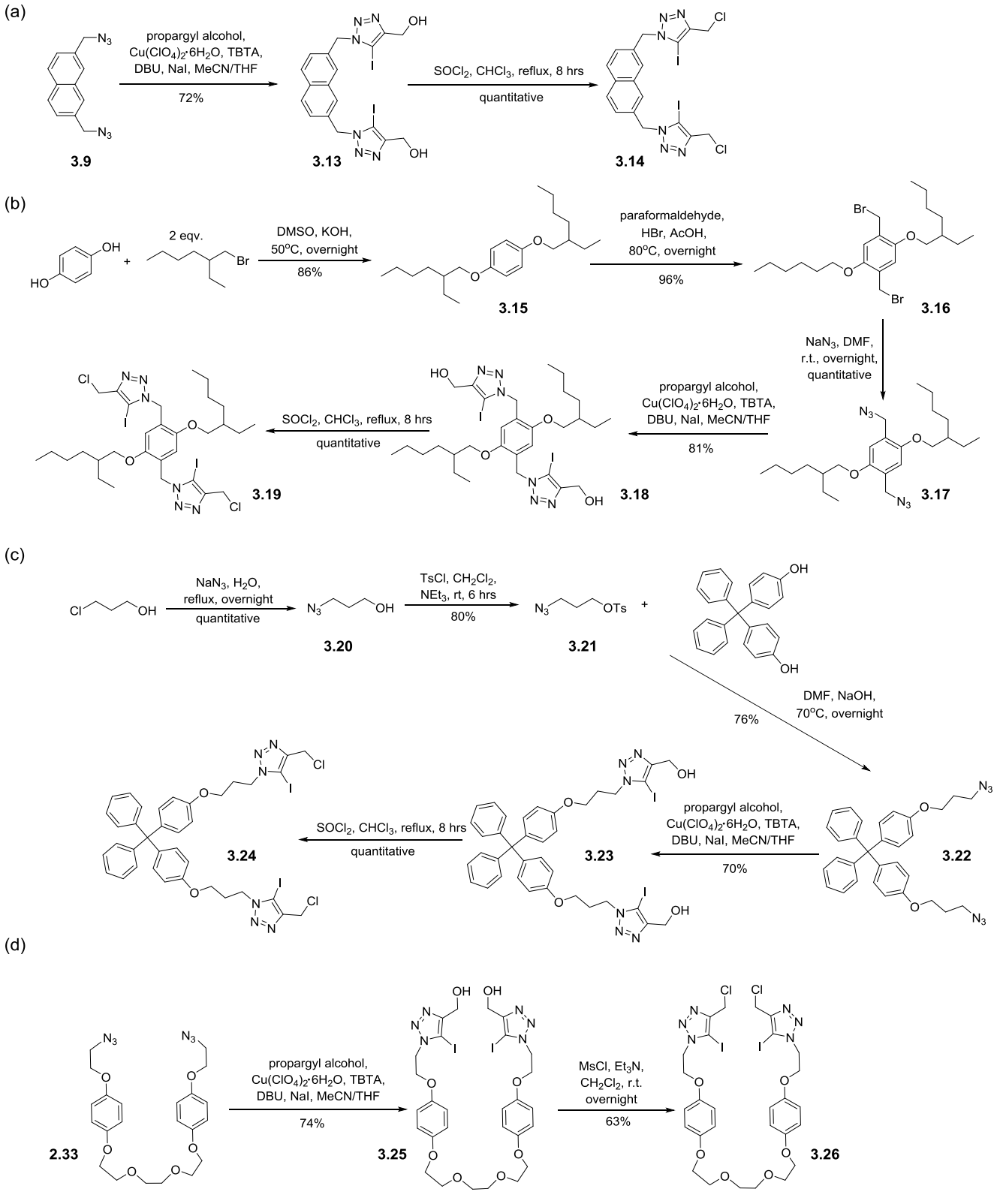


Scheme 3.2. Synthesis of XB macrocycle **3.12**.

3.2.2.2 Synthesis of XB Bridges

Having prepared the XB macrocycle, a variety of bis-chloro methylene-iodotriazole containing bridges with varying spacer groups were synthesised (Scheme 3.3). Bis-azide **3.9** was reacted with propargyl alcohol using a 'one-pot' iodo-click reaction to afford **3.13** in 72% yield. Chlorination of **3.13** was achieved by reacting with $SOCl_2$ in refluxing $CHCl_3$, affording the naphthalene-based XB bridge **3.14** in quantitative yield (Scheme 3.3(a)). A hydroquinone-based XB spacer derivative **3.19** bearing alkyl chains for improved solubility in organic solvents, was also synthesised (Scheme 3.3(b)). Compound **3.15**, prepared in 86% yield by the reaction between hydroquinone with a branched alkyl bromide under basic conditions in DMF, was reacted with paraformaldehyde to afford bis-bromo compound **3.16** in 96% yield.[24] By reacting **3.16** with NaN_3 in DMF, compound **3.17** was prepared in quantitative yield and reacted with propargyl alcohol to afford **3.18** in 81% yield. XB bridge **3.19** was prepared quantitatively by reacting **3.18** and $SOCl_2$ in refluxing $CHCl_3$. Also, XB

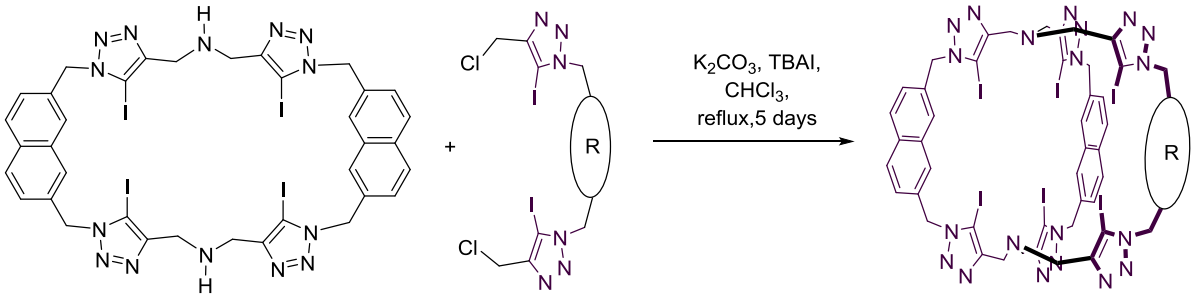
bridging linkers **3.24** and **3.26** were synthesised using analogous procedures (Scheme 3.3(c)-(d)).



Scheme 3.3. Synthesis of various potential XB bridging derivatives.

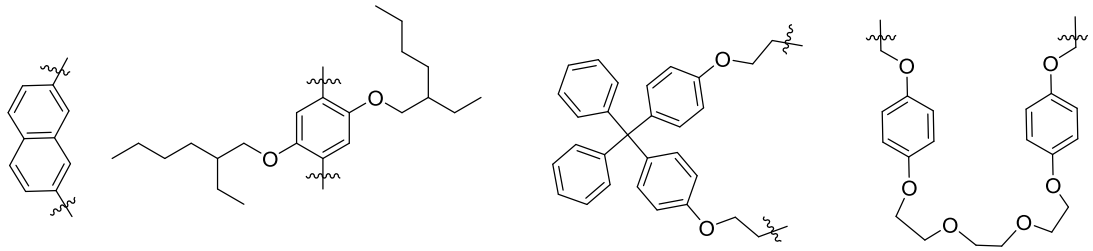
3.2.2.3 Synthesis of Target XB Cryptands

A series of XB cryptands **3.27** - **3.20** were synthesised by reacting XB macrocycle **3.12** with equimolar quantities of the respective XB bridge derivatives in refluxing $CHCl_3$ using K_2CO_3 as base and one equivalent of TBAI (Scheme 3.4). The XB cryptands were isolated in a range of yields after preparative TLC purification. The low 10% isolated yield of **3.27** may stem from its poor solubility in common organic solvents (CH_2Cl_2, $CHCl_3$, acetone, THF, acetonitrile). It is noteworthy that in the reaction of the bridging linker **3.26** and macrocycle **3.12**, the isolated yield of cryptand **3.30** was reduced significantly from 25% to 5% when the reaction was repeated in the absence of TBAI. This suggests that I^- is potentially acting in a dual role as both a catalyst and as a template.



3.12

R =



Cryptand	**3.27**	**3.28**	**3.29**	**3.30**
Yield	10%	24%	20%	25%

Scheme 3.4. Synthesis of XB cryptands.

All the cryptands were characterised by ^{1}H NMR and high-resolution ESI mass spectrometry. The ^{1}H NMR spectra of cryptands **3.27** in d_6-DMSO and **3.28** in both d_6-DMSO and $CDCl_3$ at 298K were too broad to be assigned, indicative of conformational isomers.

Indeed at higher temperatures, assignable sharp proton signals for both cryptands **3.27** and **3.28** were observed in the ^{1}H NMR spectra (Figure 3.9(a)-(b)). It is envisaged that the slow exchange on the NMR timescale between conformational isomers at room temperature may be related to the rigid bridging linkers. In contrast, cryptands **3.29** and **3.30** containing relatively longer and more flexible bridging linkers exhibited sharp and assignable proton signals in their ^{1}H NMR spectra at room temperature (Figure 3.9(c)-(d)).

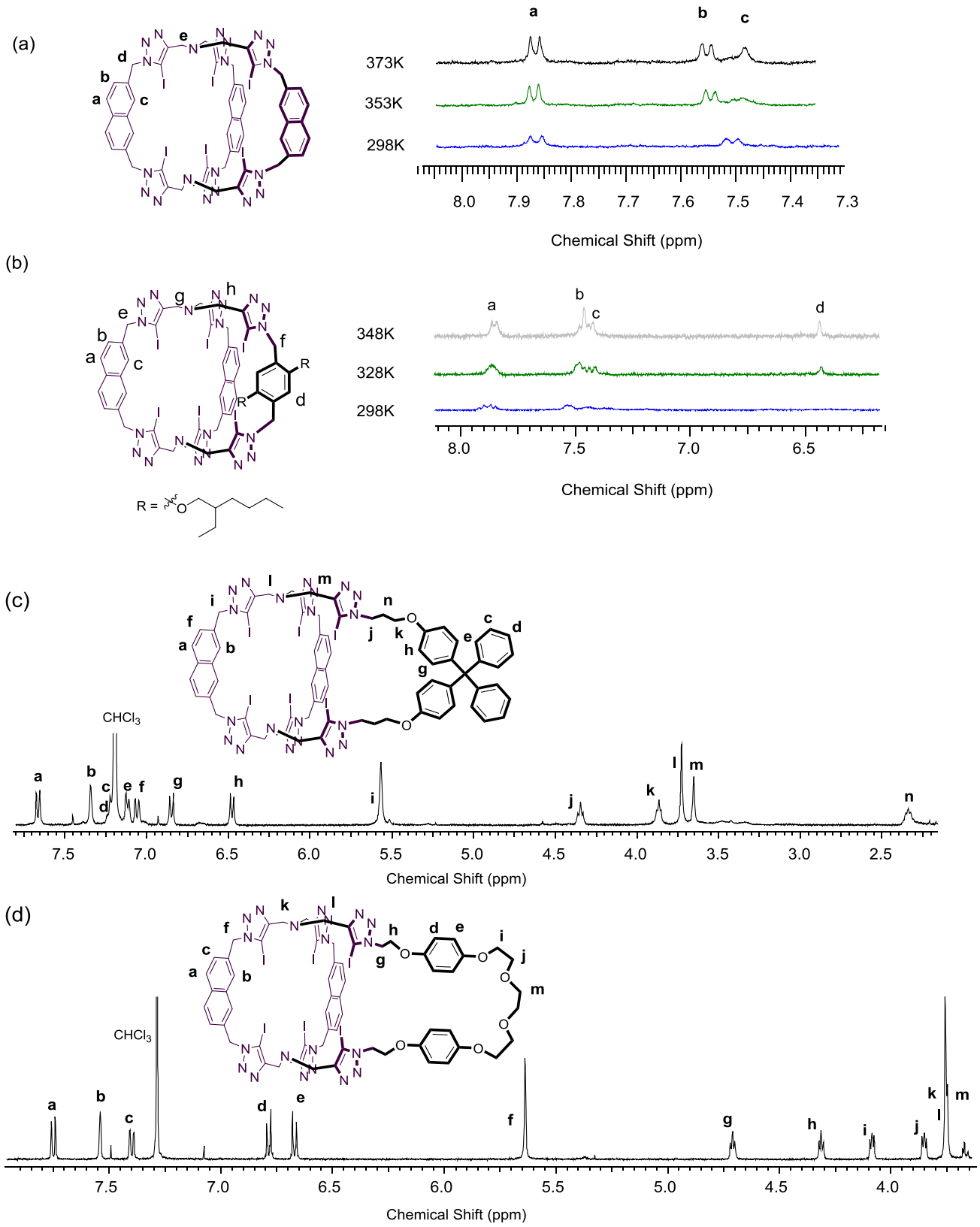


Figure 3.9. (a) Partial ^{1}H NMR spectra of cryptand **3.27** at 298 K, 353 K and 373 K in d_6-DMSO; (b) partial ^{1}H NMR spectrum of cryptand **3.28** at 298 K, 328 K and 348 K in d_6-DMSO; (c) partial ^{1}H NMR spectra of cryptand (c) **3.29** and (d) **3.30** at 298 K in $CDCl_3$.

3.2.2.4 Anion Binding Studies of XB Cryptands

The ^{1}H NMR anion binding studies of cryptand **3.30** were performed in d_6-acetone. In the case of Cl^- titration, the naphthalene proton signals arising from H_a and H_c moved upfield while naphthalene proton H_b signal moved downfield (Figure 3.10). Significant downfield shifts of methylene protons H_f and H_k, concomitant with upfield shifts of H_g, H_h and H_l as well as a coalescence of hydroquinone protons H_d and H_e were also seen. Negligible shifts of the polyether protons H_i, H_j and H_m were noted. These observations indicated that Cl^- was being encapsulated within the cryptand cavity stabilised by a combination of six XB iodotriazoles and HB C-H naphthalene interactions. Analogous proton perturbations upon addition of Br^-, NO_2^-, OAc^- and N_3^- occurred, but were of smaller magnitude, whilst no significant shifts were observed with NO_3^- and HSO_4^- indicative of no binding. Addition of I^- caused similar proton perturbations as observed with Br^- however a precipitate was formed after adding five equivalents of TBAI, so quantitative data could not be obtained.

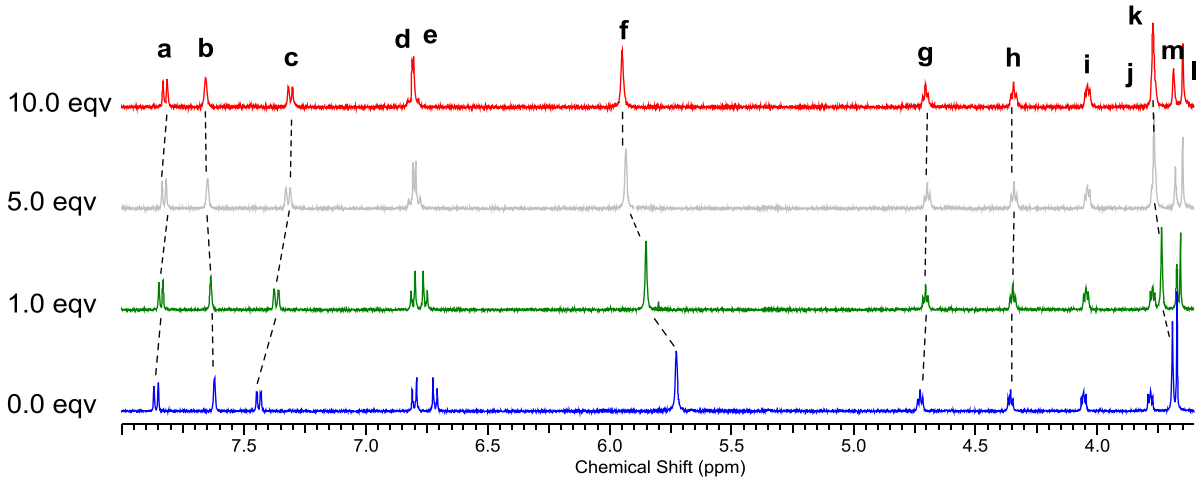


Figure 3.10. Partial ^{1}H NMR spectra of cryptand **3.30** in presence of 0.0, 1.0, 5.0, 10.0 equivalents of Cl^- ([cryptand **3.30**] = 1mM, *T* = 298K, solvent = d_6-acetone). Proton labels seen in Figure 3.9(d).

By monitoring the methylene proton H_f, which is proximal to the cryptand binding site, as a function of anion concentration (Figure 3.11), WinEQNMR2[25] analysis of the titration data determined 1:1 stoichiometric association constants which are summarised in Table 3.1. In d_6-acetone, XB cryptand **3.30** forms the strongest association with the halides Cl^- >

Br^- due to the higher charge-density of Cl^-, followed by $OAc^- > N_3^- > NO_2^- > NO_3^-$, HSO_4^-, suggesting the XB cryptand cavity is of complementary shape and size for spherical anion guest species. Analogous titrations with Cl^- and Br^- were undertaken in 1% water by volume in d_6-acetone. A significant reduction in halide binding strength of cryptand **3.30** occurs (Table 3.1) especially for the more hydrated Cl^-, which is in agreement with the Hofmeister bias anion binding trend in aqueous media.

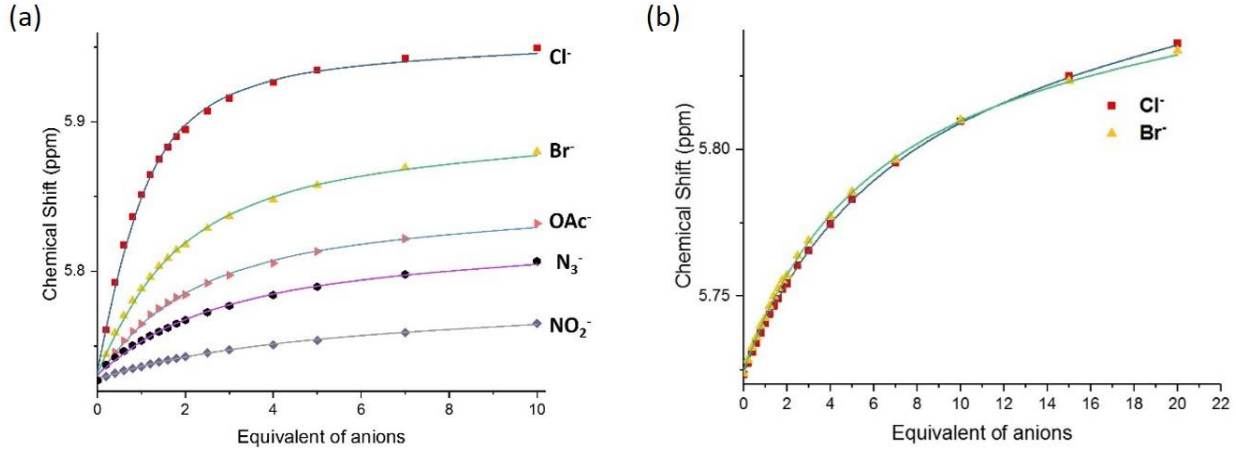


Figure 3.11. Binding isotherms of anion titrations for cryptand **3.30** with different anions in (a) d_6-acetone and (b) d_6-acetone/ D_2O 99:1 v/v. The chemical shifts of H_f were plotted as a function of equivalents of TBA salts added (T = 298 K, [host] = 1.0 mM).

Table 3.1. Association constants, K_a (M^{-1}), for cryptand **3.30** with various anions[a]

	Cl^-	Br^-	OAc^-	N_3^-	NO_2^-
d_6-acetone	2264(157)	718(40)	548(35)	371(25)	174(14)
d_6-acetone/D_2O 99:1 *v/v*	109(1)	142(5)	-[b]	-[b]	-[b]

[a] Anions added as their TBA salts, T = 298 K. The errors associated with each (< 10%) are quoted in parentheses. No binding was observed for NO_3^- and HSO_4^-.
[b] Not conducted.

Further evidence of the anion binding capability of cryptand **3.30** was obtained via preliminary fluorescence titration experiments. These experiments were undertaken in THF instead of acetone due to the fact that the excitation wavelength of naphthalene overlaps with the absorption of acetone (< 330 nm). Cryptand **3.30** exhibited a broad naphthalene emission band, with λ_{max} = 304 nm (THF, [**3.30**] = 2.0 x 10^{-5} M, λ_{ex} = 280 nm) attributed to the monomer emission of the integrated naphthalene moiety.[27] Upon addition of TBACl to a THF

solution of **3.30**, a significant emission band enhancement was observed (Figure 3.12), likely due to rigidification of the cryptand framework upon anion binding which reduces the likelihood of non-radiative decay pathways.[28–30]

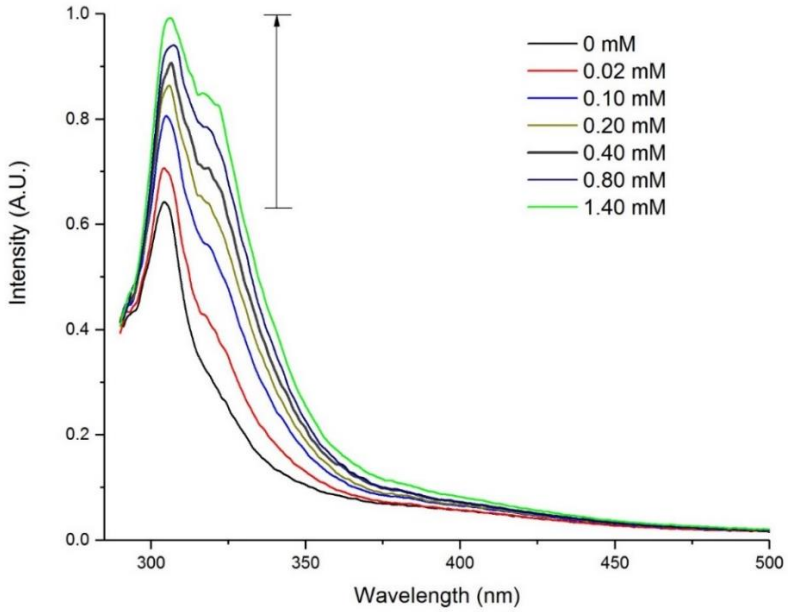


Figure 3.12. Fluorescence spectra of cryptand **3.30** in the presence of increasing concentration of Cl^- ([**3.30**] = 20 μM, T = 293 K, solvent = THF, λ_{ex} = 280 nm).

The poor solubility of cryptand **3.29** and the conformation isomers observed in the room temperature ^{1}H NMR spectra of cryptand **3.27** and **3.28**, negated anion binding studies of these cryptands being undertaken.

3.3 Towards Halogen Bonding Cryptand-based Interlocked Structures for Anion Recognition

Having prepared a series of XB cryptands, the synthesis of the corresponding cryptand-based XB interlocked rotaxane structures containing unique three-dimensional cavities for anion recognition, was attempted by active metal and HB template methods.

3.3.1 Attempted Synthesis via Active Metal Templation

Initial attempts to prepare a XB cryptand-based rotaxane were performed using cryptand **3.5** via active metal templation. The ability of tris-triazolylmethyl-amine derivatives to coordinate Cu(I) is well known. Indeed such tripodal ligands are used to stabilise the Cu(I) catalyst in CuAAC reactions.[31] Nonetheless, a ^{1}H NMR titration experiment with cryptand **3.5** with an increasing amount of $[Cu(CH_3CN)_4]PF_6$ in CD_2Cl_2 was undertaken (Figure 3.13). The addition of Cu(I) led to cryptand proton peak broadening with methylene proton H_b, which is covalently linked to the iodotriazoles, moving downfield significantly indicative of Cu(I) complexation with the N-donor atoms of the iodotriazole motifs. Thus, attempts to synthesise cryptand-based interlocked structures were performed by stirring an equimolar amount of cryptand **3.5** and $[Cu(CH_3CN)_4]PF_6$ in CH_2Cl_2, followed by addition of (a) three equivalents of stopper alkyne and three equivalents of stopper azide (Scheme 3.5(a)); or (b) three equivalents of pyridine-bis-iodoalkyne and six equivalents of stopper azide (Scheme 3.5(b)) respectively. After 72 hours in both cases, even though ESI-MS revealed the formation of target interlocked rotaxanes, only the cryptand **3.5** and the corresponding axle products were isolated from the respective reaction mixtures after preparative TLC, indicating a very low yield of rotaxane. The failure of AMT rotaxane formation may arise from the steric constraints of the cryptand's cavity, preventing the CuAAC reaction from occurring endotopically inside the cavity.

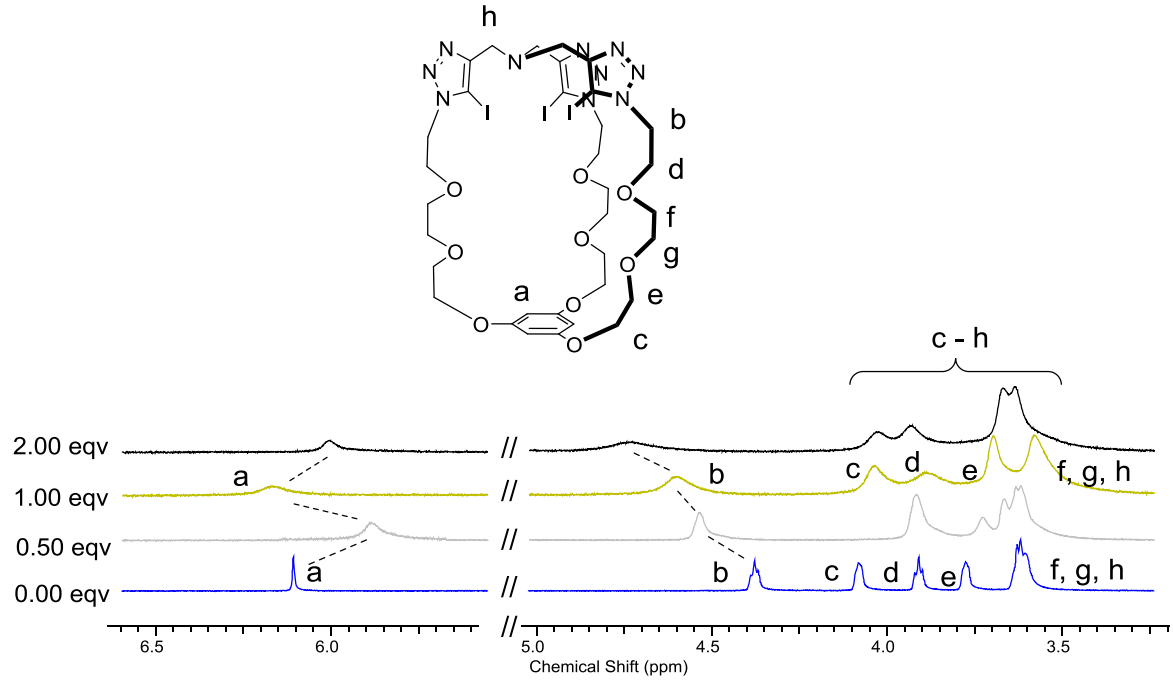
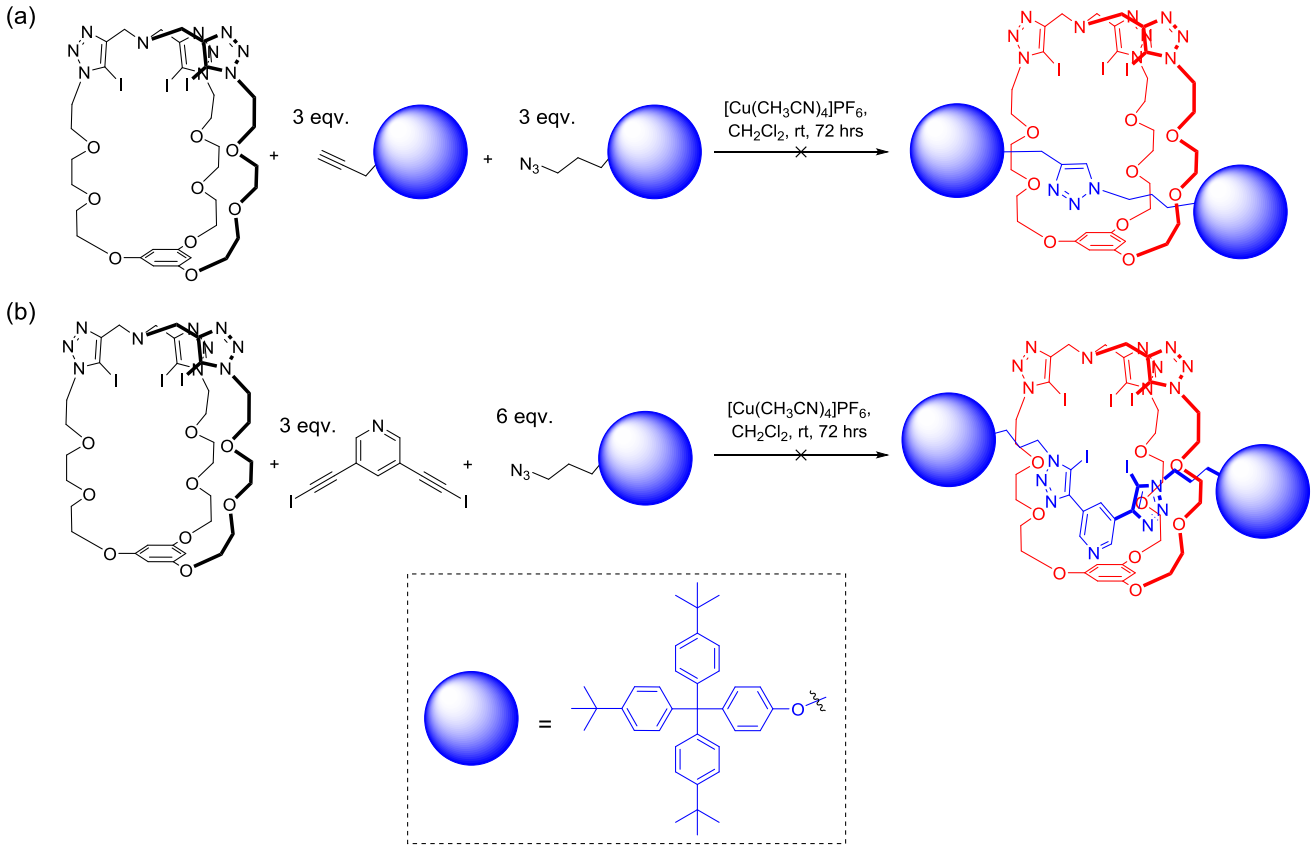


Figure 3.13. Partial ^{1}H NMR spectra of cryptand **3.5** in the presence of different amounts of $[Cu(CH_3CN)_4]PF_6$ ([**3.5**] = 1.0 mM, CD_2Cl_2, *T* = 298K).



Scheme 3.5. Attempted synthesis of cryptand-based interlocked structures using the AMT strategy.

3.3.2 Attempted Synthesis via HB Templation

The attempted synthesis of a cryptand-based rotaxane structure was also performed via HB templation. As cryptand **3.5** contains three polyether groups, a dialkylammonium thread could potentially form an interpenetrated assembly via HB interactions.[33] Qualitative ^{1}H NMR pseudo rotaxane studies were undertaken by mixing equimolar amounts of cryptand **3.5** and dibenzylammonium thread (kindly donated by Dr. Jason Lim) in CD_2Cl_2 (Figure 3.14). Promisingly, the resulting ^{1}H NMR spectrum revealed perturbations of both proton signals of the thread and cryptand. In particular, signals arising from proton H_1, H_3 and H_5 on the cryptand and H_b on the thread moved upfield in conjunction with a downfield shift of H_2 and H_c. Encouraged by these observations, an attempted synthesis of the target interlocked structure was performed by adding one equivalent of a Cu(I)-acetylide complex (kindly donated by Dr. Jason Lim) to a mixture of one equivalent of the cryptand **3.5** and the azide functionalised thread in dry CH_2Cl_2 (Scheme 3.6). After 18 hours, even though ESI-MS revealed evidence of rotaxane formation, only the corresponding axle and starting cryptand were isolated after preparative TLC.

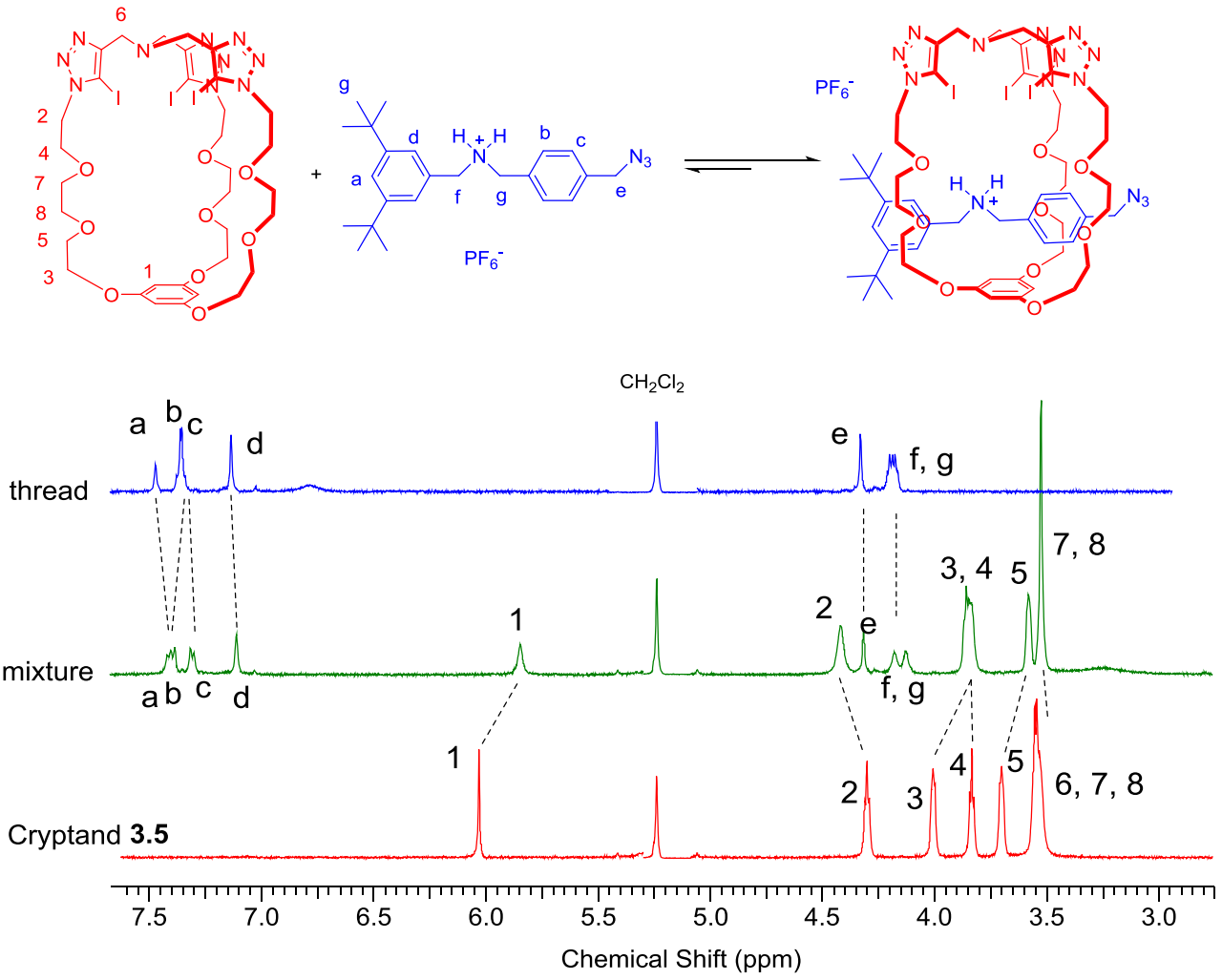
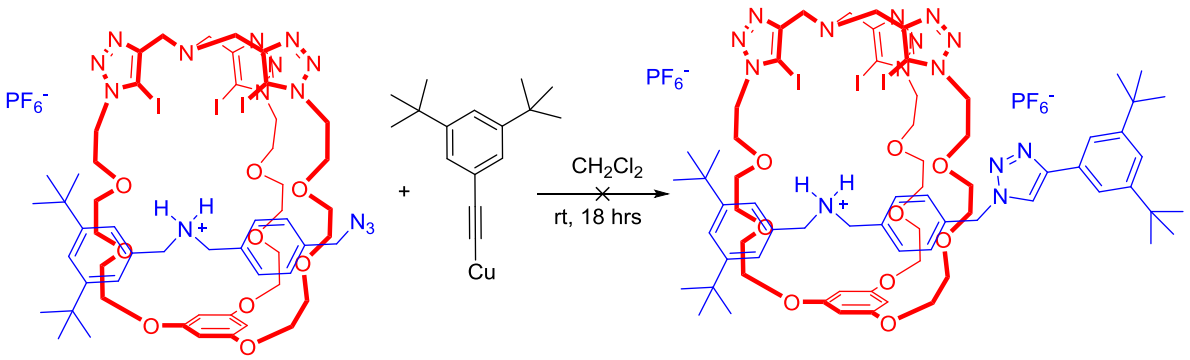


Figure 3.14. Partial ^{1}H NMR spectrum of cryptand **3.5**, the dibenzylammonium thread and their mixture. (Solvent = CD_2Cl_2, *T* = 298 K).



Scheme 3.6. Attempted synthesis of cryptand-based interlocked structures using HB templation.

3.4 Conclusions and Future Work

In conclusion, a series of XB cryptands bearing multiple iodotriazoles were constructed using tripodal capping and macrocyclic bridging synthetic approaches. By utilising a variety of bridging spacers, these XB cryptands exhibited varying solubilities and molecular conformations at room temperature. The anion binding properties of a naphthalene-containing XB cryptand were studied via ^{1}H NMR titrations in d_6-acetone, revealing its selectivity for spherical halides. The cryptand was also demonstrated to display a 'turn-on' fluorescence response upon chloride binding in THF. Attempts to prepare XB cryptand-based interlocked structures were undertaken via active metal and HB template methods. Even though ESI-MS provided evidence for rotaxane formation, no target rotaxanes were isolated likely due to the low yield.

Future work could focus on the synthesis of XB cryptands designed to function in aqueous solvent media. This could be achieved by incorporating polyether and cyclodextrin based appendages (Figure 3.15). Such hosts in an aqueous environment may adopt a conformation whereby the lipophilic XB donor iodotriazole motifs are arranged in a preorganised convergent fashion favourable for anion binding.

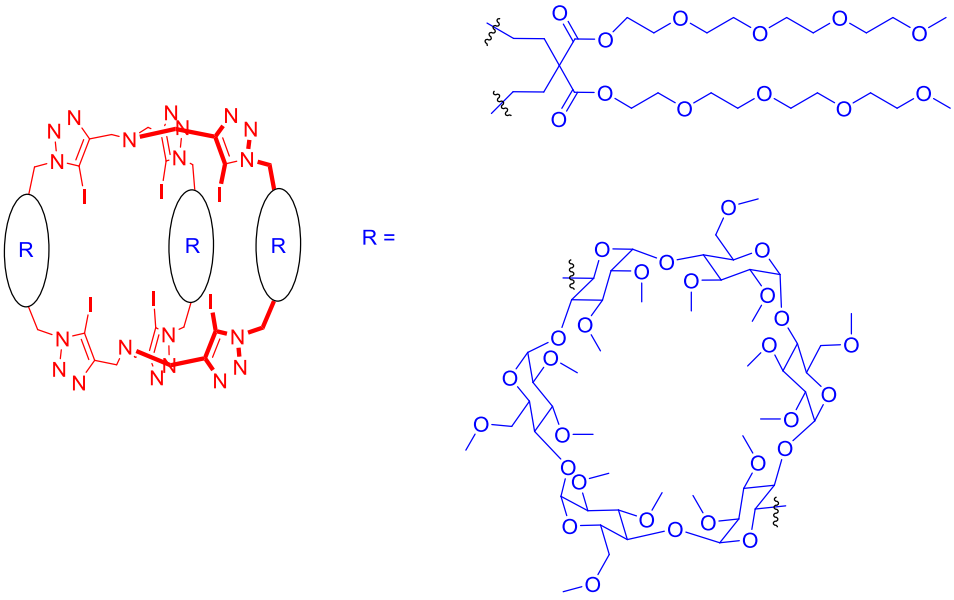


Figure 3.15. Structures of target water-soluble XB cryptands.

3.5 References:

1 B. Dietrich, J. M. Lehn and J. P. Sauvage, *Tetrahedron Lett.*, 1969, **10**, 2889–2892.
2 C. H. Park and H. E. Simmons, *J. Am. Chem. Soc.*, 1968, **90**, 2429–2431.
3 C. H. Park and H. E. Simmons, *J. Am. Chem. Soc.*, 1968, **90**, 2431–2432.
4 B. Dietrich, J.-M. Lehn, J. Guilhem and C. Pascard, *Tetrahedron Lett.*, 1989, **30**, 4125–4128.
5 J. M. Lehn, E. Sonveaux and A. K. Willard, *J. Am. Chem. Soc.*, 1978, **100**, 4914–4916.
6 J. Nelson, M. Nieuwenhuyzen, I. Pál and R. M. Town, *Dalton Trans.*, 2004, **0**, 2303–2308.
7 S. O. Kang, J. M. Llinares, V. W. Day and K. Bowman-James, *Chem. Soc. Rev.*, 2010, **39**, 3980–4003.
8 S. O. Kang, J. M. Llinares, D. Powell, D. VanderVelde and K. Bowman-James, *J. Am. Chem. Soc.*, 2003, **125**, 10152–10153.
9 S. H. Kim, J. Lee, G. I. Vargas-Zúñiga, V. M. Lynch, B. P. Hay, J. L. Sessler and S. K. Kim, *J. Org. Chem.*, 2018, **83**, 2686–2693.
10 J. M. Mahoney, R. A. Marshall, A. M. Beatty, B. D. Smith, S. Camiolo and P. A. Gale, *J. Supramol. Chem.*, 2001, **1**, 289–292.
11 F. Huang, K. A. Switek, L. N. Zakharov, F. R. Fronczek, C. Slebodnick, M. Lam, J. A. Golen, W. S. Bryant, P. E. Mason, A. L. Rheingold, M. Ashraf-Khorassani and H. W. Gibson, *J. Org. Chem.*, 2005, **70**, 3231–3241.
12 S. Li, M. Liu, J. Zhang, B. Zheng, C. Zhang, X. Wen, N. Li and F. Huang, *Org. Biomol. Chem.*, 2008, **6**, 2103–2107.
13 S. Li, M. Liu, J. Zhang, B. Zheng, X. Wen, N. Li and F. Huang, *Eur. J. Org. Chem.*, 2008, **2008**, 6128–6133.
14 M. Liu, S. Li, M. Zhang, Q. Zhou, F. Wang, M. Hu, F. R. Fronczek, N. Li and F. Huang, *Org. Biomol. Chem.*, 2009, **7**, 1288–1291.
15 J. Li, P. Wei, X. Wu, M. Xue, X. Yan and Q. Zhou, *RSC Adv.*, 2013, **3**, 21289–21293.
16 S. Li, M. Liu, B. Zheng, K. Zhu, F. Wang, N. Li, X.-L. Zhao and F. Huang, *Org. Lett.*, 2009, **11**, 3350–3353.
17 L. M. Klivansky, G. Koshkakaryan, D. Cao and Y. Liu, *Angew. Chem.*, 2009, **121**, 4249–4253.
18 A. Pun, D. A. Hanifi, G. Kiel, E. O'Brien and Y. Liu, *Angew. Chem. Int. Ed.*, 2012, **51**, 13119–13122.
19 S. M. Goldup, D. A. Leigh, P. R. McGonigal, V. E. Ronaldson and A. M. Z. Slawin, *J. Am. Chem. Soc.*, 2010, **132**, 315–320.
20 M. A. Brun, K.-T. Tan, R. Griss, A. Kielkowska, L. Reymond and K. Johnsson, *J. Am. Chem. Soc.*, 2012, **134**, 7676–7678.
21 N. C. Tansil, E. A. B. Kantchev, Z. Gao and H. Yu, *Chem. Commun.*, 2011, **47**, 1533–1535.
22 J. E. Hein, J. C. Tripp, L. B. Krasnova, K. B. Sharpless and V. V. Fokin, *Angew. Chem. Int. Ed.*, 2009, **48**, 8018–8021.
23 I. S. Choi, X. Li, E. E. Simanek, R. Akaba and G. M. Whitesides, *Chem. Mater.*, 1999, **11**, 684–690.
24 G. Iadevaia, A. E. Stross, A. Neumann and C. A. Hunter, *Chem. Sci.*, 2016, **7**, 1760–1767.
25 M. J. Hynes, *J. Chem. Soc. Dalton Trans.*, 1993, 311.
26 M. G. Sarwar, B. Dragisić, E. Dimitrijević and M. S. Taylor, *Chem. – Eur. J.*, 2013, **19**, 2050–2058.
27 S. Samanta, M. B. Roy, M. Chatterjee and S. Ghosh, *J. Lumin.*, 2007, **126**, 230–238.
28 A. Borissov, J. Y. C. Lim, A. Brown, K. E. Christensen, A. L. Thompson, M. D. Smith and P. D. Beer, *Chem. Commun.*, 2017, **53**, 2483–2486.
29 R. Martínez-Máñez and F. Sancenón, *Chem. Rev.*, 2003, **103**, 4419–4476.
30 P. D. Beer, *Acc. Chem. Res.*, 1998, **31**, 71–80.
31 P. S. Donnelly, S. D. Zanatta, S. C. Zammit, J. M. White and S. J. Williams, *Chem. Commun.*, 2008, 2459–2461.
32 M. J. Langton, Y. Xiong and P. D. Beer, *Chem. – Eur. J.*, 2015, **21**, 18910–18914.
33 M. Zhang, X. Yan, F. Huang, Z. Niu and H. W. Gibson, *Acc. Chem. Res.*, 2014, **47**, 1995–2005.

Chapter 4. Novel Rotaxane Ligands for Lanthanide Complexation

4.1 Introduction

4.1.1 Fundamental Properties of Lanthanides

The lanthanides are a series of chemical elements with atomic numbers 57-71, from lanthanum to lutetium in the Periodic Table. The +3 oxidation state dominates their coordination complexes (Ln^{3+}), acting as classic hard Lewis acids.[1–3] Lanthanide complexes are ionic in nature, hence geometric constraint is minimal, resulting in a range of coordination numbers of up to 12 and kinetic lability.[4] Lanthanides have unique photo-physical properties displaying sharp emission bands and long micro-second scale lifetimes, which facilitate the elimination of the background fluorescence from organic chromophores providing special applications in imaging and sensing.[5] As a consequence of Laporte forbidden f-f transitions, the direct excitation of lanthanides results in weak emission. To overcome this, sensitiser groups, usually termed 'antenna', are incorporated to aid the indirect excitation of the Ln^{3+} (Figure 4.1(a)). The antenna absorbs photons to produce a singlet excited state S^* where intersystem crossing (ISC) to an excited triplet state T^* and subsequent energy transfer produces the excited lanthanide centre (Figure 4.1(b)).[6,7]

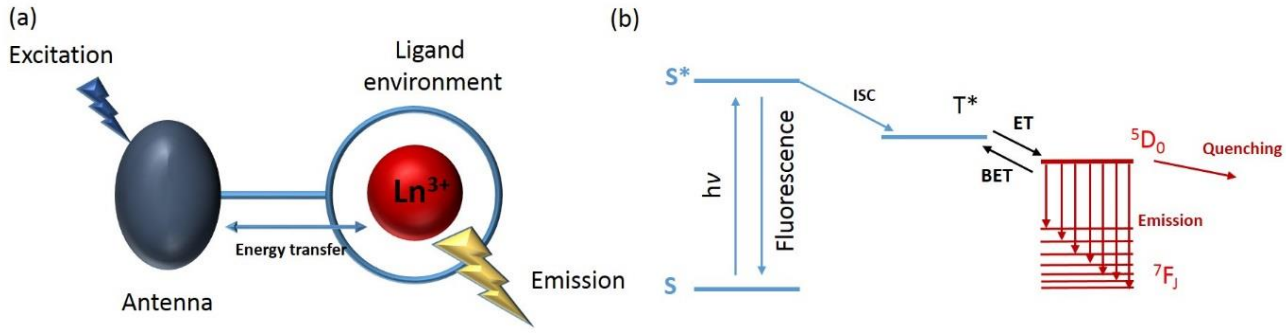


Figure 4.1. (a) Schematic illustration of luminescence from a lanthanide complex incorporating an excitable antenna; (b) energy level diagram depicting the photo-physical processes involved in sensitised Eu^{3+}emission. Adapted from reference 6.

4.1.2 Lanthanide-containing Interlocked Structures

A plethora of hard basic oxygen and nitrogen donor based ligands such as carboxylates, crown ethers and acetylacetone (acac) derivatives for lanthanide complexation have been synthesised and studied over many years. Polyaminocarboxylate-based macrocyclic ligands in particular such as DOTA (1,4,7,10-tetraazacyclododecane-1,4,7,10-tetraacetic acid) offer kinetic inertness and thermodynamic stability in lanthanide complexation. DOTA consists of a central 12-membered tetra-azacyclodecane macrocycle (known as cyclen) with the four secondary amine groups functionalised with $-CH_2CO_2H$ groups. For example, the solid state structure of a Eu·DOTA complex (Figure 4.2) reveals Eu^{3+} is coordinated by four nitrogen atoms and four carboxyl oxygen atoms on the DOTA ligand as well as by one water molecule.[8] Compared to the acyclic analogue EDTA (ethylenediaminetetraacetic acid), lanthanide DOTA complexes are several orders of magnitude more stable.[9]

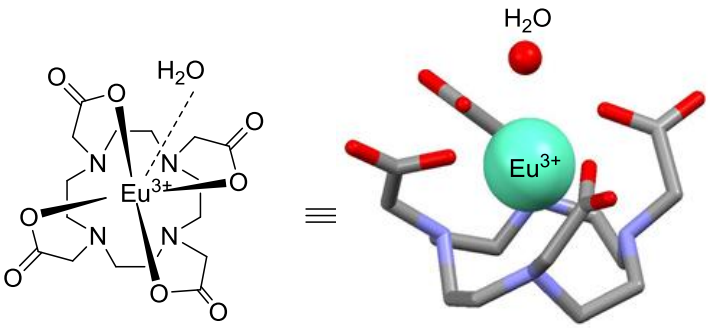


Figure 4.2. The chemical structure (left) and solid state structure (right) of Eu·DOTA·H_2O complex.[8]

In spite of the existence of numerous lanthanide complexes, examples of lanthanide-containing interlocked molecules are rare.[6] Pioneering work for incorporating lanthanides into [2]rotaxanes was performed by Beer and co-workers. For instance, a Eu·DO3A appended [2]rotaxane, prepared by the CuAAC reaction between a Eu-containing propargyl DO3A complex with a 'rotaxane' azide, exhibited Cl^- responsive luminescence behaviour (Figure 4.3(a)).[10] Also, via a 'stoppering' methodology, lanthanide rotaxanes were

synthesised by first forming pseudo-rotaxanes using lanthanide cation-pyridine N-oxide templation (Figure 4.3(b))[11] and nitrite anion templation (Figure 4.3(c))[12].

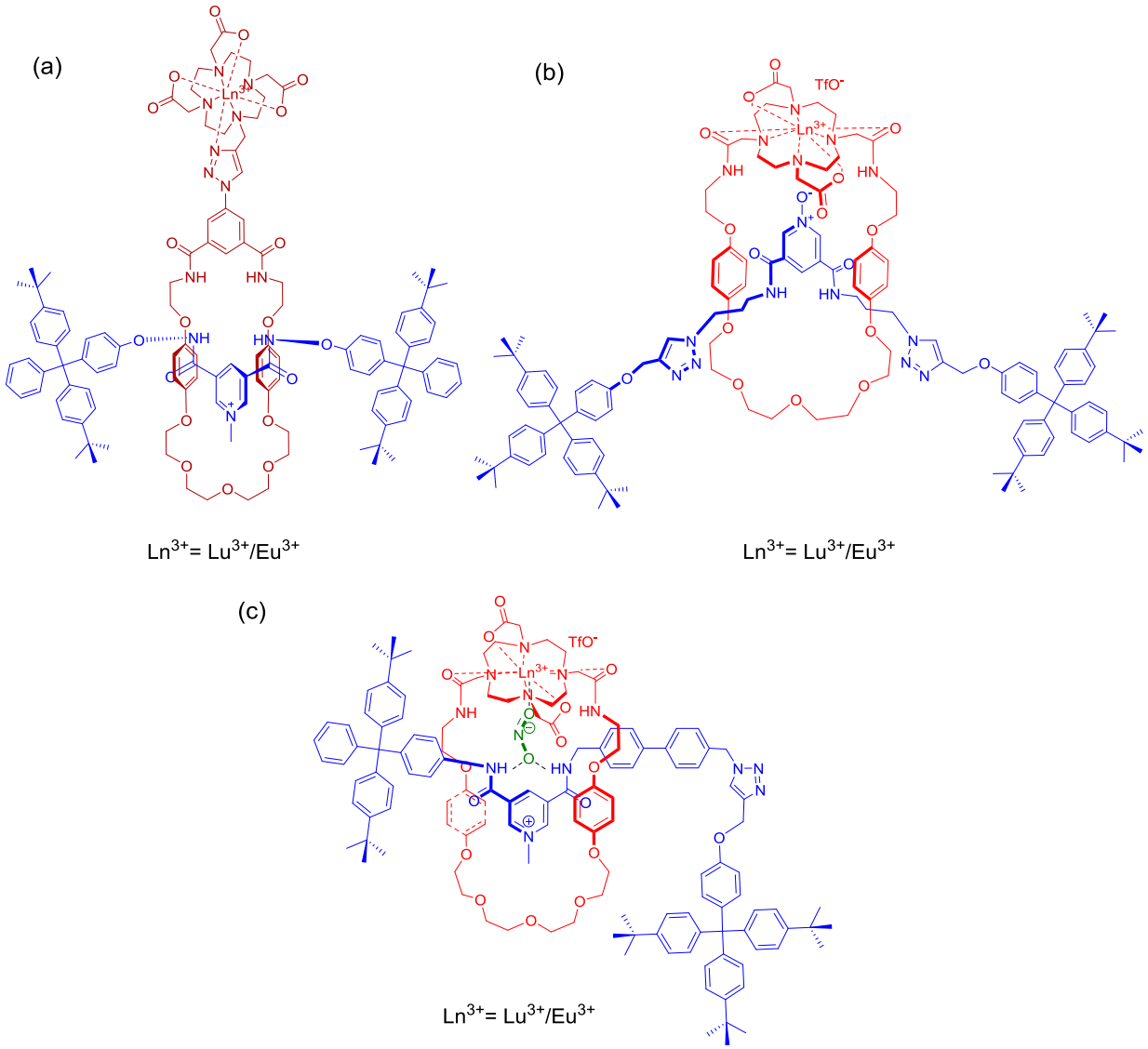


Figure 4.3. Lanthanide-containing rotaxanes.

Besides DO3A derivatives, 2,6-pyridinedicarboxamide motifs have also been exploited to synthesise interlocked lanthanide complexes. For example, a series of trefoil knots were prepared by Leigh and co-workers utilising interactions between Ln^{3+} cations and three 2,6-pyridine-dicarboxamide ligands (Figure 4.4(a)).[13–15] Similarly, mechanically interlocked [2]- and [3]catenanes were synthesised by Gunnlaugsson and co-workers using

ring-closing metathesis reactions of a Eu(III) templated pyridine-dicarboxamide bis-vinyl functionalised motif (Figure 4.4(b)).[16]

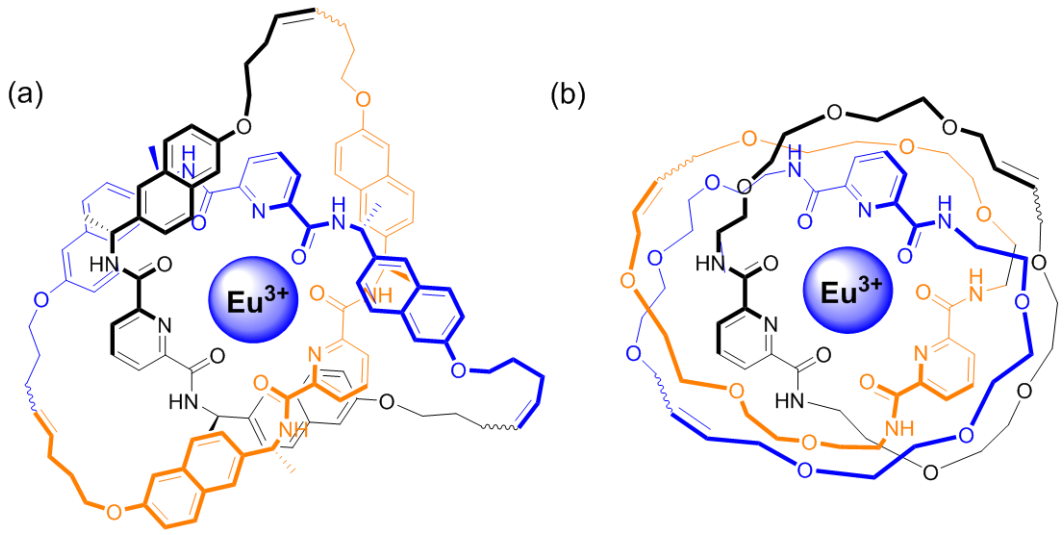


Figure 4.4. (a) Leigh's Eu-containing knots;[14] (b) Gunnlaugsson's Eu-templated [3]catenane.[16]

4.1.3 Chapter Aims

The DOTA type ligand has been extensively used for lanthanide complexation, with a wide range of coordinating amide, ester, phosphate based arms and macrocycle size variation. All these modifications however are restricted to using covalent bonds to arrange multiple donor ligands on a cyclen cyclic framework, while exploiting the mechanical bond to achieve this has not been investigated. The aim of the project described in this chapter was to construct a novel type of interlocked host for lanthanides where the covalent bonds of the cyclen cycle in DOTA are replaced by mechanical bonds resulting in a [2]rotaxane ligand (Figure 4.5). The target rotaxane cavity is flanked by multiple nitrogen donor atoms functionalised with carboxylates, which are able to encapsulate the lanthanide metal cation. Also, by varying the numbers of $NCH_2CO_2^-$ ligands and the size of macrocycle, the strength of lanthanide cation association can be modulated.

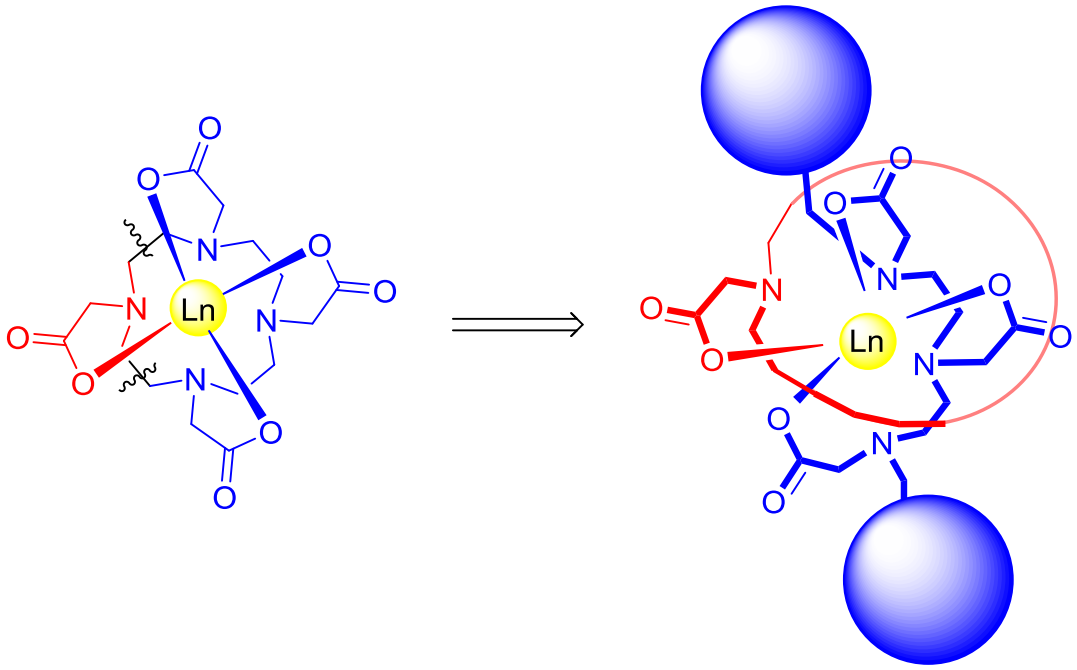
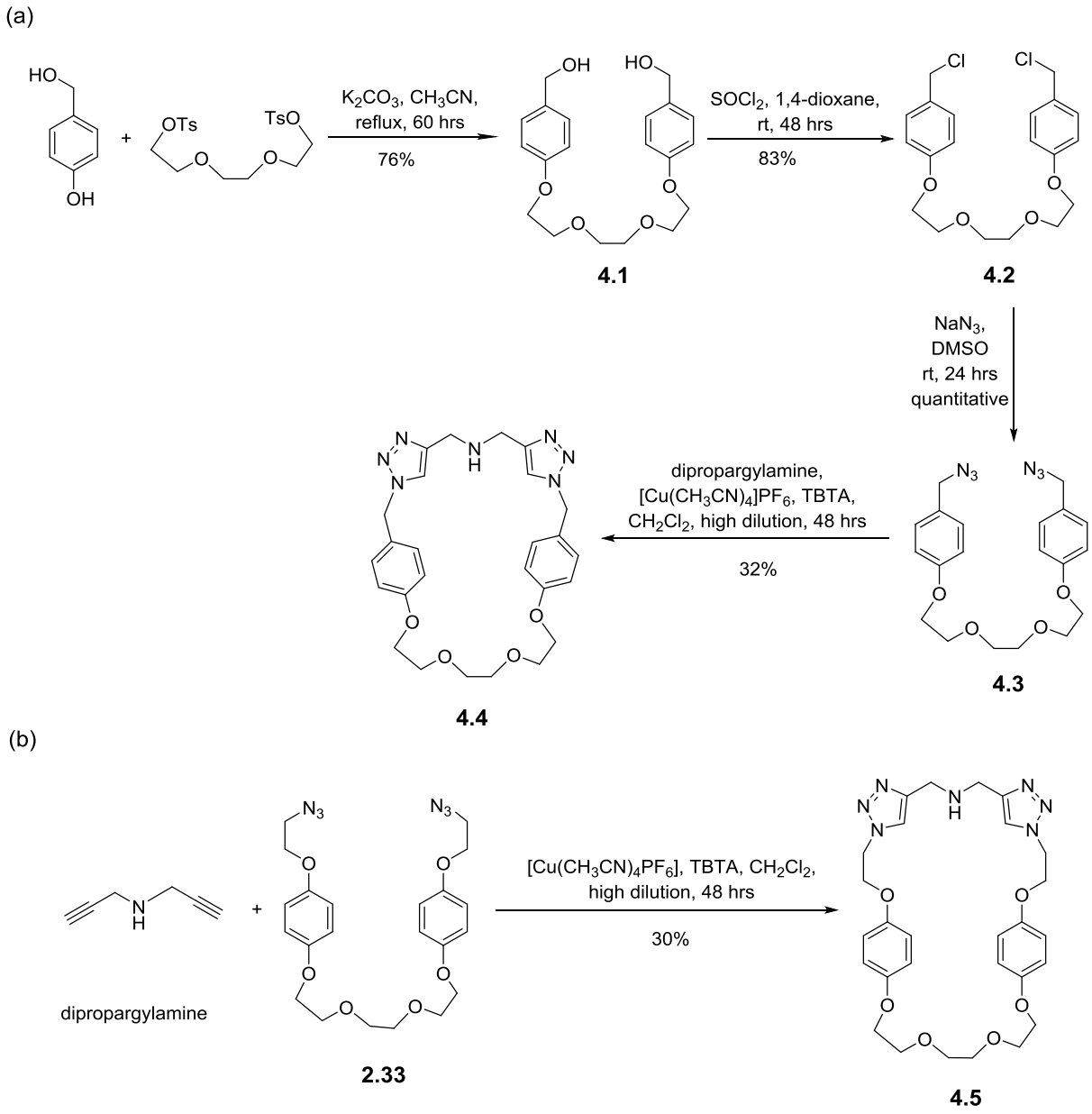


Figure 4.5. The cartoon illustration of the idea of novel rotaxane ligands for lanthanide complexation

4.2 Synthesis and Characterisation of Rotaxane Ligands

4.2.1 Synthesis of Macrocycle Components

The synthesis of the target rotaxane ligands utilised the bis-triazole-amine motif containing macrocycles to facilitate AMT mechanical bond formation. Macrocycles **4.4** and **4.5** were prepared according to Scheme 4.1. 4-Hydroxybenzyl alcohol was reacted with triethylene bis-tosylate[17] in CH_3CN under basic conditions to afford compound **4.1** in 76% yield.[18] Chlorination using thionyl chloride gave **4.2** in 83% yield,[19] which was converted to azide **4.3** in quantitative yield using NaN_3.[20] Reacting dipropargylamine and **4.3** under high-dilution CuAAC reaction conditions, followed by chromatographic purification gave macrocycle **4.4** in 32% yield (Scheme 4.1(a)). Similarly, synthesis of macrocycle **4.5** in 30% yield was achieved by CuAAC reaction with dipropargylamine and bis azide **2.33** under high dilution conditions (Scheme 4.1(b)).

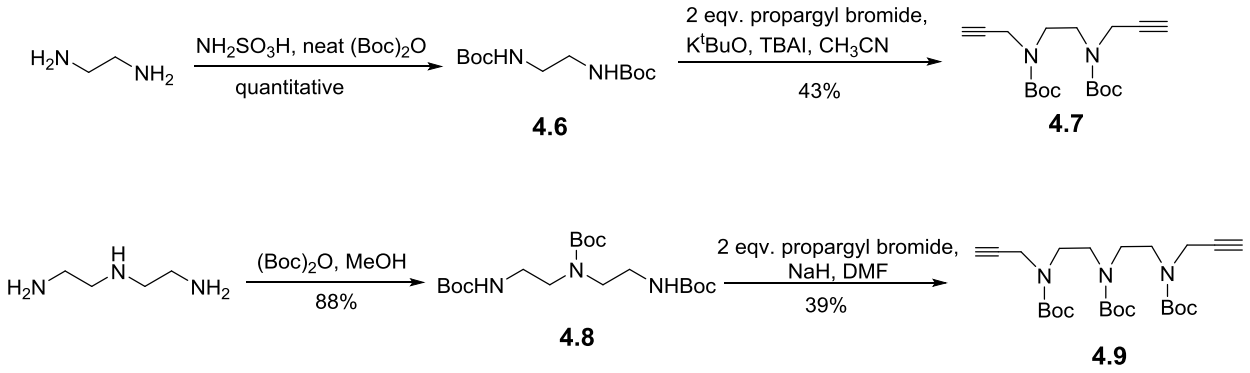


Scheme 4.1. Synthesis of macrocycle (a) **4.4** and (b) **4.5**.

4.2.2 Synthesis of Axle Components

Bis-alkyne polyamine *N*-Boc protected axle precursors were prepared as shown in Scheme 4.2. Ethylenediamine was reacted with Boc anhydride ($(Boc)_2O$) to afford compound **4.6** in quantitative yield.[21] Reaction of **4.6** with two equivalents of propargyl bromide in CH_3CN under basic conditions gave *N*-Boc-protected bis-alkyne **4.7** in 43% yield.[22] Similarly, synthesis of *N*-Boc-protected bis-alkyne **4.9** involved *N*-Boc-protection of

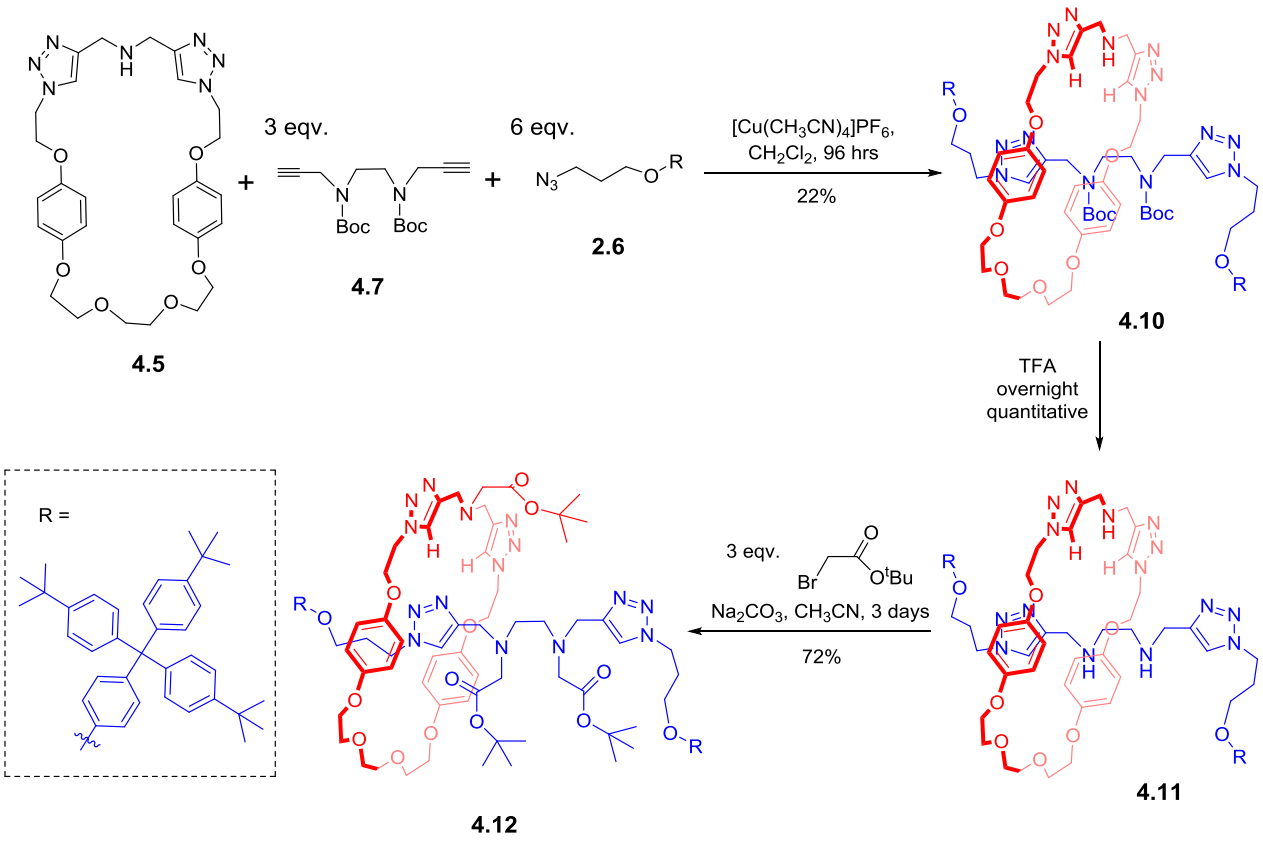
diethylenetriamine[23] and subsequent reaction with two equivalents of propargyl bromide in the presence of base.



Scheme 4.2. Synthesis of bis-alkyne **4.7** and **4.9**.

4.2.3 Synthesis and Characterisation of Rotaxanes

Rotaxanes were prepared through AMT synthesis. As shown in Scheme **4.3**, *N*-Boc protected rotaxane **4.10** was prepared in 22% isolated yield by reacting one equivalent of macrocycle **4.5**, three equivalents of bis alkyne **4.7** and six equivalents of stopper azide **2.6** in CH_2Cl_2 followed by preparative TLC purification. Rotaxane **4.10** was characterised by ^1H and ^{13}C NMR and high resolution ESI mass spectrometry. By comparing the ^1H NMR spectra of macrocycle **4.5**, rotaxane **4.10** and the corresponding free axle component which was isolated as a by-product from the AMT rotaxane forming reaction, the interlocked nature of **4.10** was evidenced from the upfield shifts of macrocycle component hydroquinone proton signals, arising from the aromatic π- π donor-acceptor interactions with the electron-deficient triazole motifs on the axle (Figure 4.6). In addition, the interlocked nature of **4.10** was further confirmed by ^1H-^1H ROESY NMR spectroscopy. Quantitative removal of *N*-Boc groups using TFA followed by reaction with three equivalents of tert-butyl bromoacetate in the presence of base afforded the rotaxane **4.12** in 72% yield.



Scheme 4.3. Synthesis of Rotaxane **4.12**.

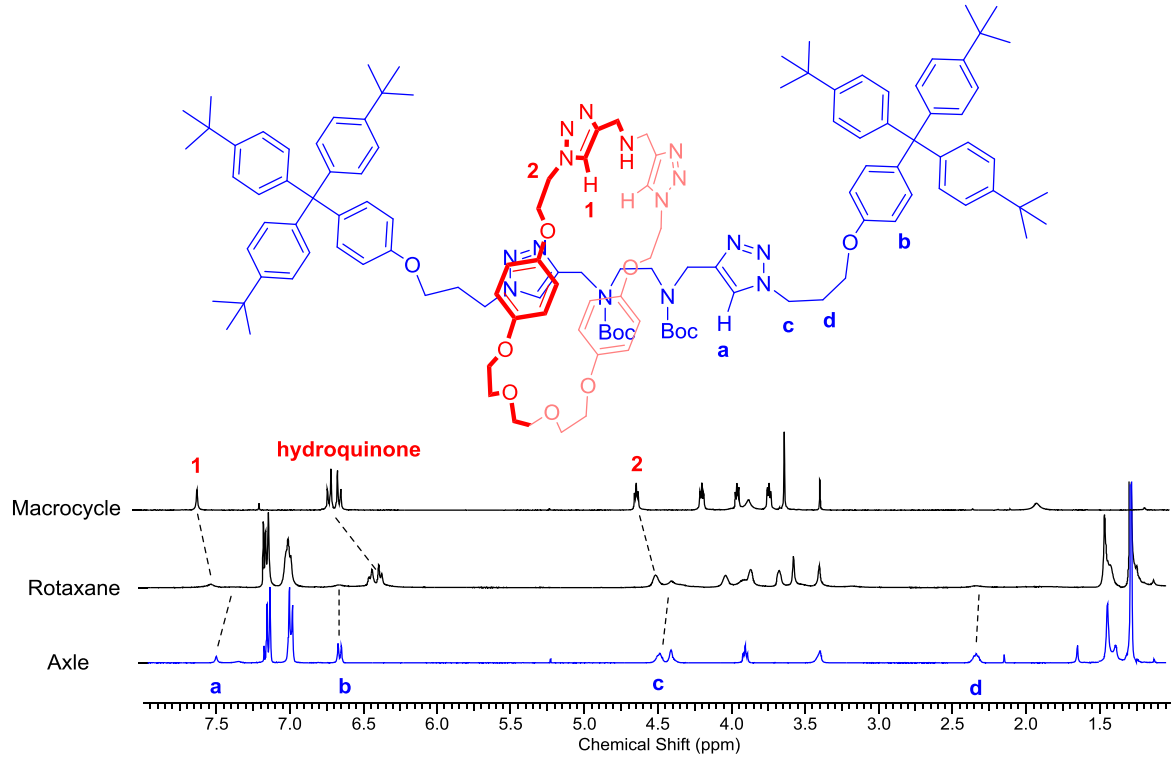


Figure 4.6. ^{1}H NMR comparison of macrocycle **4.5**, rotaxane **4.10** and corresponding axle in $CDCl_3$ (T = 298 K).

A comparison of the ^{1}H NMR spectra of rotaxanes **4.10**, **4.11** and **4.12** is shown in Figure 4.7. After removal of *N*-Boc-protecting groups, the proton signals become quite sharp and display assignable coupling patterns due to the elimination of the slow exchange N-CO bond rotation process of the *N*-Boc moieties. However, the appendage of three methylene tert-butyl acetate groups resulted in the rotaxane adopting an unsymmetric co-conformation as evidenced from the signal splitting in the ^{1}H NMR spectrum of **4.12**. Signals arising from triazole protons H_a and $H_{a'}$, stopper phenol protons H_b and $H_{b'}$, axle alkyl protons H_g and $H_{g'}$ show obvious differences while proton signals on the macrocycle component (e.g. triazole H_1 and hydroquinone protons) do not exhibit any doubling of signals. Also, the alkyl proton signals in the region between 3.0 – 4.5 ppm become more complicated and difficult to interpret compared to rotaxane **4.11**. These observations indicate that the macrocycle is stationed on one side of the axle and cannot shuttle along the axle freely, presumably because of steric hindrance from the axle's tert-butyl acetate functionalities.

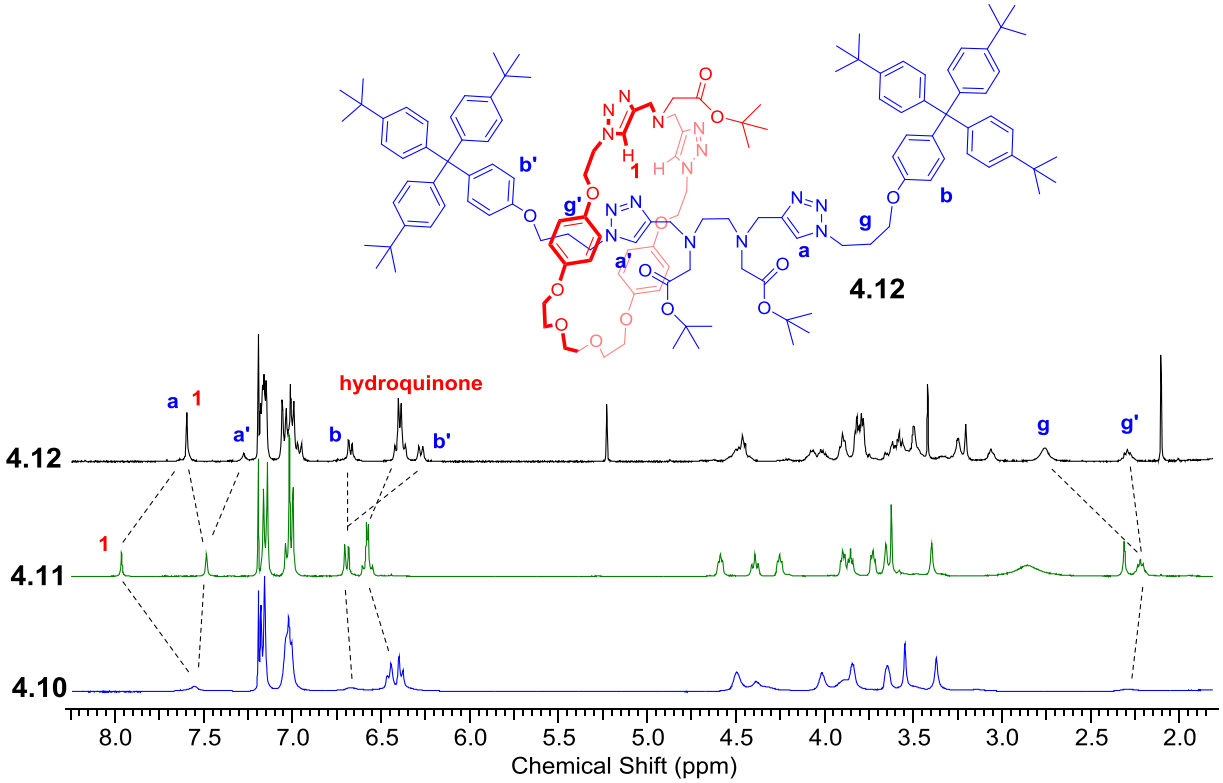
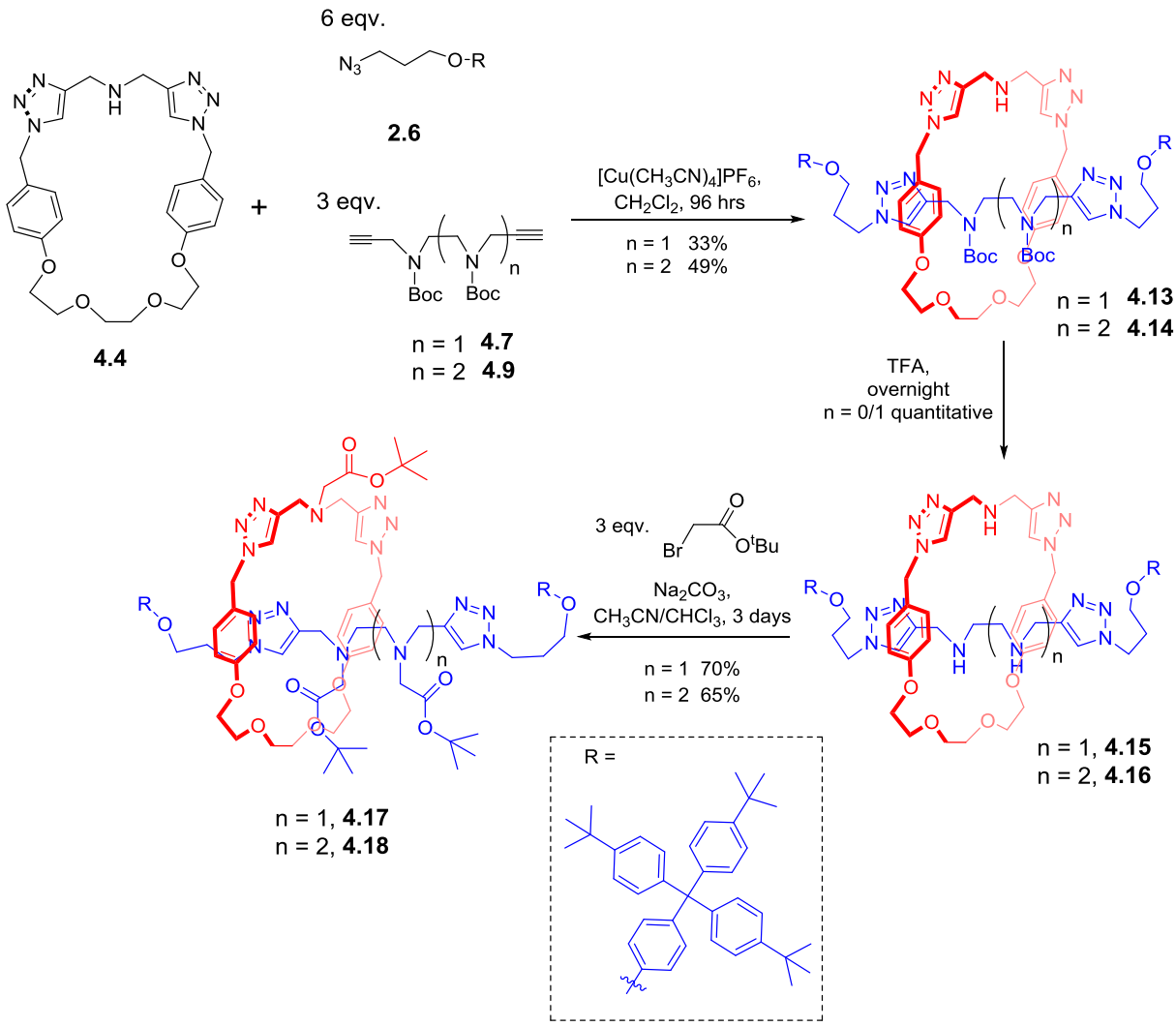


Figure 4.7. ^{1}H NMR comparison between rotaxanes **4.10**, **4.11**, **4.12** in $CDCl_3$ (*T* = 298 K).

A similar synthetic protocol (AMT rotaxane synthesis – deprotection – post-rotaxane functionalisation) was adopted to prepare rotaxanes **4.17** and **4.18** (Scheme 4.4). It is noteworthy that employing the smaller macrocycle **4.4** improved the rotaxane yields up to 49%. This observation is in agreement with previously reported results that smaller sized 2,2'-bipyridine containing macrocycles gave higher rotaxane yields using the AMT synthetic protocol.[24] Rotaxanes **4.17** and **4.18** were characterised by ^{1}H, ^{13}C and ^{1}H-^{1}H ROESY NMR and high resolution ESI mass spectrum. As expected, both rotaxanes **4.17** and **4.18** containing the smaller sized macrocycle component exhibit unsymmetric ^{1}H NMR spectra suggesting the macrocycle for steric reasons cannot shuttle along the respective axle (Figure 4.8).



Scheme 4.4. Synthesis of rotaxanes **4.17** and **4.18**.

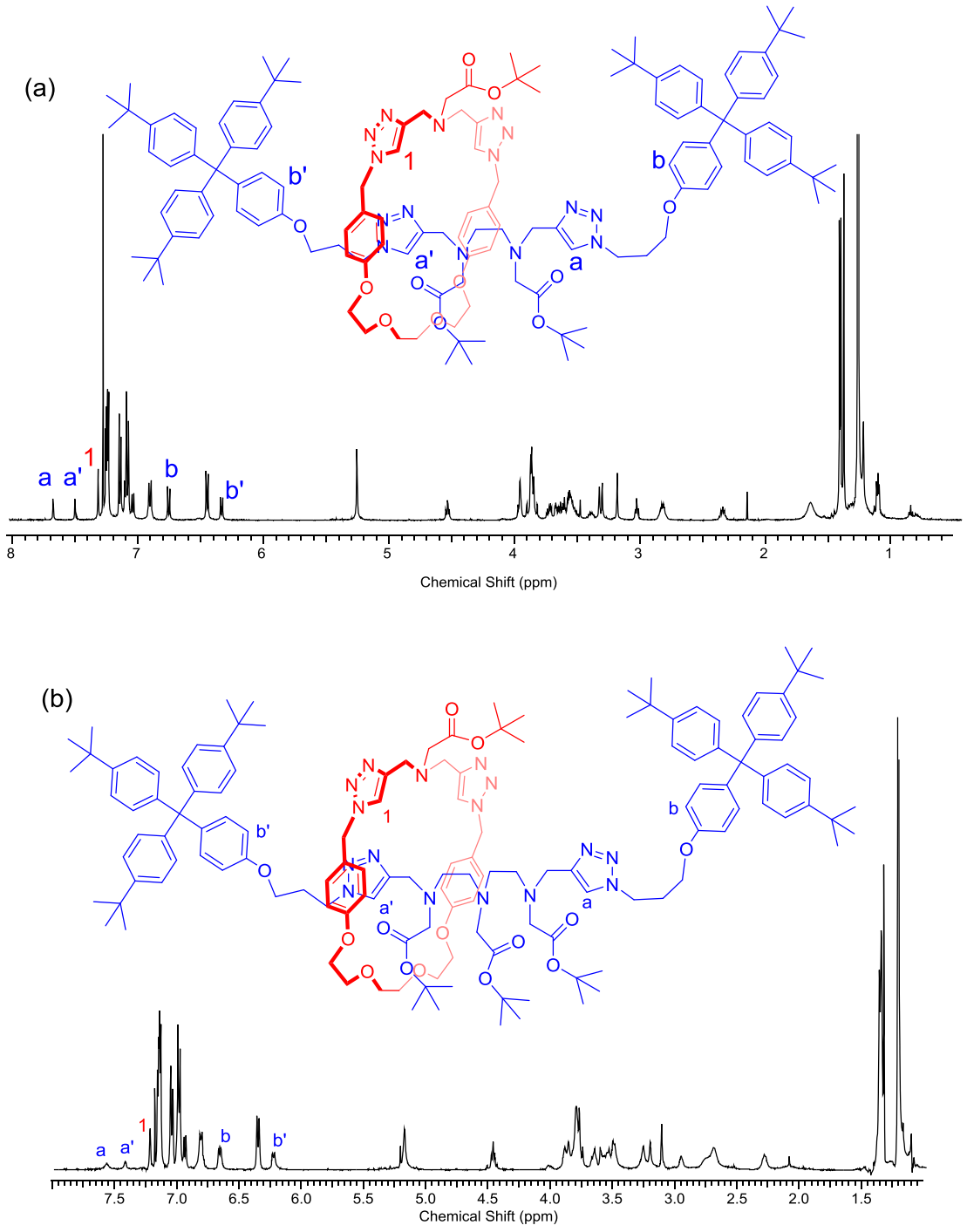
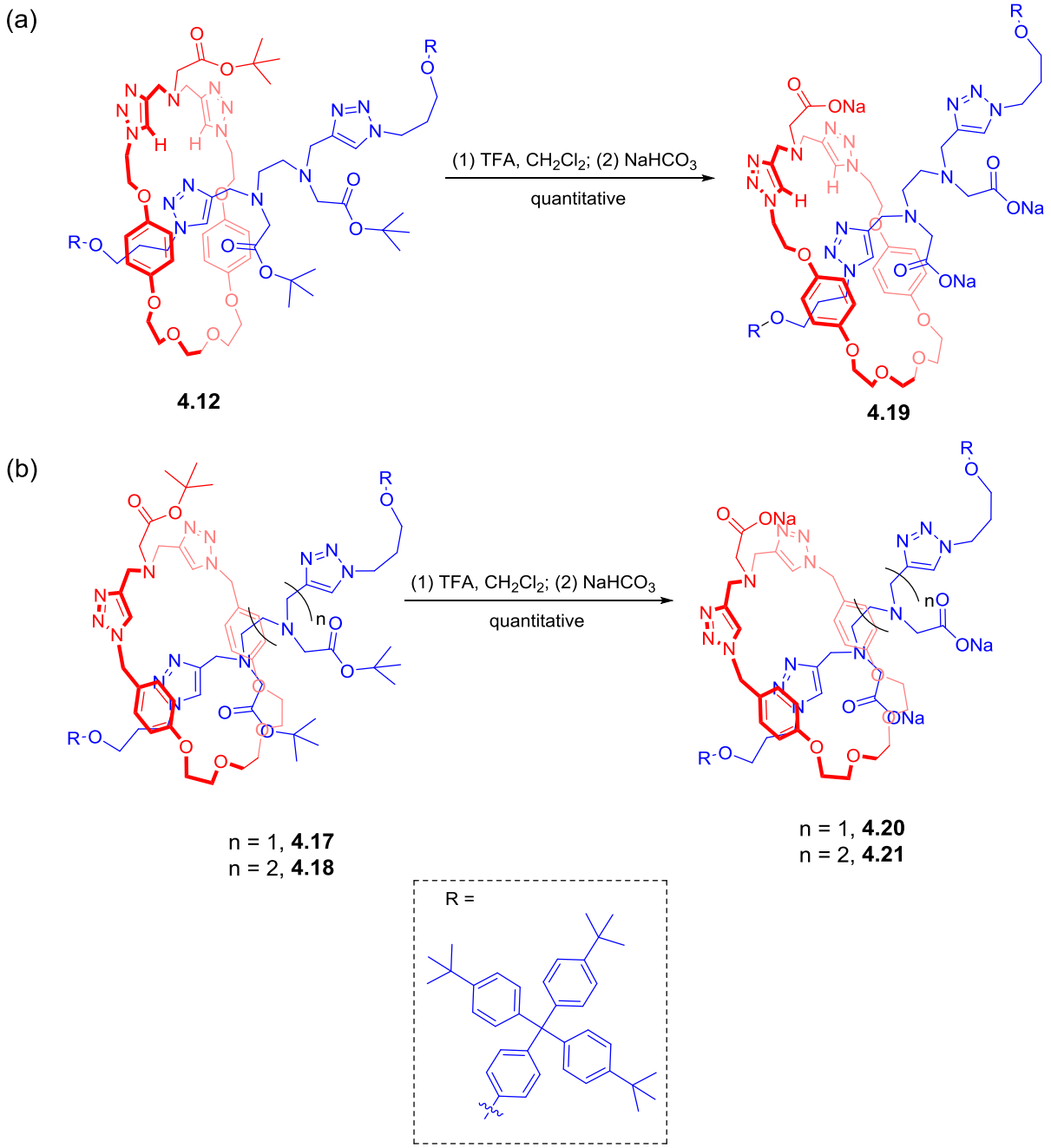


Figure 4.8. ^{1}H NMR spectrum of rotaxane (a) **4.17** and (b) **4.18** in $CDCl_3$ (T = 298 K)**.**

Removal of the tert-butyl protecting groups using TFA followed by washing with saturated $NaHCO_3$ aqueous solution produced the corresponding rotaxane sodium salts **4.19**, **4.20**, **4.21** (Scheme 4.5). For example, ^{1}H NMR spectrum of **4.21** (Figure 4.9) shows

the disappearance of the tert-butyl signals and ESI mass spectrometry also confirmed the removal of all the protecting groups.



Scheme 4.5. Synthesis of rotaxane ligands (a) **4.19** (b) **4.20** and **4.21**.

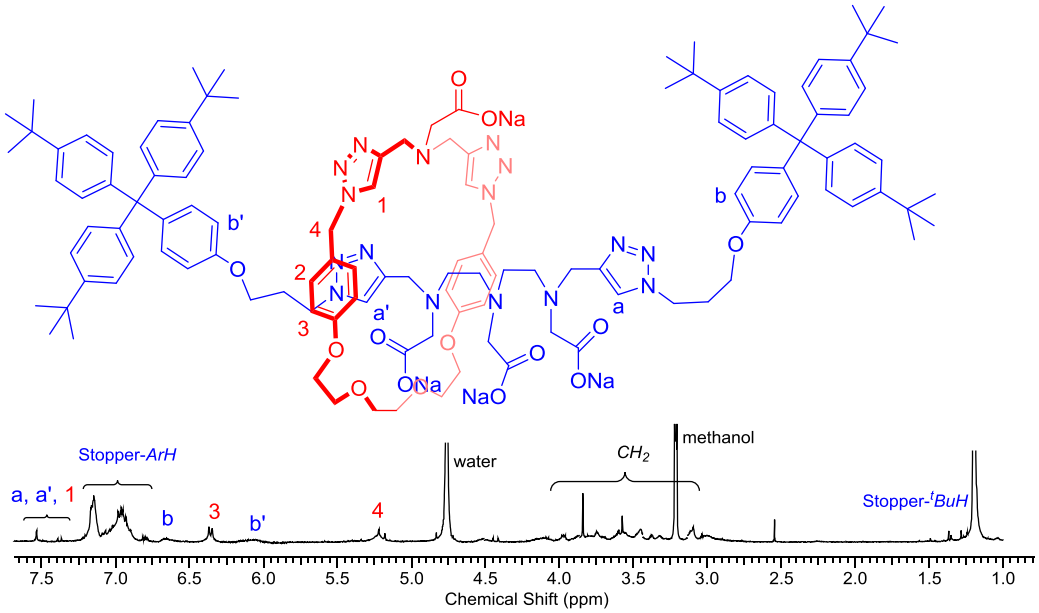
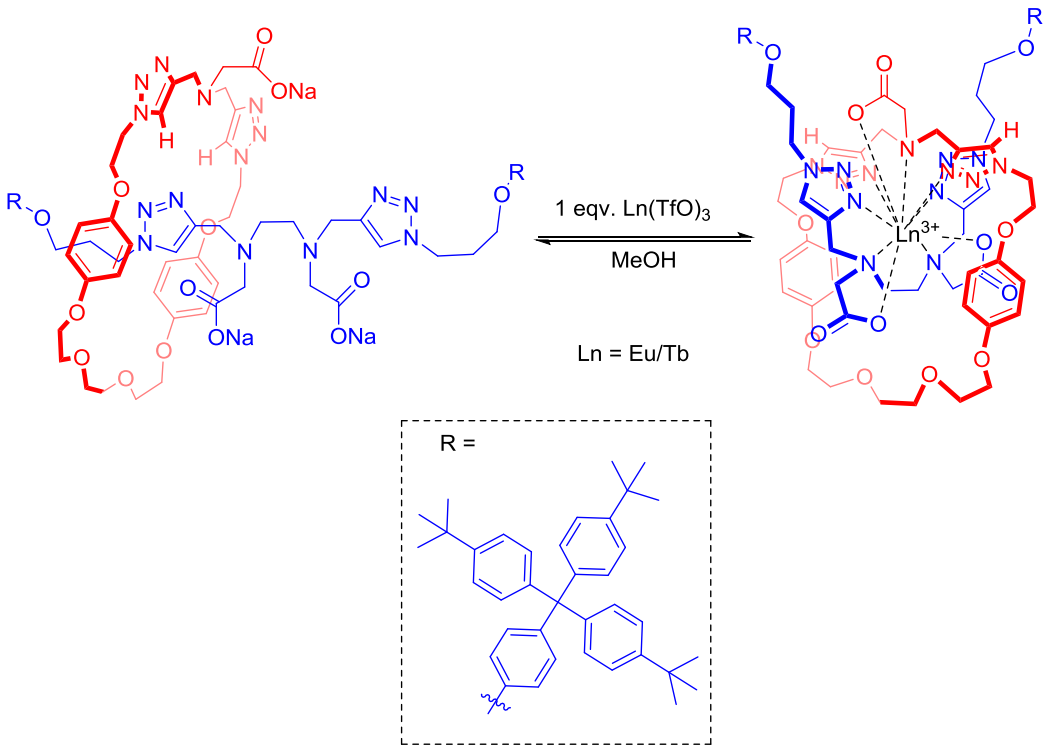


Figure 4.9. ^{1}H NMR of **4.21** in CD_3OD (T = 298 K).

4.3 Lanthanide Binding Studies*

4.3.1 Preliminary Qualitative Complexation Studies

Preliminary qualitative lanthanide complexation experiments were initially performed by adding one equivalent of $Eu(TfO)_3$ or $Tb(TfO)_3$ to methanolic solutions of rotaxane ligand **4.19** (Scheme 4.6) and monitoring the luminescence properties of the resulting mixture.



Scheme 4.6. Preliminary Eu^{3+}/Tb^{3+} complexation with rotaxane **4.19**.

Upon the addition of Eu^{3+}, the excitation spectrum of the resulting complex **4.19Eu** showed a broad ligand-metal charge transfer (LMCT) band with a sharp peak at 315 nm (Figure 4.10(a)). Importantly, the corresponding emission spectrum (excited at 315 nm) reveals low intensity luminescence, suggesting the emission of the Eu-containing systems was quenched by the LMCT process. It was hypothesised that the acyl-triazole chromophore was unable to sensitise Eu^{3+} effectively due to a dislocation between the lowest triplet state in the triazole motif and excited state of Eu^{3+}, favouring back energy transfer from the excited state of Eu^{3+} to the triazoles. Though further investigation is required before verifying these

*These experiments were undertaken in collaboration with Mr. Xuejian Zhang in Professor Stephen Faulkner's group.

hypotheses, it was clear that Eu^{3+} was not a suitable candidate for studying lanthanide cation complexation to the rotaxane ligands. By contrast, **4.19Tb** displayed stronger excitation and emission intensities, suggesting that Tb^{3+} luminescence was less strongly affected by LMCT processes due to the higher energy of its excited states (Figure 4.10(b)). The complex displayed classic terbium-centred emission, with four bands corresponding to $^5D_4 \rightarrow {}^7F_6$, $^5D_4 \rightarrow {}^7F_5$, $^5D_4 \rightarrow {}^7F_4$ and $^5D_4 \rightarrow {}^7F_3$ transitions. The moderate luminescence intensity observed may result from intramolecular energy transfer from the antenna chromophore triazole motifs to the Tb^{3+} centre. Similar luminescence spectra were noted with the in-situ formed Tb^{3+} complexes of **4.20** and **4.21**.

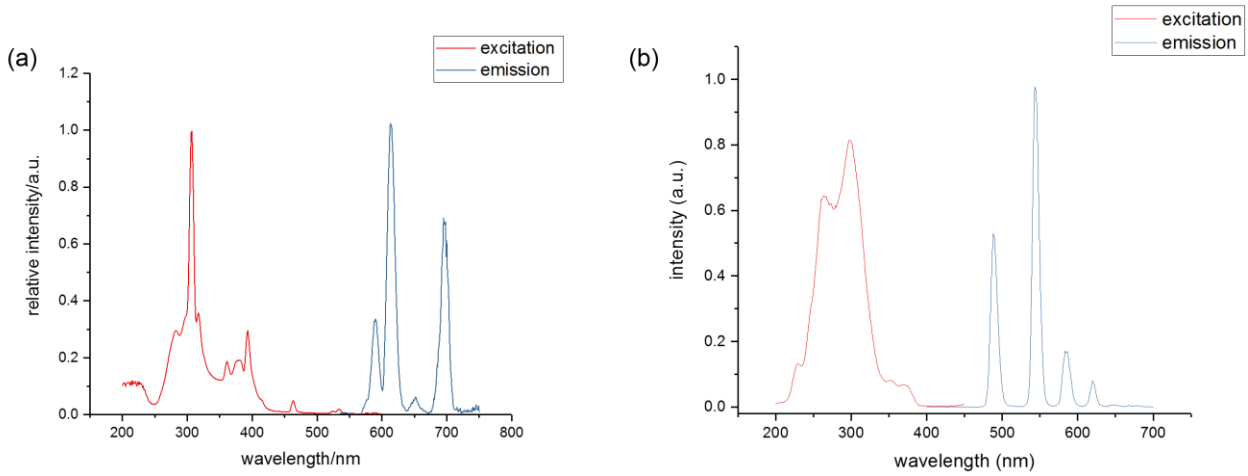


Figure 4.10. (a) Excitation spectrum (red line, λ_{em} = 615 nm) and emission spectrum of **4.19Eu** (blue line, λ_{ex} = 315 nm); (b) excitation spectrum (red line, λ_{em} = 475 nm) and emission spectrum of **4.19Tb** (blue line, λ_{ex} = 298 nm). The intensity scales are normalised respectively. Concentration = 5 x 10^{-5} M, solvent = MeOH.

Further evidence for Tb^{3+} complexation was obtained by high-resolution ESI mass spectrometry and ^{1}H NMR spectroscopy. High resolution ESI mass spectrometry confirmed the successful complexation between all three rotaxane ligands and Tb^{3+} ions (e.g. observed m/z = 2208.07099, assigned as [**4.19Tb**+H]$^+$, $C_{122}H_{149}O_{14}N_{15}Tb$, theoretical calculated 2208.06900). Also, **4.21Tb** displayed a paramagnetic shift in the ^{1}H NMR spectrum. Compared to the free ligand **4.21**, **4.21Tb** (Figure 4.11) showed a ^{1}H NMR spectral range of

over 100 ppm with line broadening arising from the paramagnetic nature of the rotaxane complexed Tb^{3+}.

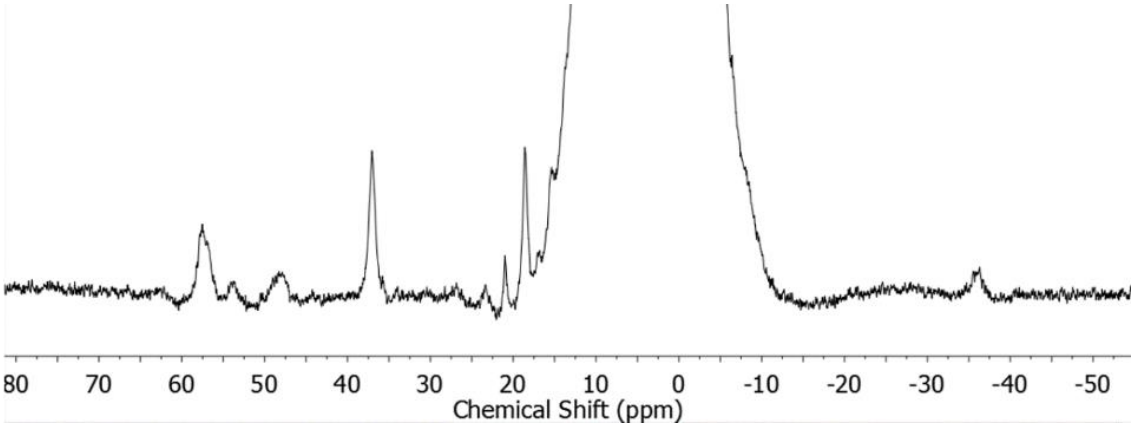


Figure 4.11. ^{1}H NMR spectra of **4.21Tb** in CD_3OD.

To further elucidated the nature of the local coordination environment of the lanthanide ions, the hydration number (q_{H_2O}), which indicates the number of water molecules coordinating to the lanthanide centre, was determined for the lanthanide rotaxane complexes **4.19Tb** and **4.21Tb**. By measuring the lifetime τ in deuterated and non- deuterated methanol, q_{H_2O} can be calculated via the Horrocks equation:

$$q_{H_2O} = 2 * A\left(\frac{1}{\tau_{MeOH}} - \frac{1}{\tau_{MeOD}} - B\right)$$

where A is a parameter which is specific to each lanthanide and B is the correction factor.[25] The curve was fitted with single exponential luminescence decays in MeOH and d_4-MeOD with the parameters of Beeby et al. (A = 5.0, B = 0.06),[26] affording an average hydration number of 2.2 for **4.21Tb** (Figure 4.12). Compared to **4.21Tb**, the hydration number of the complex **4.19Tb** is much larger (around 5), reflecting the availability of more coordination sites as a result of the lower denticity of the rotaxane ligand **4.19**. This implies the cavity of ligand **4.21** has more coordinating donors to complex the lanthanide, in particular one more $NCH_2CO_2^-$ on the axle. Multi-exponential fitting attempts were unsuccessful, indicating that no free Tb^{3+} ions were present in solution for both **4.19** and **4.21**.

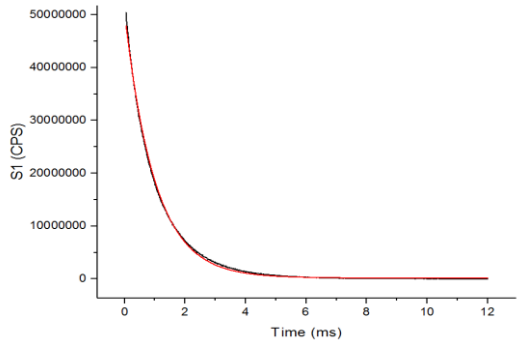
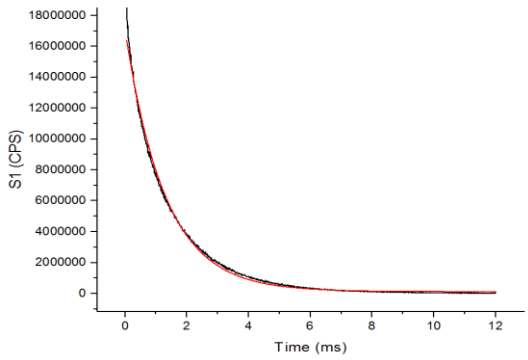
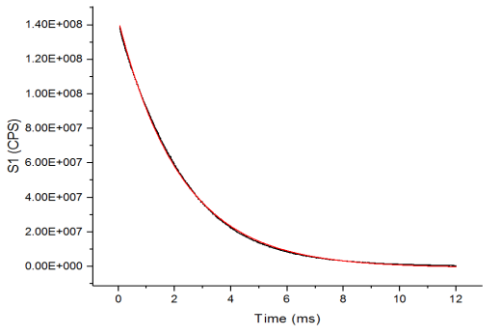
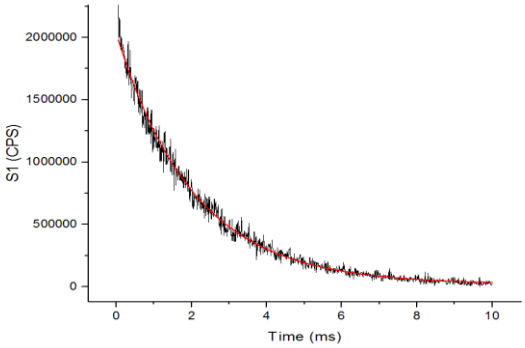
Complex	**4.19Tb**	**4.21Tb**
τ_{MeOH}		
	1.00 ms	1.29 ms
τ_{MeOD}		
	2.23 ms	2.03 ms
q_{H_2O}	4.9	2.2

Figure 4.12. Lifetimes and hydration states for **4.19Tb** and **4.21Tb**. (Fitted curved: red, observed curve: black)

Preliminary computational studies were performed to provide further insights into the structure of **4.21Tb**. MOPAC 2016, a quantum chemistry program designed to study lanthanide complexes on the basis of Dewar and Thiel's NDDO approximation, implemented with Sparkle Model parameters with RM1 (a semi-empirical molecular orbital model) was exploited to predict the geometry of **4.21Tb**.[27] Compared to conventional DFT method, MOPAC has certain advantages such as low computational cost and relative high accuracy.

Throughout the MOPAC optimization, **4.21Tb** presents a non-linear axle with distorted macrocyclic components (Figure 4.13). The rotaxane coordinates to the Tb^{3+} centre via four direct electrostatic interactions between carboxylate arms and the lanthanide cation. The optimised structure demonstrates the binding event does not occur within the cavity of the macrocyclic ring, which can be rationalised by steric effects arising from the bulky nature

of the interlocked ligand. The average bond length between Tb^{3+} and the coordinate carboxylate oxygen atoms is 2.23 Å which is relatively close to the Tb-oxygen distance (2.35 Å) observed in Tb-DOTA systems.[28]

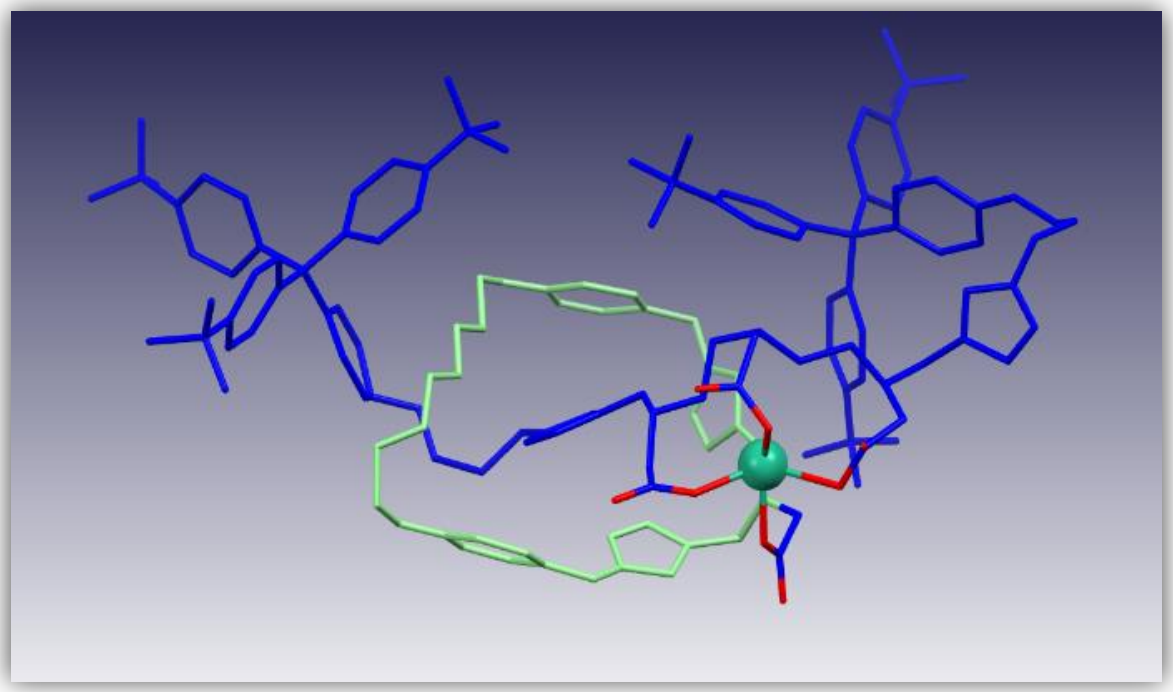


Figure 4.13. Calculated structure of **4.21Tb**, optimized using MOPAC2016. red atom: oxygen; grey atom: terbium cation.

4.3.2 Association Constant Determination

After performing qualitative Tb^{3+} complexation studies with rotaxane ligands **4.19**, **4.20** and **4.21**, the complex stoichiometries and association constants between the rotaxane ligands and Tb^{3+} in methanol were determined by luminescence titrations, which were undertaken by adding an increasing amount of $Tb(TfO)_3$ into methanol solutions of the interlocked ligands. The addition of Tb^{3+} resulted in greatly increased emission intensity (Figure 4.14) while a control experiment showed that no emission was observed on addition of Tb^{3+} into pure methanol. Moreover, by plotting the integrated luminescence intensities (J = - 2 or J = -1) against the concentration of Tb^{3+} cation and analyzing the resulting titration curves using Dynafit[29] (Figure 4.15), 1:1 stoichiometric association constants were obtained

(Table 4.1). It is envisaged that the bulky and encapsulating nature of the rotaxane ligands prevents the formation of higher order complexes with greater host/guest ratios.

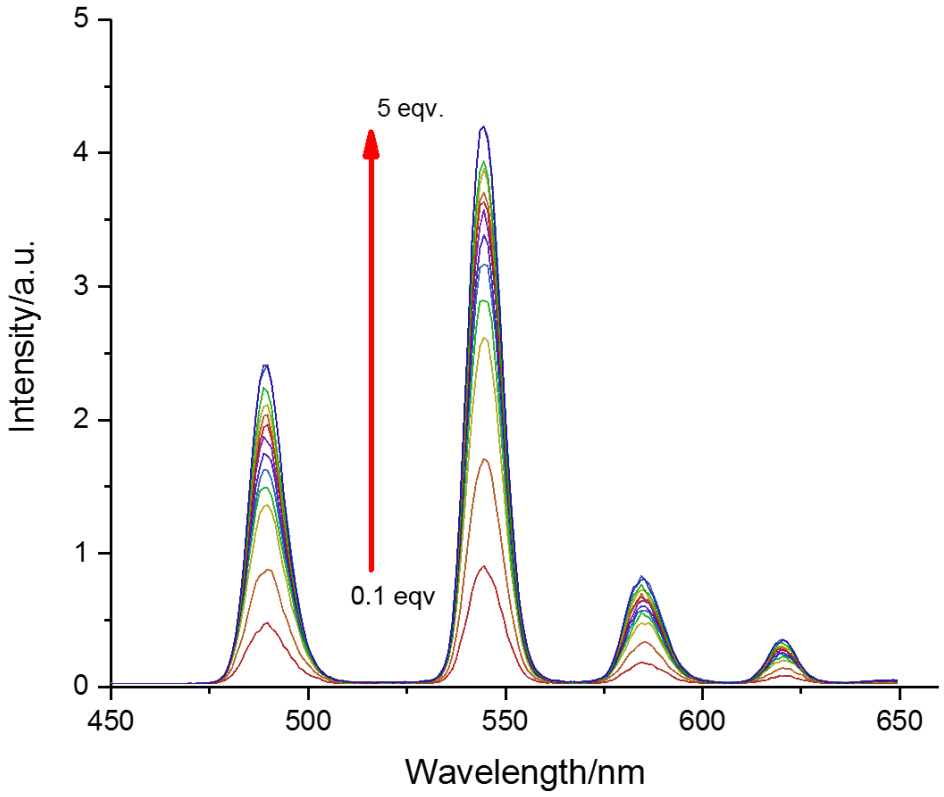


Figure 4.14. Phosphorescence spectra: titration of free Tb^{3+} cation into a MeOH solution of the rotaxane ligand **4.19** (excitation at 298 nm, exit slit = 5 nm, gated time = 0.1 ms, [**4.19**] = 5 x 10^{-5} M).

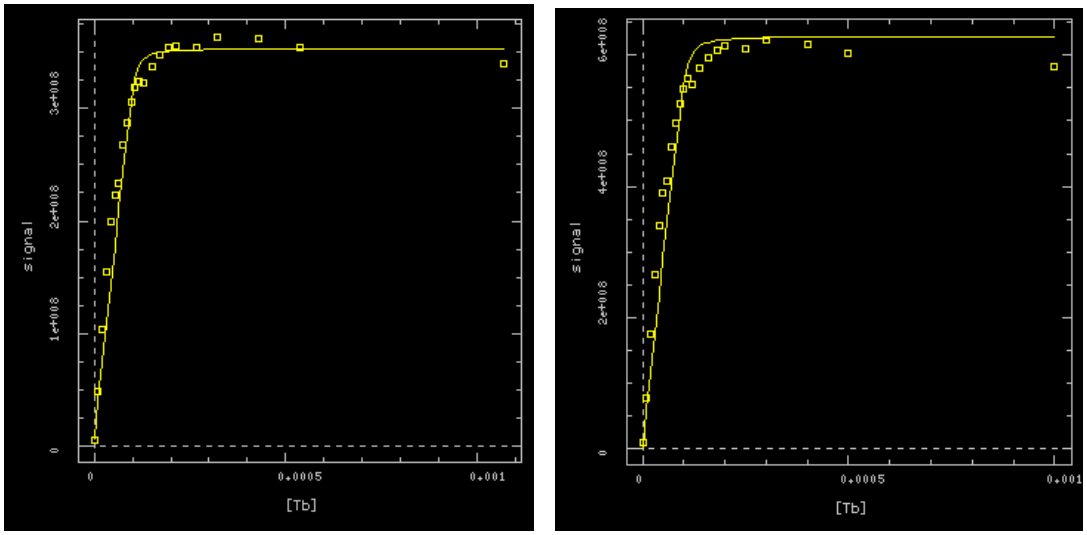


Figure 4.15. Binding curve fitting (ΔJ = -2 (left) and ΔJ = -1 (right)). Vertical axis: integrated luminescence intensity; horizontal axis: concentration of Tb^{3+} cation.

Table 4.1. Association constants for formation of 1:1 complexes between of different rotaxane ligands with Tb^{3+} and rotaxane ligands **4.19**, **4.20** and **4.21**.

Ligand	Log (K_a/M^{-1})[a]	
	J = -2	J = -1
4.19	5.04 ± 0.09	5.12 ± 0.07
4.20	5.30 ± 0.08	5.37 ± 0.09
4.21	6.17 ± 0.04	6.08 ± 0.05
[a] Solvent = CH_3OH, T = 293 K.		

Both rotaxanes **4.19** and **4.20** have three carboxylic acid functionalities with the latter containing a smaller macrocycle component. The greater affinity between Tb^{3+} and **4.20** illustrates that the smaller macrocycle size results in greater complex stability, likely due to the increased preorganisation and fewer degrees of conformational freedom associated with the smaller macrocycle component. Comparing the Tb^{3+} association constant values of rotaxane ligands **4.20** and **4.21**, both of which have the same macrocycle component, **4.21** forms the strongest complex as a consequence of having an additional $NCH_2CO_2^-$ carboxylate coordinate donor incorporated into the rotaxane's axle component.

4.4 Conclusions and Future Work

A series of novel rotaxane ligands capable of lanthanide complexation were prepared via AMT rotaxane synthesis followed by post-functionalisation. Quantitative lanthanide complexation experiments proved the successful binding of Tb^{3+} cations to the three rotaxane ligands, which was demonstrated by luminescence experiments, ^{1}H NMR spectroscopy and high resolution mass spectrometry. Further understanding of the environment of the interlocked ligand complexed lanthanide centre was obtained by calculating the hydration numbers of Tb^{3+} complexes, as well as by performing computational modelling studies. Association constants for 1:1 stoichiometric rotaxane:Tb^{3+} binding were determined by luminescent spectroscopic titrations. The large association constant values not only proved the successful formation of stable complexes between the rotaxane ligands and Tb^{3+}, but also indicated that complex stability was enhanced with increasing the number of $NCH_2CO_2^-$coordinate donor groups on the rotaxanes' axle component, and with increasing preorganisaton of the interlocked host through contraction of the macrocycle component.

Future work will focus on incorporating other sensitisers such as ferrocene derivatives into the rotaxane ligand framework (Figure 4.16). The ferrocene motif will potentially act as an efficient antenna for other lanthanide guest metal cations such as Eu^{3+} leading to unique photo-physical properties. Importantly, a redox addressable antenna can also allow the resulting lanthanide complex to switch sensitised emission electrochemically.[30]

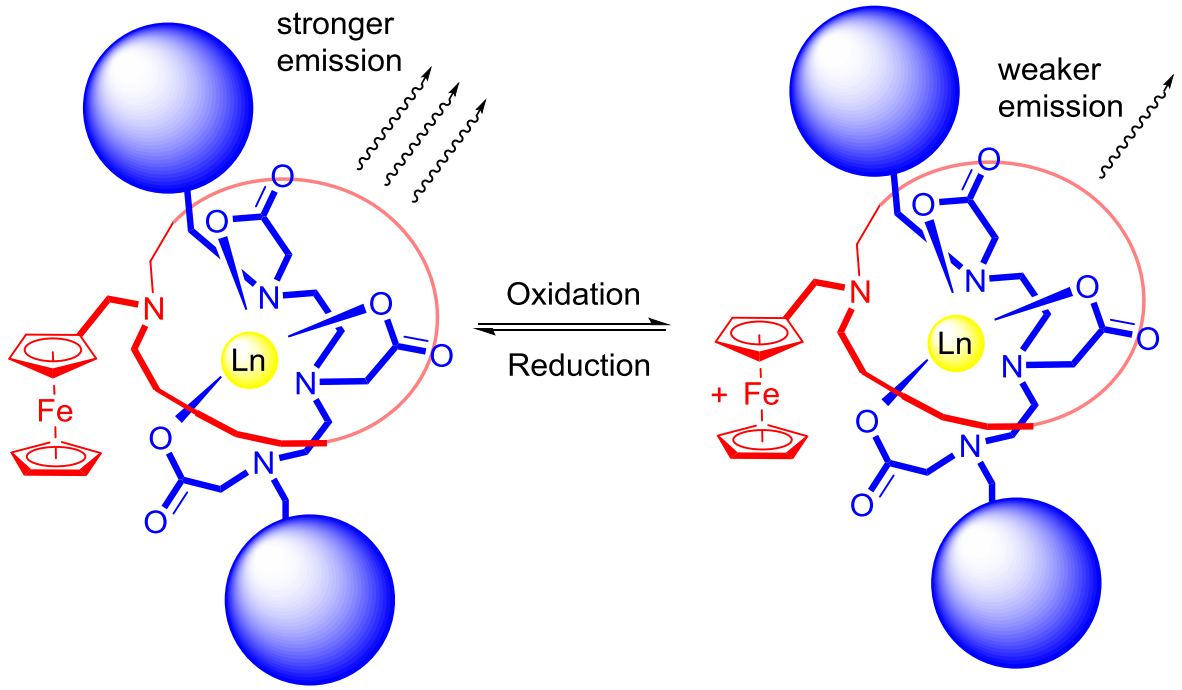


Figure 4.16. A ferrocene-containing interlocked lanthanide complex potentially capable of electrochemical switching of luminescence.

4.5 References

1 R. G. Pearson, *J. Am. Chem. Soc.*, 1963, **85**, 3533–3539.
2 R. G. Pearson, *J. Chem. Educ.*, 1968, **45**, 581.
3 R. G. Pearson, *J. Chem. Educ.*, 1968, **45**, 643.
4 J.-C. G. Bünzli, *J. Coord. Chem.*, 2014, **67**, 3706–3733.
5 L. G. Nielsen, A. K. R. Junker and T. J. Sørensen, *Dalton Trans.*, 2018, **47**, 10360–10376.
6 J. Lehr, P. D. Beer, S. Faulkner and J. J. Davis, *Chem. Commun.*, 2014, **50**, 5678–5687.
7 M. C. Heffern, L. M. Matosziuk and T. J. Meade, *Chem. Rev.*, 2014, **114**, 4496–4539.
8 M. R. Spirlet, J. Rebizant, J. F. Desreux and M. F. Loncin, *Inorg. Chem.*, 1984, **23**, 359–363.
9 W. P. Cacheris, S. K. Nickle and A. D. Sherry, *Inorg. Chem.*, 1987, **26**, 958–960.
10 C. Allain, P. D. Beer, S. Faulkner, M. W. Jones, A. M. Kenwright, N. L. Kilah, R. C. Knighton, T. J. Sørensen and M. Tropiano, *Chem. Sci.*, 2012, **4**, 489–493.
11 F. Zapata, O. A. Blackburn, M. J. Langton, S. Faulkner and P. D. Beer, *Chem. Commun.*, 2013, **49**, 8157–8159.
12 M. J. Langton, O. A. Blackburn, T. Lang, S. Faulkner and P. D. Beer, *Angew. Chem. Int. Ed.*, 2014, **53**, 11463–11466.
13 G. Gil-Ramírez, S. Hoekman, M. O. Kitching, D. A. Leigh, I. J. Vitorica-Yrezabal and G. Zhang, *J. Am. Chem. Soc.*, 2016, **138**, 13159–13162.
14 G. Zhang, G. Gil-Ramírez, A. Markevicius, C. Browne, I. J. Vitorica-Yrezabal and D. A. Leigh, *J. Am. Chem. Soc.*, 2015, **137**, 10437–10442.
15 D. A. Leigh, L. Pirvu, F. Schaufelberger, D. J. Tetlow and L. Zhang, *Angew. Chem. Int. Ed.*, 2018, **57**, 10484–10488.
16 C. Lincheneau, B. Jean-Denis and T. Gunnlaugsson, *Chem. Commun.*, 2014, **50**, 2857–2860.
17 S. J. Bora, R. Dutta, D. J. Kalita and B. Chetia, *Spectrochim. Acta. A. Mol. Biomol. Spectrosc.*, 2018, **204**, 225–231.
18 M. J. Gunter, T. P. Jeynes, M. R. Johnston, P. Turner and Z. Chen, *J. Chem. Soc. Perkin 1*, 1998, 1945–1958.
19 A. Yıldırım and S. Öztürk, *Phosphorus Sulfur Silicon Relat. Elem.*, 2015, **190**, 1535–1550.
20 S. Lal, J. McNally, A. J. P. White and S. Díez-González, *Organometallics*, 2011, **30**, 6225–6232.
21 D. J. Upadhyaya, A. Barge, R. Stefania and G. Cravotto, *Tetrahedron Lett.*, 2007, **48**, 8318–8322.
22 G. A. Bailey, E. W. Price, B. M. Zeglis, C. L. Ferreira, E. Boros, M. J. Lacasse, B. O. Patrick, J. S. Lewis, M. J. Adam and C. Orvig, *Inorg. Chem.*, 2012, **51**, 12575–12589.
23 T.-T. Truong, G. W. Coates and H. D. Abruña, *Chem. Commun.*, 2015, **51**, 14674–14677.
24 H. Lahlali, K. Jobe, M. Watkinson and S. M. Goldup, *Angew. Chem. Int. Ed.*,2011, **50**, 4151–4155.
25 P. Dissanayake, Y. Mei and M. J. Allen, *ACS Catal.*, 2011, **1**, 1203–1212.
26 A. Beeby, I. M. Clarkson, R. S. Dickins, S. Faulkner, D. Parker, L. Royle, A. S. de Sousa, J. A. G. Williams and M. Woods, *J. Chem. Soc. Perkin Trans. 2*, 1999, 493–504.
27 M. A. M. Filho, J. D. L. Dutra, G. B. Rocha, R. O. Freire and A. M. Simas, *RSC Adv.*, 2013, **3**, 16747–16755.
24 D. Parker, H. Puschmann, A. S. Batsanov and K. Senanayake, *Inorg. Chem.*, 2003, **42**, 8646–8651.
29 P. Kuzmič, *Anal. Biochem.*, 1996, **237**, 260–273.
30 M. Tropiano, N. L. Kilah, M. Morten, H. Rahman, J. J. Davis, P. D. Beer and S. Faulkner, *J. Am. Chem. Soc.*, 2011, **133**, 11847–11849.

Chapter 5: Conclusions

The work in this thesis highlights the application of interlocked host structures for anion recognition and lanthanide complexation. In the case of interlocked structures as anion hosts, the utility of halogen bonding as an intermolecular interaction has been established, demonstrating that the unique three dimensional cavities of interlocked structures flanked with multiple XB iodotriazole motifs facilitate anion binding affinity and selectivity. The arrangement of $NCH_2CO_2^-$ donor groups integrated into the macrocycle and axle components of [2]rotaxanes leads to a novel type of host molecule for lanthanide cations.

Chapter 2 underscored the bifunctional properties of XB bis-iodotriazole derivatives where their Lewis basic N-donors are used for metal coordination and Lewis acidic XB C-I donors are used for anion recognition. Using AMT methodology, a series of XB rotaxane hosts were prepared. Coordinating a Re(I) functionality to a cationic XB rotaxane resulted in enhanced affinity and selectivity for spherical halide anions in competitive aqueous solvent media. Furthermore, incorporating a XB bis-iodotrizole-amine motif into rotaxane frameworks generated XB rotaxanes capable of acid-regulated switching of metal cation and anion guest binding (Figure 5.1). When neutral, the rotaxanes were able to bind transition metals strongly and exhibited relatively weaker anion binding affinity. Addition of acid producing the protonated rotaxane analogue greatly enhanced the strength of anion binding and switched off metal cation binding. Importantly, the protonated XB rotaxane host displayed a rare anti-Hofmeister anion binding bias, $Cl^- > Br^- > NO_3^-$ with no binding of I^- and ReO_4^-.

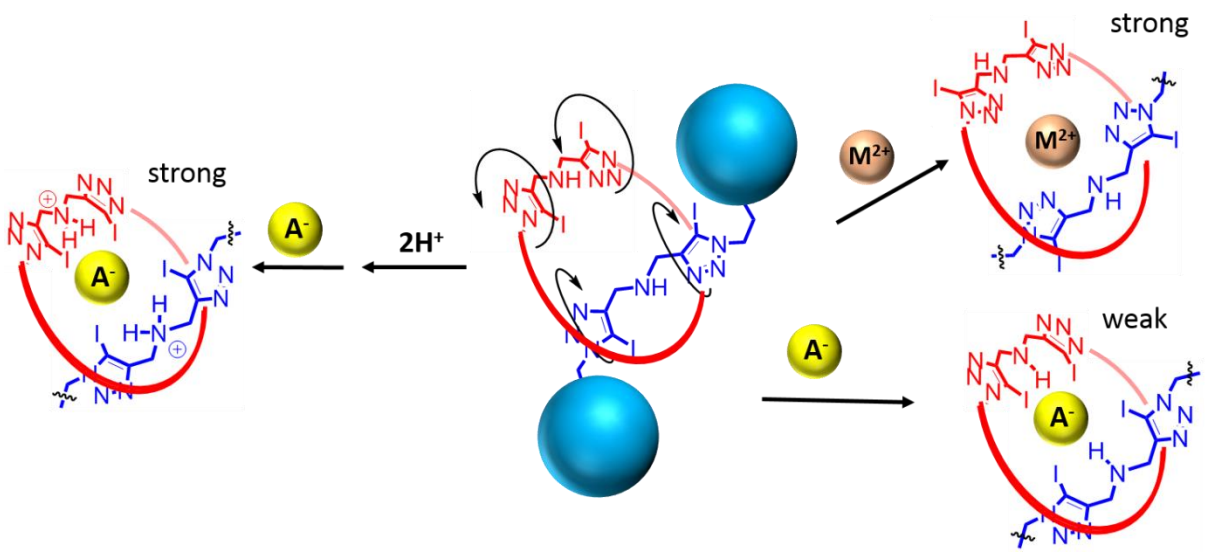


Figure 5.1. Cartoon illustration of a bis-iodotriazole-amine motif containing XB rotaxane capable of acid-regulated switching of metal cation and anion guest binding.

In Chapter 3 XB cryptand hosts bearing multiple iodotriazole groups for anion recognition were prepared using tripodal capping and macrocyclic bridging synthetic approaches. It was established that incorporating a variety of bridging covalently linked spacer groups into such cryptand frameworks had a significant influence on cryptand solubility and molecular conformation. A naphthalene-containing XB cryptand (Figure 5.2) was demonstrated to act as a selective chloride anion host and fluorescent sensor. Efforts to prepare unprecedented XB cryptand-based interlocked anion hosts were undertaken via AMT and HB template approaches. Although evidence of formation of the target hosts was observed by ESI-MS, no interlocked products could be isolated.

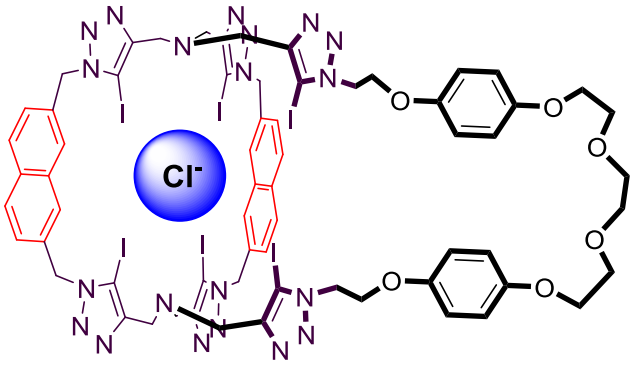


Figure 5.2. A multiple XB iodotriazole functional groups containing cryptand capable of selective spherical Cl^- recognition and sensing.

Chapter 4 described a series of novel interlocked ligands for lanthanide complexation (Figure 5.3). These rotaxane ligands were prepared via AMT mechanical bond synthesis followed by post-rotaxane functionalisation. The successful formation of stable complexes between the rotaxane ligands and Tb^{3+} was observed as evidenced from photo-physical investigations. In addition, increasing the number of $NCH_2CO_2^-$ donor groups on the rotaxanes' axle component together with preorganisaton of the interlocked host through contraction of the macrocycle component was demonstrated to enhance the stability of the Tb^{3+} complex. Further modification of the rotaxane ligand framework by altering the arrangement of the $NCH_2CO_2^-$ donor groups and incorporating a variety of antennas such as ferrocene motifs will produce lanthanide complexes with potential applications in sensing and imaging

.

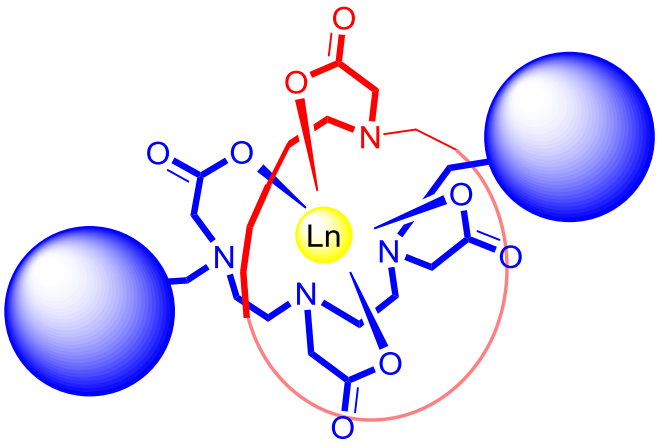


Figure 5.3. Cartoon illustration of a new class of novel rotaxane ligand for lanthanide complexation.

In summary, the results described in this thesis demonstrate that interlocked molecules, prepared by AMT methodologies, can act as unique hosts for anions and lanthanides. Furthermore, elaborate modification of such interlocked host molecules has proven to be an efficient approach to tune their guest binding affinity and selectivity.

Chapter 6: Experimental

6.1 General Considerations

6.1.1 Instrumentation

NMR spectra were recorded on Bruker Avance III 400 HD nanobay NMR spectrometers equipped with 9.4T magnets, or Bruker Avance 500 machines equipped with 11.75T magnets. All chemical shifts are noted in parts per million (ppm) (nearest 0.01 ppm for ^{1}H NMR and nearest 0.1 for ^{13}C NMR). Signal splittings are denoted as singlet (s), doublet (d), triplet (t), quartet (quart.), quintet (quint.), septet (sep.) and multiplet (m). 2D techniques such as COSY and ROESY are used to assign proton signals in some cases. Spectra are recorded relative to the residual solvent peak (for ^{1}H and ^{13}C), or the solvent with greatest number of deuterium atoms in the case of mixed solvent systems. Low and high resolution ESI mass spectra were carried out on Waters LCT premier and Bruker microTOF spectrometers respectively. Fluorescence and UV-Vis spectra were recorded on a Horiba Fluorolog 3, T60U (PG Instruments Ltd) spectrophotometer and Applied Photophysics Chirascan instrument respectively. Terbium luminescence spectra were collected in phosphorescence mode exciting at 298 nm using a flash delay of 0.1 ms.

6.1.2 ^{1}H NMR Titration Protocols

All deuterated solvents and tetrabutylammonium (TBA) salts used were purchased from chemical suppliers. All TBA salts need to be stored in vacuum dessicators at room temperature in the presence of P_2O_5 dessicant for at least a week. In a typical titration experiment, the initial sample volumes were 0.5 mL, at a concentration of 1.0 mM of host where a solution of the anion of interest as its tetrabutylammonium (TBA) salt was added to the host solution. The resulting chemical shifts of the appropriate protons were monitored for at least 17 data points. The observed chemical shift values at each guest concentration were entered into the WinEQNMR2 software[1] for every titration point. Estimates for the binding constant and limiting chemical shifts were performed. The parameters were refined using

non-linear squares analysis under a host-guest 1:1 binding model to obtain the best fit between the observed and calculated chemical shifts during convergence of the best-fit binding constant values and their errors.

6.1.3 Luminescence Titration Protocols

Luminescence spectroscopy was performed on a HORIBA Fluorolog. In each case, spectra were recorded at 293 K using standard 3 mL quartz cuvettes with sample volumes of 2.5 mL and path length of 1 cm. In order to maintain the receptor concentration, the guest species of interest (anions or lanthanide cations) was dissolved in the same receptor solution. In a typical experiment, an aliquot of the guest species solution was added to the receptor solution in the cuvette and the mixture was thoroughly mixed using a pipette before the luminescence spectra were recorded.

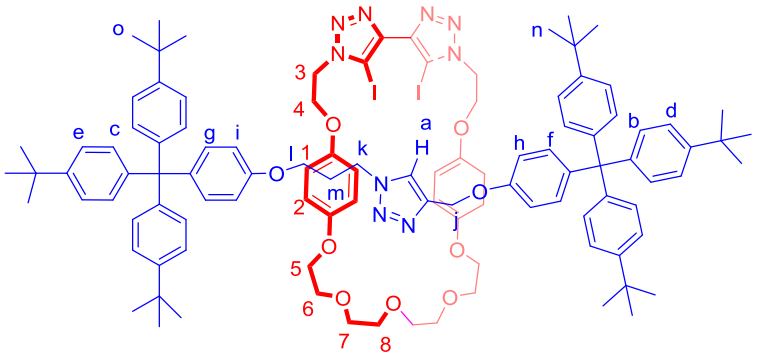
6.2 Synthetic Procedures

6.2.1 Solvents and Reagents

All solvents and reagents were purchased from commercial suppliers and used as received. Dry organic solvents were degassed with nitrogen and then dehydrated by passing through an MBraun MPSP-800 column. De-ionised water was obtained using a Milli-Qr Millipore machine. Triethylamine was distilled from potassium hydroxide and stored over the same base at ambient conditions while TBTA was synthesised as described.[2] Brine refers to a saturated aqueous solution of NaCl and basic EDTA solution is a 0.02 M aqueous solution of EDTA in a 1 % NH_3 solution. 0.1 M HBF_4 solution was prepared by dissolving $HBF_4{\cdot}Et_2O$ complex in $CDCl_3$ and the solution was stored in fridge. Thin layer chromatography (TLC) analysis was undertaken using Merck silica Kieselgel 60 F_{254} 0.25 mm with spots visualised under UV light (254 or 365 nm) or staining with $KMnO_4$ solution. Purification of compounds were performed using silica gel column chromatography (particle size 40-63 uM) or preparative TLC plates (20 x 20 cm with 1 mm silica thickness). Microwave-assisted reactions were undertaken in sealed standard Biotage pyrex-glass microwave vials with a Biotage® Initiator 2.0 reactor.

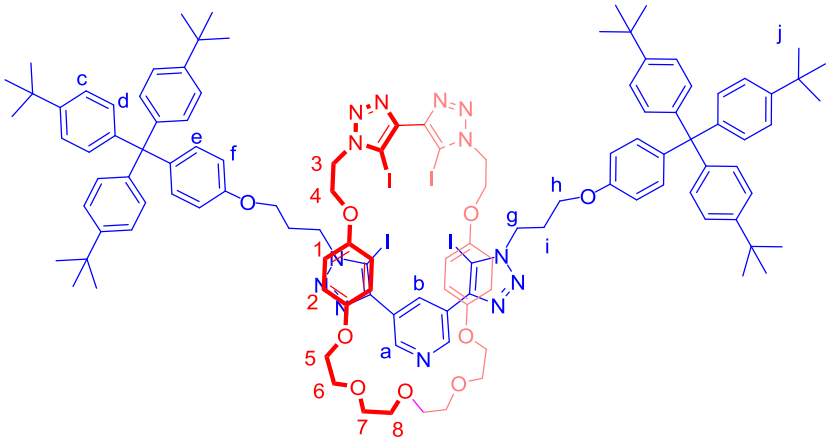
6.2.2 Synthesis of Novel Compounds from Chapter 2

Rotaxane **2.7H**



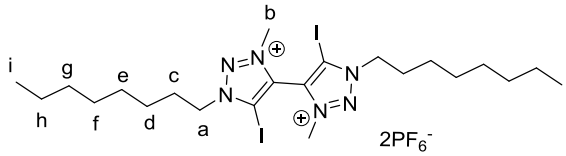
To a solution of macrocycle **2.3** (44 mg, 0.054 mmol) in dry CH_2Cl_2 (5 mL) under N_2 was added $[Cu(CH_3CN)_4]PF_6$ (20 mg,0.054 mmol) and stirred for 5 min. Stopper-azide **2.6** (126 mg, 0.216 mmol) and stopper-alkyne **2.5** (117 mg, 0.216 mmol) were then added and the solution was left to stir at room temperature for 48 hrs. The reaction mixture was diluted with CH_2Cl_2 (20 mL), washed with an EDTA solution (3 x 5 mL), water (2 x 5 mL) and then dried over $MgSO_4$. The rotaxane was purified using preparative TLC chromatography (97:3 CH_2Cl_2/CH_3OH) to afford the rotaxane **2.7H** as a white solid (21 mg, yield = 20%). **^{1}H NMR** (500 MHz, $CDCl_3$) δ (ppm): 7.80 (1H, s, H_a), 7.25-7.08 (28H, m, H_b-H_g), 6.80 (2H, d, ^3J = 8.9 Hz, H_h), 6.60 (2H, d, ^3J = 8.9 Hz, H_i), 6.55-6.38 (8H, m, H_1 + H_2), 4.95 (2H, s, H_j), 4.79 (4H, m, H_3), 4.32 (4H, t, ^3J = 5.1 Hz, H_4), 3.99 (2H, t, ^3J = 7.5 Hz, H_k), 3.59-3.47 (18H, m, H_5–H_8 + H_l), 1.85 (2H, quin, ^3J = 7 Hz, H_m), 1.31(27H, s, H_n), 1.30 (27H, s, H_o); **^{13}C NMR** (125 MHz, $CDCl_3$) δ (ppm): 156.3, 156.2, 153.1, 151.9, 148.3, 144.2, 142.9, 142.6, 139.9, 139.7, 132.2, 132.1, 130.7, 124.1, 115.9, 115.2, 113.3, 113.1, 70.7, 69.5, 67.5, 64.3, 63.1, 61.5, 49.7, 47.1, 34.3, 31.4, 31.4, 29.7, 29.5; **HRMS** (ESI +ve) m/z= 1949.79245 ($[M+H]^+$, $C_{108}H_{130}I_2N_9O_9$, calc. 1949.79525).

Rotaxane **2.9**



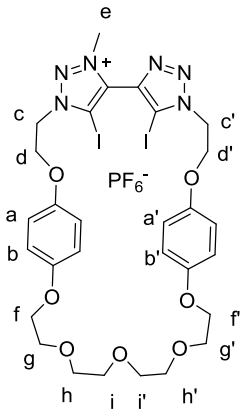
To a solution of macrocycle **2.3** (20 mg, 0.024 mmol) in dry CH_2Cl_2 (2.4 mL) under N_2 was added $[Cu(CH_3CN)_4]PF_6$ (18 mg, 0.048 mmol) and stirred for 5 min. Stopper azide **2.6** (112 mg, 0.192 mmol) and 3,5-bis-iodoalkyne pyridine **2.8** (36 mg, 0.096 mmol) were added and the solution was left to stir at room temperature for 96 hrs. The reaction mixture was diluted with $CHCl_3$ (20 mL), washed with an EDTA solution (10mL x 2), water (5 mL) and then dried with $MgSO_4$. After preparative TLC chromatography (97:3 CH_2Cl_2/CH_3OH), the rotaxane **2.9** was gained as a white solid (14 mg, 24% yield). **^{1}H NMR** (500 MHz, $CDCl_3$) δ (ppm): 9.23 (2H, s, H_a), 8.77 (1H, s, H_b), 7.26-7.24 (12H, d, ^3J = 9.0 Hz, H_c), 7.13-7.11 (16H, d, ^3J = 9.0, H_d + H_e), 6.68 (4H, d, ^3J = 8.7 Hz, H_f), 6.37 (4H, d, ^3J = 9.0 Hz, H_1), 6.33 (4H, d, ^3J = 9.0 Hz, H_2), 4.86 (4H, t, ^3J = 4.2 Hz, H_3), 4.24 (4H, t, ^3J = 4.2 Hz, H_4), 4.17 (4H, t, ^3J = 5.9 Hz, H_g), 3.78-3.63 (20H, m, H_5-H_8 + H_h), 2.02 (4H, quintet, ^3J = 5.9 Hz, H_i), 1.32 (54H, s, H_j); **^{13}C NMR** (125 MHz, $CDCl_3$) δ (ppm) 156.3, 153.0, 151.8, 148.3, 144.2, 141.9, 139.8, 132.3, 132.2, 130.7, 124.1, 114.9, 114.9, 113.1, 79.3, 70.7, 70.6, 69.5, 67.6 67.3, 64.0, 63.1, 50.2, 47.9, 34.3, 31.4, 29.7, 29.4, 22.7, 14.1; **HRMS** (ESI +ve) m/z = 2373.6608 ($[M+H]^+$, $C_{117}H_{134}O_9N_{13}I_4$, calc. 2373.6634).

Compound **2.14**



Compound **2.13** (184mg, 0.3 mmol) was dissolved in dry CH_2Cl_2 (5 mL) before $[Me_3O]BF_4$ (93.2 mg, 0.63 mmol) was added. The mixture was stirred for two days under N_2. A drop of CH_3OH was added to quench reaction and the solvent was removed under vacuum to give a light yellow solid which was then purified by preparative TLC chromatography (9:1 CH_2Cl_2/CH_3OH). Anion exchange to the PF_6^- salt was achieved by washing a $CHCl_3$ solution (20 mL) of the product with a 0.1 M NH_4PF_6 aqueous solution (20 mL x 10). The solution was dried over $MgSO_4$ and the solvent was removed under vacuum to afford the compound **2.14** as an off-white solid (168 mg, 60% yield). **^{1}H NMR** (400 MHz, CD_3CN) δ (ppm): 4.64 (4H, t, ^3J = 6.0 Hz, H_a), 4.19 (6H, s, H_b), 2.06 (4H, quin, ^3J = 5.8 Hz, H_c), 1.50-1.31 (20H, m, H_d - H_h), 0.91 (6H, t, ^3J = 5.5 Hz, H_i); **^{19}F NMR** (376 MHz, CD_3CN) δ (ppm): -72.4 (d, $^1J_{F\text{-}P}$ = 712 Hz); **^{31}P NMR** (142 MHz, CD_3CN) δ (ppm): -144.8 (sep., $^1J_{F\text{-}P}$ = 712 Hz); **MS** (ESI +ve) m/z= 321.1 ($[M - 2PF_6]^{2+}$, $C_{22}H_{40}N_6I_2$, calc. 321.1).

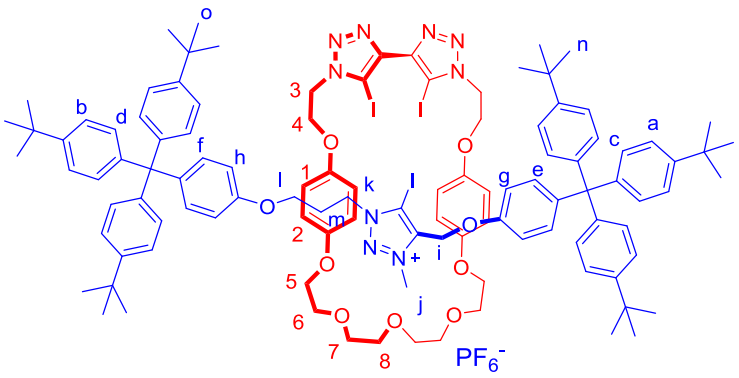
Compound **2.15**



Macrocycle **2.3** (10mg, 0.0122 mmol) was dissolved in dry CH_3CN (5 mL) in a microwave vial before $[Me_3O]BF_4$ (7.2 mg, 0.0488 mmol) was added. The mixture was

stirred at 80 °C for seven days. A drop of CH_3OH was added to quench reaction and the solvent was removed under vacuum to give a light yellow solid which was then purified by preparative TLC chromatography (9:1 CH_2Cl_2/CH_3OH) to afford an off-white solid. Anion exchange of the product to the PF_6^- salt was achieved by washing a $CHCl_3$ solution (20 mL) of the product with a 0.1 M NH_4PF_6 aqueous solution (20 mL x 10). The solution was dried over $MgSO_4$ and the solvent was removed under vacuum to afford the compound **2.15** as an off-white solid (11.2 mg, 94% yield). **^{1}H NMR** (400 MHz, $CDCl_3$) δ (ppm): 6.87-6.62 (8H, m, H_a + $H_{a'}$ +H_b + $H_{b'}$), 5.04 (2H, t, ^3J = 4.3 Hz, H_c), 4.88 (2H, t, ^3J = 4.3 Hz, $H_{c'}$), 4.62 (2H, t, ^3J = 4.3 Hz, H_d), 4.54(2H, t, ^3J = 4.54 Hz, $H_{d'}$), 4.23 (3H, s, H_e), 4.08 (2H, t, ^3J = 4.5Hz, H_f), 4.01 (2H, t, ^3J = 4.5 Hz, H_f), 3.78 (4H, m, H_g + $H_{g'}$), 3.65 (8H, m, H_h + $H_{h'}$ + H_i + $H_{i'}$); **^{13}C NMR** (100 MHz, $CDCl_3$) δ (ppm): 153.0, 152.6, 151.0, 149.8, 137.6, 134.4, 115.4, 114.8, 114.6, 69.8, 69.6, 68.7, 68.6, 67.4, 67.0, 66.1, 64.3, 53.0, 52.4, 50.3, 39.0, 28.7; **^{19}F NMR** (376 MHz, $CDCl_3$) δ (ppm): -72.4 (d, $^1J_{F-P}$ = 712 Hz); **^{31}P NMR** (142 MHz, $CDCl_3$) δ (ppm): -144.8 (sep., $^1J_{F-P}$ = 712 Hz); **MS** (ESI +ve) m/z = 833.1 ([M–PF_6]$^+$, $C_{29}H_{35}O_7N_6I_2$, calc. 833.1).

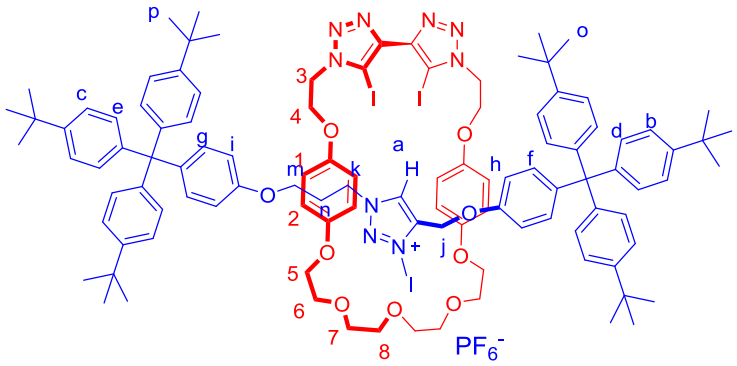
Rotaxane **2.16I**



To a solution of neutral rotaxane **2.7I** (8 mg, 0.004mmol) in 1 mL of $CHCl_3$ was added CH_3I (30 mg, 0.21 mmol) and stirred at 30°C until all the starting material was consumed. The solvent was removed to afford a light yellow solid which was then purified through preparative TLC chromatography (95:5 CH_2Cl_2/CH_3OH). Anion exchange of the

purified product to the PF_6^- salt was achieved by washing a $CHCl_3$ solution (20 mL) of the product with a 0.1 M NH_4PF_6 aqueous solution (20 mL x 10). The solvent was removed under vacuum to afford the product as a white solid (6.4 mg, 80% yield). **^{1}H NMR** (500 MHz, $CDCl_3$) δ (ppm): 7.26-7.22 (12H, m, H_a + H_b), 7.18-7.11 (16H, m, H_c- H_f), 6.77 (2H, d, ^3J = 8.7 Hz, H_g), 6.66 (2H, d, ^3J = 8.7 Hz, H_h), 6.37 (4H, d, ^3J = 9.2 Hz, H_1), 6.35 (4H, d, ^3J = 9.2 Hz, H_2), 4.89 (4H, m, H_3), 4.47 (2H, s, H_i), 4.26 (4H, m, H_4), 3.95 (3H, s, H_j), 3.82-3.40 (20H, m, H_5–H_8 + H_k + H_l), 1.80 (4H, quintet, ^3J = 6.8 Hz, H_m), 1.32 (27H, s, H_n), 1.31 (27H, s, H_o); **^{13}C NMR** (125 MHz, $CDCl_3$) δ (ppm): 156.1, 154.5, 152.7, 151.8, 148.3, 144.1, 144.0, 141.7, 140.1, 130.6, 124.2, 124.1, 115.0, 114.9, 113.2, 88.9, 78.5, 70.6, 70.0, 67.7, 67.1, 63.1, 57.9, 51.5, 50.2, 39.3, 34.3, 31.4, 29.7, 27.7; **^{19}F NMR** (376 MHz, $CDCl_3$) δ (ppm): -72.4 (d, $^1J_{F\text{-}P}$ = 712 Hz); **^{31}P NMR** (142 MHz, $CDCl_3$) δ (ppm): -144.8 (sep., $^1J_{F\text{-}P}$ = 712 Hz); **HRMS** (ESI +ve) m/z = 2089.6969 ([M–PF_6]$^+$, $C_{109}H_{129}O_9N_9I_3$, calc. 2089.7075).

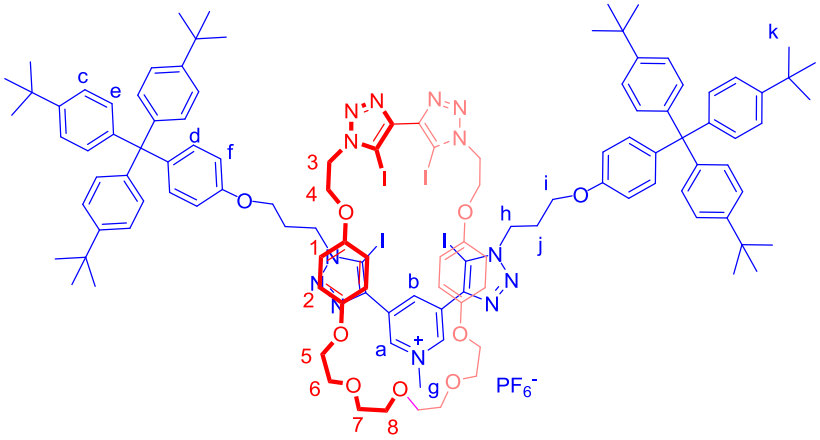
Rotaxane **2.16H**



To a solution of neutral rotaxane **2.7H** (8 mg, 0.004mmol) in 1 mL of $CHCl_3$ was added CH_3I (30 mg, 0.21 mmol) and stirred at 30°C until all the starting material was consumed. The solvent was removed to afford a light yellow solid which was purified through preparative TLC chromatography (95:5 CH_2Cl_2/CH_3OH). Anion exchange of the purified product to the PF_6^- salt was achieved by washing a $CHCl_3$ solution (20 mL) of the product with a 0.1 M NH_4PF_6 aqueous solution (20 mL x 10). The solvent was removed under

vacuum to afford the rotaxane **2.16H** as a white solid (6.0 mg, 75% yield). **^{1}H NMR** (400 MHz, $CDCl_3$) δ (ppm): 8.74 (1H, s, H_a), 7.26-7.10 (28H, m, H_b – H_g), 6.81 (2H, d, ^{3}J = 8.9 Hz, H_h), 6.67 (2H, d, ^{3}J = 8.9 Hz, H_i), 6.48 (4H, d, ^{3}J = 9.0 Hz, H_1), 6.40 (4H, d, ^{3}J = 9.0 Hz, H_2), 5.12 (2H, s, H_j), 4.81 (4H, t, ^{3}J = 5.1 Hz, H_3), 4.41(2H, t, ^{3}J = 7.7 Hz, H_k), 4.34 (4H, t, ^{3}J = 5.1 Hz, H_4), 3.77 (3H, s, H_l), 3.75 (2H, t, ^{3}J = 5.8 Hz, H_m), 3.67 – 3.54 (16H, m, H_5 – H_8), 2.12 (2H, quintet, ^{3}J = 6.4 Hz, H_n), 1.31 (54H, s, H_o + H_p); **^{13}C NMR** (125 MHz, $CDCl_3$) δ (ppm): 157.9, 154.5, 152.7, 151.8, 144.2, 144.1, 141.7, 140.1, 130.6, 130.2, 124.1, 115.2, 114.0, 112.1, 88.9, 78.5, 70.6, 70.0, 67.7, 67.1, 63.2, 52.1, 51.6, 50.2, 39.3, 34.3, 31.4, 30.1, 27.9; **^{19}F NMR** (376 MHz, $CDCl_3$) δ (ppm): -72.4 (d, $^{1}J_{F\text{-}P}$ = 712 Hz); **^{31}P NMR** (142 MHz, $CDCl_3$) δ (ppm): -144.8 (sep., $^{1}J_{F\text{-}P}$ = 712 Hz); **MS** (ESI +ve) m/z = 1963.8 ($[M - PF_6]^+$, $C_{109}H_{130}O_9N_9I_2$, calc.1963.8).

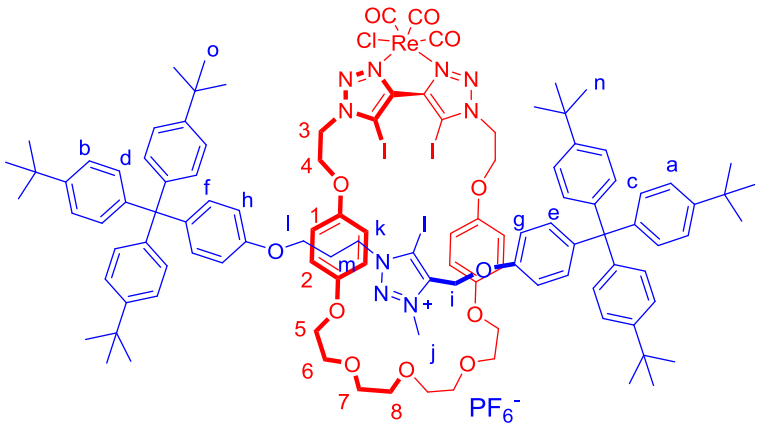
Rotaxane **2.17**



To a solution of rotaxane **2.9** (10 mg, 0.004 mmol) in dry CH_2Cl_2 (1 mL) was added CH_3I (3 mg, 0.02 mmol). The reaction mixture was stirred overnight. The solvent was removed to afford the rotaxane I^- salt. Anion exchange of the product to the PF_6^- salt was achieved by washing a $CHCl_3$ solution (20 mL) of the product with a 0.1 M NH_4PF_6 aqueous solution (20 mL x 10). The solvent was removed under vacuum to afford the rotaxane **2.17** as a white solid. (7 mg, 70% yield). **^{1}H NMR** (500 MHz, $CDCl_3$) δ (ppm): 9.35 (2H, s, H_a),

8.29 (1H, s, H_b), 7.21 (12H, d, ^3J = 8.7, H_c), 7.15 (4H, d, ^3J = 8.7, H_d), 7.08 (12H, d, ^3J = 8.7, H_e), 6.88 (4H, d, ^3J = 8.7 Hz, H_f), 6.26 (4H, d, ^3J = 9.0 Hz, H_1), 5.95 (4H, d, ^3J = 9.0 Hz, H_2), 4.77 (4H, t, ^3J = 4.4 Hz, H_3), 4.65 (3H, s, H_g), 4.61 (4H, t, ^3J = 7.1 Hz, H_h), 4.11 (8H, m, H_4 + H_i), 3.73-3.45 (16H, m, H_5–H_8), 2.49 (4H, quintet, ^3J = 6.2 Hz, H_j), 1.31 (54H, s, H_k); **^{13}C NMR** (125 MHz, $CDCl_3$) δ (ppm): 156.4, 152.6, 152.0, 148.4, 144.1, 142.3, 142.2, 141.7, 140.2, 133.5, 132.4, 130.7, 130.5, 124.1, 116.2, 115.2, 114.4, 113.2, 81.3, 79.9, 70.9, 69.9, 67.6, 67.4, 64.1, 63.1, 50.3, 49.0, 48.3, 41.0, 34.3, 31.9, 31.4, 29.7, 22.7, 14.1; **^{19}F NMR** (376 MHz, $CDCl_3$) δ (ppm): -72.4 (d, $^1J_{F\text{-}P}$ = 712 Hz); **^{31}P NMR** (142 MHz, $CDCl_3$) δ (ppm): -144.8 (sep., $^1J_{F\text{-}P}$ = 712 Hz); **HRMS** (ESI +ve) m/z = 2387.6802 ($[M - PF_6]^+$, $C_{118}H_{136}O_9N_{13}I_4$, calc. 2387.6790).

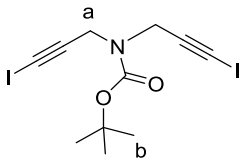
Rotaxane **2.18**



$Re(CO)_5Cl$ (1.7 mg, 0.0048 mmol) was heated under reflux in dry CH_3CN (4 mL) for 3 hrs, before the solvent was removed under vacuum and the residue was redissolved in dry CH_2Cl_2 (2 mL). This solution was added to a solution of rotaxane **2.16I** (9 mg, 0.0043 mmol) in dry CH_2Cl_2 (2 mL) and stirred at room temperature under N_2 for 16 hrs. The solvent was removed under vacuum and the cationic Re(I)-rotaxane **2.18** was isolated as a white solid (7 mg, 75% yield) after purification by preparative TLC chromatography (97:3 CH_2Cl_2/CH_3OH). **^{1}H NMR** (500 MHz, $CDCl_3$) δ (ppm): 7.26-7.20 (12H, m, H_a + H_b), 7.16-7.13 (16H, m, H_c-H_f),

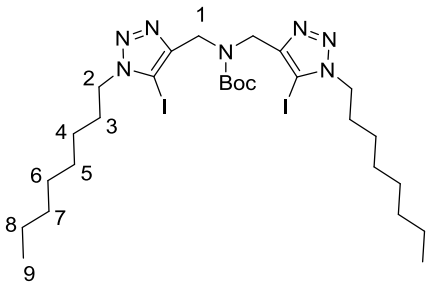
6.92 (2H, d, ^3J = 8.3 Hz, H_g), 6.86 (2H, d, ^3J = 8.3 Hz, H_h), 6.69 (4H, d, ^3J = 8.6 Hz, H_1), 6.33 (4H, d, ^3J = 8.6 Hz, H_2), 5.04-4.89 (4H, m, H_3), 4.73 (2H, s, H_i), 4.41 (3H, s, H_j), 4.29 (4H, m, H_4), 3.94-3.04 (20H, m, H_5–H_8 + H_k + H_l), 2.59 (2H, m, H_m), 1.32 (27H, s, H_n), 1.31 (27H, s, H_o); **^{13}C NMR** (125 MHz, $CDCl_3$) δ (ppm): 195.2, 156.2, 155.0, 152.7, 152.0, 148.4, 145.2, 144.1, 142.3, 141.6, 140.9, 132.9, 132.3, 130.7, 130.6, 124.2, 115.7, 114.7, 113.3, 70.9, 70.6, 70.1, 68.5, 67.1, 63.2, 57.3, 52.0, 39.6, 34.3, 31.4, 29.7, 26.7; **^{19}F NMR** (376 MHz, $CDCl_3$) δ (ppm): -72.4 (d, $^1J_{F\text{-}P}$ = 712 Hz); **^{31}P NMR** (142 MHz, $CDCl_3$) δ (ppm): -144.8 (sep., $^1J_{F\text{-}P}$ = 712 Hz); **HRMS** (ESI +ve) m/z = 2395.6064 ($[M–PF_6]^+$, $C_{112}H_{129}O_{12}N_9ClI_3Re$, calc. 2395.6169).

Compound **2.20I**



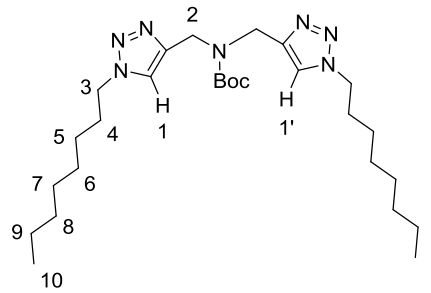
Compound **2.20H** (100mg, 0.52mmol) was dissolved in 2 mL of CH_3OH. 0.5 mL of KOH (146mg, 2.6mmol) aqueous solution was added at 0 ^{o}C and the mixture was stirred for 10 min. Iodine (290mg, 1.14mmol) was added in one portion. The solution was warmed to room temperature and left to stir overnight. Subsequently, the solution was poured into water (20 mL) and extracted with Et_2O (20 ml x 3). The organic layers were combined, washed with saturated $Na_2S_2O_3$ solution (20 mL), brine (20 mL) and then dried with $MgSO_4$. The solvent was removed under vacuum to afford the product **2.20I** as a light yellow solid (230mg, quantitative yield). **^{1}H NMR** (400 MHz, $CDCl_3$) δ (ppm): 4.30 (4H, s, H_a), 1.48 (9H, s, H_b); **^{13}C NMR** (100 MHz, $CDCl_3$) δ (ppm): 154.0, 89.3, 81.3, 37.2, 28.3; **HRMS** (ESI +ve) m/z = 467.89269 ($[M + Na]^+$, $C_{11}H_{13}I_2NO_2Na$, calc. 467.89279).

Compound **2.21I**



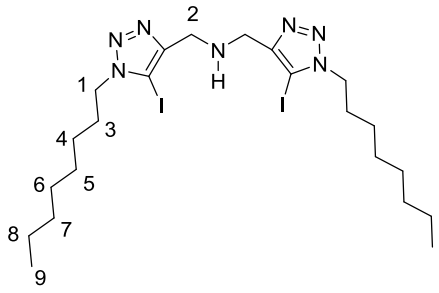
Compound **2.20I** (100 mg, 0.225 mmol), octyl azide **2.12** (77 mg, 0.495 mmol) and TBTA (12 mg, 0.023 mmol) were dissolved in 2 mL of dry degassed THF before $[Cu(CH_3CN)_4]PF_6$ (21 mg, 0.056 mmol) was added in one portion. The reaction mixture was stirred under N_2 at room temperature for 2 days. The solvent was removed under vacuum before 20 mL of $CHCl_3$ was added. The solution was washed with an EDTA solution (10 mL x 2), brine (20 mL x 2) and then dried with $MgSO_4$. The solvent was removed under vacuum to afford a yellow oil. Purification of the compound was achieved by silica gel column chromatography (97:3 CH_2Cl_2/CH_3OH) to give the product **2.21I** as an off-white solid (130 mg, 78% yield). **^{1}H NMR** (400 MHz, $CDCl_3$) δ (ppm): 4.65 (4H, s, H_1), 4.35 (4H, t, ^3J = 5.5 Hz, H_2), 1.88 (4H, quin, ^3J = 5.5 Hz, H_3), 1.45 (9H, s, Boc), 1.35-1.20 (20H, m, H_4-H_8), 0.88 (6H, t, ^3J = 5.5 Hz, H_9); **^{13}C NMR** (100 MHz, $CDCl_3$) δ (ppm): 155.5, 148.1, 51.0, 31.5, 30.0, 28.7, 28.5, 26.2, 23.7, 14.0; **HRMS** (ESI +ve) m/z = 756.19485 ($[M + H]^+$, $C_{27}H_{48}I_2N_7O_2$, calc. 756.19534).

Compound **2.21H**



Compound **2.20H** (130 mg, 0.67 mmol), octyl azide **2.12** (208 mg, 1.34 mmol) and TBTA (18 mg, 0.03 mmol) were dissolved in 2 mL of dry degassed CH_2Cl_2 before $[Cu(CH_3CN)_4]PF_6$ (25 mg, 0.067 mmol) was added in one portion. The reaction mixture was stirred under N_2 at room temperature for 2 days. The solvent was removed under vacuum before 20 mL of $CHCl_3$ was added. The organic solution was washed with an EDTA solution (10 mL x 2), brine (20 mL x 2) and then dried with $MgSO_4$. The solvent was removed under vacuum to afford a yellow oil. Purification of the compound was achieved by silica gel column chromatography (97:3 CH_2Cl_2/CH_3OH) to give the product **2.21H** as an off-white solid (287mg, 85% yield). **^{1}H NMR** (400 MHz, $CDCl_3$) δ (ppm): 7.49 (1H, s, H_1), 7.37 (1H, s, $H_{1'}$), 4.47 (4H, s, H_2), 4.24 (4H, t, ^3J = 5.5 Hz, H_3), 1.81 (4H, quin, ^3J = 5.5 Hz, H_4), 1.38 (9H, s, Boc), 1.23-1.18 (20H, m, H_5-H_9), 0.80 (6H, t, ^3J = 5.5 Hz, H_{10}); **^{13}C NMR** (100 MHz, $CDCl_3$) δ (ppm): 155.2, 144.8, 122.6, 121.8, 80.3, 50.2, 42.2, 41.5, 31.6, 30.2, 28.9, 28.3, 26.4, 22.5, 14.0; **HRMS** (ESI +ve) m/z = 504.40168 ($[M + H]^+$, $C_{27}H_{49}I_2N_7O_2$, calc. 504.40205).

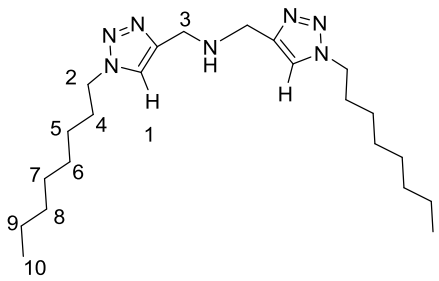
Compound **2.22I**



To a solution of compound **2.21I** (30 mg, 0.04 mmol) in dry CH_2Cl_2 (2 mL) was added trifluoroacetic acid (0.06 mL, 91 mg, 0.8 mmol) and then left to stir overnight. The reaction mixture was diluted with 10 mL of $CHCl_3$ and washed with a 1 M $NaHCO_3$ aqueous solution (10 mL x 2), brine (10 mL x 2) and then dried with $MgSO_4$. The solvent was removed under vacuum to afford the product **2.22I** as a light yellow solid (27 mg, quantitative yield). **^{1}H NMR**

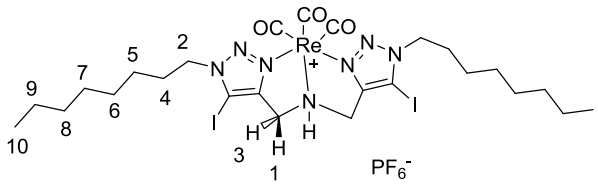
(400 MHz, $CDCl_3$) δ (ppm): 4.35 (4H, t, ^3J = 5.5 Hz, H_1), 3.90 (4H, s, H_2), 1.88 (4H, quin, ^3J = 5.5 Hz, H_3), 1.35-1.20 (20H, m, H_4-H_8), 0.88 (6H, t, ^3J = 5.5 Hz, H_9); **^{13}C NMR** (100 MHz, $CDCl_3$) δ (ppm): 148.1, 51.0, 44.0, 31.5, 30.0, 28.7, 28.5, 26.2, 23.7, 14.0; **HRMS** (ESI +ve) m/z = 656.14279 ($[M + H]^+$, $C_{22}H_{40}I_2N_7$, calc. 656.14291).

Compound **2.22H**



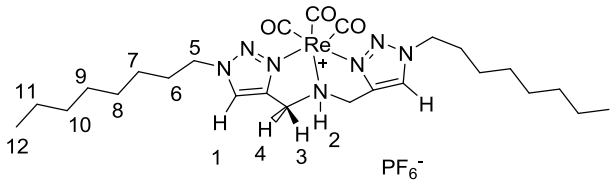
To a solution of compound **2.21H** (20 mg, 0.04 mmol) in dry CH_2Cl_2 (2 mL) was added trifluoroacetic acid (0.06 mL, 91 mg, 0.8 mmol) and then left to stir overnight. The reaction mixture was diluted with 10 mL of $CHCl_3$ and washed with a 1 M $NaHCO_3$ aqueous solution (10 mL x 2), brine (10 mL x 2) and then dried with $MgSO_4$. The solvent was removed under vacuum to afford the product **2.22H** as a light yellow solid (16 mg, quantitative yield). **^{1}H NMR** (400 MHz, $CDCl_3$) δ (ppm): 7.44 (1H, s, H_1), 4.25 (4H, t, ^3J = 5.5 Hz, H_2), 3.87 (4H, s, H_3), 1.81 (4H, quin, ^3J = 5.5 Hz, H_4), 1.23-1.18 (20H, m, H_5-H_9), 0.80 (6H, t, ^3J = 5.5 Hz, H_{10}); **^{13}C NMR** (100 MHz, $CDCl_3$) δ (ppm): 145.0, 120.7, 49.3, 42.7, 30.7, 29.3, 28.0, 27.9, 25.5, 25.3, 21.6, 13.1; **HRMS** (ESI +ve) m/z = 404.34970 ($[M + H]^+$, $C_{22}H_{42}N_7$, calc. 404.34962).

Compound **2.23I**



Bis-iodotriazole-amine **2.22I** (36 mg, 0.054 mmol) and $Re[(CO)_3(H_2O)_3]Br$ (22 mg, 0.054 mmol) were suspended in 0.5 mL of CH_3OH in a microwave vial and then the reaction mixture was heated at 100 ^oC for 5 min under microwave reaction conditions. The reaction mixture was diluted using 1 mL of CH_3OH and stirred with NH_4PF_6 powder (8.8 mg, 0.054 mmol) at 0 ^oC for 30 min. Subsequently, 10 mL of saturated NH_4PF_6 aqueous solution was added in one portion. The resulting white precipitate was collected by filtration, washed with H_2O (2 x 5 mL) and then dried with high vacuum to afford the product **2.23I** as a white solid (40 mg, 68%). **^{1}H NMR** (400 MHz, CD_3OD) δ (ppm): 4.54 (2H, d, ^2J = 16.6 Hz, H_1), 4.40 (4H, t, ^3J = 6.8 Hz, H_2), 4.34 (2H, d, ^2J = 16.6 Hz, H_3), 1.86 (4H, quin, ^3J = 7.2 Hz, H_4), 1.34–1.22 (20H, m, H_5-H_9), 0.91 (6H, t, ^3J = 7.1 Hz, H_{10}); **^{13}C NMR** (100 MHz, CD_3OD) δ (ppm): 153.7, 78.5, 52.9, 51.7, 31.5, 29.3, 29.0, 28.8, 28.4, 25.7, 22.3, 13.0; **^{19}F NMR** (376 MHz, CD_3OD) δ (ppm): -74.0 (d, $^1J_{F\text{-}P}$ = 752 Hz); **^{31}P NMR** (162 MHz, CD_3OD) δ (ppm): -144.6 (sep., $^1J_{F\text{-}P}$ = 752 Hz); **HRMS** (ESI +ve) m/z = 926.07493 ($[M - PF_6]^+$, $C_{25}H_{39}O_3N_7I_2Re$, calc. 926.07558).

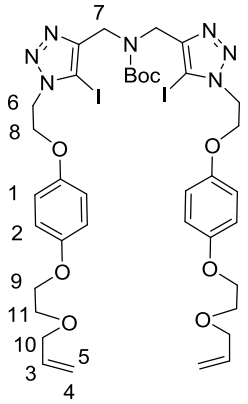
Compound **2.23H**



Bis-triazole-amine **2.22H** (20 mg, 0.0496 mmol) and $Re[(CO)_3(H_2O)_3]Br$ (20 mg, 0.0495 mmol) were suspended in 0.5 mL of CH_3OH in a microwave vial and then the reaction mixture was heated at 100 ^oC for 5 min under microwave reaction conditions. The reaction was diluted using 1 mL of CH_3OH and stirred with NH_4PF_6 powder (8.1 mg, 0.0496 mmol) at 0 ^oC for 30 min. Subsequently, 10 mL of saturated NH_4PF_6 aqueous solution was added in one portion. The resulting white precipitate was collected by filtration, washed with H_2O (2 x 5 mL) and then dried with high vacuum to afford the product **2.23H** as a white solid (28 mg, 70%). **^{1}H NMR** (400 MHz, $CDCl_3$) δ (ppm): 7.65 (2H, s, H_1), 5.83 (1H, s, H_2), 4.48

(4H, m, H_3 + H_4), 4.33–4.20 (4H, m, H_5), 1.85 (4H, quin, ^3J = 6.1 Hz, H_6), 1.29–1.28 (20H, m, H_7–H_{11}), 0.89 (6H, t, ^3J = 7.1 Hz, H_{12}); **^{13}C NMR** (125 MHz, $CDCl_3$) δ (ppm):194.5, 147.9, 122.7, 53.1, 52.1, 31.7, 29.7, 29.0, 28.8, 26.2, 22.6, 14.1; **^{19}F NMR** (376 MHz, $CDCl_3$) δ (ppm): -71.4 (d, $^1J_{F\text{-}P}$ = 757 Hz); **^{31}P NMR** (162 MHz, $CDCl_3$) δ (ppm): -144.3 (sep., $^1J_{F\text{-}P}$ = 757 Hz); **HRMS** (ESI +ve) m/z = 674.28189 ([M – PF_6]$^+$, $C_{25}H_{41}O_3N_7Re$, calc. 674.28229).

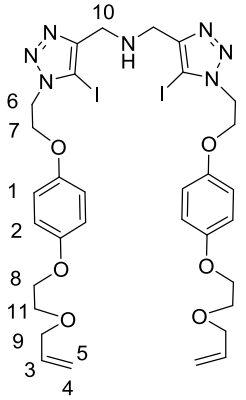
Compound **2.25**



Compound **2.20I** (200 mg, 0.45 mmol), vinyl azide **2.24** (237 mg, 0.9 mmol) and TBTA (13 mg, 0.025 mmol) were dissolved in 2 mL of dry degassed THF before $[Cu(CH_3CN)_4]PF_6$ (19 mg, 0.05 mmol) was added in one portion. The reaction mixture was stirred under N_2 at room temperature for 2 days. The solvent was removed under vacuum before 20 mL of $CHCl_3$ was added. The organic solution was washed with an EDTA solution (10 mL x 2), brine (20 mL x 2) and then dried with $MgSO_4$. The solvent was removed under vacuum to afford a yellow oil. Purification of the compound was achieved by silica gel column chromatography (98:2 CH_2Cl_2/CH_3OH) to give the product **2.25** as a white solid (362 mg, 83% yield). **^{1}H NMR** (400 MHz, $CDCl_3$) δ (ppm): 6.83–6.76 (8H, m, H_1 + H_2), 5.96–5.89 (2H, m, H_3), 5.31–5.18 (4H, m, H_4 + H_5), 4.70 (4H, t, ^3J = 4.5 Hz, H_6), 4.64–4.56 (4H, m, H_7), 4.34 (4H, t, ^3J = 4.5 Hz, H_8), 4.09–4.05 (8H, m, H_9 + H_{10}), 3.76 (4H, t, ^3J = 3.8 Hz, H_{11}), 1.44 (9H, s, Boc); **^{13}C NMR** (100 MHz, $CDCl_3$) δ (ppm): 155.1, 153.5, 152.1, 148.0, 134.6, 117.4,

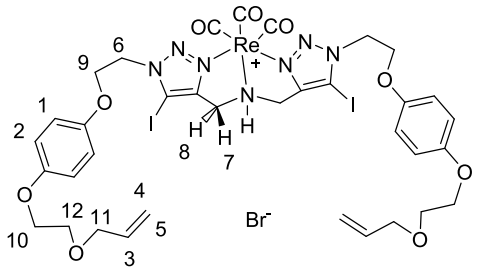
115.7, 80.5, 72.4, 68.6, 68.1, 66.7, 49.6, 28.5; **HRMS** (ESI +ve) m/z = 994.14621 ($[M + Na]^+$, $C_{37}H_{47}I_2N_7O_8Na$, calc. 994.14677).

Compound **2.26**



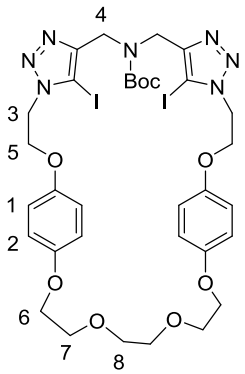
To a solution of compound **2.25** (200 mg, 0.206 mmol) in dry CH_2Cl_2 was added trifluoroacetic acid (0.12 mL, 182 mg, 1.6 mmol) and then left to stir overnight. The reaction mixture was diluted with 10 mL of $CHCl_3$ and washed with a 1 M $NaHCO_3$ aqueous solution (10 mL x 2), brine (10 mL x 2) and then dried with $MgSO_4$. The solvent was removed under vacuum to afford the product **2.26** as a light yellow solid (179 mg, quantitative yield). **^{1}H NMR** (400 MHz, $CDCl_3$) δ (ppm): 6.84–6.78 (8H, m, H_1 + H_2), 5.97–5.89 (2H, m, H_3), 5.31–5.19 (4H, m, H_4 + H_5), 4.71 (4H, t, ^3J = 4.5 Hz, H_6), 4.34 (4H, t, ^3J = 4.5 Hz, H_7), 4.08–4.05 (8H, m, H_8 + H_9), 3.89 (4H, s, H_{10}), 3.76 (4H, t, ^3J = 3.8 Hz, H_{11}); **^{13}C NMR** (100 MHz, $CDCl_3$) δ (ppm): 152.5, 151.1, 148.6, 133.5, 116.3, 114.6, 114.5, 79.3, 71.3, 67.6, 67.0, 65.7, 48.6, 43.0; **HRMS** (ESI +ve) m/z = 872.11190 ($[M + H]^+$, $C_{32}H_{39}I_2N_7O_6$, calc. 872.11239).

Compound **2.27**



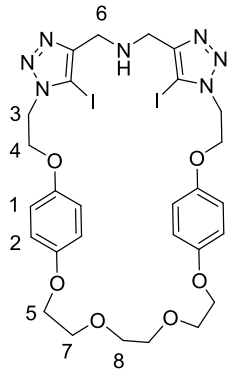
Compound **2.26** (20 mg, 0.023 mmol) and $Re[(CO)_3(H_2O)_3]Br$ (9.3 mg, 0.023 mmol) was suspended in 0.5 mL of CH_3OH in a microwave vial and the reaction mixture was heated at 100 ^oC for 5 min under microwave reaction conditions. The reaction was added 5 mL of H_2O and the resulting white precipitate was collected by filtration, washed with H_2O (2 x 5 mL) and then dried with high vacuum to afford the product **2.27** as a white solid (16 mg, 57%). **^{1}H NMR** (400 MHz, CD_3OD) δ (ppm): 6.88–6.71 (8H, m, H_1 + H_2), 5.97–5.88 (2H, m, H_3), 5.32–5.15 (4H, m, H_4 + H_5), 4.52–4.48 (6H, m, H_6 + H_7), 4.33 (2H, d, ^2J = 16.5 Hz, H_8), 4.27–4.19 (4H, m, H_9), 4.07–4.05 (8H, m, H_{10} + H_{11}), 3.76 (4H, t, ^3J = 4.5 Hz, H_{12}); **^{13}C NMR** (100 MHz, CD_3OD) δ (ppm): 194.4, 153.7, 153.4, 152.0, 134.5, 116.1,115.4, 80.5, 71.8, 68.5, 67.8, 66.3, 52.8, 50.9; **HRMS** (ESI +ve) m/z = 1142.04310 ($[M – Br]^+$, $C_{35}H_{39}O_9N_7I_2Re$, calc. 1142.04506).

Macrocycle **2.34**



Compound **2.20I** (30 mg, 0.068 mmol), bis-azide **2.33** (32 mg, 0.068 mmol) and TBTA (9 mg, 0.017mmol) were dissolved in 20 mL of dry degassed THF before $[Cu(CH_3CN)_4]PF_6$ (13mg, 0.034mmol) was added in one portion. The reaction was stirred under N_2 at room temperature for 2 days. The solvent was removed under vacuum before 20 mL of $CHCl_3$ was added. The organic solution was washed with an EDTA solution (10 mL x 2), brine (20 mL x 2) and then dried with $MgSO_4$. The solvent was removed under vacuum to afford a yellow oil. Purification of the compound was achieved by preparative TLC chromatography (97:3 CH_2Cl_2/CH_3OH) to give the product **2.34** as an off-white solid (60% yield). **^{1}H NMR** (400 MHz, $CDCl_3$) δ (ppm): 6.82-6.72 (8H, m, H_1 + H_2), 4.66 (4H, t, ^3J = 5.6 Hz, H_3), 4.58 (4H, s, H_4), 4.31 (4H, t, ^3J = 5.6 Hz, H_5), 4.02 (4H, t, ^3J = 4.8 Hz, H_6), 3.80 (4H, t, ^3J = 4.8 Hz, H_7), 3.71 (4H, s, H_8), 1.51 (9H, s, Boc); **^{13}C NMR** (100 MHz, $CDCl_3$) δ (ppm): 154.3, 152.6, 151.1, 146.4, 115.1, 114.5, 79.6, 69.9, 68.8, 67.4, 65.8, 48.4, 27.5; **HRMS** (ESI +ve) m/z = 918.11515 ($[M + H]^+$, $C_{33}H_{42}I_2N_7O_8$, calc. 918.11787).

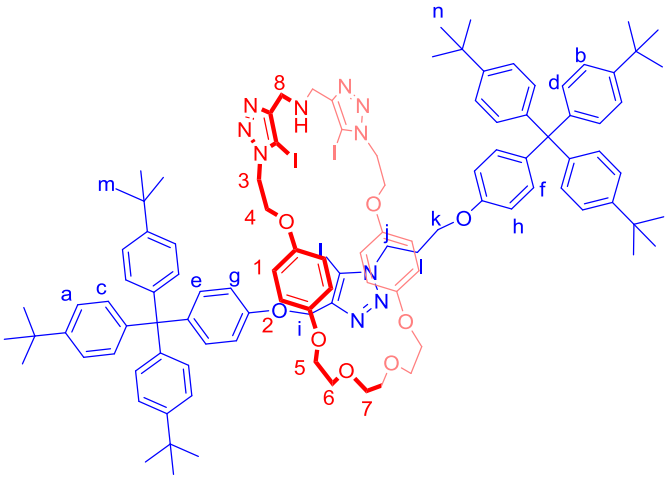
Macrocycle **2.35**



To a solution of macrocycle compound **2.34** (15 mg, 0.016 mmol) in dry CH_2Cl_2 (2 mL) was added trifluoroacetic acid (0.024 mL, 36 mg, 0.32 mmol) and then left to stir overnight. The reaction mixture was diluted with 10 mL of $CHCl_3$ and washed with a 1 M $NaHCO_3$ aqueous solution (10 mL x 2), brine (10 mL x 2) and then dried with $MgSO_4$. The solvent was removed under vacuum to afford the macrocycle **2.35** as a white solid (13 mg,

quantitative yield). **^{1}H NMR** (400 MHz, $CDCl_3$) δ (ppm): 6.81-6.70 (8H, m, H_1 + H_2), 4.69 (4H, t, ^{3}J = 5.1 Hz, H_3),), 4.31 (4H, t, ^{3}J = 5.1 Hz, H_4), 4.03 (4H, t, ^{3}J = 4.8 Hz, H_5), 3.86 (4H, s, H_6), 3.79 (4H, t, ^{3}J = 4.8 Hz, H_7), 3.69 (4H, s, H_8); **^{13}C NMR** (100 MHz, $CDCl_3$) δ (ppm): 152.9, 151.1, 148.5, 115.0, 114.5, 79.7, 69.9, 68.8, 67.4, 66.0, 48.6, 42.6, 28.7; **HRMS** (ESI +ve) m/z = 818.06490 ($[M + H]^+$, $C_{28}H_{34}I_2N_7O_6$, calc. 818.06544).

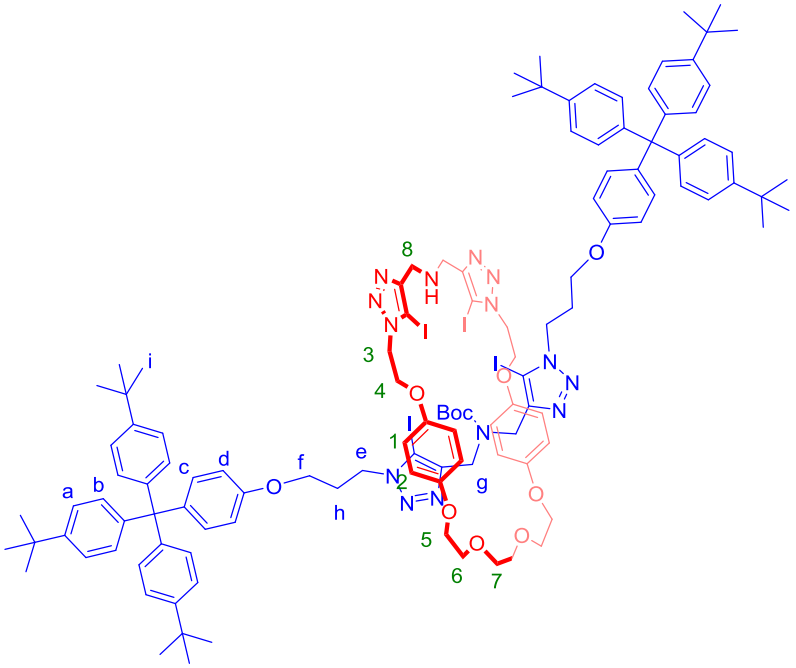
Rotaxane **2.36**



Macrocycle **2.35** (15 mg, 0.018 mmol) and $[Cu(CH_3CN)_4]PF_6$ (6.8 mg, 0.018 mmol) were dissolved in 2 mL of dry degassed CH_2Cl_2 and left to stir for 5 min. Stopper azide **2.6** (53 mg, 0.09 mmol) and stopper iodo-alkyne **2.4** (60 mg, 0.09 mmol) were added to the solution. The reaction was stirred under N_2 at room temperature for 2 days. The reaction mixture was diluted with 20 mL of $CHCl_3$, washed with an EDTA solution (10 mL x 2), brine (20 mL x 2) and then dried with $MgSO_4$. The solvent was removed under vacuum to afford a yellow solid. Purification of the compound was achieved by preparative TLC chromatography (97:3 CH_2Cl_2/CH_3OH) to give the product **2.36** as a cream solid (11 mg, 30% yield). **^{1}H NMR** (400 MHz, $CDCl_3$) δ (ppm): 7.18-7.00 (28H, m, H_a - H_f), 6.81 (2H, d, ^{3}J = 8.4 Hz, H_g), 6.50 (2H, d, ^{3}J = 8.4 Hz, H_h), 6.32-6.22 (8H, m, H_1 + H_2), 4.80 (2H, s, H_i), 4.55 (4H, m, H_3), 3.95-3.55 (22H, m, H_4–H_8 + H_j), 3.31 (2H, m, H_k), 1.38 (2H, m, H_l), 1.23 (27H, s, H_m), 1.22 (27H, s, H_n); **^{13}C NMR** (100 MHz, $CDCl_3$) δ (ppm): 155.3, 155.1, 152.0, 150.6, 148.1, 147.2, 145.4,

143.2, 138.6, 131.2, 129.7, 123.1, 115.1, 113.7, 112.4, 112.1, 69.7, 68.6, 66.6, 65.7, 62.0, 33.2, 30.4, 28.7, 13.1; **HRMS** (ESI +ve) m/z = 2074.70543 ($[M + H]^+$, $C_{108}H_{128}I_3N_{10}O_8$, calc. 2074.70787).

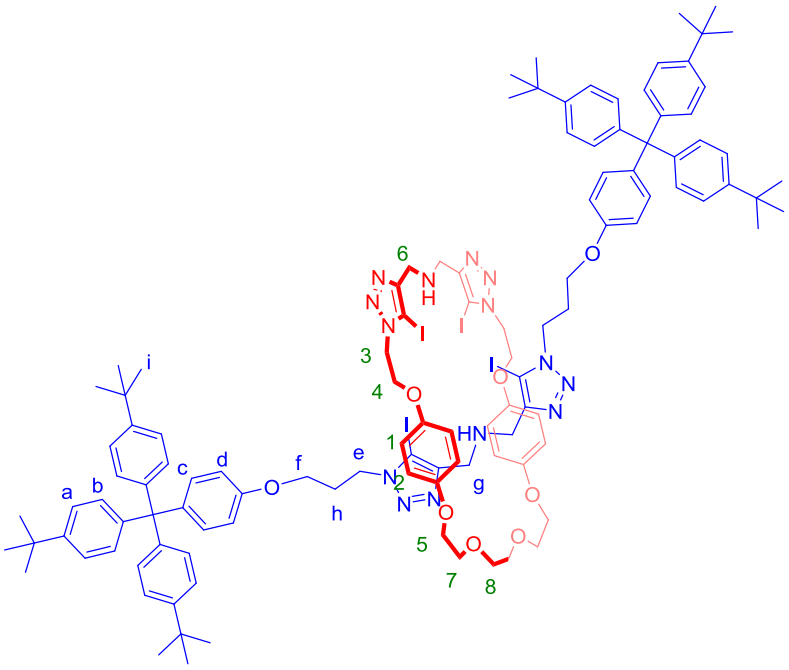
Rotaxane **2.38**



Macrocycle **2.35** (10 mg, 0.0122 mmol) and $[Cu(CH_3CN)_4]PF_6$ (4.5 mg, 0.0122 mmol) were dissolved in 1 mL of dry degassed CH_2Cl_2 and left to stir for 5 min. Stopper azide **2.6** (57 mg, 0.0976 mmol) and bis-iodoalkyne **2.20I** (22 mg, 0.0488 mmol) were added into the solution. The reaction was stirred under N_2 at room temperature for 2 days. The reaction mixture was diluted with 20 mL of $CHCl_3$, washed with an EDTA solution (10 mL x 2), brine (20 mL x 2) and then dried with $MgSO_4$. The solvent was removed under vacuum to afford a yellow solid. Purification of the compound was achieved by preparative TLC chromatography (97:3 CH_2Cl_2/CH_3OH) to give the product **2.38** as a white solid (10 mg, 34% yield). **^{1}H NMR** (400 MHz, d_6-acetone) δ (ppm): 7.32-7.26 (28H, m, H_a + H_b + H_c), 7.07 (4H, d, ^3J = 6.8 Hz, H_d), 6.47 - 6.42 (8H, m, H_1 + H_2), 4.72 (4H, t, ^3J = 3.7 Hz, H_3), 4.48 (4H, m, H_e), 4.14 (4H, t, ^3J = 3.7 Hz, H_4), 3.91-3.60 (24H, m, H_4–H_8 + H_f + H_g), 2.87 (4H, m ,H_h), 1.48 (9H, s, Boc), 1.30 (54H, s, H_i); **^{13}C NMR** (100 MHz, d_6-acetone) δ (ppm): 154.9, 153.1, 152.1, 149.5,

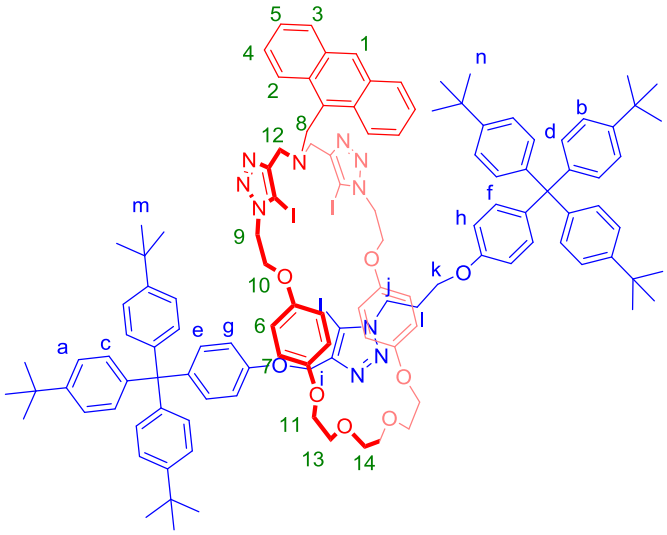
148.2, 144.5, 131.8, 130.6, 124.2, 116.0, 115.3, 114.8, 113.3, 81.2, 79.5, 70.4, 69.3, 67.7, 66.9, 64.2, 63.1, 49.8, 44.9, 34.0, 30.8; **HRMS** (ESI +ve) m/z = 2438.73642 ($[M + H]^+$, $C_{119}H_{145}I_4N_{14}O_{10}$, calc. 2438.74749).

Rotaxane **2.39**



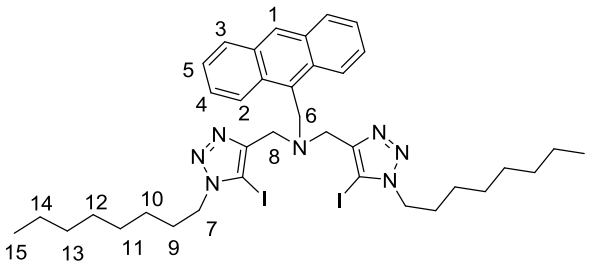
To a solution of rotaxane **2.38** (10 mg, 0.004 mmol) in dry CH_2Cl_2 (2 mL) was added trifluoroacetic acid (0.008 mL, 9 mg, 0.08 mmol) and then left to stir overnight. The reaction mixture was diluted with 10 mL of $CHCl_3$ and washed with a 1 M $NaHCO_3$ aqueous solution (10 mL x 2), brine (10 mL x 2) and dried with $MgSO_4$. The solvent was removed under vacuum to afford the product **2.39** as a white solid (13 mg, 95% yield). **^{1}H NMR** (400 MHz, d_6-acetone) δ (ppm): 7.34-7.14 (24H, m, H_a + H_b), 7.08 (4H, d, ^3J = 7.1 Hz, H_c), 6.71 (4H, d, ^3J = 7.1 Hz, H_d), 6.48-6.41 (8H, m, H_1 + H_2), 4.72 (4H, t, ^3J = 4.0 Hz, H_3), 4.18-4.12 (8H, m ,H_4 + H_e), 3.95 (4H, t, ^3J = 4.0 Hz, H_5), 3.90 (4H, s, H_6), 3.75-3.65 (12H, m , H_f + H_g + H_7), 3.60 (4H, s, H_8), 2.02 (4H, m, H_h), 1.27 (54H, s, H_i); **^{13}C NMR** (100 MHz, d_6-acetone) δ (ppm): 156.6, 153.0, 152.1, 148.2, 144.5, 139.4, 131.2, 130.6, 124.2, 115.2, 114.8, 113.3, 78.3, 70.5, 69.3, 67.7, 67.2, 66.9, 64.2, 63.1, 49.8, 47.2, 44.7, 43.9, 34.0, 30.8; **HRMS** (ESI +ve) m/z = 2338.68266 ($[M + H]^+$, $C_{114}H_{137}I_4N_{14}O_8$, calc. 2338.69506).

Rotaxane **2.40**



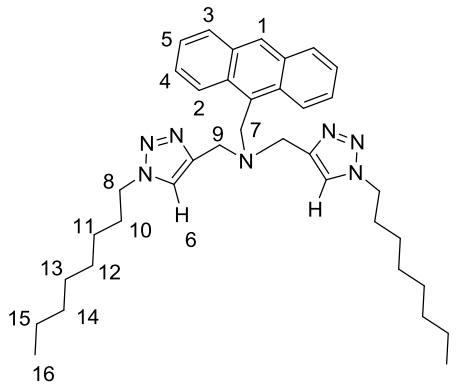
To a solution of rotaxane **2.36** (8 mg, 0.004 mmol) in $CHCl_3/CH_3CN$ (1 mL/ 1 mL) was added 9-chloromethyl-anthracene (3 mg, 0.012 mmol) and K_2CO_3 (8 mg, 0.06 mmol). The reaction was left to stir at room temperature for 2 days. The reaction mixture was diluted with 10 mL of $CHCl_3$, washed with water (10 mL x 2), brine (10 mL x 2) and then dried with $MgSO_4$. The solvent was removed under vacuum to afford a light yellow solid. Purification of the compound was achieved by preparative TLC chromatography (98:2 CH_2Cl_2/CH_3OH) to give the product **2.40** as a white solid (5.2 mg, 60% yield). **^{1}H NMR** (400 MHz, $CDCl_3$) δ (ppm): 7.34-7.33 (3H, m , H_1 + H_2), 7.86 (2H, d, ^3J = 6.0 Hz, H_3), 7.30-7.25 (4H, m ,H_4 + H_5), 7.21-7.00 (24H, m, H_a-H_d), 6.98 (2H, d, ^3J = 7.1 Hz, H_e), 6.93 (2H, d, ^3J = 7.1 Hz, H_f), 6.77 (2H, d, ^3J = 7.1 Hz, H_g), 6.38-6.33 (10H, m, H_6 + H_7 + H_h), 4.80 (2H, s, H_8), 4.66 (2H, s, H_i), 4.52 (4H, t, , ^3J = 4.6 Hz, H_9), 4.09 (4H, m ,H_{10}), 3.94 (2H, t, , ^3J = 5.5 Hz, H_j), 3.79 (4H, m, H_{11}), 3.66 (4H, s, H_{12}), 3,52 (4H, t, ^3J = 3.6 Hz, H_{13}), 3.44 (4H, m , H_{14}), 3.34 (2H, t, ^3J = 5.0 Hz, H_k), 1.71 (2H, m, H_l), 1.16 (27H, s, H_m), 1.16 (27H, s, H_n). **^{13}C NMR** (100 MHz, $CDCl_3$) δ (ppm): 207.3, 156.2, 153.1, 151.7, 148.3, 146.9, 144.3, 144.1, 140.1, 139.6, 132.2, 131.4, 130.7, 128.8, 124.2, 115.6, 115.2, 113.5, 113.2, 70.8, 69.7, 67.5, 66.6, 64.0, 63.1, 50.1, 34.3, 31.4, 30.2; **HRMS** (ESI +ve) m/z = 2264.77740 ($[M + H]^+$, $C_{123}H_{138}I_3N_{10}O_8$, calc. 2264.78612).

Compound **2.41I**



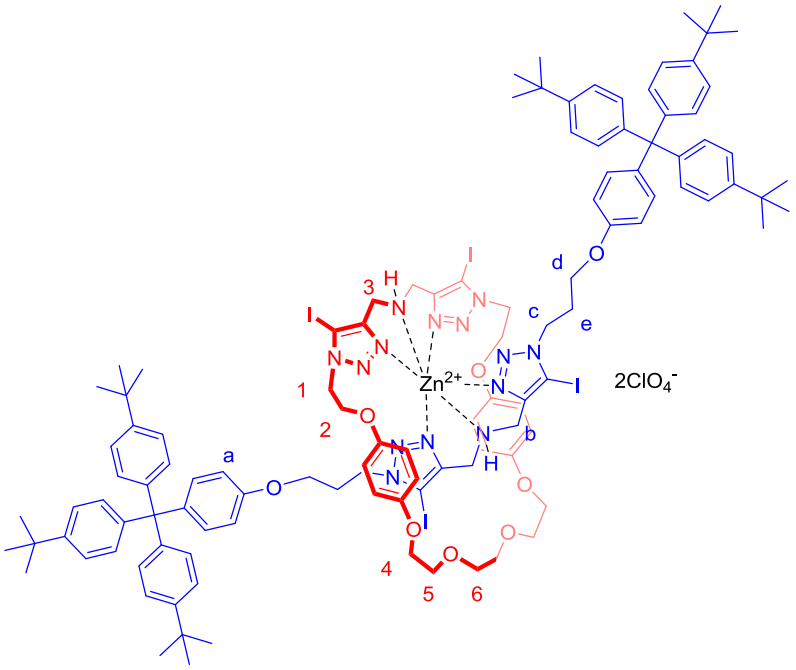
To a solution of compound **2.22I** (30 mg, 0.046 mmol) in $CHCl_3$/CH_3CN (1 mL / 1 mL) was added 9-chloromethyl-anthracene (12 mg, 0.055 mmol) and K_2CO_3 (32 mg, 0.23 mmol). The mixture was left to stir 2 days. The reaction mixture was diluted with 10 mL of $CHCl_3$, washed with water (10 mL x 2), brine (10 mL x 2) and then dried with $MgSO_4$. The solvent was removed under vacuum to afford a light yellow solid. Purification of the compound was achieved by silica gel column chromatography (99:1 CH_2Cl_2/CH_3OH) to give the product **2.41I** as an off-white solid (26 mg, 68% yield). **^{1}H NMR** (400 MHz, $CDCl_3$) δ (ppm): 8.33 (1H, s, H_1), 8.15 (2H, d, ^3J = 6.7 Hz, H_2), 7.88 (2H, d, ^3J = 6.1 Hz, H_3), 7.35-7.30 (4H, m, H_4 + H_5), 4.60 (2H, s, H_6), 4.22 (4H, t, ^3J = 5.8 Hz, H_7), 3.71 (4H, s, H_8), 1.77 (4H, quin, ^3J = 5.4 Hz, H_9), 1.24-1.16 (20H, m, H_{10}-H_{14}), 0.78 (6H, t, ^3J =5.2 Hz, H_{15}); **^{13}C NMR** (100 MHz, $CDCl_3$) δ (ppm): 147.5,133.1, 130.7, 130.4, 128.8, 127.8, 126.5, 124.5, 124.4, 123.7, 79.2, 49.6, 48.8, 47.7, 30.6, 29.0, 28.0, 25.3, 21.6, 13.0; **HRMS** (ESI +ve) m/z = 846.22112 ($[M + H]^+$, $C_{37}H_{50}I_2N_7$, calc. 846.2116).

Compound **2.41H**



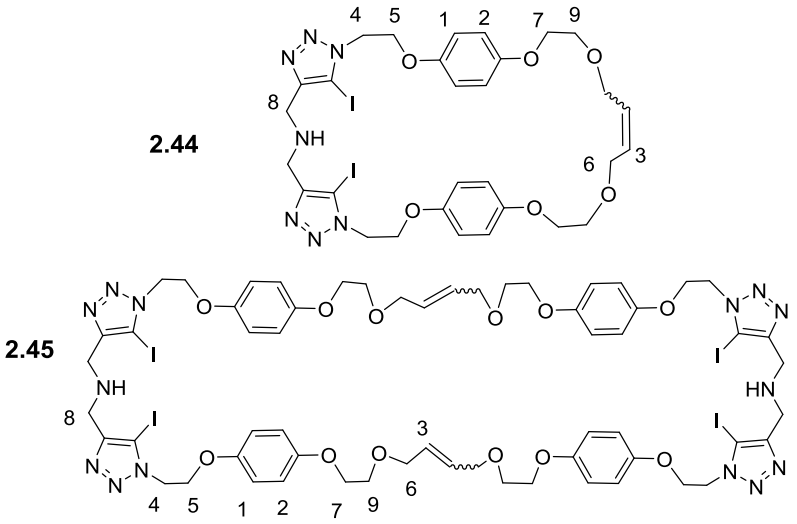
To a solution of compound **2.22H** (19 mg, 0.046 mmol) in $CHCl_3/CH_3CN$ (1 mL / 1 mL) was added 9-chloromethyl-anthracene (12 mg, 0.055 mmol) and K_2CO_3 (32 mg, 0.23 mmol). The mixture was left to stir 2 days. The reaction mixture was diluted with 10 mL of $CHCl_3$, washed with water (10 mL x 2), brine (10 mL x 2) and then dried with $MgSO_4$. The solvent was removed under vacuum to afford a light yellow solid. Purification of the compound was achieved by silica gel chromatography column (99:1 CH_2Cl_2/CH_3OH) to give the product as an off-white solid (19 mg, 70% yield). **^{1}H NMR** (400 MHz, $CDCl_3$) δ (ppm): 8.33 (3H, m, $H_1 + H_2$), 7.90 (2H, d, ^3J = 7.2 Hz, H_3), 7.41-7.36 (4H, m, $H_4 + H_5$), 7.32 (2H, s, H_6), 4.62 (2H, s, H_7), 4.22 (4H, t, ^3J = 5.8 Hz, H_8), 3.77 (4H, s, H_9), 1.78 (4H, quin, ^3J = 5.5 Hz, H_{10}) 1.22-1.16 (20H, m, H_{11}-H_{15}), 0.78 (6H, t, ^3J = 5.4 Hz, H_{16}); **^{13}C NMR** (100 MHz, $CDCl_3$) δ (ppm): 144.7, 131.4, 128.9,127.6, 125.6, 125.1, 124.9, 123.2, 50.5, 50.3, 47.4, 31.7, 30.3, 29.0, 28.9, 26.5, 22.6, 14.1; **HRMS** (ESI +ve) m/z = 594.42744 ($[M + H]^+$, $C_{37}H_{52}N_7$, calc. 594.42787).

Rotaxane **2.39**·$Zn(ClO_4)_2$



Rotaxane **2.39** (5 mg, 0.002 mmol) and $Zn(ClO_4)_2·6H_2O$ (0.83 mg, 0.002 mmol) were dissolved in CH_2Cl_2/CH_3OH (0.5 mL / 0.5 mL). The reaction mixture was left to stir for 30 min at room temperature. The solvent was removed under vacuum to give the product as a white solid (5.8 mg, quantitative yield). **^{1}H NMR** (400 MHz, d_6-acetone) *δ* (ppm): 7.37-7.15 (30H, m, stopper-Ar*H*), 6.76 (2H, d, ^3J =7 Hz, H_a), 7.67-7.51 (8H, m, hydroquinone-*H*), 4.72 (4H, t, ^{3}J = 4 Hz, H_1), 4.39-4.36 (16H, m ,H_2 + H_3 + H_b + H_c), 4.03 (4H, m, H_4), 3.90 (4H, m, H_d), 3.72 (4H, m, H_5), 3.66 (4H, s, H_6), 2.11 (4H, m, H_e), 1.32 (54H, s, stopper-^{t}Bu*H*); **^{13}C NMR** (100 MHz, d_6-acetone) δ (ppm): 156.4, 153.3, 152.2, 148.9, 148.3, 144.4, 139.7, 131.9, 130.5, 124.5, 115.2, 113.3, 80.4, 79.4, 70.8, 69.7, 66.3, 64.0, 63.1, 51.4, 48.7, 44.4, 34.0, 30.8; **HRMS** (ESI +ve) m/z = 1200.80437 ($[M - 2ClO_4^-]^{2+}$, $C_{114}H_{136}I_4N_{14}O_8Zn$, calc. 1200.80792).

Compound **2.44** and **2.45**



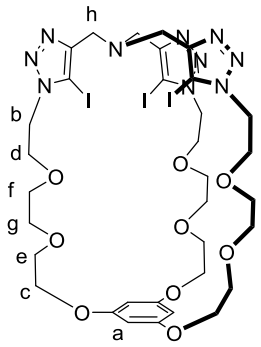
Bis-iodotriazole-amine-vinyl **2.26** (5.10 mg, 5.86 x 10^{-3} mmol) was dissolved in degassed CH_2Cl_2 (1.5 mL) followed by addition of $Ni(ClO_4)_2{\cdot}6H_2O$ (1.07 mg, 2.93 x 10^{-3} mmol). The mixture was stirred for 5 min and then 0.5 mg of Stewart-Grubbs' Catalyst was added. The reaction was left to stir at room temperature for 2 days before it was diluted using 20 mL of $CHCl_3$, washed with an EDTA solution (10 mL x 4), brine (20 mL x 2) and then dried with $MgSO_4$. The solvent was removed under vacuum to afford a light yellow solid. Purification of the compound was achieved by preparative TLC chromatography (96:4 CH_2Cl_2/CH_3OH) to give the product as a white solid.

Compound **2.44**: 2.1 mg, 41 % yield. **^{1}H NMR** (400 MHz, $CDCl_3$) δ (ppm): 6.83–6.72 (8H, m, H_1 + H_2), 5.82 (2H, m, H_3), 4.72 (4H, t, ^3J = 5.1 Hz, H_4), 4.32 (4H, t, ^3J = 5.1 Hz, H_5), 4.06–4.04 (8H, m, H_6 + H_7), 3.88 (4H, s, H_8), 3.74 (t, ^3J = 4.6 Hz, H_9); **HRMS** (ESI +ve) m/z = 844.08118 ($[M + H]^+$, $C_{30}H_{36}O_6N_7I_2$, calc. 844.08109).

Compound **2.45**: 2.0 mg (39 % yield).**^{1}H NMR** (400 MHz, $CDCl_3$) δ (ppm): 6.83–6.74 (8H, m, H_1 + H_2), 5.84 (2H, m, H_3), 4.71 (4H, t, ^3J = 5.1 Hz, H_4), 4.34 (4H, t, ^3J = 5.1 Hz, H_5), 4.07 (4H, m, H_6), 4.05 (4H, t, ^3J = 4.6 Hz, H_7), 3.89(4H, s, H_8), 3.75 (t, ^3J = 4.6 Hz, H_9); **HRMS** (ESI +ve) m/z = 1687.15112 ($[M + H]^+$, $C_{60}H_{71}O_{12}N_{14}I_4$, calc. 1687.15491).

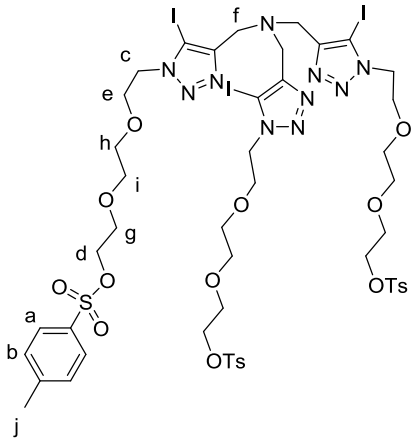
6.2.3 Synthesis of Novel Compounds from Chapter 3

Cryptand **3.5**



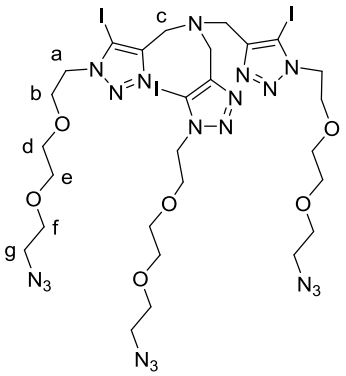
Tris-azide **3.3** (75 mg, 0.126 mmol), tris-iodoalkyne **3.4** (64 mg, 0.126 mmol) and TBTA (6.9 mg, 0.013 mmol) were dissolved in 20 mL of dry degassed THF before CuI (2.5 mg, 0.013 mmol) was added in one portion. The reaction was stirred under N_2 at 60 ^{o}C for 5 days. The solvent was removed under vacuum and 20 mL of $CHCl_3$ was added. The organic solution was washed with an EDTA solution (10 mL x 3), brine (20 mL x 2) and then dried with $MgSO_4$. The solvent was removed under vacuum to afford a yellow solid. Purification of the compound was achieved by preparative TLC chromatography (97:3 CH_2Cl_2/CH_3OH) to give the product as an off-white solid (17 mg, 12% yield). **^{1}H NMR** (400 MHz, $CDCl_3$) δ (ppm): 6.15 (3H, s, H_a), 4.40 (6H, t, ^{3}J = 5.4 Hz, H_b), 4.11 (6H, t, ^{3}J = 4.2 Hz, H_c), 3.94 (6H, t, ^{3}J = 5.4 Hz, H_d), 3.83 (6H, t, ^{3}J = 4.2 Hz, H_e), 3.68-3.65 (18H, m, H_f + H_g + H_h); **^{13}C NMR** (100 MHz, $CDCl_3$) δ (ppm): 160.7, 148.8, 94.5, 82.9, 70.9, 70.3, 69.7, 69.4, 67.3, 49.9, 48.1; **HRMS** (ESI +ve) m/z = 1107.05803 ([M + H^+] = $C_{33}H_{46}O_9N_{10}I_3$, calculated 1107.05888).

Compound **3.6**



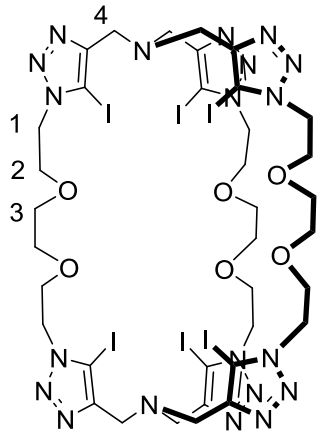
Azide-tosylate **3.2** (520 mg, 1.58 mmol), tris-iodoalkyne **3.4** (243 mg, 0.0478 mmol) and TBTA (25 mg, 0.048 mmol) were dissolved in 10 mL of dry degassed THF before CuI (9.1 mg, 0.048 mmol) was added in one portion. The reaction was stirred under N_2 at room temperature overnight. The solvent was removed under vacuum and 20 mL of $CHCl_3$ was added. The organic solution was washed with an EDTA solution (10 mL x 3), brine (20 mL x 2) and then dried with $MgSO_4$. The solvent was removed under vacuum to afford an off-yellow solid. Purification of the compound was achieved by silica gel column chromatography (98:2 CH_2Cl_2/CH_3OH) to give the product as an off-white solid (580 mg, 81% yield). **^{1}H NMR** (400 MHz, $CDCl_3$) δ (ppm): 7.79 (6H, d, ^3J = 8.2 Hz, H_a), 7.35 (6H, d, ^3J = 8.1 Hz, H_b), 4.48 (6H, t, ^3J = 5.0 Hz, H_c), 4.15 (6H, t, ^3J = 4.8 Hz, H_d), 3.94 (6H, t, ^3J = 5.0 Hz, H_e), 3.75 (6H, s, H_f), 3.66 (6H, t, ^3J = 4.8 Hz, H_g), 3.60-3.55 (12H, m, H_h + H_i), 2.44 (9H, s, H_j); **^{13}C NMR** (100 MHz, $CDCl_3$) δ (ppm): 149.2, 145.0, 132.9, 129.9, 127.9, 83.0, 70.7, 70.0, 69.2, 69.1, 68.7, 49.6, 47.8, 21.7; **HRMS** (ESI +ve) m/z = 1519.07033 ($[M + Na]^+$ = $C_{48}H_{63}I_3N_{10}O_{15}S_3Na$, calculated 1519.06627).

Compound **3.7**



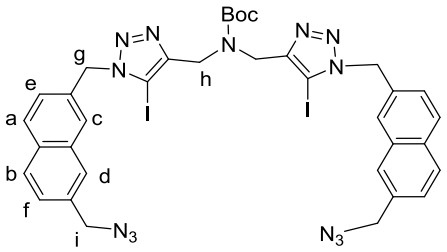
To a solution of compound **3.7** (580 mg, 0.388 mmol) in dry DMF (10 mL) was added NaN_3 (83 mg, 1.28 mmol) and left to stir overnight at 60 ^oC. The reaction mixture was diluted with 50 mL of EtOAc, washed with H_2O (10 mL x 2), brine (10 mL x 2) and then dried with $MgSO_4$. The solvent was removed under vacuum to afford the product as a white solid (430 mg, quantitative yield). **^{1}H NMR** (400 MHz, $CDCl_3$) δ (ppm): 4.50 (6H, t, ^3J = 5.4 Hz, H_a), 3.99 (6H, t, ^3J = 5.4 Hz, H_b), 3.77 (6H, s, H_c), 3.68-3.61 (18H, m, H_d + H_e + H_f), 3.39 (6H, t, ^3J = 4.8 Hz, H_g); **^{13}C NMR** (100 MHz, $CDCl_3$) δ (ppm): 149.2, 82.8, 70.6, 70.2, 70.1, 69.1, 50.7, 49.7, 47.8; **HRMS** (ESI +ve) m/z = 1132.06109 ($[M + Na]^+$ = $C_{27}H_{42}I_3N_{19}O_6Na$, calculated 1132.06158).

Cryptand **3.8**



Compound **3.7** (100 mg, 0.09 mmol), tris-iodoalkyne **3.4** (45 mg, 0.09 mmol) and TBTA (4.8 mg, 0.009 mmol) were dissolved in 15 mL of dry degassed THF before CuI (34 mg, 0.18 mmol) was added in one portion. The reaction was stirred under N_2 at 60 ^oC for 5 days. The solvent was removed under vacuum and 100 mL of $CHCl_3$ was added. The organic solution was washed with an EDTA solution (20 mL x 3), brine (20 mL x 2) and then dried with $MgSO_4$. The solvent was removed under vacuum to afford a yellow solid. Purification of the compound was achieved by preparative TLC chromatography (97:3 CH_2Cl_2/CH_3OH) to give the product as an off-white solid (14.7 mg, 10% yield). **^{1}H NMR** (400 MHz, $CDCl_3$) δ (ppm): 4.52 (12H, t, ^3J = 5.6 Hz, H_1), 3.97 (12H, t, ^3J = 5.6 Hz, H_2), 3.77 (12H, s, H_3), 3.64 (12H, s, H_4); **^{13}C NMR** (100 MHz, $CDCl_3$) δ (ppm): 149.2, 83.0, 70.6, 70.1, 69.2, 49.6, 47.8; **HRMS** (ESI +ve) m/z = 1640.82486 ([M + H^+] = $C_{38}H_{47}O_6N_{20}I_6$, calculated 1640.82500).

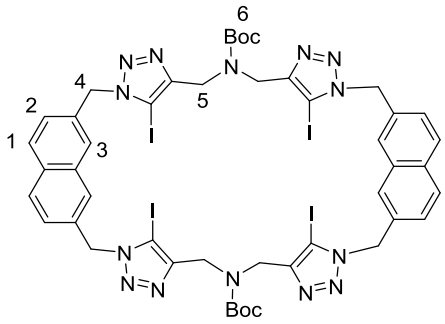
Compound **3.10**



Bis-azide **3.9** (428 mg, 1.8 mmol), $[Cu(CH_3CN)_4]PF_6$ (17 mg, 0.045 mmol) and TBTA (12 mg, 0.023 mmol) were dissolved in dry degassed THF (5 mL) before a degassed solution of *N*-Boc-protected bis-alkyne (40 mg, 0.09 mmol) in THF (2 mL) was added dropwise in 4 hrs. The reaction mixture was left to stir at room temperature under N_2 for 2 days before all the solvent was removed under vacuum. The residue was dissolved in $CHCl_3$ (50 mL), washed with an EDTA solution (20 mL x 3), H_2O (3 x 30 mL) and then dried over $MgSO_4$. The solvent was removed under vacuum to afford a yellow solid. Purification of the product was achieved by silica gel column chromatography (98:2 $CHCl_3/CH_3OH$) to afford

the product as a white solid (51 mg, 62% yield). **^{1}H NMR** (400 MHz, $CDCl_3$) δ (ppm): 7.85 (2H, d, ^3J = 8.8 Hz, H_a), 7.83 (2H, d, ^3J = 9.0 Hz, H_b), 7.75 (2H, s, H_c), 7.68 (2H, s, H_d), 7.45 (2H, d, ^3J = 8.8 Hz, H_e), 7.40 (2H, d, ^3J = 9.0 Hz, H_f), 5.70 (4H, s, H_g), 4.67 (4H, br., H_h), 4.50 (4H, s, H_i), 1.42 (9H, s, Boc); **^{13}C NMR** (125 MHz, $CDCl_3$) δ (ppm): 154.1, 147.6, 132.7, 132.0, 131.7, 131.4, 127.7, 127.6, 126.2, 126.1, 125.5, 124.7, 79.5, 53.8, 53.1, 49.8, 41.0, 40.7, 27.4; **HRMS** (ESI +ve) m/z = 944.08604, ($[M + Na]^+$, $C_{35}H_{33}I_2O_2N_{13}Na$, calculated 944.08617).

Macrocycle **3.11**



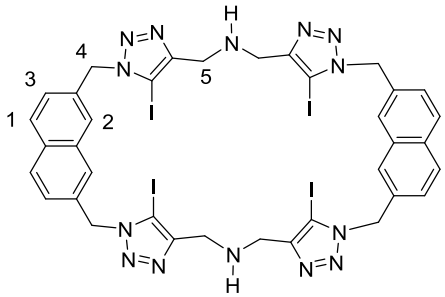
Entry 1: Compound **3.9** (428 mg, 1.8 mmol), bis-iodoalkyne **2.20I** (800 mg, 1.8 mmol) and TBTA (120 mg, 0.23 mmol) were dissolved in dry degassed THF (300 mL) before $[Cu(CH_3CN)_4]PF_6$ (170 mg, 0.45 mmol) was added in one portion. The reaction mixture was left to stir at room temperature under N_2 for 2 days before all the solvent was removed under vacuum. The residue was dissolved in $CHCl_3$ (50 mL), washed with an EDTA solution (20 mL x 3), H_2O (3 × 30 mL) and then dried over $MgSO_4$. The solvent was removed under vacuum to afford a yellow solid. Purification of the compound was achieved by silica gel column chromatography (98:2 $CHCl_3$/CH_3OH) to afford the product as a white solid (270 mg, 22% yield).

Entry 2: Compound **3.10** (200 mg, 0.22 mmol), bis-iodoalkyne **2.20I** (98 mg, 0.22 mmol) and TBTA (27 mg, 0.05 mmol) were dissolved in degassed THF (50 mL) before $[Cu(CH_3CN)_4]PF_6$ (37 mg, 0.1 mmol). The reaction mixture was left to stir at room

temperature under N_2 for 2 days before all the solvent was removed under vacuum. The residue was dissolved in $CHCl_3$ (50 mL), washed with an EDTA solution (20 mL x 3), H_2O (3 x 30 mL) and then dried over $MgSO_4$. The solvent was removed under vacuum to afford a yellow solid. Purification of the compound was achieved by silica gel column chromatography (98:2 $CHCl_3/CH_3OH$) to afford the product as a white solid (150 mg, 50% yield).

^{1}H NMR (500 MHz, d_6-DMSO) δ (ppm):7.92 (4H, d, ^3J = 8.6 Hz, H_1), 7.53 (4H, d, ^3J =8.4 Hz, H_2), 7.23 (4H, br., H_3), 5.73 (8H, s, H_4), 4.43 (8H, m, H_5), 1.38 (18H, s, H_6); **^{13}C NMR** (125 MHz, d_6-DMSO) δ (ppm): 154.9, 134.1, 133.1, 132.2, 128.6, 126.4, 80.0, 68.7, 53.5, 28.5, 26.4; **HRMS** (ESI +ve) m/z = 1388.99101, ($[M + Na]^+$, $C_{46}H_{46}I_4O_4N_{14}Na$, calculated 1388.98974).

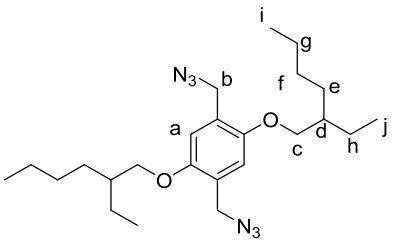
Macrocycle **3.12**



Compound **3.11** (200 mg, 0.146 mmol) was suspended in dry CH_2Cl_2 (2 mL) before trifluoroacetic acid (0.06 mL, 90 mg, 0.8 mmol) was added in one portion. The reaction was left to stir at room temperature overnight before it was diluted with 10 mL of $CHCl_3$. The organic solution was washed with a 1 M $NaHCO_3$ aqueous solution (10 mL x 2), brine (10 mL x 2) and then dried with $MgSO_4$. The solvent was removed under vacuum to afford the product as a white solid (170 mg, 100% yield). **^{1}H NMR** (500 MHz, d_6-DMSO) δ (ppm): 7.90 (4H, d, ^3J = 8.6 Hz, H_1), 7.53 (4H, s, H_2), 7.41 (4H, d, ^3J = 8.7 Hz, H_3), 5.75 (8H, s, H_4), 3.66 (8H, s, H_5); **^{13}C NMR** (125 MHz, d_6-DMSO) δ (ppm): 150.0, 134.1, 132.9, 132.3, 128.8,

126.6, 126.2, 84.1, 53.7, 43.7; **MS** (ESI +ve) m/z = 1166.90, ($[M + H]^+$, $C_{36}H_{31}I_4N_4$, calculated 1166.90).

Compound **3.17**



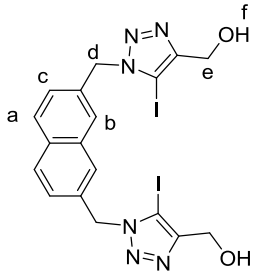
To a solution of compound **3.16** (100 mg, 0.19 mmol) in dry DMF (3 mL) was added NaN_3 (123 mg, 1.9 mmol). The reaction mixture was left to stir for 2 days at room temperature before it was diluted with 50 mL of EtOAc, washed with H_2O (10 mL x 2), brine (10 mL x 2) and then dried with $MgSO_4$. The solvent was removed under vacuum to afford the product as a white solid (84 mg, 100% yield). **^{1}H NMR** (500 MHz, $CDCl_3$) δ (ppm): 6.87 (2H, s, H_a), 4.40 (4H, s, H_b), 3.88 (4H, d, ^3J = 5.2 Hz, H_c), 1.77 (2H, sep, ^3J = 6.1 Hz, H_d), 1.56–1.34 (16H, m, H_e-H_h), 0.97–0.93 (12H, m, H_i + H_j); **^{13}C NMR** (125 MHz, $CDCl_3$) δ (ppm): 150.8, 124.6, 113.2, 71.1, 49.9, 39.6, 30.6, 29.1, 24.0, 23.1, 14.1, 11.2.

General protocol for synthesis of bis-OH compounds **3.13**, **3.18**, **3.23** and **3.25***:*

To a bis-azide (0.25 mmol) solution in THF (3 mL), NaI (290 mg, 2.0 mmol), $Cu(ClO_4)_2{\cdot}6H_2O$ (370 mg, 1.0 mmol) and TBTA (6.6 mg, 0.013 mmol) were added and the resulting mixture was left to stir for 5 min in the dark. Subsequently, an CH_3CN solution (3 mL) of DBU (76 mg, 0.5 mmol) was added to the reaction mixture followed by addition of propargyl alcohol (28 mg, 0.5 mmol). The reaction was left to stir at room temperature in the dark for 18 hrs. The mixture was diluted with 30 mL of $CHCl_3$, washed with an EDTA solution (20 mL x 3), H_2O (3 x 30 mL) and then dried over $MgSO_4$. The solvent was removed under

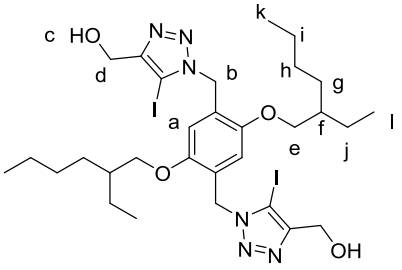
vacuum to afford an off-white solid. Purification of the compound was achieved by silica gel column chromatography (98:2 $CHCl_3/CH_3OH$) to afford the product as a white solid.

Compound **3.13**



Prepared from bis-azide **3.9**, 108 mg, 72% yield. **^{1}H NMR** (500 MHz, d_6-DMSO) δ (ppm): 7.93 (2H, d, ^3J = 8.4 Hz, H_a), 7.68 (2H, s, H_b), 7.34 (2H, d, ^3J = 8.4 Hz, H_c), 5.79 (4H, s, H_d), 5.17 (2H, t, ^3J = 5.5 Hz, H_e), 4.44 (4H, d, ^3J = 5.5 Hz, H_f); **^{13}C NMR** (125 MHz, d_6-DMSO) δ (ppm): 151.7, 134.2, 132.9, 128.9, 126.8, 126.1, 84.4, 55.3, 53.7; **HRMS** (ESI +ve) m/z = 624.93128, ($[M + Na]^+$, $C_{18}H_{16}I_2O_2N_6Na$, calculated 624.93163).

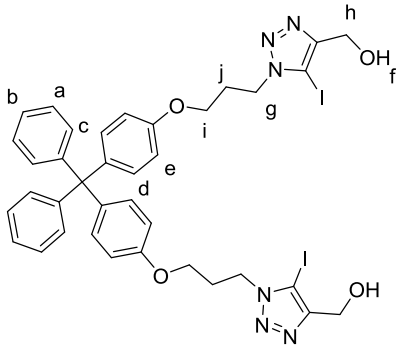
Compound **3.18**



Prepared from bis-azide **3.17**, 164 mg, 81%, yield. **^{1}H NMR** (500 MHz, d_6-DMSO) δ (ppm): 6.61 (2H, s, H_a), 5.48 (4H, s, H_b), 5.15 (2H, t, ^3J = 5.5 Hz, H_c), 4.43 (4H, d, ^3J = 5.5 Hz, H_d), 3.70 (4H, d, ^3J = 5.7 Hz, H_e),1.60 (2H, sep, ^3J = 6.2 Hz, H_f), 1.37–1.20 (16H, m, H_g–H_j), 0.87–0.81 (12H, m, H_k + H_l); **^{13}C NMR** (125 MHz, $CDCl_3$) δ (ppm): 151.3, 150.3, 124.3,

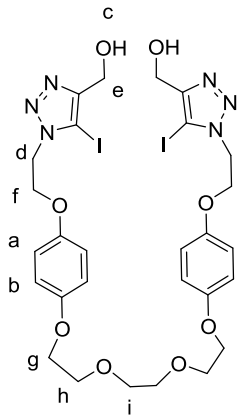
113.9, 84.3, 71.2, 55.3, 49.2, 30.3, 28.9, 23.7, 23.0, 14.4, 11.4; **HRMS** (ESI +ve) m/z = 809.17410, ($[M + H]^+$, $C_{30}H_{47}I_2O_4N_6$, calculated 809.17427).

Compound **3.23**



Prepared from bis-azide **3.22**, 154 mg, 70% yield. **^{1}H NMR** (500 MHz, d_6-DMSO) δ (ppm): 7.29 (4H, t, ^3J = 7.9 Hz, H_a), 7.19 (2H, t, ^3J = 7.3 Hz, H_b), 7.11 (4H, d, ^3J = 7.3 Hz, H_c), 6.99 (4H, d, ^3J = 8.9 Hz, H_d), 6.86 (4H, d, ^3J = 8.9 Hz, H_e), 5.15 (4H, t, ^3J = 5.5 Hz, H_f), 4.51 (4H, t, ^3J = 7.0 Hz, H_g), 4.42 (4H, d, ^3J = 5.5 Hz, H_h), 3.96 (4H, t, ^3J = 6.0 Hz, H_i), 2.25 (4H, quin, ^3J = 6.3 Hz, H_j); **^{13}C NMR** (125 MHz, $CDCl_3$) δ (ppm): 156.6, 151.2, 147.4, 139.2, 132.0, 130.9, 128.1, 126.3, 113.9, 83.9, 64.5, 63.6, 55.3, 47.5, 29.7; **HRMS** (ESI +ve) m/z = 883.09624, ($[M + H]^+$, $C_{37}H_{37}I_2O_4N_6$, calculated 883.09602).

Compound **3.25**

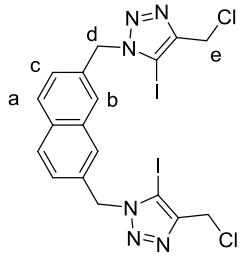


Prepared from bis-azide **2.33**, 155 mg, 74% yield. **^{1}H NMR** (400 MHz, $CDCl_3$) δ (ppm): 6.85–6.80 (8H, m, H_a + H_b), 5.16 (2H, br., H_c), 4.70 (4H, t, ^3J = 5.1 Hz, H_d), 4.43 (4H, br., H_e), 4.34 (4H, t, ^3J = 5.1 Hz, H_f), 3.99 (4H, t, ^3J = 4.6 Hz, H_g), 3.70 (4H, t, ^3J = 4.6 Hz, H_h), 3.58 (4H, s, H_i); **^{13}C NMR** (100 MHz, $CDCl_3$) δ (ppm): 153.3, 152.3, 151.1, 115.9, 115.8, 84.8, 70.4, 69.5, 68.0, 57.1, 55.3, 49.8; **HRMS** (ESI +ve) m/z = 837.05970, ($[M + H]^+$, $C_{28}H_{35}I_2O_8N_6$, calculated 837.06002).

General protocol for synthesis of bis-Cl compounds **3.14**, **3.19** and **3.24***:*

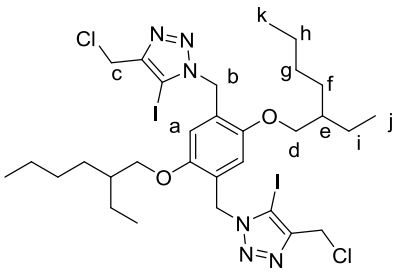
Bis-OH compound (0.20 mmol) was suspended in 3 mL of $CHCl_3$ before 0.1 mL of $SOCl_2$ (excess) was added. The reaction was heated under reflux for 8 hrs. The reaction was diluted with 20 mL of $CHCl_3$, washed with a saturated $NaHCO_3$ aqueous solution (20 mL), H_2O (20 mL x 2) and then dried with $MgSO_4$. The solvent was removed under vacuum to afford the product as a light yellow solid.

Compound **3.14**



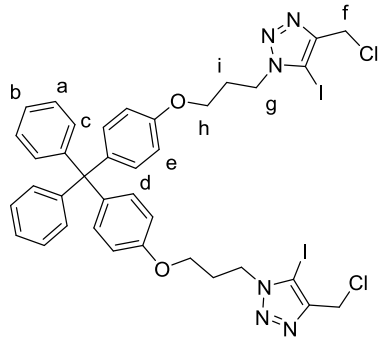
Prepared from compound **3.13**, 127 mg, quantitative yield. **^{1}H NMR** (400 MHz, $CDCl_3$) δ (ppm): 7.84 (2H, d, ^3J = 8.4 Hz, H_a), 7.67 (2H, s, H_b), 7.44 (2H, d, ^3J = 8.4 Hz, H_c), 5.75 (4H, s, H_d), 4.68 (4H, s, H_e); **^{13}C NMR** (125 MHz, d_6-DMSO) δ (ppm): 148.7, 132.9, 128.9, 127.3, 125.9, 54.5, 36.1, 30.9; **HRMS** (ESI +ve) m/z = 638.88159, ($[M + H]^+$, $C_{18}H_{15}I_2Cl_2N_6$, calculated 638.88191).

Compound **3.19**



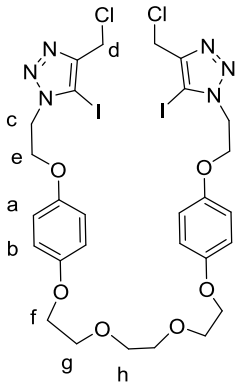
Prepared from compound **3.18**, 168 mg, quantitative yield. **^{1}H NMR** (500 MHz, d_6-DMSO) δ (ppm): 6.62 (2H, s, H_a), 5.50 (4H, s, H_b), 4.76 (4H, s, H_c), 3.69 (4H, d, ^{3}J = 5.4 Hz, H_d), 1.59 (2H, sep, ^{3}J = 6.2 Hz, H_e), 1.35–1.17 (16H, m, H_f – H_i), 0.87–0.80 (12H, m, H_j + H_k); **^{13}C NMR** (125 MHz, $CDCl_3$) δ (ppm): 150.4, 148.0, 124.0, 113.9, 86.6, 71.4, 49.8, 30.2, 28.8, 23.7, 23.0, 14.4, 11.4; **HRMS** (ESI +ve) m/z = 845.10670, ($[M + H]^+$, $C_{30}H_{45}I_2O_4N_6Cl_2$, calculated 845.10649).

Compound **3.24**



Prepared from compound **3.23**, 184 mg, quantitative yield. **^{1}H NMR** (500 MHz, d_6-DMSO) δ (ppm): 7.29 (4H, t, ^{3}J = 7.7 Hz, H_a), 7.19 (2H, t, ^{3}J = 7.2 Hz, H_b), 7.11 (4H, d, ^{3}J = 7.7 Hz, H_c), 7.00 (4H, d, ^{3}J = 8.9 Hz, H_d), 6.83 (4H, d, ^{3}J = 8.9 Hz, H_e), 4.75 (4H, s, H_f), 4.53 (4H, t, ^{3}J = 6.7 Hz, H_g), 3.97 (4H, t, ^{3}J = 5.7 Hz, H_h), 2.26 (4H, quin, ^{3}J = 6.3 Hz, H_i); **^{13}C NMR** (125 MHz, $CDCl_3$) δ (ppm): 156.6, 147.8, 147.3, 139.2, 132.0, 130.9, 128.1, 126.3, 113.9, 86.3, 64.6, 58.9, 48.0, 29.5, 15.6; **HRMS** (ESI +ve) m/z = 919.02878, ($[M + H]^+$, $C_{37}H_{35}I_2O_2N_6Cl_2$, calculated 919.02824).

Compound **3.26**



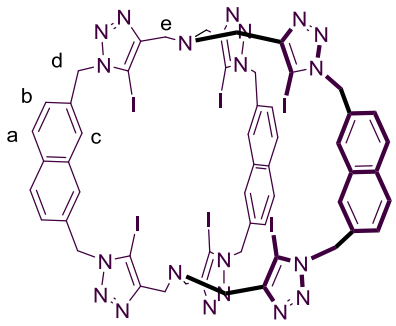
Compound **3.25** (100 mg, 0.12 mmol) was suspended in 3 mL of dry CH_2Cl_2 before Et_3N (51 mg, 0.50 mmol) was added. The mixture was cooled down to 0 ^oC and left to stir for 5 min. Subsequently, a CH_2Cl_2 solution (3 mL) of MsCl (33 mg, 0.29 mmol) was added dropwise in 30 min. The reaction was warmed to room temperature and left to stir overnight. The mixture was diluted with 30 mL of $CHCl_3$, washed with H_2O (20 mL x 2) and then dried with $MgSO_4$. The solvent was removed under vacuum to afford a yellow solid. The purification of the compound was achieved by silica gel column chromatography (98:2 CH_2Cl_2/CH_3OH) to give the product as a white solid (68 mg, 63%). **^{1}H NMR** (400 MHz, $CDCl_3$) δ (ppm): 6.85–6.75 (8H, m, H_a + H_b), 4.75 (4H, t, ^3J = 5.5 Hz, H_c), 4.68 (4H, s, H_d), 4.37 (4H, t, ^3J = 5.5 Hz, H_e), 4.06 (4H, t, ^3J = 5.0 Hz, H_f), 3.83 (4H, t, ^3J = 5.0 Hz, H_g), 3.74 (4H, s, H_h); **^{13}C NMR** (100 MHz, d_6-DMSO) δ (ppm): 153.3, 152.3, 147.7, 116.0, 115.8, 87.2, 70.4, 69.5, 68.0, 67.0, 50.2, 37.6; **HRMS** (ESI +ve) m/z = 894.97412, ($[M + Na]^+$, $C_{28}H_{32}I_2O_6N_6Cl_2Na$, calculated 894.97420).

General protocol for synthesis of cryptands **3.27** – **3.30***:*

Macrocycle **3.12** (23 mg, 0.02 mmol), bis-Cl compound (0.02 mmol), TBAI (6.4 mg, 0.02 mmol) and K_2CO_3 (13.8 mg, 0.1 mmol) were dissolved in 2 mL of $CHCl_3$ and the reaction was stirred under reflux for 5 days. The reaction mixture was diluted with 20 mL of $CHCl_3$, washed with H_2O (20 mL x 3), brine (20 mL x 2) and then dried with $MgSO_4$. The

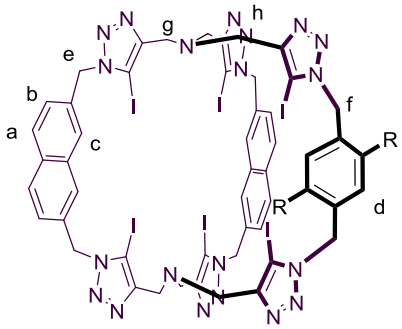
solvent was removed under vacuum to afford a yellow solid. Purification of the compound was achieved by preparative TLC chromatography (97:3 CH_2Cl_2/CH_3OH) to give the product as an off-white solid.

Cryptand **3.27**



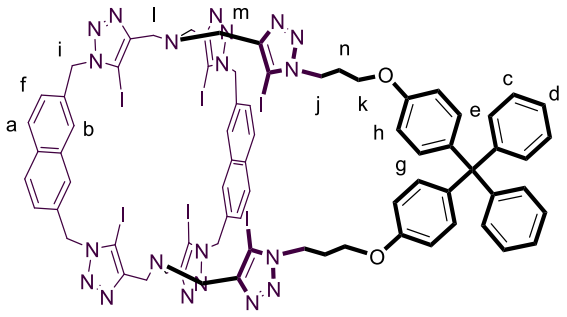
Prepared from compound **3.14**, 3.5 mg, 10% yield. **^{1}H NMR** (400 MHz, $CDCl_3$) δ (ppm): 7.88 (6H, d, ^3J = 7.8 Hz, H_a), 7.53 (6H, t, ^3J = 7.8 Hz, H_b), 5.75 (4H, s, H_d), 3.56 (4H, s, H_e); **HRMS** (ESI +ve) m/z = 1732.82314, ($[M + H]^+$, $C_{54}H_{43}I_6N_{20}$, calculated 1732.82422).

Cryptand **3.28**



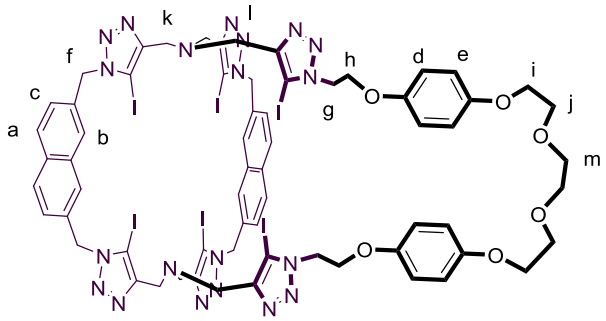
Prepared from compound **3.19**, 9.3 mg, 24% yield. ^{1}H NMR signals are too broad to be identified at 298 K; **HRMS** (ESI +ve) m/z = 1939.04766, ($[M + H]^+$, $C_{66}H_{73}O_2I_6N_{20}$, calculated 1939.04880).

Cryptand **3.29**



Prepared from compound **3.24**, 8.0 mg, 20% yield. **^{1}H NMR** (500 MHz, $CDCl_3$) δ (ppm): 7.75 (4H, d, ^{3}J = 8.5 Hz, H_a), 7.42 (4H, s, H_b), 7.30–7.27 (6H, m, H_c + H_d), 7.20 (4H, d, ^{3}J = 7.0 Hz, H_e), 7.14 (4H, d, ^{3}J = 7.2 Hz, H_f), 6.93 (4H, d, ^{3}J = 8.8 Hz, H_g), 6.56 (4H, d, ^{3}J = 8.8 Hz, H_h), 5.64 (4H, s, H_i), 4.42 (4H, d, ^{3}J = 6.7 Hz, H_j), 3.94 (4H, d, ^{3}J = 5.7 Hz, H_k), 3.80 (8H, s, H_l), 3.73 (4H, s, H_m), 2.42 (4H, quin, ^{3}J = 6.5 Hz, H_n); **^{13}C NMR** (125 MHz, $CDCl_3$) δ (ppm): 156.4, 149.1, 148.6, 146.9, 139.6, 133.0, 132.6, 131.1, 129.8, 127.6, 126.3, 125.4, 113.1, 96.1, 82.8, 81.7, 63.6, 63.2, 54.0, 48.8, 46.7, 39.6, 31.9, 31.0, 29.7, 29.4, 28.9, 22.7, 14.1; **HRMS** (ESI +ve) m/z = 2012.97075, ($[M + H]^+$, $C_{73}H_{63}O_2I_6N_{20}$, calculated 2012.97055).

Cryptand **3.30**

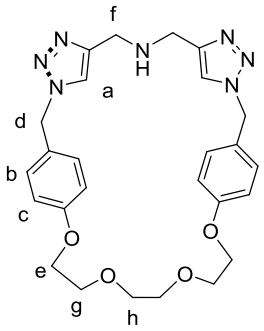


Prepared from compound **3.26**, 9.8 mg, 25% yield. **^{1}H NMR** (500 MHz, $CDCl_3$) δ (ppm): 7.74 (4H, d, ^{3}J = 8.4 Hz, H_a), 7.52 (4H, s, H_b), 7.39 (4H, d, ^{3}J = 8.4 Hz, H_c), 6.78 (4H, d, ^{3}J = 9.2 Hz, H_d), 6.66 (4H, d, ^{3}J = 9.1 Hz, H_e), 5.62 (4H, s, H_f), 4.69 (4H, d, ^{3}J = 4.9 Hz, H_g), 4.30 (4H, d, ^{3}J = 4.9 Hz, H_h), 4.07 (4H, d, ^{3}J = 4.8 Hz, H_i), 3.83 (4H, d, ^{3}J = 4.8 Hz, H_j),

3.74-3.73 (16H, m, H_k + H_l +H_m) ;**^{13}C NMR** (125 MHz, $CDCl_3$) δ (ppm): 149.2, 148.7, 132.9, 132.5, 128.6, 126.8, 125.9, 115.9, 115.6, 96.1, 70.8, 69.8, 68.1, 67.1, 53.9, 49.9, 48.4, 30.7, 29.7, 17.4; **HRMS** (ESI +ve) m/z = 1988.89782, ($[M + Na]^+$, $C_{64}H_{60}O_6I_6N_{20}$, calculated 1988.91650).

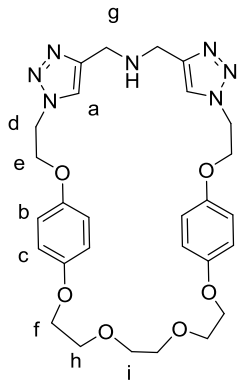
6.2.4 Synthesis of Novel Compounds from Chapter 4

Macrocycle **4.4**



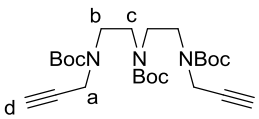
To a solution of dipropargylamine (49 mg, 0.53 mmol), bis-azide **4.3** (220 mg, 0.53 mmol) and TBTA (26 mg, 0.05 mmol) in dry degassed CH_2Cl_2 (150 mL) was added $[Cu(CH_3CN)_4]PF_6$ (37 mg, 0.10 mmol) in one portion. The reaction mixture was stirred at room temperature for 48 hrs. Subsequently, the mixture was washed with an EDTA solution (20 mL x 3), H_2O (3 x 30 mL) and then dried over $MgSO_4$. The solvent was removed under vacuum to afford a light yellow solid. Purification of the compound was achieved by preparative TLC chromatography (95:5 $CHCl_3/CH_3OH$) to afford the product as a beige solid (86 mg, 32% yield). **^{1}H NMR** (500 MHz, $CDCl_3$) δ (ppm): 7.24 (2H, s, H_a), 7.20 (4H, d, ^3J = 8.0 Hz, H_b), 6.87 (4H, d, ^3J = 8.0 Hz, H_c), 5.38 (4H, s, H_d), 4.09 (4H, t, ^3J = 3.8 Hz, H_e), 3.90 (4H, s, H_f), 3.84 (4H, t, ^3J = 3.8 Hz, H_g), 3.71 (4H, s, H_h); **^{13}C NMR** (125 MHz, $CDCl_3$) δ (ppm): 159.2, 146.8, 130.0, 126.7, 121.1, 115.1, 70.9, 69.6, 67.7, 53.8, 44.8, 30.9; **HRMS** (ESI + ve) m/z = 506.25162 ($[M + H]^+$, $C_{26}H_{32}N_7O_4$, calculated 506.25103).

Macrocycle **4.5**



To a solution of dipropargylamine (17 mg, 0.18 mmol), bis-azide **2.33** (85 mg, 0.18 mmol) and TBTA (4.8 mg, 0.009 mmol) in dry CH_2Cl_2 (60 mL) was added $[Cu(CH_3CN)_4]PF_6$ (6.7 mg, 0.018 mmol) in one portion. The reaction mixture was stirred at room temperature for 48 hrs before it was washed with an EDTA solution (20 mL x 3), H_2O (3 × 30 mL) and then dried over $MgSO_4$. The solvent was removed under vacuum to give a light yellow solid. The purification of the compound was achieved by preparative TLC chromatography (95:5 CH_2Cl_2/CH_3OH) to afford the product as a beige solid (31 mg, 30% yield). **^{1}H NMR** (400 MHz, $CDCl_3$) δ (ppm): 7.70 (2H, s, H_a), 6.80 - 6.71 (8H, m, H_b + H_c), 4.71 (4H, t, ^3J = 4.6 Hz, H_d), 4.26 (4H, t, ^3J = 4.6 Hz, H_e), 4.02 (4H, t, ^3J = 4.9 Hz, H_f), 3.94 (4H, s, H_g), 3.80 (4H, t, ^3J =4.9 Hz, H_h), 3.70 (4H, s, H_i); **^{13}C NMR** (125 MHz, $CDCl_3$) δ (ppm): 153.8, 152.1, 146.3, 130.1, 124.1, 123.1, 115.9, 115.6, 70.9, 68.3, 67.2, 49.9, 43.9, 34.3, 31.4, 29.7; **HRMS** (ESI + ve) m/z = 566.27197, ($[M+H]^+$, $C_{28}H_{36}O_6N_7$, calculated 566.27216).

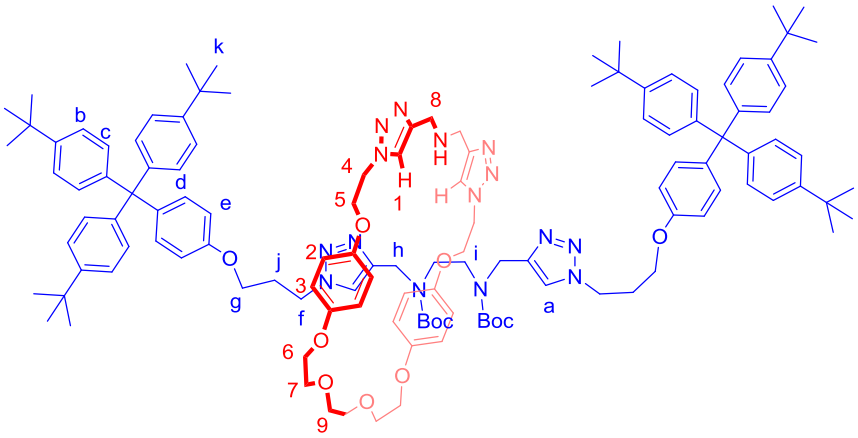
Compound **4.9**



Compound **4.8** (400 mg, 1 mmol) was dissolved in 3 mL of dry DMF, followed by portionwise addition of NaH (88 mg, 2.2 mmol, 60% in minerals). The resulting mixture was left to stir at room temperature for 30 min before propargyl bromide (262 mg, 2.2 mmol) was

added dropwised. The reaction mixture was left to stir at room temperature overnight and then 50 mL of H_2O was added. The aqueous solution was extracted by Et_2O (30 mL x 3) and the combined organic layers were dried over $MgSO_4$. The solvent was removed under vacuum to give a dark brown oil which was then purified by silica gel column chromatography (hexane/EtOAc = 1/9) to afford the product as a light yellow oil (186 mg, 39% yield). **^{1}H NMR** (400MHz) δ (ppm): 4.07-3.98 (4H, broad, H_a), 3.43-3.33 (8H, m, H_b + H_c), 2.20 (2H, s, H_d), 1.44 (18H, s, Boc), 1.43 (9H, s, Boc); **^{13}C NMR** δ (ppm): 155.2, 154.8, 80.5, 80.3, 79.8, 79.5, 71.8, 71.4, 71.2, 45.2, 44.6, 44.0, 37.1, 36.1, 28.4; **HRMS** (ESI +ve) m/z = 502.28863, ($[M+Na]^+$, $C_{25}H_{41}O_6N_3Na$, calculated 502.28876).

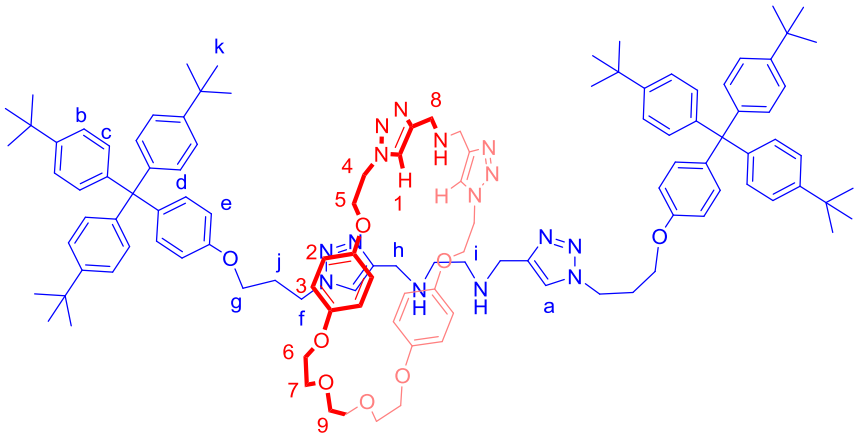
Rotaxane **4.10**



To a solution of macrocycle **4.5** (26 mg, 0.046 mmol) in dry CH_2Cl_2 (4 mL) was added $[Cu(CH_3CN)_4]PF_6$ (17 mg, 0.046 mmol) and the mixture was left to stir at room temperature for 5 min under N_2. Stopper azide **2.6** (166 mg, 0.276 mmol) and bis-alkyne **4.7** (46 mg, 0.138 mmol) were added and the solution was left to stir at room temperature for 96 hours. The reaction mixture was diluted with $CHCl_3$ (20 mL), washed with an EDTA solution (10mL x 2), water (5 mL x 2) and then dried with $MgSO_4$. The solvent was removed under vacuum to afford a light yellow solid. Purification of the compound was achieved by preparative TLC chromatography (96:4 $CHCl_3$/CH_3OH) to afford the product as a white solid (21 mg, 22% yield). **^{1}H NMR** (500 MHz, $CDCl_3$) δ (ppm): 7.63 (4H, m, H_1 + H_a), 7.25-6.75 (32H, m, H_b-H_e),

6.54-6.45 (8H, m, H_2 + H_3), 4.57-3.45 (40H, m, H_f-H_i, H_4–H_9), 2.37 (4H, m, H_j) 1.49-1.43 (18H, m, Boc), 1.31 (27H, s, stopper-^{t}Bu); **^{13}C NMR** (125 MHz, $CDCl_3$) δ (ppm): 156.2, 153.2, 151.8, 148.3, 144.2, 139.9, 132.2, 130.7, 124.1, 123.1, 115.4, 113.0, 70.8, 69.7, 67.9, 66.7, 64.1, 63.1, 49.6, 47.1, 46.9, 44.8, 44.3, 41.6, 34.3, 31.4, 28.5; **HRMS** (ESI +ve) m/z = 2078.25351 ($[M + H]^+$, $C_{126}H_{162}O_{12}N_{15}$, calculated 2078.2555).

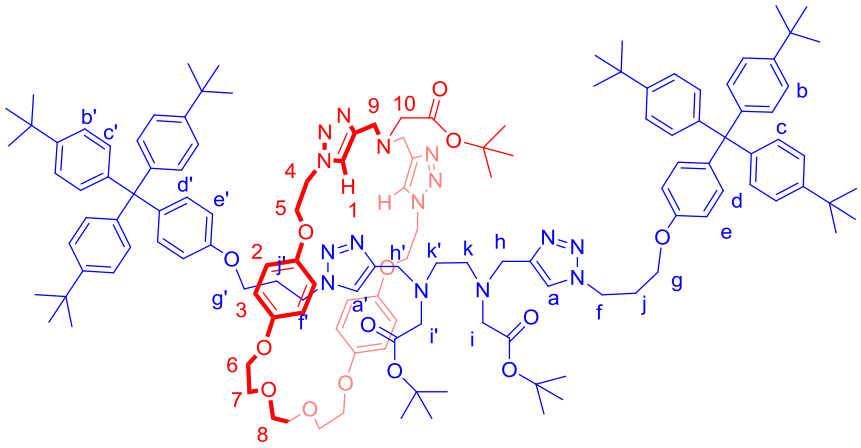
Rotaxane **4.11**



To a solution of rotaxane **4.10** (20 mg, 0.00963 mmol) in dry CH_2Cl_2 (2 mL), TFA (0.1 mL, excess) was added. The reaction mixture was left to stir overnight at room temperature before it was diluted with 20 mL of $CHCl_3$. The solution was washed with a saturated $NaHCO_3$ solution (20 mL), H_2O (20 mL x 2) and then dried with $MgSO_4$. The solvent was removed under vacuum to give the product as a light yellow solid (18 mg, quantitative yield). **^{1}H NMR** (500 MHz, $CDCl_3$) δ (ppm): 8.05 (2H, s, H_1), 7.56 (2H, s, H_a), 7.24-7.07 (28H, m, H_b + H_c + H_d), 6.78 (4H, d, ^3J = 9.0 Hz, H_e), 6.68-6.63 (8H, m, H_2 + H_3), 4.66 (4H, t, ^3J = 4.8 Hz, H_4), 4.47 (4H, t, ^3J = 7.1 Hz, H_f), 4.33 (4H, t, ^3J = 4.8 Hz, H_5), 3.97 (4H, t, ^3J = 4.9 Hz, H_6), 3.93 (4H, t, ^3J = 5.9 Hz, H_g), 3.80 (4H, t, ^3J = 4.9 Hz, H_7), 3.74 (4H, s, H_8), 3.70 (4H, s, H_9), 3.47 (4H, s, H_h), 2.39 (4H, s, H_i), 2.30 (4H, quin, ^3J = 6.3 Hz, H_j), 1.30 (54, s, H_k); **^{13}C NMR** (125 MHz, $CDCl_3$) δ (ppm): 156.3, 153.4, 152.0, 148.3, 144.1, 142.3, 140.1, 132.3, 130.7, 124.1, 115.6, 115.3, 113.0, 70.8, 69.7, 68.2, 66.7, 64.0, 63.1, 50.1, 47.3, 46.0, 44.1, 42.7,

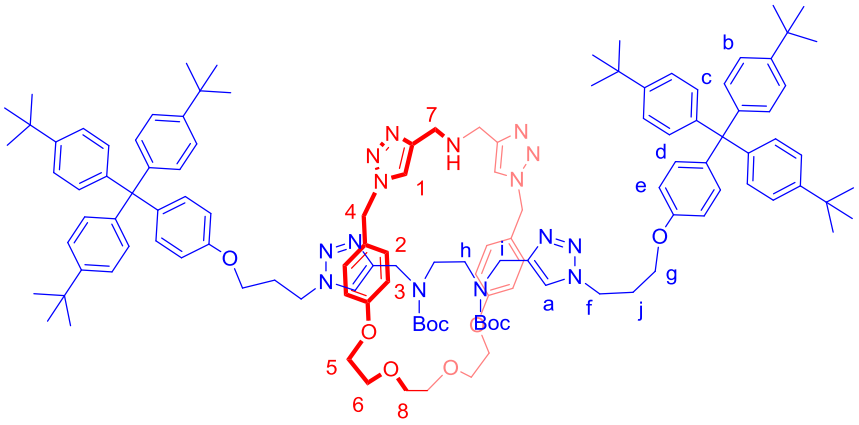
34.3, 31.4, 29.7, 22.7, 14.1; **HRMS** (ESI + ve) m/z = 1878.14633 ($[M+H]^+$, $C_{116}H_{146}O_8N_{15}$, calculated1878.15069).

Rotaxane **4.12**



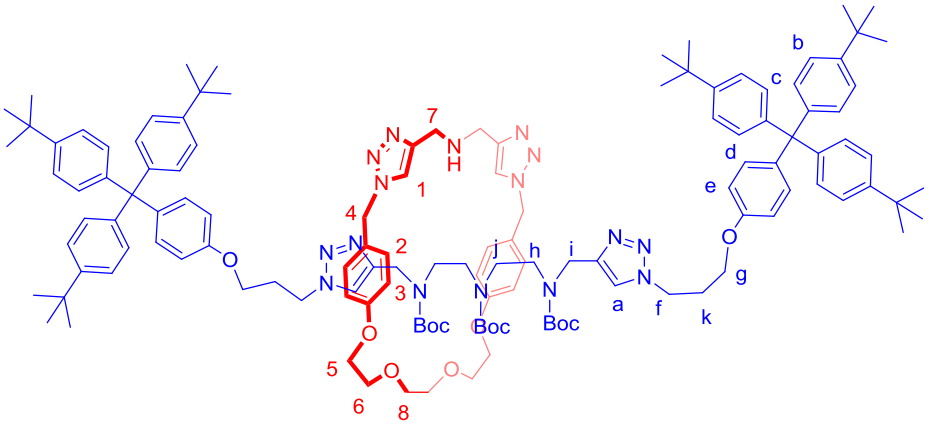
Rotaxane **4.11** (25 mg, 0.0133 mmol) and tert-butyl-2-bromoacetate (11 mg, 0.04 mmol) were dissolved in dry CH_3CN (2 mL) before Na_2CO_3 (28 mg, 0.26 mmol) was added in one portion. The reaction was left to stir at room temperature for 3 days. The mixture was diluted with 20 mL of $CHCl_3$, washed with H_2O (20 mL x 2), brine (20 mL) and then dried with $MgSO_4$. The solvent was removed under vacuum to afford a light yellow solid. Purification of the compound was achieved by preparative TLC chromatography (96:4 $CHCl_3/CH_3OH$) to afford the product as an off-white solid (18 mg, 72% yield). **^{1}H NMR** (400 MHz, $CDCl_3$) δ (ppm): 7.67 (3H, m, H_1 + H_a), 7.35 (1H, s, $H_{a'}$), 7.26-7.03 (28H, m, H_b + H_c + H_d + $H_{b'}$ + $H_{c'}$ + $H_{d'}$), 6.76 (2H, d, ^3J = 8.3 Hz, H_e), 6.50-6.44 (8H, m, H_2 + H_3), 6.36 (4H, d, ^3J = 8.7 Hz, $H_{e'}$), 4.61-4.52 (8H, m, H_4 + H_f + $H_{f'}$), 4.15-4.08 (4H, m, H_5), 3.98-3.96 (4H, m, H_g + $H_{g'}$), 3.90-3.29 (26H, m, H_6 - H_{10}, H_h + $H_{h'}$, H_i +$H_{i'}$), 3.14 (2H, m, H_j), 2.37 (2H, m, $H_{j'}$), 2.18 (4H, m, H_k + $H_{k'}$), 1.44-1.43 (27H, m, acetate-^{t}Bu), 1.30 (54H, s, stopper-^{t}Bu); **^{13}C NMR** (125 MHz, $CDCl_3$) δ (ppm): 153.2, 151.8, 148.3, 144.3, 144.1, 132.3, 130.7, 130.6, 124.2, 124.1, 115.9, 115.6, 115.3, 113.0, 70.7, 69.7, 67.8, 66.8, 63.1, 49.5, 48.2, 34.3, 33.2, 31.9, 31.4, 31.4, 29.7, 29.4, 28.2, 22.7, 17.5, 17.4, 14.2, 10.9; **HRMS** (ESI + ve) m/z = 2220.35289 ($[M+H]^+$, $C_{134}H_{176}N_{15}O_{14}$, calculated 2220.35493).

Rotaxane **4.13**



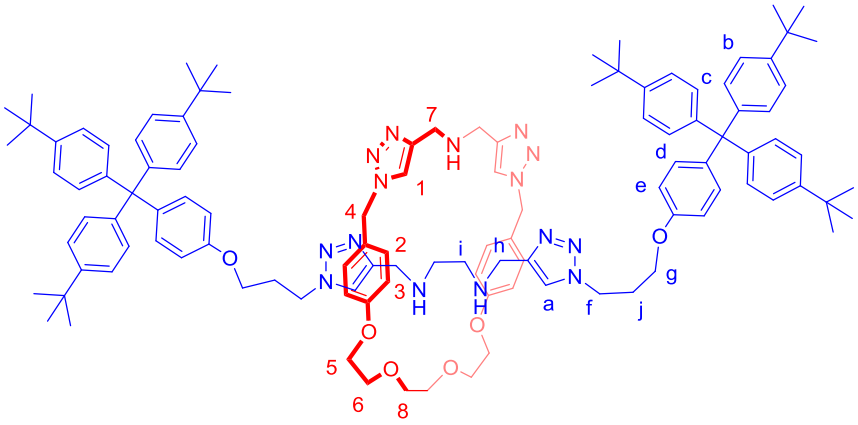
To a solution of macrocycle **4.4** (10 mg, 0.0198 mmol) in dry CH_2Cl_2 (2 mL) was added $[Cu(CH_3CN)_4]PF_6$ (7.5 mg, 0.0198 mmol) and the mixture was left to stir at room temperature for 5 min under N_2. Stopper azide **2.6** (70 mg, 0.1188 mmol) and bis-alkyne **4.7** (20 mg, 0.0594 mmol) were added and the solution was left to stir at room temperature for 96 hrs. The reaction mixture was diluted with $CHCl_3$ (20 mL), washed with an EDTA solution (10 mL x 2), water (5 mL x 2) and then dried with $MgSO_4$. The solvent was removed under vacuum to afford a light yellow solid. Purification of the compound was achieved by preparative TLC chromatography (95:5 $CHCl_3/CH_3OH$) to afford the product as a white solid (13 mg, 33% yield). **^{1}H NMR** (500 MHz, $CDCl_3$) δ (ppm): 7.63-7.36 (4H, m, H_a + H_1), 7.25-7.07 (28H, m, H_b + H_c + H_d), 6.94 (4H, d, ^3J = 7.9 Hz, H_2), 6.76 (4H, d, ^3J = 9.0 Hz, H_e), 6.50 (4H, d, ^3J = 7.9 Hz, H_3), 6.27-6.26 (4H, m, H_4), 4.57-4.40 (4H, m, H_f), 3.98-3.92 (8H, m, H_5 + H_g), 3.78-3.47 (20H, m, H_6 + H_7 + H_8 + H_h + H_i), 2.38 (4H, m, H_j), 1.50 (18H, m, Boc), 1.31 (54H, s, stopper-^{t}Bu); **^{13}C NMR** (125 MHz, $CDCl_3$) δ (ppm): 158.6, 156.2, 156.0, 155.5, 155.4, 148.4, 148.3, 144.3, 144.1, 140.1, 139.9, 132.4, 130.7, 130.6, 129.8, 126.7, 124.2, 124.1, 114.6, 113.1, 112.9, 80.2, 70.9, 69.6, 67.5, 64.0, 63.1, 53.6, 47.3, 46.7, 45.0, 44.9, 34.3, 34.3, 31.4, 30.1, 28.6; **HRMS** (ESI + ve) m/z = 2018.23710, ($[M + H]^+$, $C_{124}H_{158}N_{15}O_{10}$, calculated 2018.23442).

Rotaxane **4.14**



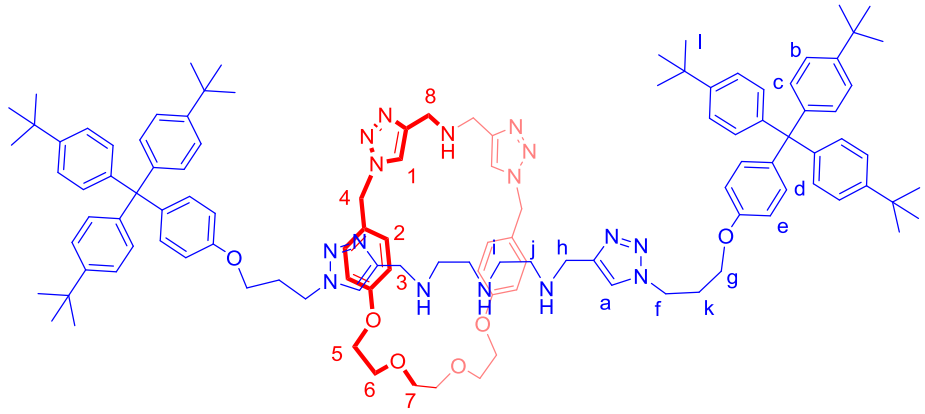
To a solution of macrocycle **4.4** (25 mg, 0.05 mmol) in dry CH_2Cl_2 (2 mL) was added $[Cu(CH_3CN)_4]PF_6$ (19 mg, 0.05 mmol) and the mixture was left to stir at room temperature for 5 min under N_2. Stopper azide **2.6** (176 mg, 0.3 mmol) and bis-alkyne **4.9** (72 mg, 0.15 mmol) were added and the solution was left to stir at room temperature for 96 hrs. The reaction mixture was diluted with $CHCl_3$ (20 mL), washed with an EDTA solution (10 mL x 2), water (5 mL x 2) and then dried with $MgSO_4$. The solvent was removed under vacuum to afford a light yellow solid. Purification of the compound was achieved by preparative TLC chromatography (95:5 $CHCl_3/CH_3OH$) to afford the product as a white solid (52 mg, 49% yield). **^{1}H NMR** (500 MHz, $CDCl_3$) δ (ppm): 7.61-7.39 (4H, m, H_a + H_1), 7.25-7.07, 6.75 (32H, m, H_b-H_e), 6.93 (4H, d, ^3J = 8.5 Hz, H_2), 6.50 (4H, m, H_3), 5.27–5.26 (4H, m, H_4), 4.60-4.41 (4H, m, H_f), 4.09-3.43 (36H, m, H_5–H_8, H_g-H_j), 2.38 (4H, m, H_k), 1.50 (27H, m, Boc), 1.30 (54H, s, stopper-^{t}Bu); **^{13}C NMR** (125 MHz, $CDCl_3$) δ (ppm): 158.5, 156.2, 155.4, 155.3, 148.4, 148.3, 144.3, 144.1, 140.1, 139.9, 132.4, 132.0, 130.7, 130.6, 129.8, 126.7, 124.2, 124.1, 114.6, 114.5, 113.1, 112.9, 80.2, 70.9, 69.6, 67.5, 64.0, 63.1, 63.0, 53.6, 53.5, 47.3, 46.7, 45.0, 34.3, 31.4, 30.1, 28.6; **HRMS** (ESI + ve) m/z = 1081.16878, ($[M + 2H]^{2+}$, $C_{131}H_{172}N_{16}O_{12}$, calculated 1081.16816).

Rotaxane **4.15**



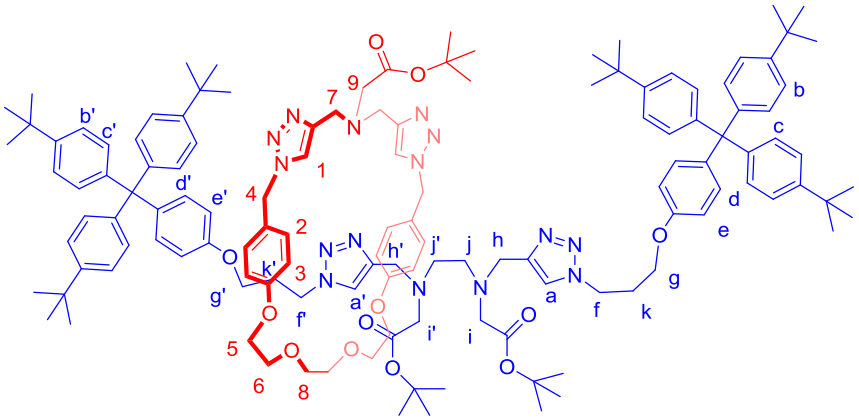
To a solution of rotaxane **4.13** (20 mg, 0.0099 mmol) in dry CH_2Cl_2 (2 mL), TFA (0.1 mL, excess) was added. The reaction was left to stir overnight at room temperature before it was diluted with 20 mL of $CHCl_3$. The solution was washed with a saturated $NaHCO_3$ solution (20 mL), H_2O (20 mL x 2) and then dried with $MgSO_4$. The solvent was removed under vacuum to give the product as a light yellow solid (18 mg, quantitative yield). **^{1}H NMR** (500 MHz, $CDCl_3$) δ (ppm): 7.62 (2H, s, H_a), 7.44 (2H, s, H_1), 7.23 - 7.08 (32H, H_b-H_e), 6.77 (4H, d, ^3J = 8.8 Hz, H_2), 6.61 (4H, d, ^3J = 8.8 Hz, H_3), 5.36 (4H, s, H_4), 4.42 (4H, t, ^3J = 6.8 Hz, H_f), 3.91 (8H, m, H_g + H_5), 3.77 (4H, t, ^3J = 4.0 Hz, H_6), 3.70 (4H, s, H_7), 3.66 (4H, s, H_8), 3.42 (4H, s, H_h), 2.57 (4H, s, H_i), 2.28 (4H, quin, ^3J = 5.9 Hz, H_j), 1.30 (54H, s, stopper-^{t}Bu); **^{13}C NMR** (125 MHz, $CDCl_3$) δ (ppm): 158.7, 156.3, 148.3, 144.1, 140.1, 132.3, 130.7, 130.2, 127.8, 124.1, 122.4, 114.4, 113.0, 70.8, 69.6, 67.7, 64.1, 63.1, 53.5, 47.2, 44.5, 42.8, 34.3, 31.4, 31.0, 29.8; **HRMS** (ESI + ve) m/z = 1818.13129 ($[M+H]^+$, $C_{114}H_{142}N_{15}O_6$, calculated 1818.12956).

Rotaxane **4.16**



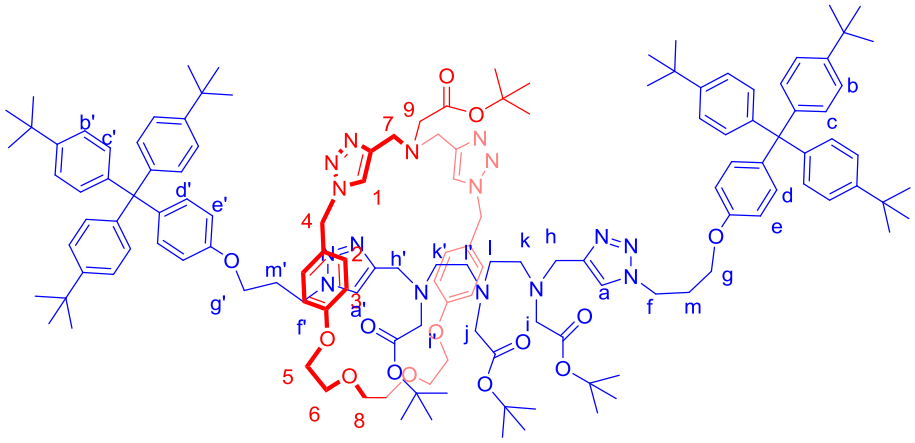
To a solution of rotaxane **4.14** (50 mg, 0.023 mmol) in dry CH_2Cl_2 (2 mL), TFA (0.1 mL, excess) was added. The reaction mixture was left to stir overnight at room temperature before it was diluted with 20 mL of $CHCl_3$. The solution was washed with a saturated $NaHCO_3$ solution (20 mL), H_2O (20 mL x 2) and then dried with $MgSO_4$. The solvent was removed under vacuum to give the product as a light yellow solid (43 mg, quantitative yield). **^{1}H NMR** (400 MHz) δ (ppm): 7.93 (2H, s, H_1), 7.48 (2H, s, H_a), 7.29 (2H, d, ^3J = 8.3 Hz, H_2), 7.22-7.07 (28H, m, H_b + H_c + H_d), 6.76 (4H, d, ^3J = 8.7 Hz, H_e), 6.68 (4H, d, ^3J = 8.3 Hz, H_3), 5.35 (4H, s, H_4), 4.45 (4H, t, ^3J = 6.6 Hz, H_f), 3.95 (4H, br, H_5), 3.90 (4H, t, ^3J = 5.2 Hz, H_g), 3.78 (4H, br, H_6), 3.73 - 3.69 (8H, m, H_7 + H_8), 3.45 (4H, s, H_h), 2.43 (8H, s, H_i + H_j), 2.28 (4H, quin, ^3J = 5.8 Hz, H_k), 1.29 (54H, s, H_l); **^{13}C NMR** (400 MHz) δ (ppm): 157.8, 155.3, 147.3, 144.2, 143.0, 139.0, 131.3, 129.7, 129.3, 126.6, 123.0, 121.8, 113.6, 111.9, 69.8, 68.5, 66.7, 63.0, 62.0, 52.5, 46.1, 45.7, 44.7, 43.5, 42.0, 33.3, 30.6, 28.9; **HRMS** (ESI +ve) m/z = 1861.17954 ($[M + H]^+$, $C_{116}H_{147}O_6N_{16}$, calculated 1861.17176).

Rotaxane **4.17**



Rotaxane **4.15** (17 mg, 0.00936 mmol) and tert-butyl-2-bromoacetate (6 mg, 0.028 mmol) were dissolved in $CHCl_3$/CH_3CN (1 mL/1 mL) before Na_2CO_3 (20 mg, 0.187 mmol) was added in one portion. The reaction mixture was left to stir at room temperature for 3 days before it was diluted with 20 mL of $CHCl_3$. The solution was washed with H_2O (20 mL x 2), brine (20 mL) and then dried with $MgSO_4$. The solvent was removed under vacuum to afford a light yellow solid. Purification of the compound was achieved by preparative TLC chromatography (96:4 $CHCl_3$/CH_3OH) to afford the product as an off-white solid (14 mg, 70% yield). **^{1}H NMR** (500 MHz, $CDCl_3$) δ (ppm): 7.66 (1H, s, H_a), 7.49 (1H, s, $H_{a'}$), 7.31 (2H, s, H_1), 7.25-7.03 (28H, m, H_b + H_c + H_d + $H_{b'}$ + $H_{c'}$ + $H_{d'}$), 6.91 (4H, d, ^3J = 8.4 Hz, H_2), 6.76 (2H, d, ^3J = 9.0 Hz, H_e), 6.46 (4H, d, ^3J = 8.4 Hz, H_3), 6.34 (2H, d, ^3J = 8.9 Hz, $H_{e'}$), 5.26 (4H, s, H_4), 4.55 (2H, t, ^3J = 7.1 Hz, H_f), 3.99–2.84 (36H, m, H_g + H_h + H_i + H_j + H_k + $H_{g'}$ + $H_{h'}$ + $H_{i'}$ + $H_{j'}$ + H_5-H_9), 2.38 (2H, quin, ^3J = 6.5 Hz, $H_{k'}$), 1.45 (9H, s, Boc), 1.44 (9H, s, Boc), 1.42 (9H, s, Boc), 1.31 (27H, s, stopper-^{t}Bu), 1.30 (27H, s, stopper-$_t$Bu); **^{13}C NMR** (125 MHz, $CDCl_3$) δ (ppm): 170.7, 170.6, 170.2, 158.5, 156.3, 155.9, 148.3, 148.2, 145.2, 145.1, 144.3, 144.1, 140.0, 139.6, 132.3, 131.8, 130.7, 130.6, 129.7, 126.6, 124.2, 124.1, 123.4, 123.3, 122.6, 114.6, 113.1, 113.0, 80.9, 80.8, 70.9, 69.6, 67.4, 64.1, 63.9, 63.1, 63.1, 55.8, 55.7, 54.3, 53.6, 51.9, 51.9, 49.2, 49.1, 47.2, 46.8, 34.3, 31.4, 31.4, 30.2, 29.8, 29.1, 28.2, 22.8, 17.5, 17.4, 14.1; **HRMS** (ESI +ve) m/z = 1080.67127, ($[M+2H]^{2+}$, $C_{132}H_{173}N_{15}O_{12}$, requires1080.67054).

Rotaxane **4.18**

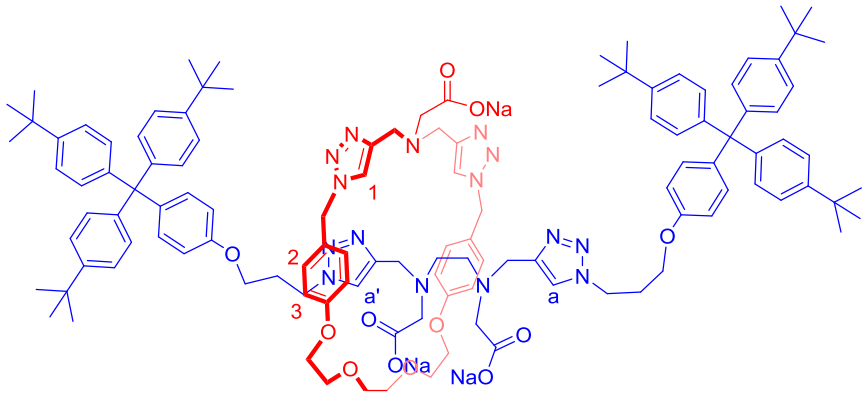


Rotaxane **4.16** (50mg, 0.027 mmol) and tert-butyl-2-bromoacetate (16 mg, 0.081 mmol) were dissolved in $CHCl_3/CH_3CN$ (1 mL/1 mL) before Na_2CO_3 (57 mg, 0.54 mmol) was added in one portion. The reaction mixture was left to stir at room temperature for 3 days before it was diluted with 20 mL of $CHCl_3$. The solution was washed with H_2O (20 mL x 2), brine (20 mL) and then dried with $MgSO_4$. The solvent was removed under vacuum to afford a light yellow solid. Purification of the compound was achieved by preparative TLC chromatography (95:5 $CHCl_3/CH_3OH$) to afford the product as an off-white solid (41 mg, 65% yield). **^{1}H NMR** (500 MHz, $CDCl_3$) δ (ppm): 7.65 (1H, s, H_a), 7.51 (1H, s, $H_{a'}$), 7.30 (2H, s, H_1), 7.25 - 7.02 (28H, m, H_b + H_c + H_d + $H_{b'}$ + $H_{c'}$ + $H_{d'}$), 6.91 (4H, d, ^3J = 7.8 Hz, H_2), 6.76 (2H, d, ^3J = 7.9 Hz, H_e), 6.45 (4H, d, ^3J = 7.8 Hz, H_3), 6.33 (2H, d, ^3J = 7.9 Hz, $H_{e'}$), 5.26 (4H, s, H_4), 4.55 (2H, t, ^3J = 7.0 Hz, H_f), 3.99–2.78 (40H, m, H_g – H_m, $H_{g'}$ – $H_{l'}$, H_5 -H_9), 2.37 (2H, quin, ^3J = 6.5 Hz, $H_{m'}$), 1.45-1.41 (36H, m, Boc), 1.30 (54H, s, stopper-^{t}Bu); **^{13}C NMR** (125 MHz, $CDCl_3$) δ (ppm): 169.1, 157.5, 155.3, 154.8, 147.3, 147.2, 144.1, 144.3, 143.0, 140.0, 138.5, 132.3, 131.3, 129.7, 128.6, 125.5, 123.1, 123.0, 121.6, 111.9, 79.8, 80.8, 69.8, 68.5, 66.3, 63.9, 62.9, 62.0, 62.0, 54.7, 52.5, 48.2, 46.2, 45.8, 33.3, 30.4, 29.1, 28.0, 27.2; **HRMS** (ESI +ve) m/z = 2317.43487, ($[M + H]^+$, $C_{140}H_{187}N_{16}O_{14}$, calculated 2317.44408).

General protocol for synthesis of rotaxane **4.19**, **4.20** and **4.21***:*

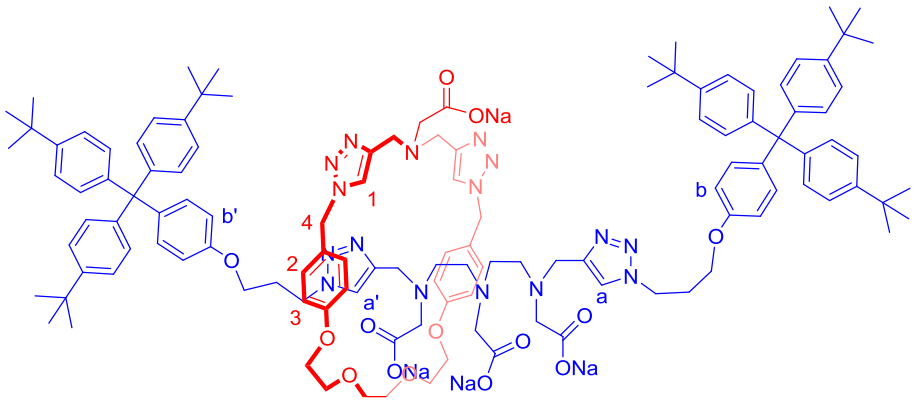
To a solution of rotaxane (0.005 mmol) in dry CH_2Cl_2 (2 mL), TFA (0.1 mL, excess) was added. The reaction mixture was left to stir overnight at room temperature before it was diluted with 20 mL of $CHCl_3$. The solution was washed with a saturated $NaHCO_3$ solution (20 mL x 2) and then dried with $MgSO_4$. The solvent was removed under vacuum to give the product as a yellow solid (quantitative yield). Even though significant evidence of removal of tert-butyl groups are revealed from ^{1}H NMR spectra of rotaxane **4.19**, **4.20** and **4.21**, the proton signals are very broad and hard to assign.

Rotaxane **4.20**



^{1}H NMR (500 MHz, d_4-methanol) δ (ppm): 7.73–7.27 (4H, m, H_1 + H_a + $H_{a'}$), 7.18–6.48 (40H, m, stopper- Ar*H* + H_2 + H_3), 4.56–2.90 (46H, m, *C*H_2), 1.20 (54H, s, stopper-^{t}Bu*H*).

Rotaxane **4.21**



^{1}H NMR (500 MHz, d_4-methanol) δ (ppm): 7.53–7.36 (4H, m, H_1 + H_a + $H_{a'}$), 7.16–6.78 (36H, m, stopper- Ar*H* + H_2), 6.67 (2H, *br.*, H_b), 6.37 (4H, d, ^{3}J = 8.6 Hz, H_3), 6.06 (2H, *br.*, $H_{b'}$), 5.22 (4H, s, H_4), 4.44-3.00 (48H, m, CH_2), 1.20 (54H, s, stopper-^{t}Bu*H*); **MS** (ESI +ve) m/z = 2093.282, ($[M-3Na+4H]^{+}$, $C_{124}H_{154}N_{16}O_{14}$, calculated 2093.193).

6.3 References

1 M. J. Hynes, *J. Chem. Soc. Dalton Trans.*, 1993, 0, 311–312.

2 *Tetrahedron Lett.*, 2006, 47, 5105–5109.

Appendix A: Crystallographic Data

Data collection

Single crystal X-ray diffraction data for compounds **2.14** and **2.23I** were collected using synchrotron radiation at 100(2) K at Diamond Light Source (DLS), Beamline I19[1] using a Cryostream N_2 open-flow cooling device on the diffractometer[2]. Cell parameters and intensity data (including inter-frame scaling) were processed using CrysAlis Pro (CrysAlis Pro, Agilent Technologies, 2010). Subsequently, the structure was solved using charge-flipping methods using SUPERFLIP,[3] and refined using full-matrix least-squares on F^2 within the CRYSTALS suite[4,5] by Dr. Jason Lim. For macrocycle **2.34**, the data was collected using the Supernova diffractometer at the University of Oxford with Cu radiation at 150 K and solved by Dr. Antonio Martinez-Martinez. All non-hydrogen atoms were refined with anisotropic displacement parameters. Where appropriate, disordered portions were modelled using refined partial occupancies, and geometric and vibrational restraints were applied to ensure that the models were physically reasonable. The majority of the hydrogen atoms were located from the difference map, while those which were not visible were repositioned geometrically. The H atoms were initially refined with soft restraints on the bond lengths and angles to regularise their geometry and U_{iso}(H), after which the positions were refined with riding constraints.[6]

Following the construction of a stable and physically-plausible model, the weights were optimised using the Chebyshev F^2 weighting scheme,[7] anomalous reflections were omitted and for poorly-diffracting samples (e.g. Compound 2), the absent high-angle data were pruned using the Wilson plot. This approach generally led to refinement convergence to give the final structure.

Compound **2.14**

Crystals suitable for X-ray diffraction structural analysis were obtained leaving a PF_6^-/ Cl^- salt of compound **2.14** to slowly crystallise from $CDCl_3$ in an NMR tube at room temperature. Due to the small size of the crystals, synchrotron radiation was necessary.

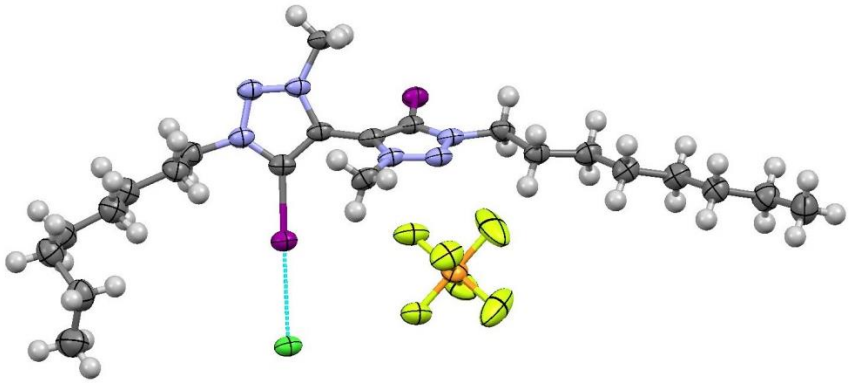


Figure A1. *X-ray crystal structure of the major component of dicationic compound* ***2.14*** *as a salt of chloride and PF_6^-. Thermal ellipsoids are displayed at the 50 % probability level.*

Table A1. Crystal structure data and refinement details for compound **2.14** as its chloride salt.

Experimental details	
Chemical formula	$C_{22}H_{40}ClF_6I_2N_6P$
M_r	822.82
Crystal system, space group	Monoclinic, $P2_1/n$
Temperature/ K	100(2)
a, b, c/ Å	8.0369 (10), 32.4865 (10), 12.3971 (10)
β / °	91.849 (10)
Unit cell volume/ Å^3	3235.1 (5)
Z	4
μ/ mm^{-1}	2.13
Crystal size/ mm	0.03 x 0.03 x 0.02
No. of measured, independent and observed [$I > 2.0\sigma(I)$] reflections	69387, 15549, 5909
R_{int}	0.057
$(\sin \theta/\lambda)_{max}$ / Å^{-1}	0.847
Refinement	
$R[F^2 > 2\sigma(F^2)]$, $wR(F^2)$, S	0.044, 0.120, 0.92
No. of reflections	6668
No. of parameters	343
$\Delta\rho_{max}$, $\Delta\rho_{min}$ (e Å^{-3})	2.23, −1.03

Complex **2.23I**

Small and poorly-diffracting crystals of complex **2.23I** were obtained by slow evaporation of solvent from a solution of the PF_6^- salt of Re(I) complex **2.23I** in methanol. Despite using synchrotron radiation, relatively low quality data were obtained due to crystal damage sustained from the X-ray beam during data collection. Nevertheless, the structure of the complex and position of the counteranion could be unambiguously determined. Some disorder of the counteranion were observed, which was successfully modelled as partially occupied PF_6^- (85 %) and iodide (10 and 5 % split over two sites). Due to poor data quality, the ellipsoids of the octyl chains on the receptor were rather large, and thus restraints to bond lengths and angles, as well as thermal and vibrational ellipsoid parameters had to be applied for the refinement to be chemically sensible. All the H atoms except that on the central bridging N atom (triazole-CH_2-**NH**-CH_2-triazole) could be located on the difference map, and thus that on the pertinent N atom was repositioned geometrically.

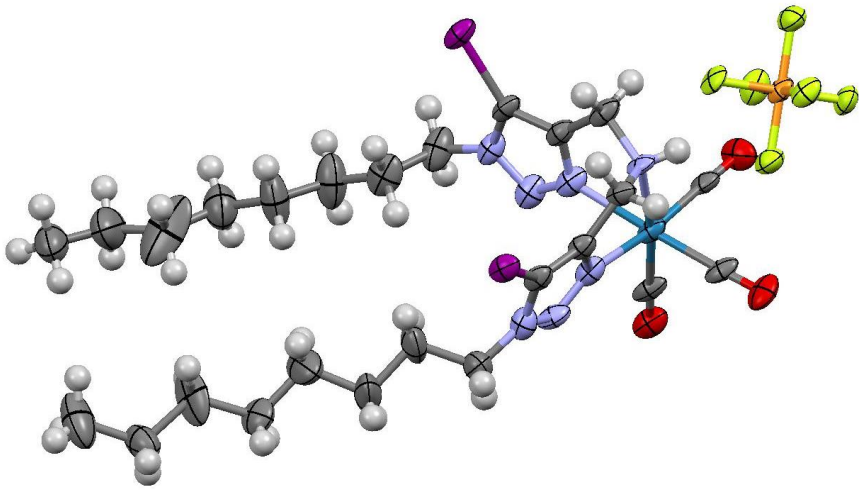


Figure A2. *X-ray crystal structure of the major component of complex* ***2.23I*** *as its PF_6^- adduct. Thermal ellipsoids are displayed at the 50 % probability level.*

Table A2. Crystal structure data and refinement details for complex **2.23I** as its PF_6 salt.

Experimental details	
Chemical formula	$C_{25}H_{39}F_6I_2N_7O_3PRe$
M_r	1067.89
Crystal system, space group	Triclinic, *P*-1
Temperature/ K	100(2)
a, *b*, *c*/ Å	7.5074 (6), 11.6898 (2), 21.0344 (8)
α, β, γ / °	98.809 (2), 96.736 (6), 90.006 (4)
Unit cell volume/ Å^3	1811.31 (17)
Z	2
μ/ mm^{-1}	5.29
Crystal size/ mm	0.02 x 0.02 x 0.01
No. of measured, independent and observed [$I > 2.0\sigma(I)$] reflections	35524, 16111, 10389
R_{int}	0.153
$(\sin \theta/\lambda)_{max}$ / Å^{-1}	0.855
Refinement	
$R[F^2 > 2\sigma(F^2)]$, $wR(F^2)$, *S*	0.112, 0.354, 0.95
No. of reflections	16071
No. of parameters	424
No. of restraints	27
$\Delta\rho_{max}$, $\Delta\rho_{min}$ (e Å^{-3})	9.25, −7.40

Macrocycle **2.34**

Crystals of macrocycle **2.34** were obtained by slow evaporation of dichloromethane from a saturated solution of the compound in a mixture of dichloromethane and hexane (ratio 1:1). Nonetheless, the crystal was still amenable for data collection in-house with Cu radiation. Although significant disorder was present, the connectivity of the atoms could be unambiguously determined. A molecule of dichloromethane was also encapsulated within the macrocycle cavity (c.a. 50 % occupancy).

Table A3. Crystal structure data and refinement details for macrocycle **2.34**.

Experimental details	
Chemical formula	$C_{33}H_{41}I_2N_7O_8 \cdot 0.5(CH_2Cl_2)$
M_r	959.99
Crystal system, space group	Triclinic, *P*-1
Temperature/ K	150
a, *b*, *c*/ Å	7.22638 (19), 14.1639 (6), 22.0908 (6)
α, β, γ / °	72.292 (3), 88.764 (2), 89.135 (3)
Unit cell volume/ Å^3	2153.35(12)
Z	2
μ/ mm^{-1}	12.48
Crystal size/ mm	0.12 x 0.10 x 0.04
No. of measured, independent and observed [$I > 2.0\sigma(I)$] reflections	20407, 8168, 7083
R_{int}	0.036
$(\sin \theta/\lambda)_{max}$ / Å^{-1}	0.610
Refinement	
$R[F^2 > 2\sigma(F^2)]$, $wR(F^2)$, *S*	0.053, 0.162, 1.04
No. of reflections	8168
No. of parameters	899
No. of restraints	2005
$\Delta\rho_{max}$, $\Delta\rho_{min}$ (e Å^{-3})	1.79, -1.01

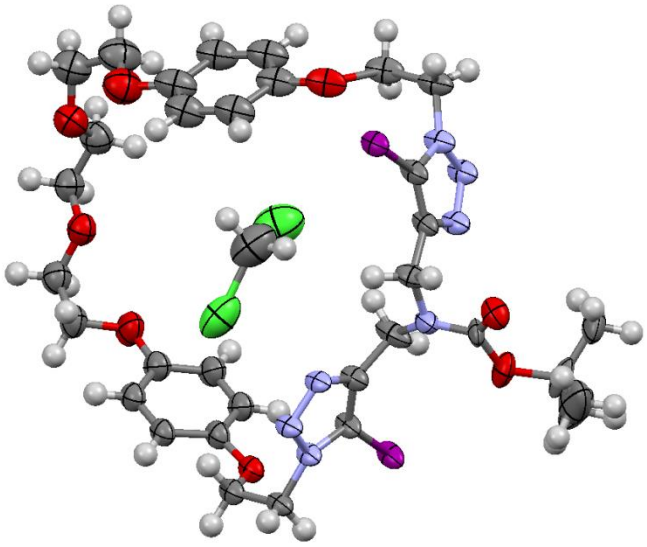


Figure A3. *X-ray crystal structure of the major component of macrocycle* ***2.34*** *with a molecule of dichloromethane. Thermal ellipsoids are displayed at the 50 % probability level.*

Appendix B: Computational Studies

The optimised geometry of **4.21Tb** (Figure A4) was calculated using MOPAC 2016 and the work was conducted by Mr. Xuejian Zhang from Professor Stephen Faulkner's group.[8] Some aspects of the calculation are shown in Table A4. A document containing more details is included in the disk.

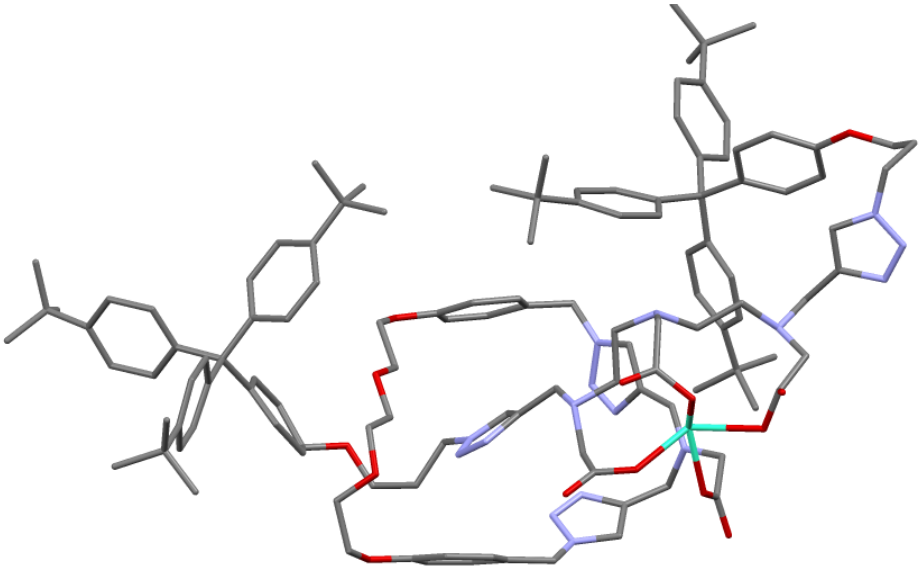


Figure A4. *Optimised geometry of* ***4.21Tb*** *using MOPAC2016*

Table A4. Some computational details of MOPAC geometry optimisation of **4.21Tb**.

SUMMARY OF AM1 CALCULATION, Site No: 26763 MOPAC2016 (Version: 17.270W)	
AM1 SPARKLE CHARGE=-1 BFGS GNORM=0.25 XYZ AUX	
THE LINE MINIMIZATION FAILED TWICE IN A ROW. SCF FIELD WAS ACHIEVED	
HEAT OF FORMATION	1069.51035 KJ/MOL
TOTAL ENERGY	-25158.94111 EV
ELECTRONIC ENERGY	-564704.86057 EV
CORE-CORE REPULSION	539545.91946 EV
GRADIENT NORM	88.82460
DIPOLE	23.22488 DEBYE POINT GROUP: C1
NO. OF FILLED LEVELS	392
CHARGE ON SYSTEM	-1
IONIZATION POTENTIAL	4.079163 EV
HOMO LUMO ENERGIES (EV)	-4.079 -2.381
MOLECULAR WEIGHT	2201.3773
COSMO AREA	1459.64 SQUARE ANGSTROMS
COSMO VOLUME	2598.41 CUBIC ANGSTROMS
SCF CALCULATIONS	356
WALL-CLOCK TIME	11 HOURS 32 MINUTES AND 24.519 SECONDS

Appendix C: Terbium Titrations Spectra

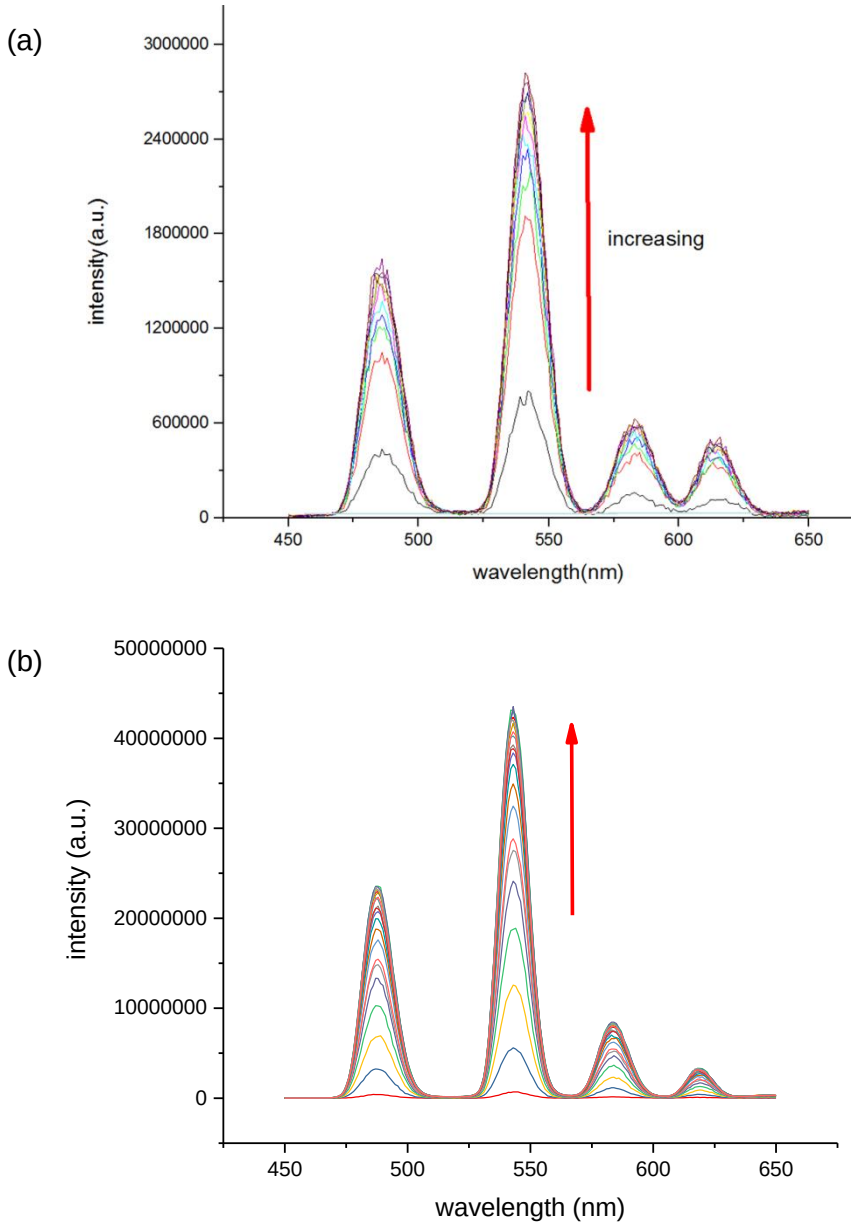


Figure A5. Phosphorescence spectra: titration of free Tb^{3+} cation into a MeOH solution of the rotaxane ligand (a) **4.20** and (b) **4.21** (from 0.0 to 5.0 eqv. Tb^{3+}, excitation at 298 nm, exit slit = 5 nm, gated time = 0.1 ms, [host] = 5 x 10^{-5} M).

References

1 H. Nowell, S. A. Barnett, K. E. Christensen, S. J. Teat and D. R. Allan, *J. Synchrotron Radiat.*, 2012, **19**, 435–441.
2 J. Cosier and A. M. Glazer, *J. Appl. Crystallogr.*, 1986, **19**, 105–107.
3 L. Palatinus and G. Chapuis, *J. Appl. Crystallogr.*, 2007, **40**, 786–790.
4P. W. Betteridge, J. R. Carruthers, R. I. Cooper, K. Prout and D. J. Watkin, *J. Appl. Crystallogr.*, 2003, **36**, 1487.
5 P. Parois, R. I. Cooper and A. L. Thompson, *Chem. Cent. J.*, 2015, **9**, 30.
6 R. I. Cooper, A. L. Thompson and D. J. Watkin, *J. Appl. Crystallogr.*, 2010, **43**, 1100–1107.
7 J. R. Carruthers and D. J. Watkin, *Acta Crystallogr. Sect. A*, 1979, **35**, 698–699.
8 M. A. M. Filho, J. D. L. Dutra, G. B. Rocha, R. O. Freire and A. M. Simas, *RSC Adv.*, 2013, **3**, 16747–16755.